Hydraulic Response and Stability Analysis of Earthen Dams subjected to Drainage Clogging and Hydraulic Fracturing

A Thesis

Submitted in Partial Fulfillment of the Requirements

for the Degree of

DOCTOR OF PHILOSOPHY

by

Priyanka Talukdar

Department of Civil Engineering

Indian Institute of Technology Guwahati

Guwahati – 781039, India

April 2020

STATEMENT

I do hereby declare that the matter embodied in this thesis is the result of investigations carried out by me in and with the aid of the Department of Civil Engineering, Indian Institute of Technology Guwahati, Assam, India.

In keeping with the general practice of reporting scientific observations, due acknowledgements have been made wherever the work described is based on the findings of other investigators.

Priyanka Talukdar.

Date: 19/04/2020 **(Priyanka Talukdar)**

Place: IIT Guwahati

CERTIFICATE

This is to certify that the thesis entitled **"Hydraulic Response and Stability Analysis of Earthen Dams subjected to Drainage Clogging and Hydraulic Fracturing"** submitted by **Priyanka Talukdar,** Roll No. 146104025, to the Indian Institute of Technology, Guwahati, for the award of the degree of Doctor of Philosophy in Civil Engineering, is a record of bonafide research work carried out by her under my supervision and guidance. The thesis work, in my opinion, has reached the requisite standard fulfilling the requirement for the degree of Doctor of Philosophy.

The results contained in this thesis have not been submitted in part or full to any other University or Institute for award of any degree.

Arindam Dey

Date: 19/04/2020
Place: IIT Guwahati

(Dr. Arindam Dey)
Associate Professor
Department of Civil Engineering
Indian Institute of Technology Guwahati
Guwahati-781039, India

ACKNOWLEDGMENTS

I owe my sincere gratitude to a number of persons whose unending support and patronage enabled me to pursue my research studies and submit the thesis for PhD. First and foremost, I would like to express my heartfelt thanks and deep sense of gratitude to my thesis supervisor and research guide Dr. Arindam Dey, for his meticulous guidance, encouragement, patience and support during my entire PhD study. He is one of the finest persons I have ever met in my life so far. I am very grateful to him for sparing his precious time and efforts throughout the entire work. His enthusiasm, integral view on research and his mission for providing high-quality work, has made a deep impression on me. During our course of interaction, I have learnt extensively from him, including how to raise new possibilities, how to regard an old question from a new perspective, how to approach a problem by systematic thinking, data-driven decision making and exploiting serendipity. I am highly obliged to him for all the insightful discussions, affection and kind suggestions, which helped me to complete the work successfully. I have been fortunate and blessed enough to have him as my research guide, whose able guidance and valuable advice will help me a long way in moulding my future career.

I extend my gratitude to my doctoral committee members Prof. A. Murali Krishna, Dr. Suresh Kartha, Dr. Ravi K and Dr. Sachin Gautam for reviewing my work and providing their valuable inputs that helped in improving my thesis. I would also like to thank all the other faculty members in the Civil Engineering Department for their suggestions and support during my PhD. I owe great thanks to the staffs of Geotechnical Engineering, Mr. Hariram Upadhyay, and Mr. Samarjyoti Kalita for kind help in conducting the research. I thank all office staffs of Civil Engineering Department for their help and cooperation in pursuing my work.

Most importantly, I owe my deepest gratitude to my parents for their immeasurable love and care. They have always encouraged me to explore my potential and pursue my dreams. I am always thankful towards my better half, Kaustav Jyoti Borah, for his eternal support and understanding of my goals and aspirations. His infallible love and support has always been my strength. His patience and sacrifice will remain my inspiration throughout my life. Without his help, I would not have been able to complete much of what I have done and become who I am. A special thanks to my lovely younger sister, Rajashree Talukdar for her unfailing love and support throughout the years. My heartfelt regard goes to my father in law and mother in law for their love and understanding. I would also like to thank my relatives and near and dear ones for their time-to-time encouragement during the course of my study.

Lastly, I would sincerely like to thank my friends Rubi, Devdeep, Prasun, Amalesh, Rana Dada, Chiranjib Dada, Shiv Shankar Dada, Jumrik Didi, Sudheer Bhaiya, Yagom Didi, Madhulatha, Dipjyoti Dada, Chinumoni Baa, Debasmita, Nayan, Needhi Baa, Jayshree Baa, Chandan, and many others for their companionship, support and encouragement.

Finally, I thank the Almighty for this enriching journey.

Priyanka Talukdar.

Date: 19/04/2020 PRIYANK TALUKDAR

ABSTRACT

The problem of dam failures has always sought attention of the researchers and engineers, owing to its devastating impact upon humankind and the environment. Studies have shown that poor drainage caused by clogging can result in drastic variation of the pore water pressures within the earthen dam, and can lead to substantial changes in the phreatic level with time, even reaching the higher limits of the downstream face. This scenario seriously influences the safety of the dams. Another factor that can lead to interior failure of earthen dams over a prolonged period is the hydraulic fracturing. There are documented cases of earthen dam failure within few hours after the first leakage was spotted, which is attributed to hydraulic fracturing during reservoir filling. In order to understand the detrimental effects of the above triggers, this dissertation reports about the influences of clogging of drainage blankets and hydraulic fracturing of the central impervious core in earthen dams. Primarily, the hydraulic response and stability analysis of these dams owing to these scenarios are investigated in this work with the finite-element based numerical investigations.

To assess the detrimental effect of drainage blanket clogging, firstly, different drainage blankets are introduced in the analyses, namely the horizontal toe drainage blanket and the inclined chimney drainage blanket. Homogeneous earthen dams, without or with fully functional or clogged drainage blankets, were investigated. The analyses were conducted considering different clogging scenarios for each blanket typology, and the outcomes are interpreted through the flow, stress-deformation and stability of the earthen dam. Analyses of the outcomes of different clogging scenarios aided in identifying the 'inward clogging' as the most critical clogging scenario owing to its influence in drastically raising the phreatic level in the downstream section of the dam. The investigations also helped to ascertain that inclined chimney drainage blanket would continue to serve its purpose for a long time even when it is partially clogged, and should be an inadvertent choice in designing earthen

dams. Further, considering various reservoir operational conditions (steady-state reservoir level, reservoir rise-up and reservoir drawdown), the influence of clogging rate of the drainage were also investigated. It was observed that the clogging rate had marginal influence on the response of earthen dams under transient reservoir operations (rise-up or drawdown), while a pertinent influence could be observed when the reservoir level or the phreatic surface within the body of the earthen had attained their steady-state scenarios.

Hydraulic fractures in earthen dams is also addressed in this work, in which the tentative location of hydraulic fracturing is identified for homogeneous and zoned earthen dams. The possibility of hydraulic fracturing of the slope faces of homogeneous earthen dams, comprising horizontal toe drainage blanket, are ascertained for its construction phase as well as for subsequent reservoir operations. This study is extended to zoned earthen dams where the tentative location of crack initiation on the faces of the central impervious core is identified with the aid of standard criterion correlating minimum effective principal stress and generated pore-water pressures. It was concluded that the provision of a drainage blanket does not necessarily reduce the possibility of hydraulic fracturing. Rather, the presence of an inclined chimney drainage blanket ensures the long-term performance even if there is a detected crack in the impervious core of a zoned earthen dam. Finally, utilizing the standard criterion, a recursive numerical methodology is devised to identify the path of crack propagation through central impervious core, initiating from the identified location of crack initiation.

Keywords: Earthen dams, Drainage blankets, Clogging, Hydraulic fracturing, Crack path propagation, Finite Element Analysis, Flow-deformation analysis, Stability analysis

TABLE OF CONTENTS

CHAPTER 6: HYDRAULIC FRACTURING AND CRACK PROPAGATION IN ZONED EARTHEN DAMS WITH A CENTRAL IMPERVIOUS CORE

CHAPTER 7: FINAL REMARKS AND CONCLUSIONS

LIST OF FIGURES

Figure No.	Figure Caption	Page No.
4.10	Model for the present study with no drainage blanket	107
4.11	(a) Model for the present study with horizontal toe drainage blanket (b) Model for the present study with inclined chimney drainage blanket	108
4.12	Inward clogging starting from outlet end of horizontal toe drainage blanket (a) Dam section with the clogged drain (b) Enlarged section of the clogged drain	109
4.13	Outward clogging starting from inlet end of horizontal toe drainage blanket (a) Dam section with the clogged drain (b) Enlarged section of the clogged drain	109
4.14	Upward clogging starting from the bottom of horizontal toe drainage blanket (a) Dam section with the clogged drain (b) Enlarged section of the clogged drain	110
4.15	Downward clogging starting from the top of horizontal toe drainage blanket (a) Dam section with the clogged drain (b) Enlarged section of the clogged drain	110
4.16	Random clogging starting from the outlet end of horizontal toe drainage blanket (a) Dam section with the clogged drain (b) Enlarged section of the clogged drain	111
4.17	Random clogging starting from the inlet end of horizontal toe drainage blanket (a) Dam section with the clogged drain (b) Enlarged section of the clogged drain	111
4.18	Inward clogging starting from outlet end of inclined chimney drainage blanket (a) Dam section with the clogged drain (b) Enlarged section of the clogged drain	112
4.19	Outward clogging starting from inlet end of inclined chimney drainage blanket (a) Dam section with the clogged drain (b) Enlarged section of the clogged drain	112
4.20	Upward clogging starting from the bottom of inclined chimney drainage blanket (a) Dam section with the clogged drain (b) Enlarged section of the clogged drain	113
4.21	Downward clogging starting from the top of inclined chimney drainage blanket (a) Dam section with the clogged drain (b) Enlarged section of the clogged drain	113

Figure No.	Figure Caption	Page No.
4.46	PWP contours on the 6th day representing complete rise-up of the reservoir and transient migration of the phreatic surfaces after complete rise-up (a) Horizontal toe drainage blanket (b) Inclined chimney drainage blanket (c) Horizontal toe drainage blanket with length comparable to the basal extent of inclined chimney drainage blanket	142
4.47	Deformation of the earthen dam at the end of rise-up i.e. at the 6th day (a) Upstream face (b) Downstream face	143
4.48	Vertical deformation profile of the base of earthen dam at the end of (a) Reservoir drawdown (b) Reservoir rise-up	144
4.49	Stability of the downstream face of an earthen dam with horizontal toe drainage blanket (a) NDC (b) FDC (c) CDC	146
4.50	Stability of the downstream face of an earthen dam with inclined chimney drainage blanket (a) NDC (b) FDC (c) CDC	147
4.51	Stability of the downstream face of an earthen dam values subjected to different types of clogging in (a) Horizontal toe drainage blanket (b) Inclined chimney drainage blanket	148
4.52	Stability of the earthen dam comprising various types of drainage blanket under varying operating conditions when subjected to reservoir drawdown scenario (a) Upstream face (b) Downstream face	149
4.53	Stability of the earthen dam comprising various types of drainage blanket under varying operating conditions when subjected to reservoir rise-up scenario (a) Upstream face (b) Downstream face	150
4.54	Variation of PWP along the base of the dam after the 3rd stage of clogging for different clogging rates (a) Steady-state reservoir condition (b) Reservoir rise-up condition (c) Reservoir drawdown condition	152
4.55	Influence of clogging rate on the variation of pore-water pressure within an earthen dam with horizontal toe drainage blanket and a steady-state reservoir condition (a) High rate of clogging, i.e. 1 m/day (b) Low rate of clogging, i.e. 0.01 m/day	153
4.56	Influence of clogging rate on the variation of pore-water pressure within an earthen dam with horizontal toe drainage blanket and a reservoir rise-up condition (a) High rate of clogging, i.e. 1 m/day (b) Low rate of clogging, i.e. 0.01 m/day	154

LIST OF TABLES

CHAPTER 1

INTRODUTION

1.1 GENERAL

Dams are structural barriers constructed to block or control the flow of water in rivers and streams. The dams are built to render two primary functions. Firstly, it is used as means of water storage to compensate the variations in river discharge (flow) or to meet the needs for energy and water. Secondly. It is used to increase the hydraulic head (difference in height between upstream reservoir and downstream water levels), thereby creating additional storage and head of water facilitating generation of electricity, providing water for agricultural, industrial or household needs, and controlling river navigation. The type and size of a dam exhibits a complex dependency on the amount of water available, requirement for water storage or diversion, topography, geology, the characteristics and feasibility of local materials available for construction. Although each constructed dam is recognized to be unique, it is possible to identify and classify them in different categories namely in the purview of their functions, structural and hydraulic designs, and materials used for construction. The different types of dams hold special importance, each having a unique purpose of its construction. However, among the various types of constructed dams, the earthen dams and embankments are most common and popular due to the easy availability and handling of the construction materials, lesser cost of construction and lesser restrictions in selection of sites. However, along with these advantages, there are a number of challenges suffered by the earthen dams and embankments, which might lead to disaster if not addressed properly.

Based on the literature survey, it is understood that based on the volumes of materials used in construction, earthen dams comprise the world's largest dams. The Fort Peck Dam, on River Missouri in Montana, is one of the largest embankment dams, utilizing 125 million cubic yards (92 million m^3) of earth materials for its construction (USACE, 2011). Earthen dams are built of various types of geologic materials, with an exclusion of peats and organic soils. Most earthen dams are designed to utilize the economically available on-site materials for the bulk of construction. The large earthen dams require an extraordinarily critical engineering skill for conception, planning, design and construction. Construction of earthen dams and embankments are a common practice in the North Eastern part of India as it consists of 12 % of the total flood area of the country (Das et al., 2017). Earthen dams and embankments are constructed as a flood management measure in this region to ensure protection during the excessive incessant rainfall events. Figure 1.1 portrays some of the recent embankment failure events that were witnessed in the North Eastern state of Assam, India, during the monsoon period starting from the last week of April to July 2019 when very heavy downpour was experienced by the region. These earthen embankment dams, which were constructed to control flood, failed catastrophically leaving scores of people homeless and displaced, destroying crops and damaging public properties. However, failure of these embankments for a variety of reasons (water surge, overtopping, hydraulic fracturing, settlement-induced cracking etc.) provided an eye-opener to look into the design, analysis, construction quality and understanding the mechanisms of their failure. The failure of many earthen dams provided an opportunity to inspect their internal structure and get an understanding of the presence or absence of various components supposedly to be present. In this scenario, it was noticed that many of these earthen dams were simply mounds of earth and, most probably, without proper engineered design.

Figure 1.1 A glimpse to some of the failures of earthen embankment dams in Assam, India, 2019 (a) Breaching of Haldibari embankment in Majuli (https://www.time8.in/breaking-majulis-main-embankment-gives-way/) (b) Erosion and settlement induced cracking of earthen dyke on Ranganadi river at Borbil, North Lakhimpur (https://www.apnnews.com/flood-situation-remains-grim-in-assam/) (c) Embankment breaching by the flood waters of Pagladia river, Assam (http://www.assamtribune.com/scripts/detailsnew.asp?id=apr2216/state051) (d) Embankment reeling under erosion resulting in eminent cracks on its surface in Sonitpur district of Assam (https://www.pratidintime.com/assam-reeling-under-soil-erosion-flood-threats/)

Most of the failures of such earthen embankments are related to the sudden rise-up and receding of water on their upstream side, apart from the erosion and abrasion during flooding. Such embankment failures were witnessed in the past for many years and the problem holds a lot of importance and challenge in the assessment of the cause of failure. Hence, there is lot of scope for research and development in order to understand the root cause of the degradation in the performance of such earthen dams and embankments, and control or eliminate such failures to the maximum extent possible. Therefore, it is realized that simply constructing the earthen dams and embankments, as the flood management measure, is not sufficient; rather, it is of utmost importance that proper emphasis and investment is being made to make sure that these embankments possess a longer performance life and are resilient to failure. It is very vital to pinpoint the different reasons that results in the earthen dam failures and to work rigorously to find out a solution so that future disasters could be averted to the best possible extent. Prevention of failures of these earthen dams and embankments are inextricably linked with safety of the lives of the people and the purpose for which these dams are constructed at the first place.

1.2 MOTIVATION OF THE STUDY

Earthen dams are ever subjected to different critical issues, which, if not dealt carefully, might cause terrible catastrophe. The chief drawback of earthen dams is that they are prone to be overtopped, subjected to seepage, internal erosion, piping, hydraulic fracturing and heaving. Apart from being subjected to transverse and longitudinal cracking, desiccation cracking also lead to sufficient malfunctioning. Instability of the upstream and downstream slopes of the earthen dams is another serious problem that comprise slides, displacements, slumps, slips, and sloughs under various governing and boundary conditions. Depressions, sinkholes and settlement are some common early indicators of serious problems that are also noticeable in such dams. Intense rainfall, rapid drawdown and seismic excitations (leading to internal and local liquefaction) are also cited to be the primary triggers for such failure and mishaps. Earthen dams should be assessed for the various loading conditions it is subjected to during its performance life. The range of loading conditions at various stages, from construction stage through the operational stage of the completed embankment, encompasses different cases such as the end of construction, rapid drawdown, steady seepage and partial pool of steady seepage condition. In many cases, drainage blankets are successfully used to control the flow of water through the earthen dams and prevent the majority of the dam structure from being saturated, thus enhancing the longevity of the same. However, a major problem is faced when such drainage blanket starts getting clogged and the performance of the dam severely deteriorates. In this regard, it becomes immensely important to understand the mechanism of clogging and how it changes the response of the earthen dam subjected to various operational stages. Hydraulic fracturing is another critical issue that needs to be addressed intently, as several of earthen dams, all around the world, have shown evidence of failure during their first filling and reservoir loading. Hydraulic fracturing is mostly initiated with the increase in the water load, and thereby the pore-water pressure within the dam. Either new cracks are initiated or the latent cracks are jacked open. Whatever may be the cause, it is important to identify the root-cause of hydraulic fracturing and the progression of the crack through the body of the dam, so that the influence of hydraulic fracturing on the response and failure of the earthen dams are suitably understood. With the advancement of time and technology, different mathematical, analytical and numerical models, aptly supported by physical modeling, has led to the better understanding of these phenomenon. Although these approaches have facilitated the evaluation of seepage and deformation in the earthen dams and embankments, still several critical issues need to be addressed. Thus, critical assessment of the failure of the earthen dams and embankments needs proper attention and thorough research.

1.3 OUTLINE OF THE DISSERTATION

This dissertation is organized into seven chapters as per the following outline:

- **Chapter 1** presents a general introduction to the subject matter and motivation of the dissertation work.
- **Chapter 2** deals with the background study and comprehensive literature review. Based on the critical appraisal of the reviewed literature and gap areas, the precise objectives and the scope of the study have been listed.
- **Chapter 3** provides the details of the methodologies adopted in the present study for numerical simulation.
- **Chapter 4** brings out the effects of clogging of drainage blankets on the flow-deformation-stability response of homogeneous earthen dams when subjected to different types of reservoir operations.
- **Chapter 5** describes the effect of hydraulic fracturing and cracking on the response of homogeneous earthen dam during its construction as well as operational stages with different types of reservoir conditions.
- **Chapter 6** describes the hydraulic fracturing through zoned earthen dams. The influence of drainage blankets on the performance of zoned earthen dams under the scenarios of core cracking are discussed. Further, a numerical methodology to highlight the progression of crack through the central impervious core of zoned earthen dam is also presented.
- **Chapter 7** lists out the important conclusions made from the present study. The limitation of the present study and the scope of future research work is also presented.

The chapters are followed by a list of related references considered for the dissertation. As an outcome of the dissertation work, the list of publications is also provided.

CHAPTER 2

BACKGROUND STUDY AND LITERATURE SURVEY

2.1 GENERAL

The world has many challenges to overcome on the path towards development, designing, and maintaining of infrastructure and technology in the field of geotechnical and water resource engineering. One of the most vital challenges faced in these areas concerns ‘Dam Failures’, with special consideration given to earthen embankments and dams. Emphasis is laid on these types of dams considering the fact that they are the most commonly constructed dams in the world. Further, according to the reports, the frequency of failure of such dams is about four times higher than that found for masonry and concrete dams (Lebreton, 1964). ‘Dam failures’ are referred to those incidents that result in the destruction of the dam or result in its structural failure in such a manner that it causes unintended releases or surges of impounded water (Fread, 1980). In addition, dam failure is also regarded as the loss of its ability to serve the purpose to hold the water in its reservoir (Mufute et al., 2008). The problem of dam failure should be treated with utmost importance because it is related to a nation’s environmental and economic attributes. Therefore, this problem is always given its due importance by the engineers. Special attention to such problems are laid by the hydraulic engineers in finding out the downstream valleys that are at risk of inundation against such instances of dam failures (Macchione and Sirangelo, 1988). A dam failure can take place in a number of ways; most of which are generally caused by a deficiency in the constructed dam section, an outside triggering event or a combination of the two. The embankment dams, constructed primarily using the earth and rock-fill materials, are complex structures to evaluate as it deals with problems of water ingress into the dam, erosion issues leading to piping and temporal strength degradation of constituent material, all of which requires stringent monitoring constantly. Preventing disastrous dam failures is imperative. Thus, it is important to study the crux of the problem to harness the benefits of the constructed dam for a long time.

2.2 FAILURE OF EARTHEN DAMS AND EMBANKMENTS

Failure of earthen dams occurs when the structure is breached or significantly damaged, leading to catastrophic effects. Routine monitoring of deformation and discharge from drains, in and around dams, is extremely helpful to diagnose the problems and allow remedial measures to be taken before the occurrence of failure. According to the International Humanitarian Law (Lorenz, 2003), dams are considered 'installations containing dangerous forces', since these structures have huge influence of an impending catastrophe on lives and property. The failure of the Banqiao Reservoir Dam (Figure 2.1), Upper and Lower Baoquan dams, Guxian dam, Nanwan dam, Xiaolangdi dam in Henan Province, China, 1975, are examples that resulted in more fatalities than any other dam failure in the history, leading to the death of 171,000 people and leaving 11 million people homeless (https://www.internationalrivers.org/resources/the-forgotten-legacy-of-the-banqiao-damcollapse). Thousands of people were left homeless in 2012, during the failure of Campos's dos Goytacazes dam (Figure 2.2), located in Brazil towards the northern state of Rio de Janeiro (http://planetsave.com/2012/01/06/13000-homeless-9-dead-from-dam-break-in-brazil). In India, major dam failures include the failure of Kaddam Project Dam in Andhra Pradesh (1958), Machhu Irrigation Scheme Dam in Gujarat (1979, Figure 2.3a), Kaila Dam in Gujarat (1959), Kodaganar Dam in Tamil Nadu (1977), Nanaksagar Dam in Punjab (1979), Panshet Dam in Maharashtra (1961, Figure 2.3b) and the 118-year-old Jaswant Sagar Dam situated in the Luni River basin, Jodhpur, Rajasthan (2007). Such dam failures remind that careless design and faulty or non-engineered may cause catastrophic situation on the lives and environment (Thandaveswara, 2012). Generally, the failure of dams occurs quite rapidly and without sufficient warning, thereby representing a potential to an extensive calamity. Some of the typical dam failure incidents that resulted in catastrophe are shown in Figures 2.4-2.6. Therefore, the design of dams should be scientifically done to avoid such situations as much as possible.

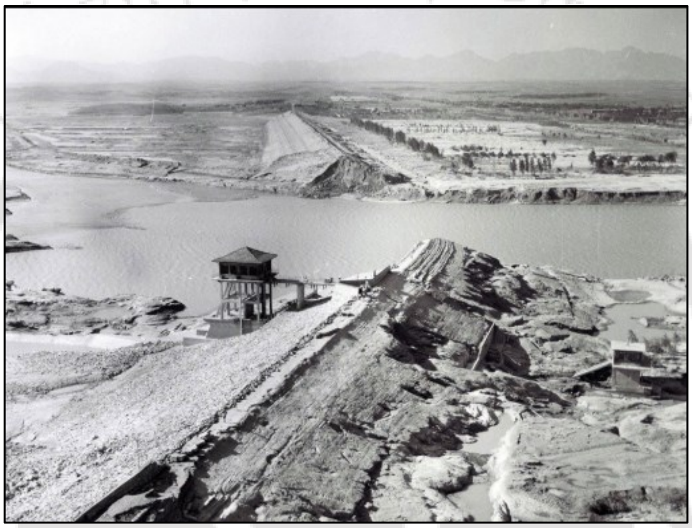

Figure 2.1 Failure of Banqiao Reservoir Dam, Henan, China, 1975

Figure 2.2 Failure of Campos's dos Goytacazes dam, Rio de Janeiro, Brazil, 2012

(a) (b)

Figure 2.3 (a) Machhu dam failure, 1979 (https://www.indiawaterportal.org/articles/machhu-dam-disaster-1979-gujarat-discussion-book-tom-wooten-and-utpal-sandesara) (b) Panshet dam disaster, Maharashtra, 1961 (https://divyamarathi.bhaskar.com/news/MAH-PUN-panshet-dam-burst-compeled-54-years-massive-flooding-in-pune-5051412-PHO.html)

Figure 2.4 Coal Ash earthen dam breach on River Dan, North Carolina, 2014 (http://duluthreader.com/articles/2018/04/26/13157_a_sampling_of_16_earthen_dam_failures)

(a) 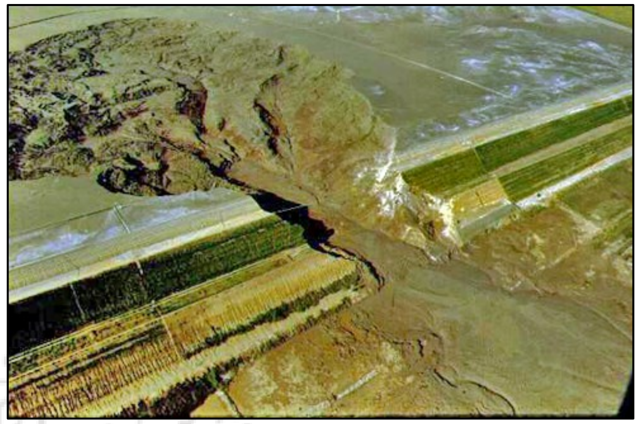(b)

Figure 2.5 (a) Tous dam failure, Valencia, 1982 (Sharma and Kumar, 2013) (b) Merriespruit dam failure, South Africa, 1994 (http://www.tailings.info/casestudies/merriespruit.htm)

Figure 2.6 Brumadinho dam disaster, Brazil, 2019 (https://www.bbc.co.uk/news/resources/idt-sh/brazil_dam_disaster)

The probability of failure of dams, due to any of the several reasons, and the high risk involved during the construction of dams has not suppressed the worldwide construction of dams. To meet the ever-growing global demand of water, the rate of dam construction is immensely high (http://www.icold-cigb.org/GB/Dams/role_of_dams.asp). This increasing demand for water would lead to an eventual steady depletion of the unevenly distributed freshwater resources around the world. During the past three centuries, the freshwater resources have depleted and the amount of water consumption has increased by a factor of 35. With the existing total storage capacity of about 6000 km^3, dam constructions definitely mark a vital contribution to the systematic management of limited and unevenly distributed resources of fresh water that are prone to tremendous seasonal variations. Hence, with over lakhs of dams already in operation around the world and many upcoming ones, proper analysis of complicacies of the dams and their safety is a major concern (http://www.un.org/waterforlifedecade/water_and_sustainable_development). Until date, in India, approximately 4862 numbers of large dams are constructed, while another 812 are under construction (NRLD, 2015). The major share of dam construction rests with the states of Maharashtra, Madhya Pradesh, Gujarat, followed by the other states and union territories that are not lacking behind in dam construction and water management.

With such a huge number of dams located across the nation, all necessary measures to assure its safety become extremely necessary and mandatory. To understand all the influencing issues, an intricate and thorough research on the functionality and failure analysis of dams is the foremost need of the hour. In the recent past, it is seen that an interest in studying the static and dynamic behavior of earthen and rock fill dams were revived. Various new analytical and numerical formulations, as well as laboratory-based procedures, were developed for estimating the behaviour and assessing the safety aspects of such dams against worst scenarios. At the same time, the vast numbers of case histories and outputs from full-scale vibration tests is continually increasing, which would eventually make it feasible to calibrate the developed procedures utilizing real field measurements. Based on such studies, it is observed that the two main causes for the hydraulic failure of earthen dams and embankments are piping and overtopping. Piping phenomenon leading to dam failure is further affected by the clogging of filters and drainage blankets, as well as hydraulic fracturing of the impervious core of an earthen dam. The following sections present a review on these issues.

2.3 PIPING INDUCED FAILURES IN EARTHEN DAMS

2.3.1 Introduction

A critical appraisal of the published literature on seepage failures reveals that since the construction of the earliest dams around 2900 BC, piping failures in dams are noticeable. In the earlier days, the construction methods did not cater the benefit of proper material zonation and filters in earthen dams, thereby leading to noticeable seepage effects. The successful dam designs evolved empirically by the first millennium AD, with the growing experience of successful construction of dams on a variety of foundation materials. A glaring example of a successful dam design is manifested by the 2,000-year service life of the Proserpina Dam constructed by the Romans (Jansen, 1983). Since then, a huge volume of work is accomplished on piping research as an outcome of global and interdisciplinary study. In the literature, there exists numerous definitions of piping, and it is a usual practice to coalesce various phenomenon and their consequences under the common been term ‘piping’. For clarity, proper understanding of definitions is important before advancing with the review (Richards and Reddy, 2007). Table 2.1 presents the various definitions of piping available and commonly used. Although all the coined terms indicate piping as a final manifestation, however, it is very important to know the intricate governing mechanism that results in piping, as the same would guide for the remedial measures to be adopted in practice.

Table 2.1 Collation of different definitions of piping existing in available literature

Researchers	**Definitions**
Terzaghi (1925, 1943)	The mechanism of ‘‘piping associated with heaving’’ was introduced. It was stated that heave takes place when a pervious zone is overlain by a semipermeable barrier under comparatively high pressure of fluid. In case of heaving, an increase in fluid pressure in the permeable zone (e.g. during flood event) may lead to a situation in which the uplift at the bottom of the semi-permeable barrier surpasses the downward effective stress provided by the overlying barrier. This type of failure takes place at a hydraulic boundary in which the water migration through the barrier is at a lower rate than the pressure-increment rate.
Terzaghi (1939), Lane (1934), Sherard *et al.,* (1963)	Defined piping as a process in which particles are gradually removed from the matrix of the soil by the tractive forces generated by water seeping through the soil. The shear resistance of the grains balances the tractive forces that mobilizes the weight of soil particle and toe filter. The greatest erosive forces are experienced at an exit point where there is concentration of the water flow, and as the removal of soil particles takes place due to erosion, the erosive forces increase due to the increased flow concentration. This type of piping is termed as ‘classic backwards-erosion type of piping’.
Jones (1981), McCook (2004), Richards and Reddy (2007)	Coined the term ‘suffusion’ to define the gentle migration of fine-grained materials through a coarser matrix, resulting into failure. This phenomenon can lead into the formation of a loose cohesionless matrix permitting comparatively high flow of water that result into disintegration of the soil skeleton. Suffusion results into high water transmissivity with the formation of high permeable zones in non-cohesive soils. It also results in increased seepage through possible outbreaks, increase in the erosive forces and probable disintegration of the soil structure skeleton.
Jones (1981)	‘Tunneling’ or ‘jugging’ are commonly seen in dispersive soils, mainly caused by erosion due to rainfall. Tunneling primarily takes place within the vadose zone and it occurs due to the chemical dispersion of clayey soils from rainfall water flowing between the open cracks or natural conduits. The occurrence of tunneling in the phreatic zone is rare, but in adverse situations, tunneling may result in the failure of dams.

Researchers	Definitions
Franco and Bagtzoglou (2002), Louis (1969), Worman and Olafsdottir (1992)	‘Internal erosion’ was defined as the flow of water through the already existing openings, e.g. cracks in cohesive material or voids along a soil-structure interface. The intergranular flow does not have much role to play in internal erosion. The hydraulics of the problem is very different as compared with backwards erosion. Internal erosion is initiated by erosive forces of water flowing through planar openings, instead of being initiated by Darcian flow at an exit point. Thus, it is assumed that internal erosion would start according to the cubic law of flow for planar openings.

2.3.2. Statistics of Piping Failures

The historic record of dam failures due to piping indicates the involvement of many factors resulting in this phenomenon. The progressive backward erosion of concentrated leaks evolves as the most serious problem from piping (Sherard et al., 1963). It has been found that repeated cycles of swelling and shrinkage in soils also results in piping (Kapadia, 2013). Numerous cases of piping are reported to occur due to progressive backward erosion, internal erosion, and incorrect design of the filter or poor maintenance. Table 2.2 shows a list of earthen dams and embankment failures due to piping, which includes examples of different failures since 1950, as obtained from various sources (Terzaghi, 1952; Lane, 1934; Jones, 1981; Foster et al., 2000a,b; Richards and Reddy, 2007; Dam Safety Organization CWC; https://en.wikipedia.org/wiki/List_of_tailings_dam_failures; http://www.wise-uranium.org/mdaf.html; National Performance of Dams Program, http://www.npdp.stanford.edu/index.html). Classical piping is a progressive backward erosion phenomenon, while internal erosion is initiated by erosive forces of water flowing through planar openings. Although internal erosion is not exactly a subset of piping, still it can be considered a causative agent of piping. It is also mentioned in the available literature that ‘internal erosion’ can take several forms, including heave, piping, concentrated leak erosion, contact erosion, and suffusion (International Commission on Large Dams, 2012). As per the assessment of the statistics of dam failures, improper design of conduits (or avoiding them altogether) significantly affects the number of piping failures.

Table 2.2 List of earthen dam and embankment failures due to piping

Sl No.	Name of the dam	Year of Failure	Height (m)	Type	Cause
1950-1960					
1	Stockton Creek dam, California, USA	1950	24.4	Rolled Earth	Abutment piping
2	Masterson dam, Oregon, USA	1951	18.3	Rolled Earth	Piping through dry fill
3	Owl Creek dam, Oklahoma, USA	1957	8.5	Earthen	Conduit piping
4	Penn Forest dam, Pennsylvania, USA	1960	46	Rolled Earth	Piping-sinkhole developed on upstream
1961-1970					
5	Panshet dam, Maharashtra, India	1961	53.8	Earthen	Piping failure
6	Baldwin Hills Reservoir Dam, California, USA	1963	48.8	Rolled Earth	Piping towards foundation resulting from fault movement
7	Jennings Creek dam, Tennessee, USA	1963	61	Earthen	Foundation piping
8	Upper Red Rock Creek dam, Oklahoma, USA	1964	7	Rockfill	Erosion tunnel piping
9	Nanak Sagar dam, Uttarakhand, India	1967	16	Earthen	Breached due to foundation piping
1971-1980					
10	D.T. Anderson dam, Colorado, USA	1974	72	Earthen	Piping through foundation

Sl No.	Name of the dam	Year of Failure	Height (m)	Type	Cause
11	Walter Bouldin dam, Alabama, USA	1975	51.8	Earthen and Rockfill	Piping towards the downstream side next to intake structure
12	Dresser dam, Missouri, USA	1975	32	Earthfill	Piping
13	Teton Dam, Idaho, USA	1976	93	Rolled Earth	Piping through abutment
14	Bad Axe Structure dam, Wisconsin, USA	1978	22.2	Earthen	Piping towards abutment foundation joints
15	Upper Lebanon Reservoir dam, Arizona, USA	1978	13.7	Earthen	Piping into embankment (tree roots)
16	Fertile Mill Dam, Iowa, USA	1979	3.4	Earthen	Piping or seepage initiated failure of slope
17	Morbi dam, Gujarat, India	1979	59.1	Earthen and Masonary	Heavy rainfall resulting in piping and breaching
18	Saint John dam, Idaho, USA	1980	11.9	Rolled Earth	Piping, sinkholes towards upstream side
1981-1990					
19	Johnston City Lake dam, Illinois, USA	1981	4.3	Earthen	Piping in badly conserved embankment
20	Roxboro Municipal Lake Dam, North Carolina, USA	1984	10	Earthen	Piping beneath paved spillway
21	Upper Red Rock Creek dam, Oklahoma, USA	1986	9.4	Earthen	Piping, into embankment
22	Little Washita River dam, Oklahoma, USA	1987	10.7	Earthen	Piping into soils, failed after 10 years of construction
23	Quail Creek dam, Utah, USA	1988	63.7	Earthen dike	Piping into foundation
1991-2000					

Sl No.	Name of the dam	Year of Failure	Height (m)	Type	Cause
24	Boyd Reservoir dam, Nevada, USA	1995	9.8	Earthen	Piping into embankment after rainfall and snowfall
25	Eureka Holding dam, Montana, USA	1995	12.2	Earthen	Piping into dike after heavy downpour
26	Bergeron Dam, New Hampshire, USA	1996	11	Earthen	Piping under spillway slab
27	Holland Dam, Texas, USA	1997	4	Earthen	Piping failure
28	Hematite dam, Kentucky, USA	1998	4	Earthen	Piping between embankment and concrete sluice contact
29	Vertrees dam, Colorado, USA	1998	8.2	Earthen and Rockfill	Piping, outlet damaged
30	Pittsfield Dredge Disposal Pond Dam, Illinois, USA	1999	10.7	Earthen	Piping after, 2 h of observed seepage
2001-2010					
31	Lake Flamingo Dam, New Jersey, USA	2001	8.2	Earthen	Piping through conduit
32	Bridgefield Lake Dam, Mississippi, USA	2001	7.6	Earthen	Piping initiated failure of slope
33	Sauk River Melrose dam, Minnesota, USA	2001	8.2	Earthen	Piping, failure of slope at the time of high water
34	Jamunia Dam, Madhya Pradesh, India	2001	15.4	Earthen	Piping failure
35	Swift dam, Washington, USA	2002	25.3	Earthen	Piping through rock foundation
36	Beech Lake Dam, North Carolina, USA	2002	6.7	Earthen	Piping, rupture of conduit under high pressure

Sl No.	Name of the dam	Year of Failure	Height (m)	Type	Cause
37	Big Bay Lake dam, Mississippi, USA	2004	17.4	Earthen	Piping into French drains
38	Jaswant Sagar dam, Rajasthan, India	2007	43.38	Earthen	Piping leading to breaching
39	Sardar Sarovar dam, Gujarat, India	2008	7.6	Earthen canal	Piping leading to breaching
40	Gararda dam, Rajasthan, India	2010	31.7	Earthen	Piping leading to breaching
2011-2019					
41	Bloom Lake mine, Fermont, Québec, Canada	2011	--	Tailing Dam	Breach in the tailing pond resulted in a release of 20,000 $m^3$of harmful materials
42	Campos dos Goytacazes dam, Brazil	2012	14	Earthen	Piping initiated due to excessive rainfall causing flooding and leaving 4000 people homeless
43	Zangezur Copper Molybdenum Combine, Kajaran, Syunik province, Armenia	2013	60	Tailing Dam	Piping initiated after the damage of the tailing pipeline
44	Dan River Steam Station, Eden, North Carolina, USA	2014	18	Tailing Dam	Drainage pipe collapsed resulting in dam breach and releasing toxic coal ash
45	Mariana dam disaster, Mariana, Minas Gerais, Brazil	2015	90	Earthen	The damage of the dam resulting in piping followed by a breach resulted in the destruction of one entire village evacuating 600 people
46	New Wales plant, Mulberry, Polk County, Florida, USA	2016	18	Tailing Dam	Internal erosion resulting in a 14 m wide sinkhole finally opening pathway for contaminated liquids

Sl No.	Name of the dam	Year of Failure	Height (m)	Type	Cause
47	Maple Lake, Paw, Michigan	2017	5	Earthen	The dam crumbled because of the heavy weight of the pond above it and resulted in its failure
48	Panjshir Valley dam, Afghanistan	2018	104	Earthen and rockfill type	Piping resulted in crumbling of the dam which further detoriated during heavy summer rains leaving 300 homeless and 13 people missing
49	Brumadinho dam disaster, Brazil	2019	87	Tailing Dam	Suffered a catastrophic failure releasing 12 million cubic meters of tailings slurry. 87 people missing

2.3.3. Early Researches on Piping Phenomenon through Earthen Dams

The process of piping was first referred in the context of landforms in loess by von Richthofen in 1886 (Jones, 1981). Bligh (1910) described piping in the purview of the dismissal of soil along the foundation of masonry dams. Such form of piping was studied, as early as in 1895, in Indian laboratories through mechanical models and laboratory prototypes (Clibborn and Bresford, 1902; Bligh, 1910). In 1898, the demolition of the Narora Dam on the Ganges River, India, was the maiden incident where piping became a concern to the engineers (Jones, 1981). Following the incident, Bligh (1910; 1911a, 1911b; 1913) proposed 'line of creep' theory to calculate the piping potential along the soil-structure interface, thereby correlating the flow path of seeping water and its length to the tractive forces responsible for the soil particle movement. The proposed theory was based on the consideration that the flow along the most likely path is not Darcian, and the flow path is defined as the summation of the vertical and horizontal distances estimated along the soil-structure interface.

Based on the same context of piping as described by Bligh (1910), with the aid of extensive case histories, Lane (1934) elucidated a clear distinction between the flow along structural interfaces and the diffused flow through granular media. The anisotropic conditions that govern fluid flow through stratified materials was taken into account by making suitable adjustments to the existing 'line of creep' theory, and accordingly the 'weighted creep method' was proposed by Griffith (1913). The foremost application of the modified-creep method was made to investigate the failure of the Prairie du Sac Dam in Wisconsin, USA (Lane, 1934). The 'weighted-creep-method' considers a modified length of flow path, which was arbitrarily chosen to be 1/3rd the length of flow path used by Bligh (1910).

Terzaghi (1929, 1939) described piping as the progressive backward erosion of particles from the exit point of the soil-structure interface. Terzaghi (1943) presented the estimation of piping potential for the case of boils and heaving in a cofferdam cell due to the vertical upward flow of groundwater into the excavated and dewatered floor of a cofferdam. Based on laboratory model tests, it was deciphered that as the critical value of hydraulic head is exceeded at the exit point, the rate of discharge increases, thereby manifesting a rise in the average permeability of the sand. A safety factor against such piping is defined by the ratio of the effective weight of a soil prism (in the expected area of heave) to the excessive upward hydrostatic pressure (Terzaghi, 1943). A critical safety factor was determined by 'trial and error method' conducted over numerous depths. According to Terzaghi et al. (1996), almost all piping failures result in a gradual reduction of the safety factor until attaining the failure point. The prevailing misperception about the non-occurrence of piping in homogeneous cohesionless was pointed out. It was highlighted that in embankments comprising homogeneous cohesionless material, development of sinkholes is commonly witnessed due to piping phenomenon through the body of the embankment or through the heterogeneous foundation. It was recommended that potentiality of piping in cohesionless embankments should never be completely neglected and should be checked with other possible failure modes.

Aitchison (1960) and Aitchison et al. (1963) stated that piping processes involved dispersion through clayey soils. Since then, a number of tests have been developed to determine the dispersivity of soil. Dispersion Index method, developed by Ritchie (1963), aids in the indication of probable tunneling failure of earth dams that comprises 33% of the soil lesser than 0.004 mm that disperses after 10 min of shaking in water. The pinhole test was found to be the most suitable method for the classification of dispersive soils (Forsythe, 1977). On the other hand, Decker and Dunnigan (1977) concluded that the dispersivity of soils, maintained in their natural moisture content, could be better predicted by the 'soil conservation services (SCS)' dispersion test. The review of literature indicates that there is obvious that no single diagnostic test for the assessment of the quality of dispersive soils. It is a proposed practice to carry out numerous tests and utilize reasonable engineering judgment when dealing with dispersive soils (Marshall and Workman, 1977).

2.3.4. Recent Developments on Piping Phenomenon in Earthen Dams

Recently, researchers have stressed on Lane's (1934) differentiation between piping and internal erosion to distinguish between the processes of seepage through coarser medium compared to the seepage through openings like cracks (McCook, 2004; Richards and Reddy, 2007). Recent works related to piping have emphasized on the formulation of mathematical models that can predict particle transport and clogging of filter (Bonala and Reddi, 1998; Reddi et al., 2000; Locke et al., 2001; Kakuturu, 2003; Kakuturu and Reddi, 2006a, 2006b). The studies on unstable dispersive soils, and their effect on natural soils, also forms a prime crux of the continuing research. Data collection to create an inventory of earlier incidents and statistically characterizing them against the various piping failure modes of earthen dams has been another attractive domain of research, thereby investigating the reasons, mechanisms and generic characteristics of piping (Foster et al., 2000a, 2000b; McCook, 2004). Researches related to the prediction of the development time of piping are attempted by few researchers (Fell et al., 2003; Annandale et al., 2004). With the advent of superior computational and constitutive modeling, the developments in numerical and laboratory studies are being widely attempted (Richards and Reddy, 2007).

Development of different physical models have gained popularity, which aids in evaluating the important parameters responsible for breaching of earthen dams due to overtopping. However, these models do not give considerable importance to dam failures due to piping (Chang and Zhang 2010). A new mathematical model was introduced to give a detailed and proper insight about the evolution process of piping mechanism in earthen dams (Xu and Zhang, 2013). In the model, two vital mechanisms were highlighted to have a better understanding of the piping process. The two mechanisms, namely the surface erosion on the wall of the pipe and global collapse of the soil mass above the pipe, were included in the model. The study presented the principles of the mathematical model along with the simulation of the historic Teton dam failure with the help of the proposed model. The well-known Teton dam failure in 1976 is shown in Figure 2.7 (https://history.info/on-this-day/1976-collapse-of-the-teton-dam-in-idaho/). Both pipe flow and weir flow equations were used to describe the flow of the fluid in the model. The results from the simulations showed that the height and width of the pipe gradually increased and the process of evolution of the pipe geometry was different for different materials having varying erodibility characteristics. Eventually, the process of piping was converted into overtopping after the soil mass above the pipe collapsed.

Figure 2.7 Historic Teton dam failure in 1976, Idaho, USA (https://history.info/on-this-day/1976-collapse-of-the-teton-dam-in-idaho/)

A number of attempts were made by different researchers to predict the time for piping failure. Different numerical approaches were attempted in this regard (Alamdari et al., 2012). Bonelli and Benahmed (2010) attempted to predict the erosion rate form Hole Erosion Test (HET). It was attempted to quantify the time required for piping in the embankments, by correlating the critical stress and coefficient of erosion to the common geotechnical soil properties. However, no prediction expression was provided for estimating the time of piping failure. Chang and Zhang (2012) described that mechanical behaviour of the soil gets affected by the internal erosion of the soil. Backward erosion (a form of internal erosion in which the soil particles are removed gradually by the action of water) results in the formation of shallow pipes in a direction opposite to the flow the water. This kind of failure occurs mostly in dams and dikes where sandy layers are covered by a cohesive layer. An indication of backward erosion is given by the occurrence of sand boils at the ground surface downstream of the structure. Such typical sand boils are often observed along the Mississippi and Waal rivers, as shown in Figure 2.8 (Van Beek, 2015). In this regard, validation of Sellmeijer model (Sellmeijer, 2006) was carried out by conducting small (1-g and n-g), medium and large-scale experiments (van Beek, 2015). The model was later readjusted such that it can take into account the effect of pipe forming erosion processes in uniform sands.

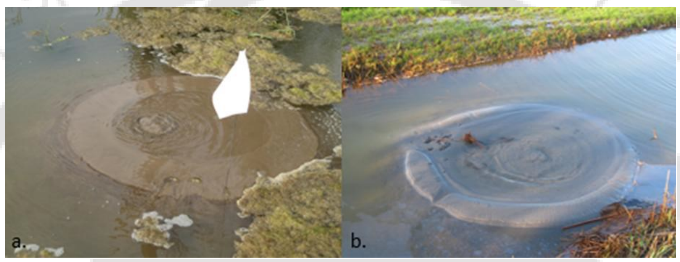

Figure 2.8: Typical sand boils observed along (a) the Mississippi River in the United States, and (b) the Waal River in the Netherlands (van Beek, 2015)

Sellmeijer model is used to predict the critical hydraulic head fall across a dike underlain by a sandy layer. This head fall is a function of geometrical parameters such as the length of the seepage path, thickness of the sand layer and several characteristics of the sand layer, like grain size, permeability and some morphological properties (van Beek et al., 2010). The basic development of the model and the original work of Sellmeijer can be obtained from Sellmeijer and Koenders (1991) and Sellmeijer (1998), respectively.

2.3.5. Modelling of Piping through Earthen Dams

The available literature provides a number of mathematical, physical and numerical models in the context of piping phenomenon and associated mechanisms in the purview of failure of earthen dams and embankments. The number of fatalities arising from a dam failure event is largely dependent on the early-warning based evacuation time obtained to shift the population at risk on the downstream part of the dam. The Unites States Bureau of Reclamation (USBR, 1987) proposes that an early warning of failure time of as little as 60 min can sufficiently reduce the number of fatalities. Thus, attempts have been made to define a reasonable prediction time, which is related to the development of breach in the dam owing to the progression of the pipe through the dam and its foundation (Fell et al., 2003). In this regard, the process of internal erosion and piping is divided into four phases: (a) the initiation stage, (b) the continuation stage leading to erosion, (c) formation of a pipe with due course of time, and (d) the development of a breach. The initiation of piping may be generated by different processes like backward erosion, suffusion or concentrated leaks. The process of continuation may be controlled by filters and transition zones. The background causes leading to the formation of piping in an embankment, or its foundation, include the capability of the soil to prevent the collapse of the roof of the pipe, and the increment and rate of increment of the pipe diameter. Furthermore, the influence of migration of filter particle from the upstream in limiting the flow through the channels through a process called ‘crack filling’ is also found to be influencing the piping mechanism. Considering all the above conditions, a generalized method has been proposed by Fell et al. (2003) to assess the likely time for the development of internal erosion and piping. For successful implementation of the proposed method, proper characterization should be made for the embankment material, its degree of saturation, the hydraulic gradient across the core, soil type, clay fraction, dry density, and the factors likely to limit the seepage flow from the upstream, to decipher their influence on the formation and progression of piping.

Erosion through concentrated leaks has resulted in a number of piping failures of dam. As the cracking of core cannot be totally avoided, the geotechnical engineers aim to construct earthen dams with such characteristics so that the closure of these core cracks takes places at the earliest, resulting in the blockage of concentrated leakage and soil erosion. The favorable condition of blockage of concentrated leakage and soil erosion is widely known as self-healing. Kakuturu and Reddi (2006a, 2006b) conducted laboratory experimental investigations to have a mechanistic understanding of the progressive erosion of core cracks in earth dams and their self-healing characteristics. It was understood that the phenomenon of self-healing is affected by the characteristics of base soils and filters, and the prevailing hydraulic, geometric, and physio-chemical conditions. The influence of partially cracked core (resulting in lesser leakage) and fully cracked core (resulting in substantial leakage) was investigated. A consistent hydraulic head was used to generate the horizontal flow through this crack. During the test, continuous monitoring of the effluent was carried out to figure out the characteristics of the progressive erosion and subsequent self-healing. Based on the experimental outcomes from various flow rates and effluent concentration with respect to time, the influence of critical seepage velocity through the filter, the surface erodibility characteristics of the base soil and the plug characteristics on self-healing were elucidated. Based on the experimental outcomes, a mechanistic 1-D continuum model for predicting self-healing characteristics was developed (Kakuturu and Reddi, 2006a, 2006b). The numerical model represented the actual core cracks as irregular cross sections in a cylinder that represented the idealized domain. 1-D flow through the domain under constant head condition was considered. At the exit point, the quantity of flow $Q(t)$ and the effluent concentration $C_e(t)$ were monitored that act as indicators of self-healing or progressive erosion. Reduction in magnitude of the two indicators represents self-healing, while an increase in any one of the indicator illustrates progressive erosion. Based on the monitored results, the temporal variation of the two indicators were estimated.

Cividini and Gioda (2004) presented a numerical model in which finite-element (FE) approach was used for the analysis of the erosion and transport of fine particles within a granular soil subjected to a seepage flow. The continuity equation for the mass of transported particles was derived considering a scheme that was conceptually similar to that applicable to the analysis of advective flow problems, followed by a finite-element formulation derived through a 'two-step' time integration procedure. A mathematical model to describe the phenomenon of piping under a dam was presented by Sellmeijer and Koenders (1991). The model analyzed the groundwater flow problem with the presence of a narrow channel under the dam. The objective was to identify any possibility of attaining equilibrium to inhibit further washing away of foundation material through the piping channel. A boundary value problem for the seepage flow, following Darcy's law, was formulated to evaluate the particle forces on the lower periphery of the piping channel. The complexity of the solution was influenced by the sudden geometrical deviations at the ends of the piping channel. A 'design rule' was formulated for the engineers to tackle all the possible realistic variations of the governing parameters.

A numerical modelling to investigate the process of erosion due to piping was developed by Alamdari et al. (2012). The piping was considered to originate from the upstream and progressively travel towards the downstream through the body of the dam, which was attributed to the enlargement of the pipe due to the axial flow of water. The numerical procedure was described by a two-phase 1-D model, wherein the soil was considered homogeneous and water-saturated. The mass and momentum conservation equations were used for the mixture of water/particle and the eroded particle phase in an Eulerian framework. In the framework of continuum mixture theory, based on solute transport, a new continuum fluid-particle coupled piping model was proposed by Luo (2012). It was assumed that the porous media comprises three phases namely the solid skeleton phase, the fluid phase and the fluidized fine particles phase, wherein the last phase is considered as a special solute migrating within the fluid matrix. The three phases interact while maintaining the mass conservation. Accordingly, a new continuum fluid-particle coupled piping model was established by introducing a 'sink term' into the mass conservation equation, which is used to elucidate the erosion of fluidized fine particles. The proposed model considered the fluid particle interaction in the evolution of piping. The model is capable of predicting the piping development of complicated structures subjected to complex boundary and flow conditions. It can also highlight the temporal changes of porosity, permeability and pore pressure induced by eroded fine particles, and can depict the unsteady, progressive failure characteristics of piping.

The issues of piping phenomenon through experimental investigations are also available in the literature. Laboratory experimental tests were carried out in the Hydraulic Laboratory, University of South Carolina on piping erosion process in earthen embankment (Sharif *et al.* 2015). The embankment comprised a mixture of sand, silt and clay, and was constructed using different construction rates. A continuous flow to the flume was supplied with the help of a pump and a control valve that was used to regulate the flow of water. It was observed that increasing the compaction of the construction layers highly increased the erosion time. However, the final average depth of erosion remained the same in all the cases. The experimental results were used to produce exponential equations to calculate the erosion depth, side area of the piping zone, and volume of eroded material. The effect of cement-bentonite treatments on erosion characteristics was studied by Wang et al. (2017) with an aim to estimate the percentage of erosion. This was further used to develop mathematical relationships between the percentage of erosion and different regimes (like curing period, erosion time, different cementitious replacement and sizes of initial holes). The developed relationships can be used in calculating the propagation of internal erosion originating from cracks in cement-bentonite seepage barriers.

Hoffmans and van Rijn (2018) developed a piping model based on Darcy's Law and incorporating Hagen–Poiseuille equation, Darcy–Weisbach equations and Shields' equations, which can be used to describe the laminar pipe flow and incipient motion of the particles. The non-uniformity of the sand mixture on pipe erosion was included in the model using the shear-stress concept developed by Grass (1970). A comparison of the developed model was made with the Sellmeijer's piping equations (Sellmeijer, 2006) by using nearly 100 laboratory experiments along with some field observations. The basic difference between the results obtained the two models was attributed to the formula used in the calculation of critical hydraulic gradient, at which backward erosion resulted in dam failures.

2.4 CLOGGING OF DRAINAGE BLANKETS IN EARTHEN DAMS

Clogging is defined as the physical buildup of material in the collection pipe, the drainage blanket, or the filter layer, to the extent that flow is significantly restricted. Clogging may be caused by the buildup of deposited soil particles, biological organisms, chemical and biochemical precipitates or the combination of all three (Bass, 1984). Literatures are available highlighting the most common forms of drain clogging and its influence on seepage under concrete dams built on permeable rock foundations (Silva, 2015). The major types of clogging mechanisms are physical, chemical, biochemical and biological mechanisms.

Physical Clogging: The simplest possible schematic picture of clogging is one where the blockage occur when particles enter a pore that is smaller than its own diameter. In general, physical mechanisms are the predominant causes of failure in drainage systems. The cause of physical clogging is mainly attributed to inhomogeneity of the particle sizes in the constituent material of the dam. Small particles move inside and block the pore hindering the seepage action, which lead to the decrease in the permeability coefficient. Clogging of drainage systems by soil sediment deposits is a common problem in agricultural drainage systems and leachate collection systems (Young et al., 1982). In this type of clogging, a significant amount of very fine particulates is removed from the adjacent soils that eventually settles in the drainage layer.

Chemical Clogging: Chemical mechanisms of clogging involve the formation of insoluble precipitates that deposits on the surface inside the drainage blankets and filters. The most common form of chemical build up is calcium carbonate. This is mostly featured when the constituent material of the earthen dam comprise soils from a borrow pit containing gypsum and calcite. However, such clogging scenarios can be controlled if proper quality and composition control is enforced for the materials chosen for the earthen dam. This form of clogging can be experienced in mine tailing dams.

Biochemical Clogging: Inorganic precipitates can also be formed in conjunction with biological systems, resulting in biochemical clogging. The principal products resulting such clogging are iron compounds, like $Fe(OH)_3$ or FeS, and manganese compounds which deposits and builds up on the drainage blankets. Reduced soluble forms of iron and manganese are metabolized by aerobic iron bacteria as an energy source producing large quantities of ferric and manganese hydroxides which biologically precipitate within and at the water entry openings of drainage blankets. Firstly, this type of clogging is not common unless the dame material should be made of borrow pit soils having iron or manganese content along with the presence of organic materials. However, such soils are generally not permitted for earthen dam construction.

Biological Clogging: Biological clogging is operative for porous media with regard to wastewater treatment, agricultural drainage and irrigation systems. Such form of clogging mostly do not affect the drainage blankets in earthen dams.

Piping can be controlled by the use of correctly designed granular filters that will retain any eroded soil particles while allowing the seepage water to flow. Empirical methods for filter design are formulated by rigorously testing different combinations of base-soil-filter under various hydraulic gradients for its stability (Sherard et al., 1984). However, while these soil filters and drainage layers are expected to serve the purpose of protecting the earthen dams, the changes in the permeability of the material over the time becomes a critical issue. There are several literature available with respect to filters, drainage blankets, and their clogging issues, when they are used in earthen dams and embankments (Peck, 1990; Vick, 1996). Studies have shown that poor drainage caused by particulate clogging can result in drastic variation of the pore water pressures within the embankment, and can lead to substantial changes in the phreatic level with time, even reaching the higher limits of the downstream face. Clogging is a ubiquitous phenomenon in nature, resulting in the reduction of porosity and permeability of the drainage layers and hampering its beneficial purpose. This scenario seriously influences the safety of the dams. Owing to the soil inhomogeneity and existence of different ions, clogging frequently occurs in tailings dams resulting in its failure. One such example is the Fonte Santa mine tailings dam in Northeast Portugal that failed on November 27 2006, because of extraordinary rainfall and eventual clogging of the spillway (Franca et al., 2008). Thus, clogging is a major public concern limiting the lifetime of the structures. Thus, it becomes essential to understand the various mechanisms of clogging. Table 2.3 collates a bunch of these available literatures related to design and clogging of filters and drainage blankets in earthen dam, and some of their important findings.

Table 2.3 Literature associated with the usage of filters and drainage blankets and the implication of their clogging on earthen dams and embankments

Researchers	**Significant interpretations and findings**
Bertram (1940)	An experimental investigation for the design of protective filters was carried out. It was found that for stability D_{15F} / D_{85B} should be equal to 6, and this ratio is independent of the shape of the soil particles. D_{15F} is that grain size diameter where 15 % by weight of the soil particles of the filter material are smaller in diameter. D_{85B} is that grain size diameter where 85 % of the base or filter soil are smaller in diameter
Arulanandan et al. (1975)	Studied the influence of eroding fluid on the surface erosion of soil. It was observed that at higher sodium concentrations, clay minerals are strongly bonded, and thus a higher critical shear stress is required to induce erosion at higher sodium contents.
Vaughan (1978)	Filter design was proposed for the protecting the dam cores subjected to cracking. It was found that permeability could be considered as a key parameter for the design of filters. The average permeability for effective filter characteristics was suggested to be 7×10^{-5} cm/sec and 2×10^{-5} cm/sec for uniform filters and graded filters, respectively.
Sherard (1979)	Suggested that cores having coarse soils are subjected to sinkholes. In this regard, it was observed that filters constructed with fine to medium-fine sands were useful preventing erosion.

Researchers	Significant interpretations and findings
Vaughan and Soares (1982)	Studied the design of filters for earthen dams comprising a clay core. It was suggested that permeability should be considered as a key parameter for measuring the performance of the filters.
Arulanandau and Perry (1983)	It was observed that the presence of some percentage fines in the filter material was necessary, as it could be useful in sustaining a crack. However, the difficulty encountered in this case was that existence of fines might make the filter act like a cohesive material.
Sherard et al. (1984)	It was found out that although D_{15F} / D_{85B} <5 was found conservative for most of the uniform filters. However, it could still be used as one of the main criteria for examining the performance of the filter.
Kenney et. al. (1985)	The performance of a filter can be judged by minimum constriction sizes along the flow path. Constriction size (D_C^*) can be defined as the maximum particle size that can pass through the filter of a particular given thickness.
das Neves (1989)	The transportation of the base material to the front of the filter is dependent on the flow velocities. Even low flow velocities (approximately 2 cm/sec) have the ability to transport the base material. However, the capability of the base material to seal itself also depends upon the cohesion of the material.
Leonards et al. (1991)	It was found through laboratory tests that in case of base materials, plasticity had no influence on the resistance to internal erosion.
Talbot and Deal (1993)	Highlighted the importance of filters and transition zones for preventing dam failures through cracking and internal erosion. It was suggested that properly designed filters could be effective in preventing concentrated leaks that can stop the dam failures.
Indraratna et al. (1996)	It was observed that uniform sand filters, of fine to medium grain size, are effective in producing a self-filtering interface; whereas, uniform coarse sand filters are ineffective in producing the same due to their porosity and permeability.
Fenton and Griffiths (1997)	The influence of spatial variability of the permeability of the dam on the development of internal hydraulic gradients was attempted. It was found that the spatial variability of the permeability does lead to a probability of higher internal gradients.

Researchers	Significant interpretations and findings
Reddi et al. (2000)	Studied the reduction of permeability of the filters due to clogging. It was observed that an increase in influent particle concentration results in faster reduction of the filter permeability. However, the filter performance was not affected by the flow rate.
Foster and Fell (2001)	Assessment of dam filters that do not satisfy filter criteria was studied. It was found that dams do not show a stable long-term performance whose filters are either too coarse (by modern standards) or which becomes segregated o the time of its construction.
Indraratna and Radampola (2002)	Analysis was carried out to find out the critical hydraulic gradient for the movement of the base particle through the filter. It was found that this gradient is a function of the minimum pore diameter, length of the pore channel, density, friction angle, orientation of the flow.
Lone et al. (2005)	An attempt was made to explain the physical behavior of porous media of different packing patterns leading to non-uniform particles size. It was observed that size D_{15} of the constituent material of the filter alone was not sufficient to ensure good filter performance, since the overall gradation of the filter was ignored.
Indraratna and Raut (2006)	Suggested that it is difficult to distinguish between uniform and well-graded filter if they have same the D_{15} size.
Indraratna et al. (2007)	Numerical models were used to demonstrate that filter selection should not be based on particle size of filter-base material. Rather it should be based on the constriction size of the voids created from self-filtration.
Reboul et. al. (2010)	A method was proposed to compute the constriction size distribution of model granular filters taking into account the relative density of the material.
Sjah and Vincens (2013)	Attempt was made to determine the cumulative constriction size distribution of granular materials by calibration of an experiment based on filtration tests.
Taylor et. al. (2015)	A new method to identify and visualize void constrictions in sands using micro-CT data was developed, with a view to assessing performance of granular filters.

Researchers	Significant interpretations and findings
Shire and o'Sullivan (2017)	The filter-base compatibility cannot be directly assessed by comparing the particle size distribution (PSD) and the constriction size distribution (CSD) of the filter base material. A conceptually simple random-walk network model, using a filter CSD derived from discrete element modelling and base PSD, is used to assess filter-base compatibility.

The migration of particles in porous media is a subject of importance in several disciplines of geotechnical and geo-environmental engineering. With the aid of probabilistic methods, Silveira (1965) examined the particle migration of base-soil into filters, and proposed the concept of pore-constriction, which states that the movement of a particle from one pore to the next is facilitated if the particle size is smaller than the pore-spaces. Based on the probabilistic comparison of the distribution of size of base soil particle and filter constriction size, a prediction model of the infiltration depth into clean filters was developed. Witt (1993) developed a 3-D pore network model comprising spheres (pores) interlinked by pipes (pore constrictions), which considers that the pore constrictions provide sufficient exits for each pore, and the movement from any pore is controlled by the largest size of adjacent pore constriction. Schuler (1996) had chosen an identical 3D void network model wherein Monte-Carlo simulations were used to assess the extent of infiltration of the base-soil particles into the filter. Indraratna and Vafai (1997) suggested a finite-difference (FD) based particle transport model, governed by mass and momentum conservation. The analysis aided in the assessing the temporal change in the distribution of particle-size, permeability and porosity of the materials at the interface of base-filter. Locke et al. (2001) developed a revised analytical model capable of capturing the movement and temporal transport of non-cohesive base-soil particles into granular filters, which can be suitably used in the design of non-cohesive, uniform, and well-graded base and filter materials. The proposed model can capture the changes in rate of flow, porosity and permeability of non-cohesive, uniform, and well-graded base and filter materials. Additionally, based on washout of fine filter particle, the revised model can further estimate internal stability, to a limited extent.

Laboratory experiments to model pipe flow and associated particle migration was conducted to understand the clogging process (Wilson et al., 2013). The corresponding numerical model was developed using Richards' equation (1931) to model the pipe flow. The modeling used two contrasting boundary conditions, constant flux (CF) and constant head (CH), to quantify pressure buildups due to pipe clogging. Wersocki (2014) reported the clogging around the drainage system of the Podgaje hydropower plant, located in the northern part of the Wielkopolska, Poland, due to the precipitation of oxidized iron that subsequently reduced the soil porosity and hydraulic conductivity.

2.5 HYDRAULIC FRACTURING / CRACKS IN EARTHEN DAMS

Cracking phenomenon is common in most geotechnical structures and there has been a renewed interest regarding this among the civil and mining engineers. These cracks constitute a threat to the overall integrity of geotechnical structures such as dams, embankments, slopes, pavements, tunnels, and foundations. Different other allied branches, for example petroleum, geo-environment mechanical, chemical and agricultural engineering, have also shown keen interest on the effect of cracks on affluent discharge from a waste deposit, hydraulic fracturing due to high fluid pressure, cracks leading to erosion of earthen dams resulting in breaching, and flow of nutrient through root zones etc.

Instability of slopes and dams, due to occurrence of cracks, is a challenging subject of research addressed by a number of researchers over decades (Nawari et al., 1997; Cho and lee, 2001; Aubeny and Lytton, 2004; Yang et al., 2004; Jimenez Rodríguez et al., 2006; Yang and Zou, 2006; Low, 2007; Li et al., 2008, Shukla et al., 2009; Cooling and Marsland, 2011). The United States of America experience slope failures every year that cause huge economic damages worth $2 billion approximately. The adverse influence of cracks on the stability of slopes is pronounced by allowing the water to flow through a preferential path, thereby increasing pore-water pressures and resulting in reduction in the strength, thereby leading to failure of the slopes. Figure 2.13 shows a deplorable condition of an embankment with cracks, which, if not protected on time, would lead to the failure of the embankment. Therefore, a clear understanding of the effect of cracks, and their propagation through the body of the embankment, is vital for safe and economical designs of earthen dams, levees and embankments.

Figure 2.13 An earthen embankment with a large crack, Morigaon, Assam, India

Researchers have grouped the occurrence of cracking occurring in an earthen embankment dam into three major categories

- ***Transverse Cracking***: These type of cracks are generally seen in the crest of the earthen dam and they appear in a direction perpendicular to the axis of the dam. These cracks usually pose a threat to the safety of the dam if they penetrate deep into the core below the reservoir level. Such deep penetration could provide the path for concentrated seepage through the core, resulting in excessive erosion and finally leading to the breaching of the embankment. Presence of these cracks indicate differential settlement within the embankment or in the underlying foundation zones.

- ***Longitudinal Cracking***: These type of cracks appear parallel to the axis of the dam. Appearance of these cracks indicate uneven settlement within the different layers of the embankment. These cracks allow the water to penetrate through it, thereby reducing the strength of the area near the crack zone, and finally resulting in slope stability failure of the dam.
- ***Desiccation Cracking***: These type of cracks occurs due to drying out and shrinkage of surficial cover materials in the earthen embankment. They usually occur in random honeycomb structure along the crest and downstream slope of the dam, as the upstream slope remains mostly protected by the reservoir water. These type of cracks are not harmful unless they are very severe. These type of cracks can pose a major threat as it results in the formation of gullies when surface runoff erosion tends to increase excessively, thereby inflicting major damage to the slopes of the earthen dam. Especially during the monsoons, heavy rain can fill these cracks, resulting in strength reduction in the cracked portion of the embankment that can cause erosion, and subsequently leading to a dam breach.

Therefore, it becomes important to understand the mechanism of cracking leading to dam failures. Although attempt has been made by the researchers to comprehend the flow of water through cracks in the soil slopes (Lytton et al., 1987; Kuhn and Zornberg, 2006), however, in actual practice, the influence of cracks in dams is not considered while designing the embankments. There are many examples that clearly indicates the requirements of millions of dollars for the repair and maintenance of the dams developing cracks during their service life. The maintenance of shallow slides in India cost approximately $960,000 as estimated by the geotechnical engineers (Hopkins et al., 1988).

The zoned earthen dams comprise a central impervious core flanked by relatively pervious shells that provide enclosure, support, and protection to the former. The upstream pervious zone affords stability against rapid drawdown, while the downstream pervious zone acts as a measure to control seepage, lower the phreatic surface, and guide the same towards the downstream exit drainages. In many cases, a filter or drainage blanket is applied between the impervious central core and the downstream shell. A drainage layer is also provided beneath the downstream shell near the toe of the earthen dam. The presence of different compartments in a zoned earthen dam, with different stiffness, accompanied by differential settlements and ingress of pore-water, can lead to hydraulic fracturing and internal failure of the earthen dams. Hydraulic fractures may develop during the first impounding causing internal erosion on the dam core. Further, successive internal erosion takes place after the occurrence of hydraulic fracture due to the migration of saturation front generating higher pore-water pressure in the already fractured region, and finally leads to the failure of the dam. Hence, in cases of dam failure and breaching originating from hydraulic fracturing, hardly any evidence remain existent for the engineers to investigate the actual cause and the pattern of the cracking leading to the failure. This issue makes the problem even more challenging and difficult to diagnose the forensic cause of hydraulic fracturing and the propagation of the crack through the body of the earthen dam. Different mechanism and theories have been postulated regarding the hydraulic fracturing phenomenon, some of which are listed in Table 2.4.

Table 2.4: Mechanism and theories associated with hydraulic fracturing in earthen dams

Researcher	Mechanisms of hydraulic fracturing
Lofquist (1957)	Probably the first researcher who indicated the phenomenon of arching in embankment dams. It was observed that arching in dam core makes it easier for the occurrence of horizontal cracks.
Morgenstern and Vaughan (1963)	It was proposed that with the increment of pore-water pressure in the potential fracturing zone, the Mohr's effective stress circle shifts to the left resulting in the occurrence of the fracture as the effective stress Mohr-Coulomb failure envelope becomes tangent to the circle.
Haimson (1968)	Studied the hydraulic fracturing phenomenon around a borehole in rock. Tests were carried out in both cylindrical and cubical specimens of porous and nonporous rock. Tests were conducted by allowing the fluid pressure increment in the borehole until fractures were initiated, determination of which was done by an abrupt drop in the internal pressure.
Kjaernsli and Torblaa (1968)	It was suggested that when the reservoir just starts to fill, there might not be any open cracks due to the distribution of compressive stresses throughout the core region. However, as the process of filling proceeds, horizontal cracks may open up since the total vertical stress in the core is much lower than the overburden pressure, owing to arching between the core and the adjacent compressible shell, thereby resulting in hydraulic fracturing
Kennard (1970)	Conducted laboratory tests for determining the safe pressures for carrying out constant head permeability tests. The tests were carried out in a specially constructed tank that could apply uniaxial or triaxial loading on the prepared specimens and was able to measure the effective stresses generated during the test. In short, the tests were carried out by applying incremental excess head, above a critical pressure, until a distinct fundamental change was observed in the flow rate i.e., when the sample experienced hydraulic fracturing.

Researcher	Mechanisms of hydraulic fracturing
Bjerrum et al., (1972)	Presented a theory for predicting the excess pressure at which hydraulic fracturing will occur in field permeability tests. From the field permeability tests, it was concluded that hydraulic fracturing could take place at excess water pressures that may be smaller than the effective overburden pressure at the point of measurement.
Sherard (1973)	Suggested that the existing closed cracks can jack open under certain conditions of reservoir pressure acting on the upstream face of the core in a zoned earthen dam. It was observed that hydraulic fracturing at certain location of the dam could occur when the total minor principal stress is less than the reservoir water pressure existing at the same location.
Nobari et al. (1973)	The mechanism of hydraulic fracture was explained as a tension failure where the fracture was formed on the plane of maximum tensile stress without any occurrence of shear failure. When the stress is non-uniform, hydraulic fracturing would generally initiate at a point of low effective stress and then would gradually propagate through the core of zoned earthen dam core, rather than forming suddenly within the core.
Vaughan (1976)	Introduced the term “wet cracks” for the cracks formed during or after the process reservoir rise-up. The occurrence of tensile failure was observed when the seepage pressure was applied rapidly to an already existing initial crack, or imperfection, leading to the undrained failure of the dam.
Massarsch (1978)	Presented a theoretical approach to the mechanism of hydraulic fracturing in soil using the concept of expanding cylindrical cavities. The approach was initially used for determining fractures in soil due to pile driving into it, which was later extended to hydraulic fracturing under undrained conditions.
Jaworski et al., (1981)	Carried out numerous laboratory tests related to fracturing in boreholes, in order to study the initiation and propagation of fracture under conditions where there could be accurate control over the stresses. The material from the core of Teton dam was used in the study. Based on the tests, it was suggested that occurrence of hydraulic fracturing was feasible only if there was some discontinuity, within which the water pressure can act to develop tension in the soil by wedging action. When the maximum tangential effective stress became tensile (or, negative) by an amount equal to the tensile strength of the soil, then hydraulic fracturing was assumed to occur.

Researcher	Mechanisms of hydraulic fracturing
Savvidou (1981)	Carried out two different types of tests on compacted samples of soil from the core of Teton Dam to study the changes in the permeability of water and air when tensile cracks jack open at low effective stresses.
Leonards and Davidson (1984), Mesri and Ali (1988)	Defined saturation settlement as the cause of core cracking due to hydraulic fracturing. Saturation settlement develops during the filling of a reservoir, when the poorly compacted soil or pervious zones and layers (comprising loose material) becomes saturated and consolidates under their own weight, before the dry or denser soil arches over it and gets the chance to saturate and collapse. A discontinuity or a crack is developed along the position of the phreatic line. Any subsequent increase in water level allows the entry of water into this crack enabling the erosion to occur. Such collapse can be either sudden or gradual.

Hydraulic fracturing is a very challenging issue to address and tackle. Cracks formed due to hydraulic fracturing are very difficult to confirm by visual inspection as it remains inside the dam and hydraulic fracturing is followed by successive erosion events, which destroys any evidence related to this phenomenon. Some of the selected case histories of earthen dams which were suspected to have experienced erosion problems because of hydraulic fracture (Mhach, 1991) are described in Table 2.5.

Table 2.5: Selected case histories of earthen dams that have experienced hydraulic fracture

Sl. No.	Dam	Hydraulic Fracturing
1.	Dale Dyke Dam, England, 1964	The dam was made up of narrow vertical core of puddle clay supported by a fill comprising stony shale that was poorly compacted and was highly permeable. The foundation of the dam was relatively incompressible. As the dam was put to operation with the water level just 0.7 m below the crest of the weir, a horizontal crack was noticed along the downstream slope near the crest. This was the only detectable damage, which was observed just before the collapse of the dam.

Sl. No.	Dam	Hydraulic Fracturing
2.	Wister Dam, Oklahoma, 1949	Heavy rainfall caused rapid rise-up of the reservoir after which eroded material appeared on the downstream slope through seepage. Once the reservoir level had receded to about 4 m, several erosion tunnels were observed intersecting the upstream slope. Hydraulic fracturing led to the formation of a concentrated leak throughout the dam section.
3.	Stockton Creek Dam, California, USA, 1950	Differential settlement led to formation of interfacial cracks. The internal stress transfer caused by differential settlement of the dam was minimal, which led to the opening of the crack by hydraulic fracturing during the reservoir filling operation, thereby causing internal erosion leading to the failure of the dam.
4.	Oklahoma and Mississippi da failures, 1950-1960	A large number of low-height homogeneous earthen embankment dams (1500 and 400, respectively) without vertical chimney drains were constructed in Oklahoma (1500) and Mississippi (400) states of USA. Out of them, failure of 11 dams in Oklahoma and 3 in Mississippi were recorded. All these failures were attributed to hydraulic fracturing as all of them occurred immediately after the first reservoir filling. In most of the cases, breaching occurred at a point along the dam length where the maximum differential settlement was expected. In addition, initial leak was detected along the downstream slope soon after the completion of the rise-up operation.
5.	Yard's Creek Upper Reservoir Dam, New Jersey, USA, 1965	Arching and differential settlement between the core and the adjacent fill material caused horizontal cracks in the core that might have opened by hydraulic fracturing. Erosion was manifested in the form of very dirty leakage emerging abruptly at the downstream toe during the first reservoir filling.
6.	Balderhead Dam, England, 1967	Due to the differential settlement across the discontinuities of the foundation, both longitudinal strains and arching were observed in various sections of the dam. The reservoir pressure was sufficiently higher than the stresses within the core to cause a hydraulic fracture.
7.	Hyttejuvet Dam, Valdalen, Norway, 1968	Hydraulic fracturing was attributed for the leakage that occurred in the upper section of the core in the dam; the core being relatively thin. The main vital factor resulting in the initiation of the crack was the vertical walls and narrow width of the core, which finally led to arching between the core and the gravel fill.

Sl. No.	Dam	Hydraulic Fracturing
8.	Teton Dam, Texas, 1976	The failure of this dam was attributed to two vital issues. The presence of highly erodible and key trench, through which the water flowed passing between joints in the unsealed rock under the grout cap, resulted in the formation of an erosion tunnel across the base of the key trench fill. The second was the differential settlement or hydraulic fracturing that resulted in development of cracks through which erosion took place.

The association of hydraulic fracturing with embankment dam failures is difficult to ascertain as it takes place within the dam and any evidence that might have existed is usually destroyed by the breach and the erosion. The existence of cracks before the reservoir rise-up and the role of the reservoir pressure in initiation and propagation of the cracks becomes very important in order to comprehend the phenomenon of hydraulic fracturing. Besides hydraulic fracture, different other mechanisms can play a vital role in the development of concentrated leaks in embankment dams. Generally, a combination of different factors lead to the collapse of the dams. Thus, formation of cracks in dams, right from its initiation to propagation, is always a challenging subject, and calls for detailed further research.

2.6 CRITICAL APPRAISAL OF LITERATURE AND RESEARCH GAP

The study gives a detailed review of the literature concerned to the hydraulic failure of earthen dams and embankments. It can be noted that the study of piping mechanism have been attempted by numerous researchers. However, to consider the range of processes that falls within the category of hydraulic failures, a lot of research is still required in order to reinforce the concepts on the evolution and progression or inhibition of piping during the performance life of the earthen dam. Individual occurrence of these phenomena, in real field conditions, is difficult to witness. In most cases, a complex combination of different processes having reciprocating influence on each other is responsible for many of the dam failure cases. Therefore, holistic methods addressing the real field condition, as closely as possible, is the need of the hour. Development of rigorous numerical models to provide precise predictions of the stated processes and elucidate the mechanisms of dam breaching from a theoretical framework is also extremely necessary. The influence of reservoir load applied on the upstream of the dam, and subsequent pore-water pressure developed inside the dam, requires a thorough scrutiny to establish mechanistic assessment of occurrence of piping and hydraulic fracturing. While piping has been defined in the previous studies strictly as a phreatic condition due to unfavorable hydraulic gradients, recent instances of piping occurring at gradients as low as 0.17 has given the indication that piping can also occur in areas where the hydraulic gradients are not that dominant (Jantzer and Knutsson, 2007). In this regard, the effect of confining pressure and seepage forces on piping should be studied, as only limited work has been attempted in this aspect (Tomlinson and Vaid, 2000). Other than the advances in filter engineering, very few works are available with respect to piping in non-cohesive soils (Skempton and Brogan, 1994; Sail et al., 2011). Minimal researches are attempted regarding piping in cohesionless soils (Aberg, 1993; Moffat and Fannin, 2006). There should be persistent attempt for the development of a constitutive model related to piping that could be utilized in a continuum model to identify the mechanism and progressive development of piping channels through earthen dams. On the other hand, studies related to the clogging phenomenon in the drainage blankets in earthen dams are not substantial, and should be attempted utilizing intricate modeling aspects. The problem of cracking and hydraulic fracturing are very complex and any predictive models describing its onset and progression to collapse would be very useful to the geotechnical community.

Based on the literature review and its critical appraisal, following is a list of gap areas where further studies should be attempted to enrich and discover the intricate mechanisms of piping though earthen dams, clogging of drainage blankets, and hydraulic fracturing in zoned earthen dams and embankments.

- Most of the researches related to piping through earthen dams were carried out for cohesive soils. However, since the earthen dams and embankments are mostly constructed with the locally available soils that may have recognizable cohesionless content, it is imperative to study the effect of piping in such locally available marginal soils as well.
- A meagre number of literatures is available with respect to the constitutive models of piping phenomenon. A constitutive behaviour of piping that could be utilized in a continuum model to estimate the nature and progression of piping in dams is yet to be developed. Such a model should incorporate flow through porous media, appended by particle migration through very narrow and tortuous channels, and guided by gravity and pressure gradients.
- Few researches are reported with regard to the estimating the time of development of piping in terms of observational instances. However, numerical and laboratory investigations should be carried out to identify the processes that can explain the time required for channel development with higher precision and confidence.
- Evaluation of the piping mechanism through unstable dispersive soils should be carried out, since internal erosion and clogging depends largely on the dispersivity of fine-grained soils.
- The processes of filtration, interface behavior, and time-dependent changes that take place within the filter and drainage blankets in earthen dams should be studied in thorough. These

drainage blankets and filters are instrumental in preventing migration of particles which otherwise can initiate piping and breach the embankment dam to failure.

- Numerical models simulating various important triggering mechanisms of earthen dam failure, especially clogging of drainage blanket and hydraulic fracturing, should be attempted, which can provide a complete picture of the failure mechanism of the dam.
- Evaluation of the water retention characteristics of the cracks in the earthen dams through simple and reliable models can be attempted, as retained water leads to higher pore pressure that eventually transpires to propagation of cracks.
- The opening and closure of cracks in an unsaturated soil embankment depends on the moisture content and the state of stresses in the soil. This opening and self-healing behaviour of the cracks should be studied through a finite element modeling approach.

2.7 OBJECTIVE AND SCOPE OF THE PRESENT STUDY

The primary objective of the dissertation work is to investigate the hydraulic response and stability of earthen dams under the influence of

- varying reservoir conditions including steady-state, rise-up and sudden drawdown,
- varying drainage configurations including horizontal and inclined drainage blankets,
- varying scenarios of clogging of drainage blankets, and
- initiation of cracking and crack propagation in the core of zoned earthen dams

In order to meet the stated objectives, the scopes of the dissertation work are listed as follows:

- Develop finite-element based numerical models of earthen dams and conduct numerical analysis to investigate the stability and hydraulic response of earthen dams.

- Validate the developed numerical models with the aid of field-monitored results obtained from case studies reported in literature.
- Investigate the response of homogeneous earthen dams without or with fully operational drainage blankets.
- Develop numerical models to simulate different scenarios of clogging (uniform clogging, end clogging, gradient clogging and random clogging of drainage blankets), and assess its influence on the response of homogeneous earthen dams.
- Investigate and assess the efficacy of drainage blankets in controlling additional distress in case of the cracking of a zoned earthen dam.
- Develop numerical models to simulate and assess the influence of sequential construction of zoned earthen dam.
- Develop numerical models to simulate hydraulic fracturing and identify the possible locations of crack initiation in homogeneous or zoned earthen dams.
- Conduct numerical analysis to identify the path of crack propagation through the core of a zoned earthen dam.

CHAPTER 3

NUMERICAL MODELLING

3.1 GENERAL

A numerical model is a mathematical simulation to a real physical process. A numerical model is different from a physical model prototype or a full-scaled field modelling. Other than being quick and providing the user a higher conditional variability, the numerical modelling is also very safe and many boundary conditions can be investigated in lesser time. In recent decades, the Finite Element Method (FEM) is used increasingly for the analysis of stress, deformation, structural forces, bearing capacity, stability and ground water flow in geotechnical engineering applications. The development in mathematics, along with the increase in the calculation prowess of computer, has led to development of various robust and user-friendly software tools. In the present study, the response of earthen dams to clogging of drainage blankets and hydraulic fracturing are extensively studied using the commercially available Finite Element program Geostudio 2012 and its corresponding modules of Seep/W, Sigma/W and Slope/W. The module Seep/W is used to model simple saturated steady-state problems or sophisticated saturated / unsaturated transient analyses with atmospheric coupling at the ground surface. It can be applied to the analysis and design of geotechnical, civil, hydrogeological, geo-environmental, and mining engineering projects. Sigma/W is a powerful finite element software product for modeling stress and deformation in earth and structural materials, and the analyses may range from simple linear elastic simulations to soil-structure interaction problems with nonlinear material models. Slope/W can effectively analyze both simple and complex stability related limit-equilibrium problems for a variety of slip surface shapes, pore-water pressure conditions, soil properties, and loading conditions.

3.2 WORKING PRINCIPLES OF VARIOUS MODULES

This section gives the theoretical basis of the three different modules of Geostudio that is used in the present study. It is important to understand the mathematical formulation working behind the simulations carried out in the present study, for which the theoretical background of each of these modules need to be explored.

3.2.1 Seep/W for Seepage Modeling

Seep/W is a finite-element module devised for analysing problems related to flow through porous media (Seep/W 2012), and is formulated based on Darcy's Law that holds validity for the flow of water through both saturated and unsaturated soil (Fredlund and Rahardjo, 1993). The working principle of Seep/W is based on the flow equilibrium, which states that the difference between the flow (flux) entering and leaving an elemental volume at a point in time is equal to the change in storage of the soil systems. The definitions is mathematically expressed as

$$q = ki \tag{3.1}$$

where, q is the specific discharge, k is the hydraulic conductivity, and i is the gradient of total hydraulic head.

Darcy's Law was originally framed for saturated soil, but later it was found that this law could also be applied to the flow of water through unsaturated soil (Richards, 1931; Childs and Collins-George, 1950). The only difference in the case of unsaturated flow is that under this condition, the hydraulic conductivity is no longer a constant. It varies with the changes in water content and indirectly varies with changes in pore-water pressure. Darcy's Law is often written as:

$$v = ki \tag{3.2}$$

where, v is the Darcian flow velocity.

It is to be noted that the actual average velocity at which water moves through the soil is the linear velocity, which is equal to Darcian flow velocity divided by the porosity of the soil. In unsaturated soil, the linear velocity is equal to Darcian flow velocity divided by the volumetric water content of the soil. Seep/W computes and presents only the Darcian flow velocity.

The general governing differential equation for three-dimensional seepage can be expressed as:

$$\frac{\partial}{\partial x}\left(k_x \frac{\partial H}{\partial x}\right)+\frac{\partial}{\partial y}\left(k_y \frac{\partial H}{\partial y}\right)+\frac{\partial}{\partial z}\left(k_z \frac{\partial H}{\partial z}\right)+Q=\frac{\partial \theta}{\partial t} \tag{3.3}$$

where, H is the total head, k_x, k_y and k_z are the hydraulic conductivities in the Cartesian directions, Q is the applied boundary flux, θ is the volumetric water content, and t is the elapsed time.

Equation 3.3 states that the difference between the flow (flux) entering and leaving an elemental volume at a point in time is equal to the change in storage of the soil systems. More fundamentally, it states that the sum of the rates of change of flows in the Cartesian directions plus the external applied flux is equal to the rate of change of the volumetric water content with respect to time. Under steady-state conditions, for a two-dimensional problem, the flux entering and leaving an elemental volume is the same at all times. The right side of Equation 3.3 consequently vanishes, and the equation reduces to

$$\frac{\partial}{\partial x}\left(k_x \frac{\partial H}{\partial x}\right)+\frac{\partial}{\partial y}\left(k_y \frac{\partial H}{\partial y}\right)+Q=0 \tag{3.4}$$

The changes in the stress state and the properties of the soil affect the changes in volumetric water content. The stress state for both saturated and unsaturated conditions can be described by two state variables (Fredlund and Morgenstern, 1976, 1977). These stress state variables are $(\sigma - u_a)$ and $(u_a - u_w)$, where σ is the total stress, u_a is the pore-air pressure, and u_w is the pore-water pressure. Seep/W is formulated for conditions of constant total stress; that is, there is no loading or unloading of the soil mass. During transient conditions, the pore-air pressure is assumed to remains constant at atmospheric pressure during Seep/W analysis. This means that $(\sigma - u_a)$ remains constant and has no effect on the change in volumetric water content. Thus, changes in the stress state variable $(u_a - u_w)$ affects the chances the volumetric water content, and with u_a remaining constant, the change in volumetric water content is a function only of pore-water pressure changes. Incorporating these changes and expressing the total head in terms of pore-water pressure, unit weight of water and elevation, the governing differential equation used in Seep/W finite element formulation is written as

$$\frac{\partial}{\partial x}\left(k_x \frac{\partial H}{\partial x}\right) + \frac{\partial}{\partial y}\left(k_y \frac{\partial H}{\partial y}\right) + \frac{\partial}{\partial z}\left(k_z \frac{\partial H}{\partial z}\right) + Q = m_w \gamma_w \frac{\partial H}{\partial t} \tag{3.5}$$

Applying the Galerkin method of weighted residual to the governing differential equation, the finite element formulation for two-dimensional seepage equation can be derived as

$$\tau \int_A \left([B]^T [C][B] \right) dA \{H\} + \tau \int_A \left(\lambda \langle N \rangle^T \langle N \rangle \right) dA \{H\},t = q\tau \int_L \left(\langle N \rangle^T \right) dL \tag{3.6}$$

where, $[B]$ is the gradient matrix, $[C]$ is the element hydraulic conductivity matrix, $\{H\}$ is the vector of nodal heads, $<N>$ is the vector of interpolating function, q is the unit flux across the edge of an element, τ is the thickness of an element, t is the elapsed time, λ is the storage term for a transient seepage equals to $m_w\gamma_w$, A is a designation for summation over the area of an element, and L is a designation for summation over the edge of an element.

In an abbreviated form, the finite element seepage equation can be expressed as

$$[K]\{H\}+[M]\{H\},t=\{Q\} \tag{3.7}$$

where, $[K]$ is the element characteristic or stiffness matrix, $[M]$ is the element mass matrix, and $\{Q\}$ is the element applied flux vector.

Equation 3.7 is the general finite element equation for a transient seepage analysis. For a steady-state analysis, the head is not a function of time and, consequently, the term $\{H\},t$ vanishes, reducing the finite element equation to be expressed as

$$[K]\{H\}=\{Q\} \tag{3.8}$$

which is identical to the abbreviated finite element form of the fundamental seepage equation, i.e. the Darcy's Law.

The finite element solution for a transient analysis is a function of time as indicated by the $\{H\},t$ term in the finite element equation. The time integration can be performed by a finite difference approximation scheme. Writing the finite element equation in terms of finite differences leads to the following equation (Segerlind, 1984):

$$\left(\omega[K]\Delta t+[M]\right)\{H\},t=\left[(1-\omega)Q_0+\omega Q_1\right]\Delta t+\left([M]-(1-\omega)[K]\Delta t\right)\{H_0\} \tag{3.9}$$

where, Δt is the time increment, ω ia a ratio between 0 and 1, H_0 is the head at beginning of time increment, H_1 is the head at end of time increment, Q_0 is the nodal flux at beginning of time increment, and Q_1 is the nodal flux at end of time increment.

Seep/W uses the Backward Difference Method, a method that sets ω to 1.0. As a result, the finite difference equation is then simplified to

$$\left([K]\Delta t+[M]\right)\{H\},t=Q_1\Delta t+[M]\{H_0\} \tag{3.10}$$

As indicated by Equation 3.10, in order to solve for the new head at the end of the time increment, it is necessary to know the head at the start of the increment, which means that the initial conditions must be known in order to perform a transient analysis. Seep/W uses Gaussian numerical integration to evaluate the element characteristic matrix [K] and the mass matrix [M]. The integrals are evaluated by sampling the element properties at specifically defined points and then summed together for the entire element.

3.2.2 Sigma/W for Stress-Deformation Modeling

This section presents the methods, equations, procedures, and techniques used in the formulation and development of the Sigma/W module. Sigma/W is formulated for either two-dimensional plane strain or axisymmetric problems using small displacement - small strain theory. In the present study, Sigma/W is used only for the two dimensional plane strain problems.

The finite element equation used in the Sigma/W formulation for a given time increment is expressed as

$$\tau\int_{V}\left([B]^{T}[C][B]\right)dV\{a\}=b\int_{V}\left(\langle N\rangle^{T}\right)dV+p\int_{A}\left(\langle N\rangle^{T}\right)dA+\{F_{n}\} \qquad (3.11)$$

where, [B] is the strain-displacement matrix, [C] is the constitutive matrix, {a} is the vector of nodal incremental x- and y-displacements, $<N>$ is the row vector of interpolating functions, A is the area along the boundary of an element, V is the volume of an element, b is the unit body force intensity, p is the incremental surface pressure, and $\{F_n\}$ is the concentrated nodal incremental load vector.

Equation 3.11 is summed over all the elements in the discretized domain. It should be noted the Sigma/W is formulated for incremental analysis. For each time step, the incremental displacements are calculated for the incremental applied load. These incremental values are then added to the values from the previous time step. The accumulated values are reported in the output files. Using this incremental approach, the unit body force is only applied when an element is subjected to analysis for the first time. For a two-dimensional plane strain analysis, Sigma/W considers all elements to be of unit thickness. For constant element thickness, *t*, Equation 3.11 is modified as

$$\tau\int_A\left([B]^T[C][B]\right)dA\{a\} = bt\int_A\left(\langle N\rangle^T\right)dA + pt\int_L\left(\langle N\rangle^T\right)dL \tag{3.12}$$

In an abbreviated form, the finite element equation is written as

$$[K]\{a\} = \{F\} = \{F_b\} + \{F_s\} + \{F_n\} \tag{3.13}$$

where, $[K]$ is the element characteristic (or stiffness) matrix, $\{a\}$ is the nodal incremental displacement vector, $\{F\}$ is the applied nodal incremental force, $\{F_b\}$ is the incremental body force vector, $\{F_s\}$ is the force vector due to surface boundary incremental pressures, and $\{F_n\}$ is the vector of concentrated nodal incremental forces.

Sigma/W solves the finite element equation for each time step to obtain incremental displacements and calculates the resultant incremental stresses and strains. It then sums all these increments since the first time step and reports the summed values in the output files. It uses Gauss-Legendre numerical integration (also termed quadrature) to form the element characteristic (or stiffness) matrix $[K]$. The variables are first evaluated at specific points within an element. These points are called integration points or Gauss points. These values are then summed for all the Gauss points within an element.

In Sigma/W, the nodal forces are included in the finite element formulation (as shown in Equation 3.13) by two different approaches. Either the nodal forces can be specified as boundary conditions, or they can be calculated internally when the elements are first provided with a stress release. For each element, the nodal forces are computed using the following expression

$$\{F\} = \int_V [B]^T \{\sigma\} dV \tag{3.14}$$

where, $\{\sigma\}$ is the vector of element stresses, $[B]$ is the strain-displacement matrix, and V is the elemental volume.

The resultant nodal forces are accumulated at each node. To simulate the removal of soils, as in an excavation, the signs on the nodal forces are reversed before these forces are incorporated into the finite element equation. In the displacement output files, Sigma/W reports the nodal forces at all nodes where displacement or boundary conditions are specified. However, in this case, the change of signs are not specified.

3.2.3 Slope/W for Slope Stability Modeling

This section explains the theory used in the development of Slope/W module. Following the basic conventions of slope stability analysis, Slope/W solves for two factor of safety equations; one equation that satisfies the force equilibrium (F_f) while the other that satisfies moment equilibrium (Fm). All the commonly used methods of slices can be visualized as special cases of the General Limit Equilibrium (GLE) solution that allows for a range of assumptions pertaining to the interrelationship between the interslice shear forced and normal forces. The interslice shear forces in the GLE method are handled with an equation proposed by Morgenstern and Price (1965), which is expressed as

$$X = E\lambda f(x) \tag{3.15a}$$

where, $f(x)$ is a function which provides the relation between the interslice normal force (E) and shear force (X), and λ is the reduction factor. However, it is to be noted that since the method is purely based on the principles of statics, and there is no mention of displacement or deformations, it is not always possible to obtain realistic stress distributions from this method.

The theory of the Finite Element Stress method is applied as an alternative to the limit-equilibrium (LE) stability analysis. This method computes the stability factor of a slope based on the stress state in the soil obtained from a finite element stress analysis. A factor of safety is defined as that factor by which the shear strength of the soil must be reduced in order to bring the soil mass into a state of limiting equilibrium along a selected slip surface. For an effective stress analysis, the shear strength is defined as

$$s = c' + (\sigma_n - u)\tan\phi' \tag{3.15b}$$

where, s is the shear strength, c' is the effective cohesion, φ' is the effective angle of internal friction, σ_n is the total normal stress, and u is the pore-water pressure.

For a total stress analysis, the strength parameters are defined in terms of total stresses and pore-water pressures are not taken into consideration. The stability analysis involves passing a slip surface through the earth mass and dividing the inscribed portion into vertical slices. The slip surface may be circular, composite (i.e., combination of circular and linear portions) or consist of any shape defined by a series of straight lines (i.e., fully specified slip surface). Slope/W conducts a slope stability analysis as described above to estimate stress-based Factor of Stability (FoS) against failure.

3.3 GEOMETRY AND MESHING

In GeoStudio, the geometry of a model is defined in its entirety prior to consideration of the discretization or meshing. In GeoStudio, the entire model is defined as a series of geometry objects. As sown in Figure 3.1, these objects can be soil regions, circular openings line objects, surface regions, and point objects.

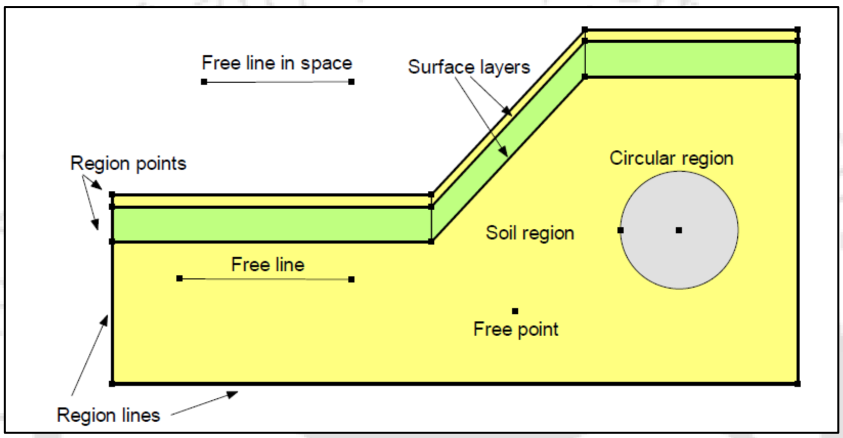

Figure 3.1 Geometry objects in Geostudio (Seep/W Manual)

GeoStudio uses the concept of regions and points to define the geometry of a problem and to facilitate discretization of the problem. The utilization of regions offers all the advantages of dividing a large domain into smaller pieces, working and analyzing the smaller pieces, and then connecting the smaller pieces together to obtain the behavior of the whole domain, similar to the fundamental concept of finite elements. The regions may be simple straight-sided shapes like quadrilaterals or triangles or a free form, multi-sided polygon.

Discretization or meshing is one of the most fundamental aspects of finite element modeling, which is used to classify any given region, surface, or line, into smaller parts to address the global response of the same from localized responses. GeoStudio has its own system and algorithms for meshing, which are designed specifically for the analysis of geotechnical and geo-environmental problems. The default scheme of meshing is fully automatic and there is no need to draw individual "finite elements" as a default mesh would be generated once the geometry regions are specified. However, the generated default mesh can be altered globally or locally according to the demand of the problem being analyzed.

One of the main features of a finite element are its constituent nodes. The nodes are used to describe the distribution of the primary unknowns within the element. All finite element equations are formed at the nodes. In a finite element formulation, it is necessary to adopt a model describing the distribution of the primary variable within the element (e.g., total head). The distribution could be linear or curved. For a linear distribution of the primary unknown, the nodes are required only at the corners of the element. With three nodes defined along an edge, a quadratic or any other higher order equation can be utilized for describing the distribution of the primary unknown within the element. The compatibility between different elements are established through their common nodes by considering the distribution of the primary unknown along the common element edge to be utilized by both the individual elements for their local estimations. The meshing algorithms in GeoStudio ensure element compatibility within regions. A special integer-based algorithm is also included to check the compatibility between regions. This algorithm ensures that common edges between regions have the same number of elements and nodes. Even though the software is very powerful and seeks to ensure mesh compatibility, the user nonetheless needs to careful about creating adjoining regions. The integer-programming algorithm in GeoStudio seeks to ensure that the same number of element divisions exist between points along a region edge. The number of element divisions are automatically adjusted in each region until this condition is satisfied. Consequently, it is often noticed that the number of divisions along the edge of a region is higher than what was specified as default.

There are different finite element mesh patterns available as default in Geostudio, namely (a) Quads and Triangles (b) Triangles only (c) Rectangular grid of Quads, and (d) Triangular grid of Quads / Triangles. In a finite element formulation, there are many integrals to be determined for achieving local scale equilibrium. For simple element shapes like 3-noded or 4-noded brick (rectangular) elements, it is possible to develop closed-formed solutions to obtain the integrals. However, for higher-order and more complex element shapes, it is necessary to conduct numerical integration. GeoStudio uses the Gauss quadrature scheme for conducting the numerical integration. This scheme is involved in sampling the element characteristics at specific points, known as Gauss points, and then adding up the sampled information. Table 3.1 lists some of the element types available in GeoStudio and their available integration points.

Table 3.1 Commonly available element types available in Geostudio and their corresponding integration points

Element Type	**Integration Points**	**Comments**
4-noded quadrilateral	4	Default
8-noded quadrilateral	4 or 9	4 is the default
3-noded triangle	1 or 3	3 is the default
6-noded triangle	3	Default

GeoStudio presents the results for a Gauss region, but the associated data is actually computed at the exact Gauss integration sampling points. In the present study, the use of mixed 'quad and triangle' unstructured mesh with 4-noded quadrilateral and 3-noded triangle element type is utilized. Figure 3.2(a) shows the typical unstructured mesh of 'quad and triangle', whereas the enlarged view is shown in Figure 3.2(b) highlights the intermixing of two types of mesh elements. The typical usage of local meshing pattern along the interface of the upstream shell and the dam core is shown in Figure 3.2 (c). In such cases, the global element size (e.g., 0.5) is used for the main regions, while refined element size is used along the interface of the core and the shell, as well as in other interconnections of regions with different material constituents. For the local refinements, the mesh elements are considered with some specific lower "ratio of the default size" (e.g., 0.3). The total number of nodes and elements used in the models depends on the number of mesh elements used and the adopted refinements.

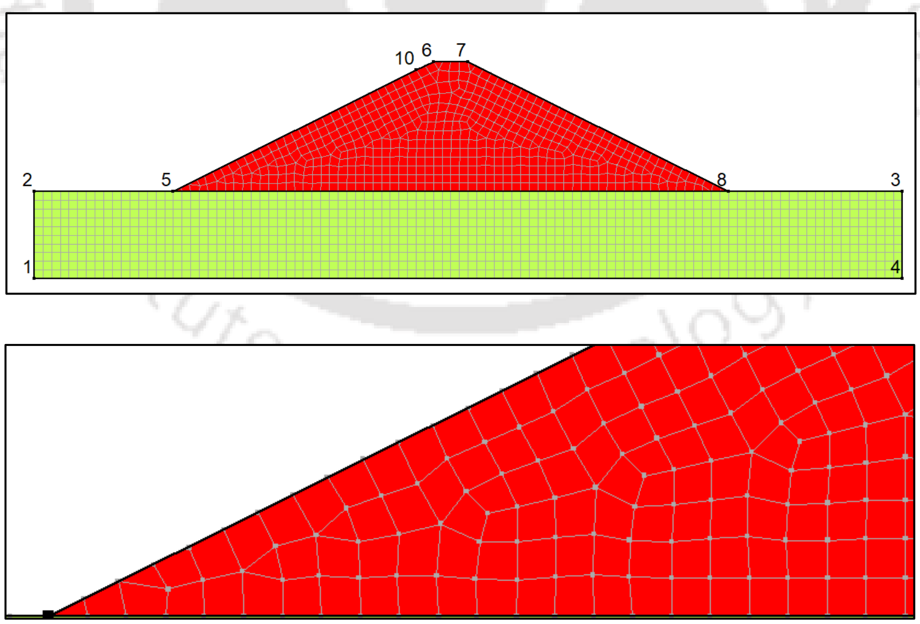

(a)

(b)

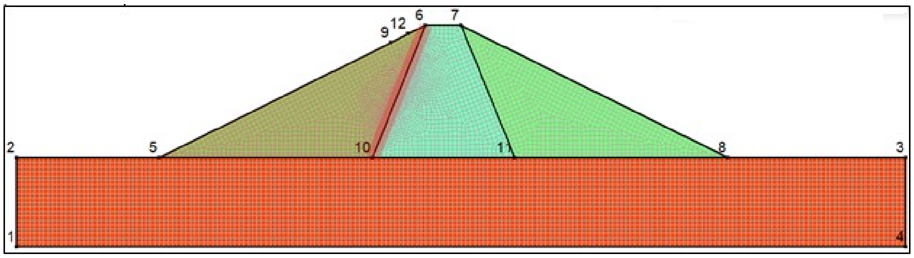

(c)

Figure 3.2 (a) Typical meshing scheme adopted to represent an earthen dam on the foundation bed: 'quad and triangle' for dam body and 'quad' for foundation (b) Enlarged meshing pattern highlighting the intermixing of mesh element types (c) Usage of global and local element size

3.4 MATERIAL MODELS AND MATERIAL PROPERTIES

This section describes the various soil models and properties in Geostudio and their influence on the generated results. Well-defined soil models and the chosen properties of the constituent materials can be critical in obtaining an efficient solution of the finite element equations and therefore it is important to have a clear understanding of them.

3.4.1 Material Models in Seep/W Analysis

There are four different material models commonly used for Seep/W analysis for different types of problems. A summary of these models and the required soil properties are discussed and provided in this section. The material models commonly consist of (a) None (when used to remove a specific part of a model from an analysis), (b) Saturated only model, (c) Saturated / Unsaturated model, and (d) Interface model. Each of these models has different behaviour and is supposed to be used according to the requirement of the project. In the simulation of flow response of homogeneous or zoned earthen dams, the 'saturated only' model and 'saturated / unsaturated model' are commonly used to analyze steady state or transient flow conditions.

The ‘saturated only’ soil model is very useful for defining a soil region that will always remain below the phreatic surface and presumably remain saturated under all conditions during the analysis. This model should not be used for soils that, at any point during the analysis, may become partially saturated. If this happens, the mathematical schemes will continue to solve the analysis, however the unsaturated zones will be considered to transmit the seepage water at the same rate as for the saturated soil. This will result in an overestimation of flow quantity and can result in an unrealistic water table or phreatic level detection. The regions where both saturated and unsaturated soil regions will be present should be simulated with ‘saturated / unsaturated model’.

Two important soil properties that needs to be defined for the ‘saturated only’ material model. The first one is the ‘saturated water content’, which is the maximum amount of water that can be stored by the soil matrix. The second parameter is the ‘saturated hydraulic conductivity’ that is the amount of water that would move vertically through a unit area of saturated soil in unit time under unit hydraulic gradient.

To use the ‘saturated / unsaturated’ material model, it is important to define the ‘hydraulic conductivity function’ and ‘volumetric water content function’. The volumetric water content function describes what portion or volume of the voids remains water-filled as the soil drains out the excess water. The three main features that characterize the volumetric water content function are the air-entry value, (AEV), the slope of the function for both the positive and negative pore-water pressure ranges (designated as m_w), and the residual water content or residual saturation (S_r). The air-entry value (AEV) corresponds to the value of negative pore-water pressure when the largest voids or pores begin to drain freely. Representing the slope of the water content function, in both the positive and negative pore-water pressure regions, can be very important in a seepage analysis, since water can be released from the soil in two different mechanisms. Firstly, water can be released by draining the water-filled voids, thereby desaturating the soil profile by gravitation forces, resulting in negative pore-water pressure. Secondly, the soil skeleton can be compressed, thereby reducing the size of the voids and effectively squeezing water out of a saturated system, resulting in positive pore-water pressure. In the positive pore-water pressure region, m_w becomes equivalent to m_v, the coefficient of volume compressibility for one-dimensional consolidation. The slope of the volumetric water content function in the negative pore-water pressure range represents the rate at which the volume of water stored within the soil changes with the pressure, ranging from the pressure corresponding to AEV until the pressure at the residual water content. Residual volumetric water content represents the volumetric water content of a soil where a further increase in negative pore-water pressure does not produce significant changes in water content. Figure 3.3 represents a typical variation of the volumetric water content function along with the demarcation of its characteristics.

Seep/W has four available methods to develop a volumetric water content function. One of these methods pertains to estimate a data point function using a predictive method based on grain size. The second method is used to develop the function based on a sample set of functions built into the software. The last two methods pertain to closed form equations based on known curve fitting parameters. For the present study, the volumetric water content curves were developed based on a sample set of functions built into the software. Seep/W provide several "typical" water content functions for different types of soils, as shown in Figure 3.4. In using these sample functions, it is required to specify the saturated water content and the residual water content (if any) based on the understanding of field conditions.

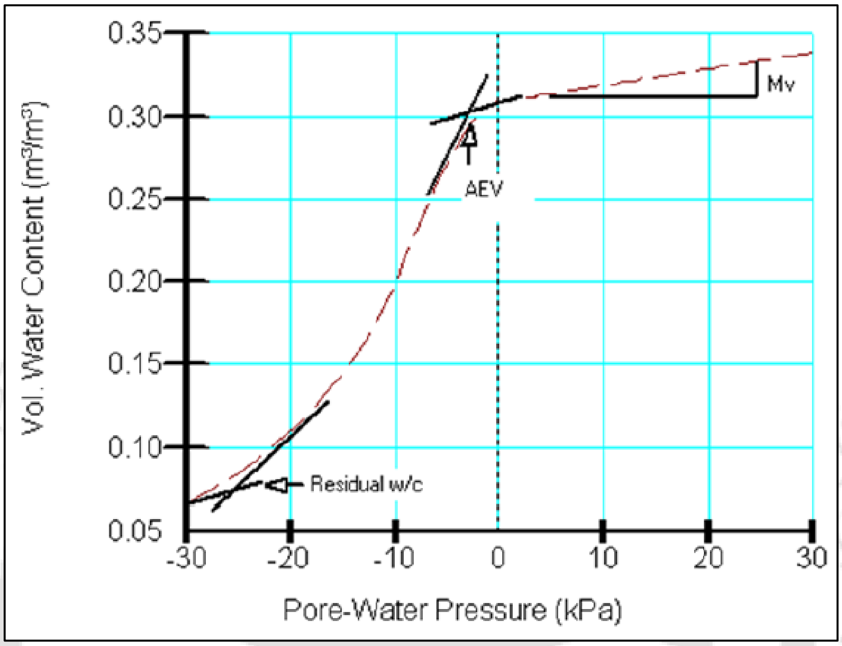

Figure 3.3 Schematic representation of the volumetric water content function of a soil (Adopted from Seep/W 2012)

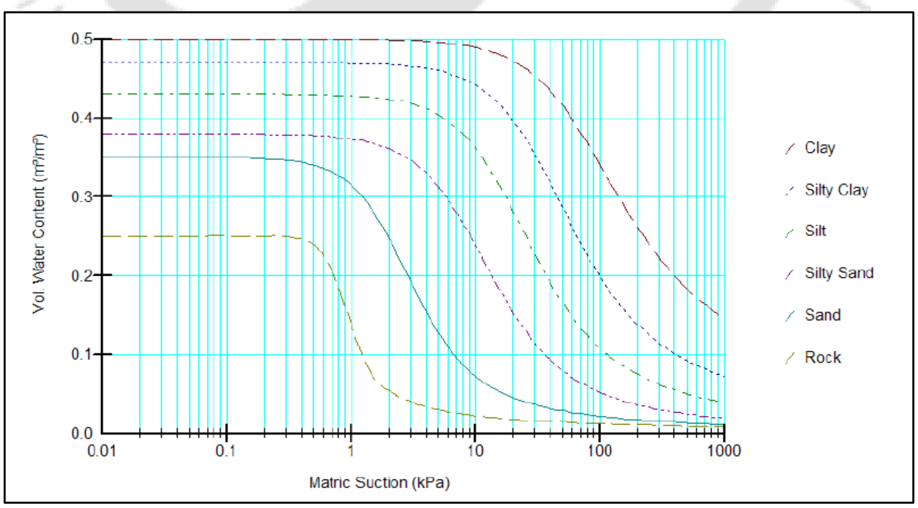

Figure 3.4 Typical volumetric water content function of soils (Adopted from Seep/W 2012)

The ability of a soil to transport or conduct water under both saturated and unsaturated conditions is reflected by the hydraulic conductivity function. In a saturated soil, all the pore spaces between the solid particles are filled with water. Once the air-entry value is exceeded, air enters the largest pores and the air-filled pores become non-conductive conduits to flow, thereby increasing the tortuosity of the flow path. As the pore-water pressure become increasingly negative, more pores become air-filled and the hydraulic conductivity decreases further. By this description, it is clear that the ability of water to flow through a soil profile depends on how much water is present in the soil matrix, which is represented by the volumetric water content function.

Seep/W module has three built-in predictive methods that can be used to estimate the hydraulic conductivity function, once the volumetric water content function and the magnitude of saturated permeability (k_s) is specified. The methods are (a) Method 1 proposed by Fredlund and Xing (1994), (b) Method 2 proposed by Green and Corey (1971), and (c) Method 3 proposed by van Genuchten (1980). In the present study, Method 3 proposed by van Genuchten (1980) is used for estimating the hydraulic conductivity function for different analysis. It the one of the most popular method for predicting the conductivity function (Kim et al., 2011). For the purpose of representation, some typical hydraulic conductivity functions of some soil types are shown in Figure 3.5.

van Genuchten (1980) proposed the following closed form equation to describe the hydraulic conductivity of a soil as a function of matric suction:

$$k_w = k_s \frac{\left[1-\left(a\Psi^{(n-1)}\right)\left(1+\left(a\Psi^{n}\right)^{-m}\right)\right]^2}{\left(\left(1+a\Psi\right)^{n}\right)^{m/2}} \tag{3.16}$$

where, k_s is the saturated hydraulic conductivity, Ψ is the required suction range, a and m are the curve fitting parameters, and $n = 1/(1-m)$

From the above equations, the hydraulic conductivity function of a soil can be estimated once the saturated conductivity and the two curve fitting parameters, a and m, are known.

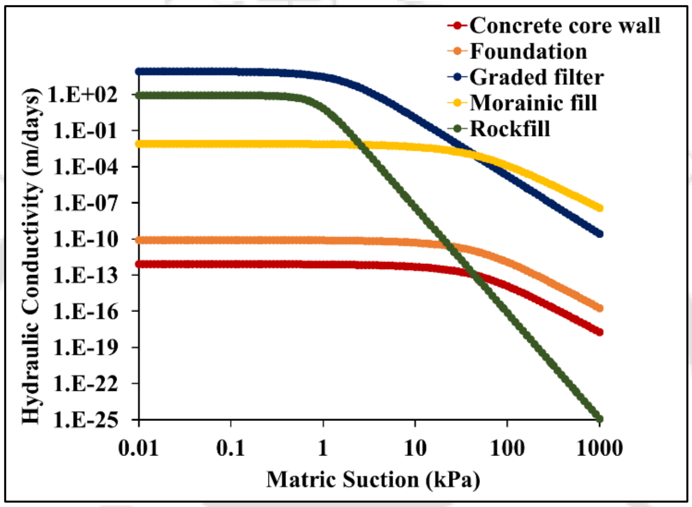

Figure 3.5 Typical hydraulic conductivity functions of some types of soils

van Genuchten (1980) showed that the curve fitting parameters can be estimated graphically based on the volumetric water content function of the soil. According to van Genuchten (1980), the best point to evaluate the curve fitting parameters is the halfway point between the residual and saturated water content of the volumetric water content function. The slope of the function can be calculated as:

$$s_p = \frac{1}{\theta_s - \theta_r} \left| \frac{d\theta_p}{d\left(\log \Psi_p\right)} \right| \tag{3.17}$$

where, θ_s and θ_r is the saturated and residual volumetric water contents respectively, θ_p is the volumetric water content at the halfway point of the volumetric water content function curve, and Ψ_p is the matric suction at the same point.

As s_p is determined, the following formulae can be used to estimate the parameters m and a:

$$m = \begin{cases} 1 - e^{-0.8 s_p} & \forall \ 0 < s_p < 1 \\ 1 - \dfrac{0.5755}{s_p} + \dfrac{0.1}{s_p^2} + \dfrac{0.025}{s_p^3} & \forall \ s_p > 1 \end{cases} \tag{3.18}$$

$$a = \frac{1}{\Psi}\left(2^{1/m} - 1\right)^{(1-n)} \tag{3.19}$$

3.4.2 Material Models in Sigma/W Analysis

Sigma/W possesses six inbuilt constitutive models for soils, as well as allows the user to create and add-in user-defined constitutive models. For each of these models, the response will be different depending on the type of stress characteristics assigned to the model, namely whether it is assigned with total stress, effective stress with no pressure change, or effective stress with pore-water pressure change. The in-built models available are (a) Linear elastic model (b) Anisotropic elastic model (c) Hyperbolic model (d) Elastic Plastic model (e) Cam Clay model, and (f) Modified Cam Clay model. For the present study, the linear elastic model and the elastic-plastic model are utilized.

The linear elastic model is the simple constitutive model for soil available in Sigma/W, wherein the stresses are considered directly proportional to the strains. The proportionality constants are Young's Modulus, E, and Poisson's Ratio, v. The stresses and strains are directly related by a constant, which is representative of pure volumetric strain. The volumetric strain tends towards zero as Poisson's ratio approaches the magnitude of 0.5. For computational purposes, v can never be 0.5. Even values greater than 0.49 is observed cause numerical problems. Consequently, Sigma/W limits the maximum value for Poisson's ratio to 0.49.

The Elastic-Plastic model in Sigma/W describes an elastic-perfectly plastic relationship. The elastic-perfectly plastic Mohr-Coulomb (M-C) model necessitates 5 input parameters, specifically the strength parameters (cohesion c, angle of internal friction φ and dilatancy angle ψ) and the stiffness parameters (Elastic modulus E and Poisson's ratio v). A typical stress-strain curve for this model is shown in Figure 3.6. The generated stress is directly proportional to the corresponding strain, until the yield point is reached. Beyond the yield point, the stress-strain curve is perfectly horizontal, indicating substantial increase in strain without change in stress.

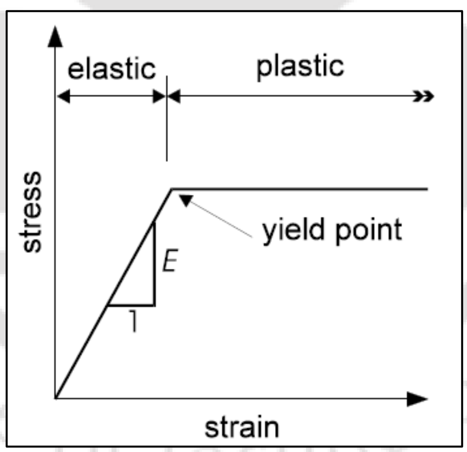

Figure 3.6 Stress-strain relationship for the elastic-perfectly plastic constitutive model

In Sigma/W, soil plasticity is formulated using the theory of incremental plasticity (Hill, 1950). Once an elastic-plastic material begins to yield, an incremental strain ($d\varepsilon$) can be divided into an elastic ($d\varepsilon^e$) and a plastic ($d\varepsilon^p$) component. Only elastic strain increments will cause changes in stress. As a result, the stress increments, $d\sigma$, can be written as follows:

$$\{d\sigma\} = [C_e]\left(\{d\varepsilon\} - \{d\varepsilon^p\}\right) \tag{3.20}$$

where, $[C_e]$ is the elastic characteristic matrix.

A function that describes the locus of the yield point is called the yield function and is defined using the symbol F. In the Elastic-Plastic model of Sigma/W, the yield point depends only on the stress state comprising of the Cartesian normal and shear stresses. Consequently, the yield function can be written as:

$$F = F\left(\sigma_x, \sigma_y, \sigma_z, \tau_{xy}\right) \tag{3.20}$$

An incremental change in the yield function is given by the matrix form

$$dF = \left\langle \frac{\partial F}{\partial \sigma} \right\rangle \{d\sigma\} \tag{3.21}$$

The theory of incremental plasticity dictates that the yield function is $F < 0$, and, when the stress state lies on the yield surface, dF should be equal to zero. This latter condition is termed the neutral loading condition, and, can be written mathematically as:

$$dF = \left\langle \frac{\partial F}{\partial \sigma} \right\rangle \{d\sigma\} = 0 \tag{3.22}$$

The plastic strain is postulated to be

$$\{d\varepsilon^p\} = \lambda \left(\frac{\partial G}{\partial \sigma} \right) \tag{3.23}$$

where, G is the plastic potential function, and λ is the plastic straining factor.

Upon substituting the plastic strain from Equation 3.23 into the incremental stress equation (Equation 3.20), the incremental stress can be expressed as

$$\{d\sigma\} = [C_e]\{d\varepsilon\} - \lambda [C_e]\left(\frac{\partial G}{\partial \sigma}\right) \tag{3.24a}$$

Substituting the incremental stress vector into the neutral loading condition, the following expression for the plastic scaling factor, λ, can be derived

$$\lambda = \frac{\left\langle \frac{\partial F}{\partial \sigma} \right\rangle [C_e]}{\left\langle \frac{\partial F}{\partial \sigma} \right\rangle [C_e]\left(\frac{\partial G}{\partial \sigma}\right)}\{d\varepsilon\} \tag{3.24b}$$

From the previous two equations, a relationship between stress increments and strain increments is derived as follows:

$$\{d\sigma\} = \left([C_e] - [C_p]\right)\{d\varepsilon\} \tag{3.25}$$

where, $[C_p]$ is the plastic characteristic matrix which is expressed as

$$[C_p] = \frac{[C_e]\left(\frac{\partial G}{\partial \sigma}\right)\left\langle \frac{\partial F}{\partial \sigma} \right\rangle [C_e]}{\left\langle \frac{\partial F}{\partial \sigma} \right\rangle [C_e]\left(\frac{\partial G}{\partial \sigma}\right)}\{d\varepsilon\} \tag{3.26}$$

To evaluate the plastic characteristic matrix $[C_p]$, the yield function (F) and the plastic potential function (G) need to be specified.

Sigma/W uses the Mohr-Coulomb yield criterion as the yield function for the Elastic-Plastic model. The Mohr-Coulomb yield criterion is commonly expressed in terms of principal stresses as follows

$$F_s = \frac{1}{2}(\sigma_1 - \sigma_3) + \frac{1}{2}(\sigma_1 + \sigma_3)\sin\phi - c\cos\phi \tag{3.27}$$

The Mohr-Coulomb criterion can also be written in terms of the stress invariants. The yield function, F, can then be written as follows (Chen and Zhang, 1991).

$$F = \sqrt{J_2}\sin\left(\theta + \frac{\pi}{3}\right) - \sqrt{\frac{J_2}{3}}\cos\left(\theta + \frac{\pi}{3}\right)\sin\phi - \frac{I_1}{3}\sin\phi - c\cos\phi = 0 \qquad (3.28a)$$

where, I_1 is the first stress invariant, J_2 and J_3 are the second and third deviatoric stress invariant, θ is the Lode angle, and c and φ are the Mohr-Coulomb shear strength parameters. These components are expressed in terms of Cartesian normal and shear stresses as follows:

$$I_1 = \sigma_x + \sigma_y + \sigma_z \qquad (3.28b)$$

$$J_2 = \frac{1}{6}\left[\left(\sigma_x - \sigma_y\right)^2 + \left(\sigma_y - \sigma_z\right)^2 + \left(\sigma_z - \sigma_x\right)^2\right] + \tau_{xy}^2 \qquad (3.28c)$$

$$\theta = \frac{1}{3}\cos^{-1}\left(\frac{3\sqrt{3}}{2}\frac{J_3}{J_2^{3/2}}\right) \qquad (3.28d)$$

$$J_3 = \sigma_x^d \sigma_y^d \sigma_z^d - \sigma_z^d \tau_{xy}^2 \qquad (3.28e)$$

When the angle of internal friction, φ, is equal to zero, the Mohr-Coulomb yield criterion becomes the Tresca criterion (Smith et al., 2014), and the same is expressed as follows:

$$F = \sqrt{J_2}\sin\left(\theta + \frac{\pi}{3}\right) - c = 0 \qquad (3.28f)$$

The plastic potential function, G, used in Sigma/W has the same form as the yield function, F, (i.e. $G = F$), except that the internal friction angle, φ, is replaced by the angle of dilatancy, Ψ. Thus, the plastic potential function is expressed as

$$G = \sqrt{J_2}\sin\left(\theta + \frac{\pi}{3}\right) - \sqrt{\frac{J_2}{3}}\cos\left(\theta + \frac{\pi}{3}\right)\sin\Psi - \frac{I_1}{3}\sin\Psi - c\cos\Psi \qquad (3.28g)$$

3.4.3 Material Models in Slope/W Analysis

The commonly available methods used to evaluate FoS in Slope/W are based on limit equilibrium formulations except for one which uses finite element computed stresses. Many different material models are available in Slope/W that can be used to calculate the FoS of slopes. These material models include 'Mohr Coulomb model', 'Undrained model', 'High Strength model', 'Bedrock or Impenetrable model', 'Bilinear strength model', 'Anisotropic Strength model', 'Spatial Mohr Coulomb model', 'Anisotropic Function model' and 'Model for Normal/Shear Function interactions'. In the present study, the Mohr Coulomb material model has been used to compute the stability of the sloping faces of the dam.

3.5 BOUNDARY CONDITIONS

The boundary conditions are, in essence, the driving force in any numerical analysis, and applying them correctly on the boundaries of a problem is one of the key components of a numerical analysis. The solutions to the numerical problems are considered as a direct response to the applied boundary conditions. The determination of the correct boundary conditions might sometimes demand an iterative process, since the boundary conditions themselves are a part of the solution. Furthermore, during a transient analysis, boundary conditions may change with time, which can substantially add to the numerical complexity. Due to the extreme importance of boundary conditions, it is essential to have a thorough understanding of this aspect of numerical modeling in order to obtain meaningful results. Most importantly, it is essential to have a clear understanding of the physical significance of the various types of boundary condition. This section discusses the various types of boundary conditions that are used in Seep/W, Sigma/W and Slope/W simulations for the present study. In GeoStudio, all the boundary conditions must be applied directly on geometry items such as region faces, region lines, free lines or free points, as shown in Figure 3.7. There is no way to apply a boundary condition directly on an element edge or node. The advantage of connecting the boundary condition with the geometry is that they become independent of the mesh and the mesh can be changed without losing the boundary condition specification. For example, a flux or stress boundary condition, which is given in units per area, can be applied to the "face" of a region.

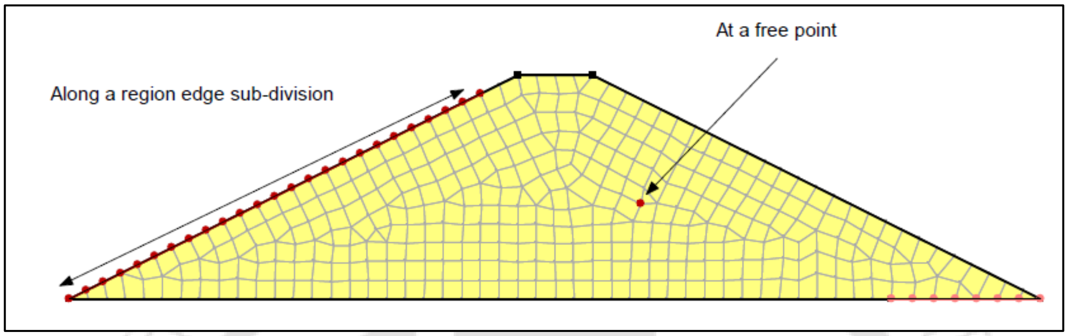

Figure 3.7 Application of different boundary conditions in an earthen dam simulation

3.5.1 Boundary Conditions in Seep/W Modeling

Seep/W is used for seepage analysis, in which the primary unknown is the total hydraulic head that is to be solved at each node. The unknowns will be computed relative to the total hydraulic head (*H*) specified at some nodes and/or the specified flow quantities (*Q*) values at some other nodes. The specified *H* or *Q* values serve as the boundary conditions. A solution cannot be obtained for the finite element equation without specifying either *H* or *Q* at some nodes. In a steady-state analysis, at least one node in the entire mesh must have a specified *H* condition. Seep/W has the facility to apply different boundary conditions that include total head (*H*), total flux (*Q*), unit flux (*q*), unit gradient (*i*) and pressure head (*P*) that can be of use for solving different problems. However, in the present study, either the constant total head (*H*) boundary condition or total head boundary varying with time (*H,t*) is used to specify the steady state or fluctuating reservoir head levels, respectively.

A typical application of the head boundary condition for a seepage analysis through the dam is shown in Figure 3.8. Along the upstream end, the full supply level of the reservoir is 24 m and thus a total head boundary of $H = 24$ m is applied. Along the downstream end of the dam, the water table is at the ground surface and the ground elevation at the bottom of the reservoir is 10 m, therefore, $H = 10$ m is applied at the downstream end.

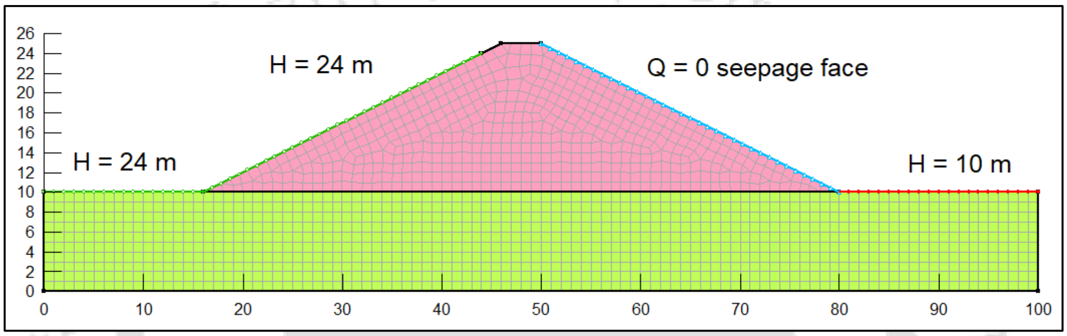

Figure 3.8 Typical boundary conditions used in the simulation of an earthen dam

On the upstream face of the dam, at the reservoir level, the water pressure is zero, but the elevation is 24 m. Then, the total head at this point is 24 m. At the bottom of the reservoir, the pressure head is 10 m of water and the elevation head is 14 m, making the total head also 24 m. Thus, the upstream boundary condition is subjected to a constant total head equal to 24 m. Similarly, along the downstream end, the pressure head is 0 m of water and the elevation is 10 m, making the total head also being 10 m. This illustrates the convenience of using total head as a boundary condition. Even though the water pressures are different at every node on the upstream sloping face under the reservoir level, the total head is nonetheless a constant. Without using total head as a boundary condition, a different pressure would have to be specified at each node on the upstream dam face; however, specifying this condition as a constant total head is more convenient.

Along the downstream face of the dam, a potential seepage face is also flagged as a boundary condition. This approach implies that at the end of each iteration, the conditions along the specified potential seepage face are "reviewed" to see if they meet the correct criteria. Considering the simplest case where the boundary conditions along the entire potential seepage face are set to Q = 0 (flux-type), it indicates that no additional flux is going to be added or removed at these nodes, and with the specification that the conditions will be reviewed and adjusted as necessary. At the end of the first iteration, after the heads are computed for all nodes along the potential seepage face, Seep/W checks if any of the nodes have a positive pressure (H greater than elevation). Nodes with computed pressures greater than zero are not allowed, as positive pressure on the surface indicates ponding, which cannot happen along the sloping boundary. This scenario implies that the specified boundary condition of $Q = 0$ is, therefore, not correct as water wants to exit the system, but the $Q = 0$ condition is not allowing the water to exit. To allow water to leave, Seep/W converts the flux-type boundary condition to a head-type boundary condition, with H equal to the y-coordinate (zero water pressure) at each node where the computed pressure was found positive. Subsequently, a new solution is computed for the altered boundary condition. At the end of the repeated solution steps, water can then leave or enter the system at the nodes that were converted from a Q-type to an H-type boundary condition. Further, the program checks to see whether the computed Q is negative (out of the system) or positive (into the system). Computed flow is acceptable to be negative, i.e. water is flowing out of the system, while a positive flow where water enters the system is unacceptable. At the nodes, along the potential seepage face, with a positive flux, Seep/W further converts the H-type boundary back to the original specified Q-type, and then repeats the analysis. The process is repeated until all the nodes on the potential seepage face has either a computed zero water pressure ($H = y$) or a nodal $Q = 0$, which is the original specified boundary condition. Upon specifying the boundary conditions along the upstream and downstream face of the dam, the total head difference between the upstream and downstream conditions was 14 m, resulting in the flow shown in Figure 3.9.

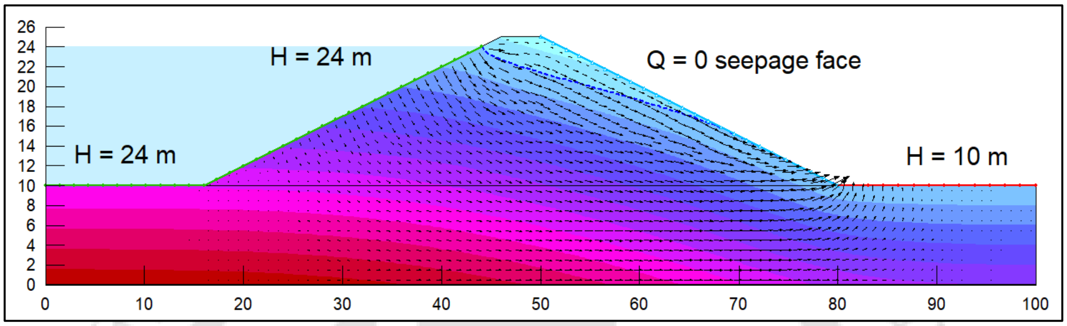

Figure 3.9 Typical flow profile due to the application of boundary conditions

Many problems in geotechnical engineering require the application of temporal boundary conditions. For example, to simulate the reservoir fluctuations and its influence on the response of an earthen dam, a time-dependent boundary condition needs to be implemented which would related to transient loading applied by the reservoir on the upstream face of the dam. In Seep/W module, there are different types of time-dependent boundary conditions available, such as (a) Total Head vs Time, (b) Total Head vs Volume, (c) Water Flux vs Time, (d) Water Unit Flux vs Time, and (e) Pressure Head vs Time. In order to simulate the operational conditions of the a reservoir, i.e. to represent the reservoir rise-up and drawdown conditions, the boundary condition conforming to 'Total Head vs Time' serves appropriate. Figure 3.10 shows a typical variation for a reservoir level that undergoes a rise-up scenario, followed by a constant reservoir level and a subsequent drawdown.

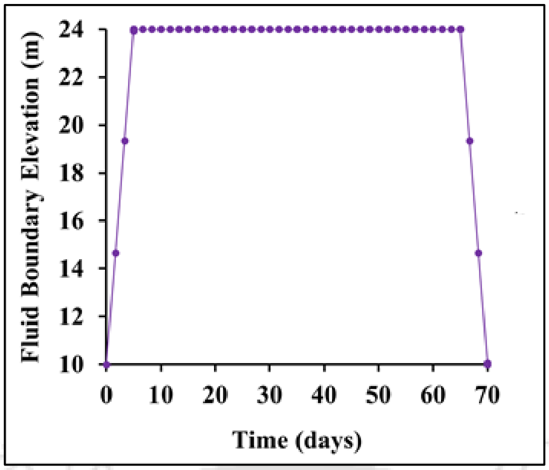

Figure 3.10 Typical representation of boundary condition functions for reservoir operations

3.5.2 Boundary Conditions in Sigma/W Modeling

In Sigma/W, multiple boundary condition types are implemented to support virtually all load-deformation modelling scenarios. Displacement, force or spring boundary conditions may be applied to points or nodes along geometry lines, while stress and fluid pressure boundary conditions may be applied to element edges on lines. Fundamentally, there are only two types of boundary conditions that can be applied to a stress-deformation analysis; namely, 'stress' and 'force or displacement' type boundary conditions. In the 'stress type' category, the hydrostatic pressure boundary condition (either maintained constant or fluid elevation varying with time) is used to simulate steady or fluctuating reservoir condition, respectively.

In all stress-deformation models, it is critical to put a "bound" the problem, which means that some parts of the geometry must be defined as 'zero displacement' boundary conditions. In general, it is common to put a bound to the left and right far boundaries of a numerical model, along with the bottom edge, by specifying as zero displacement along the Cartesian x- and/or y-directions. The base of the model is bounded in both directions, as there should not be any deformation along any direction at the base, whereas the far left and right edges are bounded in the x-direction by specifying zero displacement. Figure 3.11 shows a typical representation of the boundary condition adopted for stress-deformation analysis of an earthen dam.

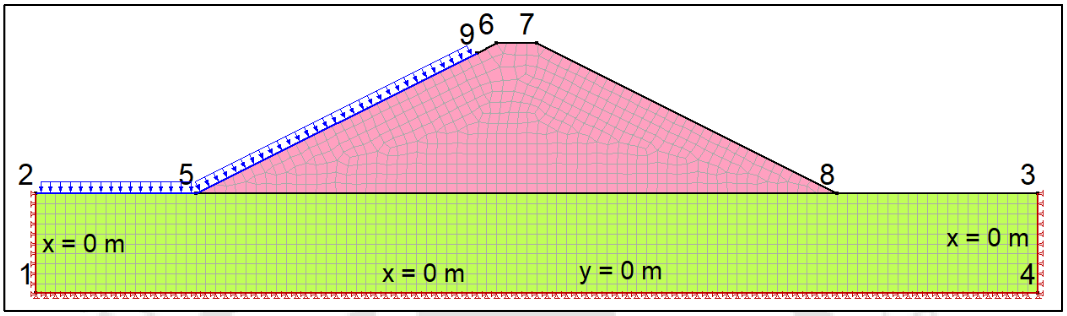

Figure 3.11 Typical representation of the application of the boundary conditions in stress-deformation analysis of earthen dam in Sigma/W

A fluid pressure boundary is defined by specifying a water surface elevation, as illustrated in Figure 3.11. The pressure is computed from the distance between the specified water surface elevation and the y-coordinate of the boundary node. All the element edges between 2-5 and 5-9 are flagged as fluid pressure boundaries. When the fluid pressure type is applied to an element edge, Sigma/W internally calculates equivalent force applied at each of the nodes comprising the edge. The nodal pressure is obtained by subtracting the nodal y-coordinate from the fluid elevation, and subsequently multiplying it by the fluid self-weight. Sigma/W will only consider positive fluid pressures. Therefore, for the fluid pressure boundary condition to have an effect, the selected edge must have a y-coordinate less than the fluid elevation. Further, identical to Seep/W, Sigma/W also facilitate transient boundary conditions; the details are same as described in Section 3.5.1.

3.5.3 Boundary Conditions in Slope/W Modeling

As Slope/W is intended to operate on the limit equilibrium analysis to identify potential facilure mechanisms through force and moment equilibrium, deformation or displacement is not involved in such analysis. Hence, through an in-built mechanism, the standard displacement boundary conditions are already imposed in the Slope/W simulation models during their creation, and need to be defined by the user. In Slope/W, the boundary conditions are also applied to the methods involved in the determination of the radius of the critical slip surface during the Limit Equilibrium (LE) based stability analysishas been described in this section. For defining the slip circles to be examined during the analysis, there are two different methods: (a) the Grid and Radius method, and (b) the Entry and Exit method. In the the Grid and Radius method, a slip circle can be defined by specifying the x-y coordinates of the centre and the radius. Figure 3.12 reflects the basic elements of the 'Grid and Radius' method for bounding the limits of the centres and radii of the trial slip surfaces. A wide variation of trial slip surfaces can be specified with a defined grid for the centres of the slipe circles and a defined range of defined radii. Each grid point represents the center of the trial slip circle. The radii of the trial slip circles are specified by the radius from the corresponding centre to the chosen tangent lines. One of the difficulties with the 'Grid and Radius' method is that it is difficult to visualize the extents and/or range of trial slip surfaces. This limitation can be overcome by specifying the location where the trial slip surfaces will likely enter the ground surface and where they will exit. This technique is called the 'Entry and Exit' method in Slope/W, as shown by the demarcating red colored lines its elements in Figure 3.13. The number of entries and exits can be specified as the number of increments along these two lines. This method is more popular in use amongst the two techniques, and is used in the present study.

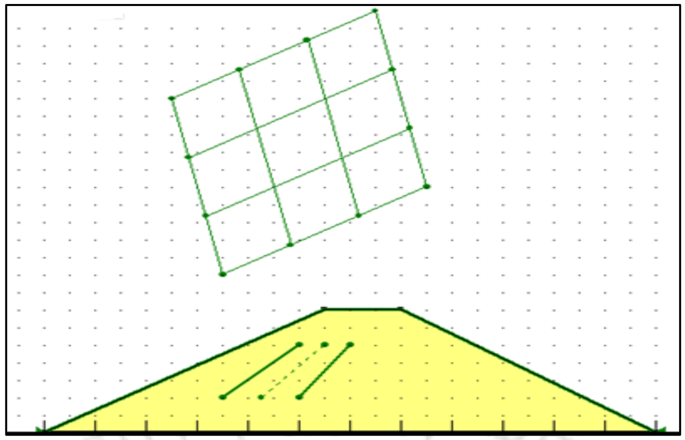

Figure 3.12 The elements of 'Grid and Radius' method for bounding trial slip circles

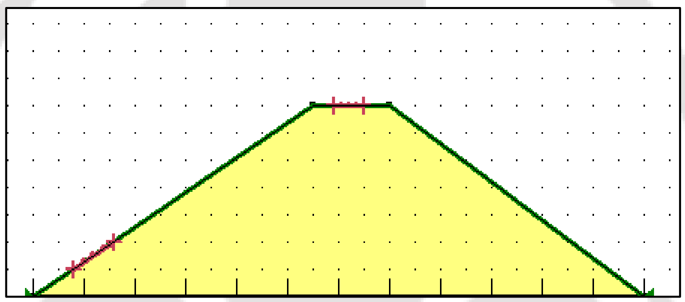

Figure 3.13 The elements of 'Entry and Exit' method for bounding trial slip circles

3.6 ANALYSES TYPES

The three different modules of Geostudio is capable of solving different types of analyses and the choice of the analyses types would depend on the objective(s) of the modelling. The more common scenario is to define multiple analyses to investigate a single problem. This section gives a brief overview about the different analyses types present in the all the three modules (Seep/W, Sigma/W and Slope/W) and describes the ones which are used in the present study.

3.6.1 Available Analyses Types in Seep/W Modeling

There are two fundamental types of finite element seepage analyses available with Seep/W modeling, namely the steady-state analysis and transient analysis. Both these types of analyses are used in the present study for various cases.

3.6.1.1 Steady State Analysis

The "steady-state" analyses describe a situation where the state of the model is steady and not changing with time. In a seepage analysis, for example, the "steady state" may indicate that the water pressures (whether hydraulic or pore-water) and flow rates have attained a steady value, and is supposed to be remaining at the achieved state for a long period, if not forever. In many cases where the geotechnical problem is exposed to nature with its cyclical changes, it is possible that a steady state will never be reached. The flow beneath a cutoff wall below a dam may come close to a steady state if the upstream conditions remain constant over time. The net surface infiltration and evaporation will never reach a long-term steady state. When simulating a constantly changing boundary condition, such as surface infiltration and evaporation, the numerical model works on the initial input parameters and tries to estimate the change in response to the boundary conditions applied over the length of time. If it is assumed that the boundary conditions are constant over time, then the model can compute the long-term outcomes. This type of analysis does not consider how long it requires achieving a steady condition. The model will reach a solved set of pressure and flow conditions for the given set of unique boundary conditions applied to it, and the time taken for the same would be considered as the extent of the analysis.

3.6.1.2 Transient State Analysis

A transient analysis, by definition, indicates a temporally varying boundary condition and a consequent temporally changing response of the numerical model, the temporal variation being dependent on the response of the model to the user-defined boundary conditions. In order to move forward in time during a transient analysis, it is important to specify the initial state of the boundary conditions and their change over the time. An incremental time sequence is required for all transient analyses, and the appropriate time sequence is problem-dependent. In most cases, it will likely be necessary to try a reasonable sequence, and then adjust the sequence as required in response to the computed results. The accuracy of the computed results depends, to some extent, on the size of the time step. Over the period of one-time increment, the process is considered linear. Each time step analysis is equivalent to a mini steady-state analysis. The incremental stepping forward in time is, in reality, an approximation of the nonlinear process. For the same rate of change, large time steps lead to more of an approximation than the smaller time steps. It follows that when the rate of change is high, the time steps should be small, whereas if the rate of change is low, the time steps may be large.

3.6.2 Available Analyses Types in Sigma/W Modeling

The Sigma/W module provides a number of analyses types, namely ‘in-situ analysis’, ‘load/deformation analysis’, ‘coupled stress/PWP analysis’, ‘stress redistribution analysis’, ‘volume change analysis’ and ‘dynamic deformation analysis’. For the present study, the former three analyses techniques are used.

3.6.2.1 In-situ Analysis

The initial stresses are established by applying the self-weight of soil by means of a body load. The specified unit weight multiplied by the element volume creates a downward nodal force. The value of Poisson's ratio (for each material) will control the development of horizontal stresses. The stiffness properties (e.g. Young's Modulus) of the materials does not influence the initial stresses. The ratio of horizontal (σ'_h) to vertical effective stresses (σ'_v) in saturated soils, having a history of one-dimensional deformation (e.g. sedimentation and possibly over consolidation), is called the coefficient of earth pressure at rest, and is expressed as

$$k_0 = \frac{\sigma_h^{'}}{\sigma_v^{'}} = \frac{\nu}{1-\nu} \tag{3.29}$$

Sigma/W limits the value of Poisson's ratio (ν) to 0.495; therefore, k_0 is limited to approximately 0.98. Overconsolidated soils generally have k_0 values that exceed this value; i.e., the effective horizontal stresses exceed the vertical effective stresses. The initial stress states with $k_0 > 0.98$ cannot be established using the 'In-situ' type of analysis. The well-established 'k_0 through gravity loading' technique is used for this type of problem.

3.6.2.3 Load / deformation analysis

The Load/Deformation Analysis is used for those problems wherein the resulting changes in stress and displacements are evaluated owing to the applied loads. Some of these problems include placement of fill and excavation or construction procedures. In the case of a fill placement analysis, the weight of the fill is added to the model on the first load step, and the resulting deformation is determined. In the case of an excavation analysis, Sigma/W calculates the resultant forces associated with the removal of the excavated elements and applies these forces as boundary loads at the nodes along the face of the excavation.

3.6.2.3 Coupled Stress / PWP Analysis

The coupled stress-PWP analysis requires the interaction of solid and fluid phases. The interaction is explained through the constitutive behavior of the soil skeleton and flow response of the water phase.

3.6.2.3.1 Constitutive Equation for Soil Structure

Considering an unsaturated soil medium, and assuming the soil to behave as an ideal elasto-plastic material, the incremental strain-stress relationship can be written as

$$\{\Delta\sigma\}-\{m\}\Delta u_a=\left([D_e]-\left[D_p\right]\right)\{\Delta\varepsilon\}-\left([D_e]-\left[D_p\right]\right)\{m_H\}\Delta\left(u_a-u_w\right) \tag{3.30}$$

where, $\{\Delta\sigma\}$ and $\{\Delta\varepsilon\}$ are the incremental stress and strain matrices respectively, u_a and u_w represents the pore-air pressure and pore-water pressure respectively. $\{m\}=\{1\ 1\ 1\ 0\ 0\ 0\}^T$ is the unit isotropic tensor, $\{m_H\} = \{1/H\ 1/H\ 0\ 0\ 0\}^T$, where, H is the unsaturated soil modulus for a soil structure with respect to matric suction $(u_a - u_w)$. $[D_e]$ and $[D_p]$ are the drained elastic and plastic constitutive matrices respectively. $[D_e]$ is the relation matrix between stress and elastic strain, while $[D_p]$ represents the impact of plastic strain on the relationship between the stress and the total strain. $[D_p]$ can be expressed as

$$\left[D_p\right]=\frac{[D_e]\left\{\dfrac{\partial G}{\partial\sigma'}\right\}\left\{\dfrac{\partial F}{\partial\sigma'}\right\}^T[D_e]}{\left\{\dfrac{\partial F}{\partial\sigma'}\right\}^T[D_e]\left\{\dfrac{\partial G}{\partial\sigma'}\right\}} \tag{3.31}$$

where, F and G denotes the yield function and plastic potential function respectively, while σ' is the effective stress.

It is assumed that the air pressure ever remained equal to the atmospheric pressure, which modified Equation 3.30 as

$$\{\Delta\sigma\}=\left(\left[D_e\right]-\left[D_p\right]\right)\{\Delta\varepsilon\}-\left(\left[D_e\right]-\left[D_p\right]\right)\{m_H\}\Delta u_w \tag{3.32}$$

Considering the soil to be completely saturated, Equation 3.32 is rewritten as

$$\{\Delta\sigma\}=\left(\left[D_e\right]-\left[D_p\right]\right)\{\Delta\varepsilon\}-\{m\}\Delta u_w \tag{3.33}$$

Upon comparing Equations 3.32 and 3.33, it can be seen that, for completely saturated soil, the following condition should be satisfied

$$\left(\left[D_e\right]-\left[D_p\right]\right)\{m_H\}=\{m\} \tag{3.34}$$

Thus, the modulus H can be obtained by solving Equation 3.34.

3.6.2.3.2 Flow Equation for the Water Phase

The equation governing the flow of water through unsaturated-saturated soils can be obtained by introducing Darcy's law into the continuity equation (Fredlund and Rahardjo, 1993). The resulting equation can be written as

$$\frac{k_x}{\gamma_w}\frac{\partial^2 u_w}{\partial x^2}+\frac{k_y}{\gamma_w}\frac{\partial^2 u_w}{\partial y^2}+\frac{\partial\theta_w}{\partial t}=0 \tag{3.35}$$

where, k_x and k_y are the hydraulic conductivities in the x- and y-directions respectively, γ_w is the unit weight of water, θ_w is the volumetric water content, u_w is the pore-water pressure, and t is the elapsed time. The volumetric water content increment, $\Delta\theta_w$, is represented by the following expressions (Dakshanamurthy et al., 1984)

$$\Delta\theta_w=\beta\Delta\varepsilon_v+\omega\Delta u_w,\quad \beta=\frac{E}{H(1-2\mu)},\quad \omega=\frac{1}{R}-\frac{3\beta}{H} \tag{3.35}$$

where, $\Delta\varepsilon_v$ is the volumetric strain increment, E is the elastic modulus, μ is the Poisson's ratio, R is a modulus relating the change in volumetric water content to the change in matric suction that can be obtained by inversing the slope of the volumetric water content curve.

The deformation compatibility equations can be used to relate the generated strains to the displacements. Considering increments in pore-water pressure and displacement as field variables, finite element method is applied to solve simultaneously the Equations 3.30 and 3.35, so that the stress, displacement and pore-water pressure could be obtained synchronously. In addition to the constitutive model of the material, the volumetric water content function and the hydraulic conductivity function are also required to carry out a 'Coupled stress – PWP analysis'.

3.6.3 Available Analyses Types in Slope/W Modeling

The different types of analysis present in Slope/W are based on the General Limit Equilibrium theory (GLE) or the Finite Element (FE) computed stresses within a limit equilibrium framework, as described in Section 3.2.2. The different methods based on GLE available are (a) Ordinary or Fellenius method (b) Bishop's simplified method (c) Janbu's simplified method (d) Spencer's method (e) Morgenstern-Price method (f) Corps of Engineers method (g) Lowe-Karafiath method (h) Sarma's method, and (i) Janbu's Generalized method. However, for the present study, the 'FE based stress' method is widely used for the determination of the factor of safety values. The use of finite element computed stresses inside a limit equilibrium framework to assess stability has many advantages. Firstly, there is no requirement to make assumptions about the interslice forces as they evolve during the analysis itself. Secondly, the stability factor is deterministically determined once the stresses are computed, and consequently, there are no issues with convergence during iterations. Thirdly, the issue of displacement compatibility is completely satisfied, and the computed ground stresses are much closer to reality. Fourthly, the stress concentrations are indirectly considered in the stability analysis, and hence, the soil-structure interaction effects are readily handled. Finally, the dynamic stresses arising from earthquake shaking can be directly considered in the stability analysis. Thus, FE computed stresses inside the LE framework finds more application while calculating the FoS through Slope/W modeling simulations.

3.7 PROJECT AND ANALYSES TREE

In Geostudio 2012, multiple analyses can be included in a single project that allows different material properties and different boundary conditions to be specified and implemented across the model as well as spanned in time. This facilitates sequential modeling of staged construction or excavation in which soil is added or removed over time and/or the boundary conditions or material properties change with time. Including multiple analyses in a single project could be used for a variety of reasons such as: (a) Conducting sensitivity analyses for variations in material properties and boundary conditions; (b) Analyzing staged construction; (c) Establishing initial conditions for a transient analysis; (d) Integrating various GeoStudio analyses modules; and, (e) Linking together multiple transient analyses.

GeoStudio uses a Parent-Child' terminology to describe the relative position of each analysis within a project. Figure 3.14 displays a typical 'Analysis Tree' combining the in-situ and coupled stress PWP analyses (utilizing Sigma/W module), seepage analysis (utilizing Seep/W module), and the slope stability analysis (utilizing the Slope/W module). The steady-state analysis assigned to Seep/W module is the 'Parent' that is used to define the initial pore-water pressure conditions and total head conditions. The initial stress conditions are generated using the in-situ analysis of Sigma/W where the pore-water pressure distributions are derived from the parent Seep/W analysis. Hence, the Sigma/W analysis becomes the 'Child' carrying the information of the 'Parent'. The

Coupled Stress/PWP analysis from Sigma/W module is used to simulate the response of a transient reservoir operation, in which the stress and pore pressure conditions are derived from the in-situ analysis. Finally, a slope stability analysis is carried out the 'Project', as a 'Child' utilizing the stress and PWP distributions from the 'Parent' i.e. the coupled stress/PWP analysis. One significant benefit of the 'Analysis tree' is that all the analyses related to a specific project are contained within a single file, and are linked to each other. It would not be necessary to refer other files to establish initial conditions or integrate the various GeoStudio products.

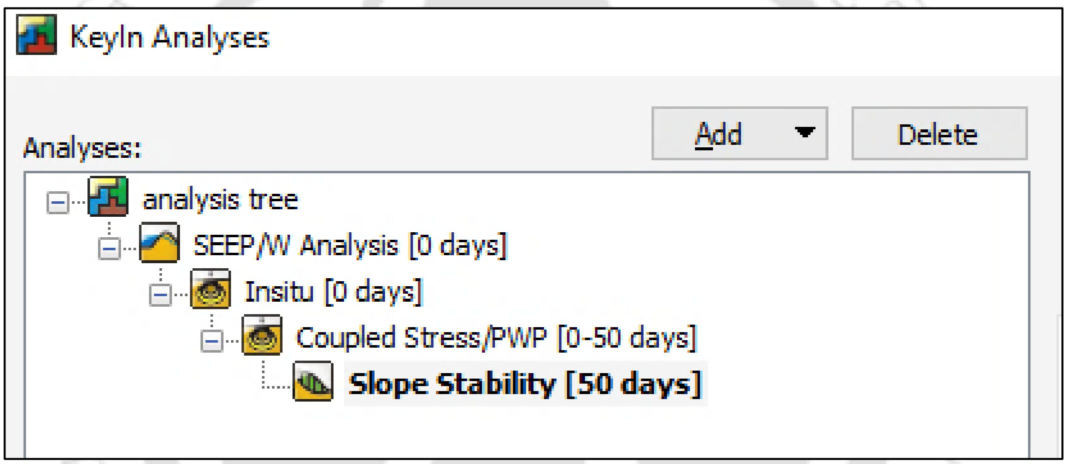

Figure 3.14 A typical representation of an 'Analysis Tree' from a GeoStudio 2012 'Project'

3.7 SUMMARY

This chapter provides a background of the numerical modelling and methods adopted in the study of the dissertation work. The working principles of various important modules of GeoStudio software package, which are used in the present study (Seep/W, Sigma/W and Slope/W), are discussed. A brief discussion is also provided about the FE modelling and its intricacies related to geometry and domain definition, meshing and mesh characteristics, as well as boundary conditions. A description is provided related to various material models, along with their constitutive behaviour and input properties, which are used in the present study. Finally, a description is provided about the various types of analyses available, their solution strategies and their mathematical formulations. The chapter gives a detailed insight about the details of various types of analysis that can be carried out in Geostudio, and which is used for the rest of the study, as would be described in the subsequent chapters of the dissertation report.

CHAPTER 4

RESPONSE OF HOMOGENEOUS EARTHEN DAM SUBJECTED TO CLOGGING OF DRAINAGE BLANKET

4.1 GENERAL

The phenomenon of transport and filtration of particulate mixtures in porous media is a challenging and important domain in science and engineering. An important application is the stability of earth and rockfill dams and embankments. Earthen dams are always associated with the seepage of water impounded in the upstream reservoir that constantly attempt to traverse the path of least resistance through the body of the dam and its foundation. Thus, the most critical requirements of a safe design of an earthen dam involves appropriate internal filtering and drainage to control the saturation level and maintain the seepage pressure at a safe level, so that the removal of fine soil particles from the critical zones in the embankment and foundation is inhibited, if not completely prevented (USBR, 1987). However, while these soil filters and drainage layers are expected to serve the purpose of protecting the earth dams in their fully functioning capability, the temporal or spatial reduction in the permeability of filters and drainage blankets becomes a very critical issue. During the service period of the dam, the soil filters and drainage blankets might undergo significant reductions in permeability owing to the progressive fine particle entrapment, a phenomenon commonly known as clogging, which is capable of seriously detrimenting the long-term stability and safety aspects of the dam. Many studies during the recent decades were fueled by unending revelations of dam failures associated with inadequate filter design (Peck, 1990; Vick, 1996). Studies have shown that poor drainage caused by particulate clogging of the pavement materials continues to cost billions of dollars to the United States (Cedergren, 1994). Koerner and

Koerner (1991) concluded that particulate clogging was a major factor in flow rate reductions of drainage layers. Researchers have discussed the most common forms of drainage clogging and its influence on seepage through foundation for concrete dams built on permeable rock foundations (Silva, 2015). Particulate clogging in porous media is a subject of importance in several disciplines, in addition to geotechnical and geo-environmental engineering (Reddi et al., 2000). A need, thus, exists to assess the impact of particulate clogging on drainage capacities of soil filters and to consider the factors responsible for the clogging in the design process. In this work, an attempt is made to understand the flow and deformation response of small earthen dams to the most common forms of clogging encountered in horizontal toe drainage blankets and inclined chimney drainage blankets.

4.2 VALIDATION STUDY: FAILURE OF GLEN SHIRA DAM, SCOTLAND

The evolution of Finite Element Method (FEM) from a research tool into a daily engineering tool has resulted in its immense application for the analysis of geotechnical engineering problems. Its ability to tackle complex real field situations has placed it next to conventional design methods. However, with many advantages provided by the usage of FEM, like every other method, it also suffers from some limitations owing to the lack of knowledge from the user in terms of the appropriate use of the same. These limitations can lead to unrealistic results as, many a time these limitations go unrecognized by the finite element users. In spite of the development of easy-to-use finite element programs, it is not always easy to create an efficient model that can capture all the uncertainties and complexities associated with the real field problem to provide a realistic prediction of the design quantities (such as displacements, stresses, pore pressures, structural forces, bearing capacity, safety factor, drainage capacity, and pumping capacity). These limitations are more likely to get pronounced in geotechnical applications as the highly non-linear and heterogeneous behaviour of the soil material makes it difficult for the numerical models to capture its character accurately. When finite element method (FEM) is used to model soil behaviour by means of a constitutive model (stress-strain relationship) formulated in a continuum, the choice of the constitutive model plays a vital role. Additionally, the corresponding set of model parameters used in modeling should also be considered carefully when creating a finite element model for a geotechnical project. The model, no matter how complex, will always be a simplified representation of the actual soil behaviour that forms one of the main limitations in the numerical modeling process. Hence, some features of soil behaviour will not be captured by the model. Therefore, validation of the numerical models with the actual field scenario becomes essential. Validation confirms the accuracy with which the model captures the reality. The correctness and acceptability of the numerical model, once established with proper validation, makes it more reliable to be used in different design process. In this work, a numerical model simulating an earthen dam subjected to the reservoir drawdown condition is validated with real field measurements.

Drawdown becomes a critical factor to assess the stability of slopes that are submerged partially or completely in their initial state. During drawdown, the removal of reservoir water results in an unloading effect, thereby leading to the reduction of the stabilizing external hydrostatic pressure. This phenomenon results in the modification of the internal pore-water pressure (PWP) within the dam body, especially towards the upstream face. The dissipation of pore-water pressure is very much dependent on the rate of drawdown. If the drawdown rate is high (i.e. rapid drawdown), then it results in a delay in the dissipation of pore-water pressure from the upstream slope, and the remaining excess pore-water pressure may induce failure of upstream slope. The effects of drawdown of reservoir water on the stability of slopes and dams are reported from different perspectives based on laboratory tests (Yan et al., 2010; Wang et al., 2012), numerical analyses (Viratjandr and Michalowski, 2006), and limit analyses (Gao et al., 2014). The solution of the uncoupled-flow problem, to evaluate the effect of hydraulic properties, are studied in previous researches (Song et al., 2015). There are investigations that are carried out to calculate the transient seepage, induced by the influence of drawdown, on slope stability using a flow program, while a coupled program is used for the deformation and stability analysis (Berilgen, 2007). There are ample examples of coupled flow-deformation analysis (Brinkgreve et al., 2015) and analysis of real cases (Zhang et al., 2010; Li et al., 2010). In addition, examples of drawdown-induced failures can be found in Sherard et al. (1963) and von Thun (1985), which highlighted the importance of measurement of pore-water pressure during the drawdown condition. The estimation of pore-water pressure distributions due to a drawdown is thus rendered an important factor in analysis of the slope stability.

Proper design, construction, and monitoring of the actual behaviour of an earthen dam, during its construction and operation, depends on its face stability and the resistance to instability (represented by factor of the safety) under several possible destabilizing conditions. Monitoring the generation of pore-water pressure in earthen dams during different operations (end of construction, reservoir filling, steady-state condition and reservoir drawdown) gives information on the behaviour of the structure and its interaction with the foundation. Field or laboratory prototype monitoring results can be used in validating the finite element models developed to perform the numerical analysis. The accuracy of the finite element models that are used to simulate the real field scenarios becomes acceptable when the data obtained from these models agrees reasonably well with the monitored data. Thus, the main objective of the work reported in this chapter is to validate a numerical model developed to simulate reservoir drawdown condition in an earthen dam. The numerical model is developed in GeoStudio, and it is used to ascertain the accuracy of numerically simulated pore-water pressure magnitudes by comparing it with the field-monitored data. To meet this objective, a finite element analysis on the Glen Shira Dam, Scotland, was performed considering a drawdown condition, and the results from the numerical analyses were compared with the field measurements.

4.2.1 Model for the Validation Study

The model used in the present study is developed for the Glen Shira Dam, which has a height of 16 m and possess a thin reinforced concrete wall at the center. The dam is mainly made of compacted well-graded non-plastic moraines. A rockfill shell covers the upstream slope of compacted moraines to increase the stability of the upstream shoulder. A detailed description of the dam and its materials is provided in Paton and Semple (1961). The stratum consists of rock structure comprising mainly soft phyllite with occasional hard bands of quartzite and quartz-schist, and an extensive zone of limestone (Paton, 1956). It is not mentioned clearly whether the foundation stratum is explicitly impervious or not. Going by the geological information provided, it can be guessed to be a mostly impervious foundation, with interstitial occurrences of cavities and fissures. A typical cross-section of the Glen Shira Dam, having the maximum width, is shown in Figure 4.1. The dam has a crest width of 3 m and it has a free board of 1 m. The foundation height and width are chosen to be 10 m and 108 m, respectively. The upstream and downstream slope inclinations are shown in Figure 4.1.

4.2.2 Material Properties

In numerical modeling, the correct assignment of the material models with proper input parameters plays an important role. In this validation study, Seep/W and Sigma/W modules of Geostudio have been used. In Seep/W analysis, the dam is modeled using a 'saturated/ unsaturated' material model, while the foundation is modeled using 'saturated only' material model. In Sigma/W, the 'elastic-plastic material' model is used to perform the analysis. The materials comprising the dam, having modeled using 'saturated/ unsaturated' material model, requires the assignment of the hydraulic conductivity function and the volumetric water content function for the analysis. These functions for the different materials used in the dam are shown in Figure 4.2.

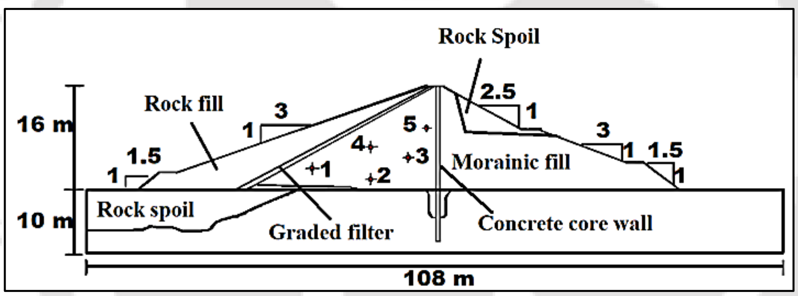

Figure 4.1 Model of Glen Shira Dam used for the validation study

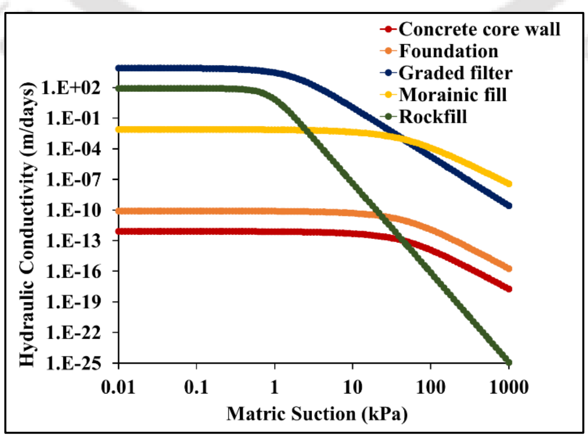

Figure 4.2 (a) Hydraulic conductivity function of materials used in validation study

The various soil properties used in the modeling are obtained from extensive literature survey (Alonso and Pinyol, 2016; Paton and Semple, 1961; USBR, 2014; Seep/W, 2012; Sigma/W, 2012) and are coupled with proper engineering judgment. The different material properties; cohesion (*c*), angle of internal friction *(ø),* unit weight of the materials (*γ*), modulus of elasticity ($E_{modulus}$) and permeability *(k)* used in the analysis, are listed in Table 4.1.

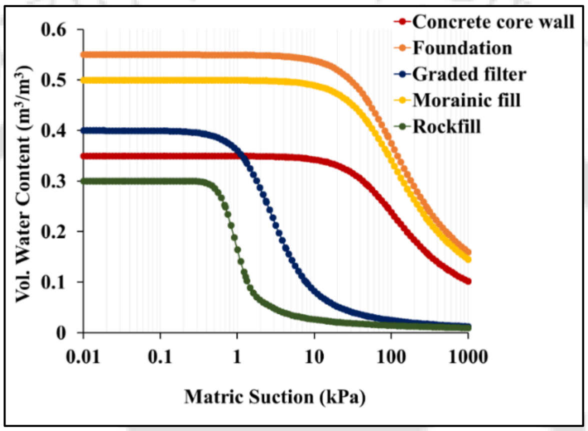

Figure 4.2 (b) Volumetric water content function of materials used in validation study

Table 4.1 Material properties used in simulation of Glen Shira Dam

Material	*c* (kPa)	*ø* (degree)	*γ* (kN/m^3)	$E_{modulus}$ (kPa)	*k* (m/s)
Morainic fill	15	25	18	5000	10^{-8}
Graded filter	0	25	16	10000	10^{-1}
Concrete core wall	12	20	18	25000	10^{-18}
Rockfill	0	30	16	15000	10^{-3}
Foundation	12	18	20	30000	10^{-16}

4.2.3 Analyses Methodology

The modeling of the Glen Shira dam construction was conducted in simple sequential steps. The present numerical study is conducted with the aid of Seep/W and Sigma/W modules of Geostudio. The main objective of this work is to ascertain the accuracy of the numerically simulated pore-water pressures in Geostudio generated during a reservoir drawdown condition in the dam. The results obtained from Geostudio was validated with field-monitored data, as well as compared with the results obtained from another finite element program Code_Bright. The field data was monitored at five (5) different points with the help of the piezometers, as shown in Figure 4.1. Barcelona Basic Model (BBM), which can capture the effect of the elastoplastic behavior observed in soils, was used in Code_Bright finite element program as an appropriate constitutive model for simulating the soil response in saturated and unsaturated conditions (Alonso and Pinyol, 2016). In Geostudio, at first, Seep/W is used to simulate the initial steady-state seepage analysis across the dam section, and the existing pore-water pressures and total head conditions are established. The initial stress conditions were generated using the in-situ analysis of Sigma/W. The drawdown of the reservoir is analyzed using the Coupled Stress/PWP analysis in Sigma/W, in which the pore-water pressure generated in the steady-state analysis and stresses generated in the in-situ analysis were used to define the initial conditions for the transient state. The rate of reservoir drawdown is a function of total head with time, as shown in Figure 4.3; and it is assigned as a boundary condition along the upstream side of the dam. The results obtained from the analyses were compared with the existing field-monitored and numerical data to check for the accuracy of the numerical model developed in Geostudio. A detailed analysis of the results obtained from the simulations along with the discussions is provided in the next section.

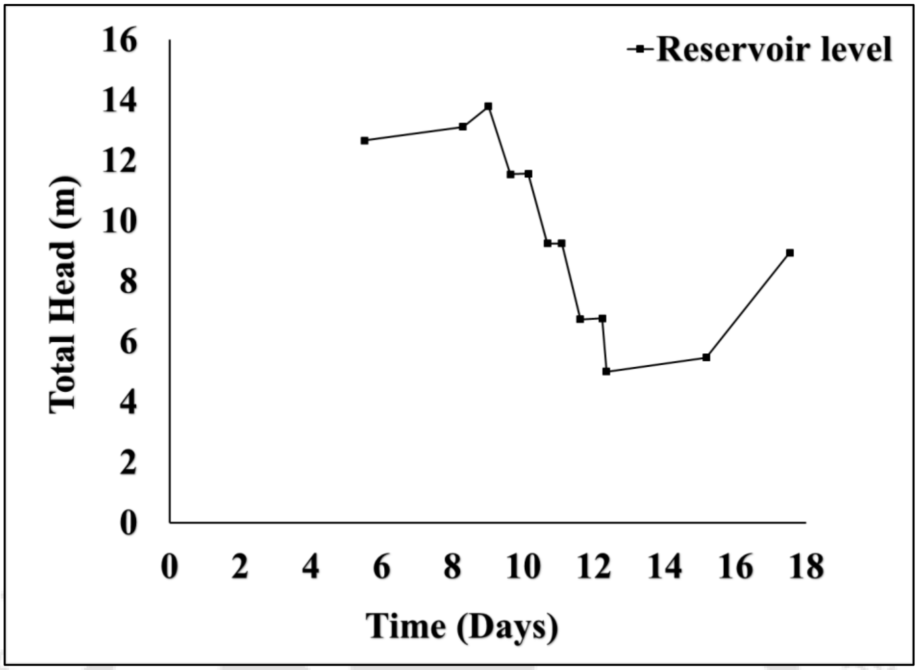

Figure 4.3 Reservoir drawdown condition as adopted in the Glen Shira Dam, Scotland

4.2.4 Results and Discussions

The variation of total head with time that is obtained from the numerical simulations performed in Geostudio are compared with the measured values obtained from the five different piezometer readings as shown in Figures 4.4-4.8; the locations of the piezometers are provided in Figure 4.1. The results from the finite element program Code_Bright, obtained from the work by Alonso and Pinyol (2016), are also plotted in the corresponding figures (Figures 4.4-4.8) to get a better understanding of the nature of the temporal variation of total head during the reservoir drawdown condition. The drawdown history of the reservoir level is also indicated in each of the figures.

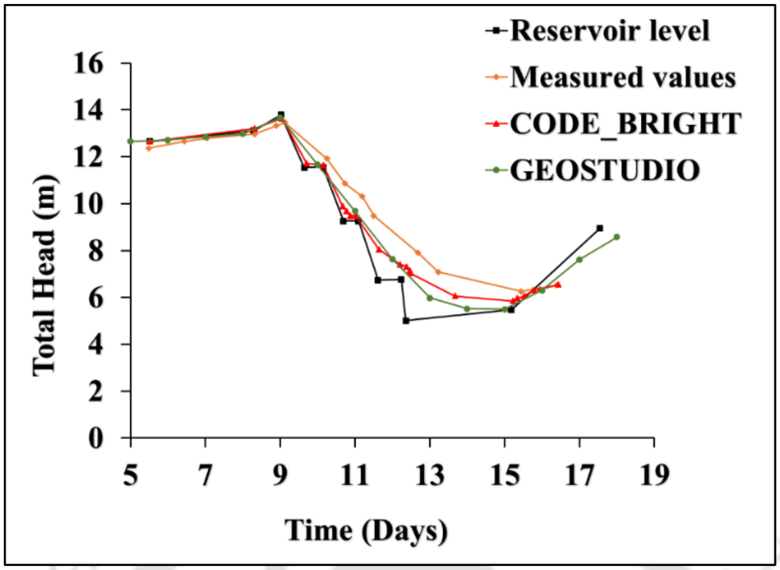

Figure 4.4 Comparison with measured pore-water pressures in Piezometer 1

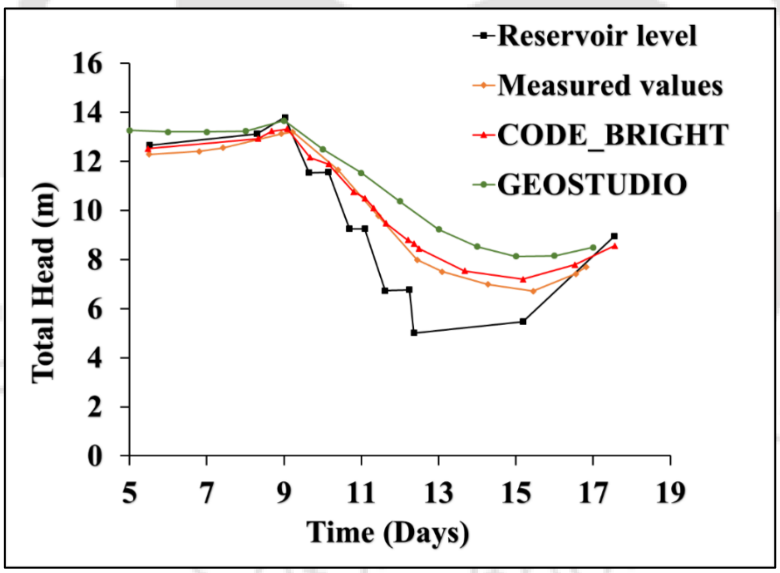

Figure 4.5 Comparison with measured pore-water pressures in Piezometer 2

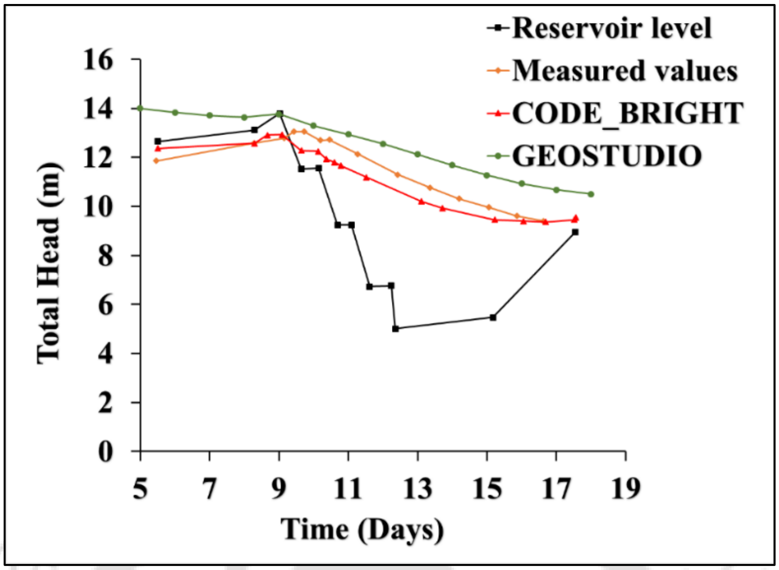

Figure 4.6 Comparison with measured pore-water pressures in Piezometer 3

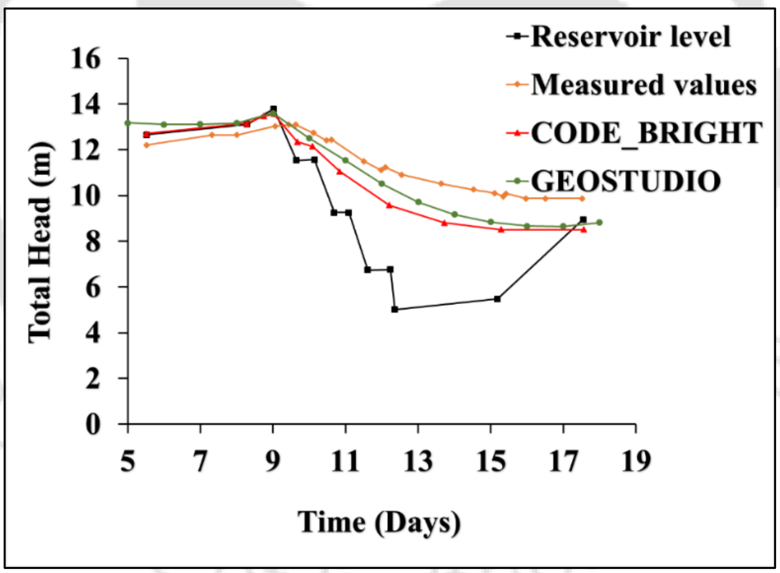

Figure 4.7 Comparison with measured pore-water pressures in Piezometer 4

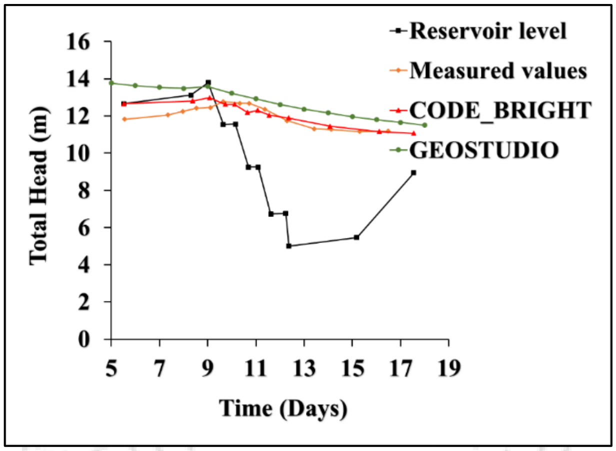

Figure 4.8 Comparison with measured pore-water pressures in Piezometer 5

The figures give a detailed comparison between the simulated values of pore-water pressures along with the corresponding measured values from the five piezometers. It is observed that the pore-water pressure values obtained from the numerical model simulated in Geostudio (using coupled flow/deformation analysis) satisfactorily agrees with the measured values from the field and as well as with the calculated values obtained from Code_Bright (simulated using a coupled flow-elastic deformation analysis for saturated/unsaturated conditions). The temporal variation of recorded pore-water pressures is appreciably captured by the numerical model. For the five field measurement points (in numbered sequence), the percentage average difference between the results come out to be 7, 11, 8, 3 and 6%, respectively. All the magnitudes being within or near the limit of 10%, and the trends being appreciably similar, the numerical results are adjudged to be in appreciable agreement with the field-measured values. A better agreement between measurements and calculations probably requires the consideration of certain field heterogeneity in the permeability and/or soil stiffness. An attempt is made to plot the total head contours obtained from Geostudio and to compare the same with the computed results from Code_Bright (Alonso and Pinyol, 2016) as well as with the interpolated values potted by Paton and Semple (1961). The distribution of total head contours inside the shell for a drawdown from 14 m to 5.2 m are shown in Figure 4.9(a-c). The total head contour values and distribution obtained from Geostudio gives very similar nature when compared with the computed and interpolated values.

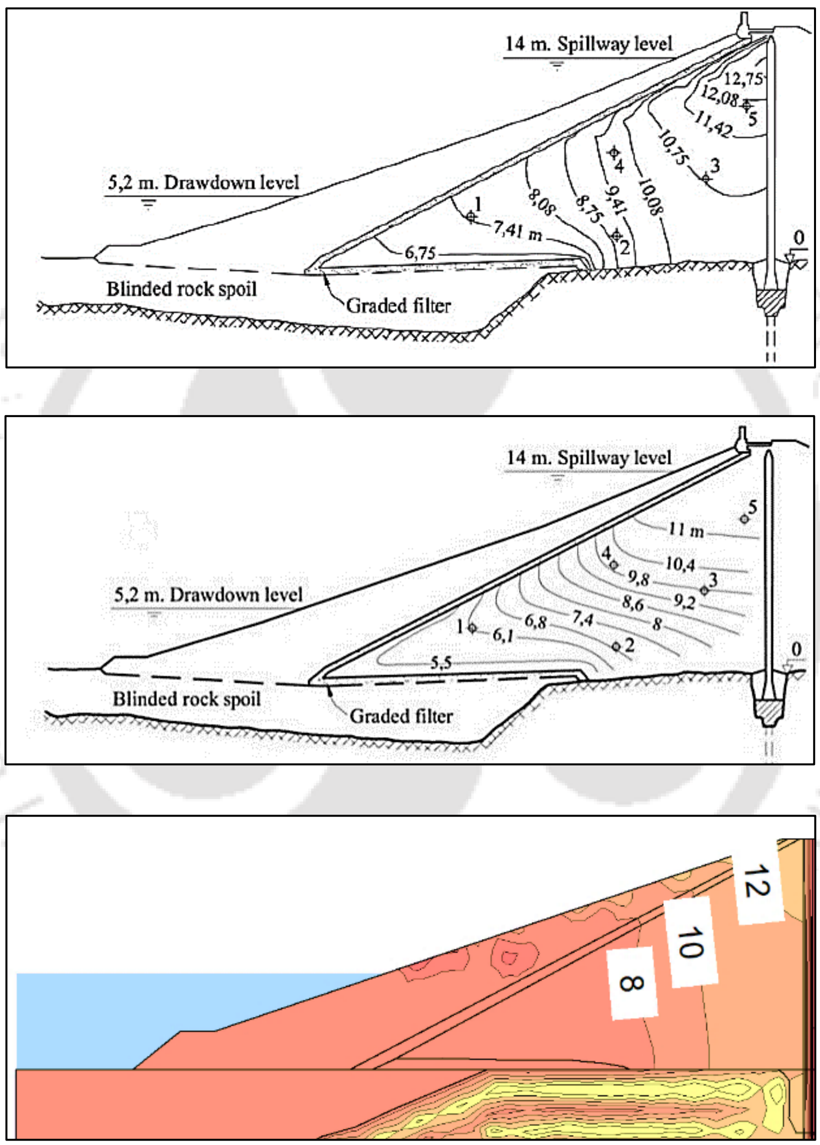

(a)

(b)

(c)

Figure 4.9 Distribution of the total head inside the shell of the Glen Shira dam for a drawdown from 14 m to 5.2 m (a) computed results from Code_Bright; (b) interpolated values plotted by Paton and Semple (1961), and (c) computed results from Geostudio

Thus, in this Section 4.2, a well-documented case history (Glen Shira Dam) was analyzed using Geostudio to provide insight into the accuracy of the numerical model in simulating drawdown problem. The dam used in this study includes soil (a compacted moraine) that has an intermediate permeability between impervious clays and free draining granular materials. It should be added that materials with this intermediate permeability are very common in dam engineering and dam construction. The fully coupled flow/deformation analysis is used to simulate this problem. The results from the analysis are compared with the calculated values obtained from Code_Bright and with the measured values from the field. The comparison shows a reasonably good agreement of the water pressure values obtained from Geostudio with that of the field measured values and the calculated values from the finite element program. Thus, it indicated that the numerical model simulated in Geostudio is capable of capturing the drawdown scenario accurately to a significant extent and it can further be used to simulate other destabilizing scenarios.

4.3 RESPONSE OF HOMOGENEOUS EARTHEN DAMS TO CLOGGING OF DRAINAGE BLANKET

Along the life of a dam, drains and drainage blankets can clog and lose their designed capacities to carry the seepage flow and control the uplift pressures. This can be observed either visually or through instrumental readings. If clogging occurs, the readings will often indicate a decrease of flow in the drains and an increase in the exit pressures in the foundations of the dam. There are many causes of drain clogging, and the most common ones include the calcium carbonate deposits from the dam concrete, the grout curtain, the foundation rock (Ruggeri, 2004) or bacterial deposits (Rutenback and Day, 1999). The other causes are the accumulation of materials from the drain walls, or that carried by seepage into the drains, or a combination of both. The effects of drain clogging generally can lead to a reduction of drain diameter, a reduction of drain length or a reduction of the drain's capacity to carry the flow. Therefore, there is a need to study the influence of drain clogging on the response of the dam. Numerical modeling makes it easier and faster to simulate the various possible scenario of clogging to have a detail understanding of its effect on dams. The study reported here was conducted using the three different modules i.e., Seep/W, Sigma/W and Slope/W of the finite element software GeoStudio. The working mechanism of these modules is already discussed elaborately in Chapter 3.

4.3.1 Model for the Present Study

In the present work, the flow and deformation response of small homogeneous earthen dams, subjected to clogging of horizontal and inclined chimney drainage blanket, is studied during both steady-state and reservoir operation conditions. The reservoir operation condition includes the rise-up and drawdown conditions. The models used in the study with its relevant dimensions are shown below in Figure 4.10 and Figure 4.11 (a, b). The height of the earthen dam is chosen 10 m and its width is selected as 50 m. The upstream slope has an inclination of 2.5H:1V and downstream slope has an inclination of 2.2H:1V. The earthen dam has a crest width of 3 m and it has a free board of 1 m. The height and width of the foundation are considered 10 m and 80 m respectively.

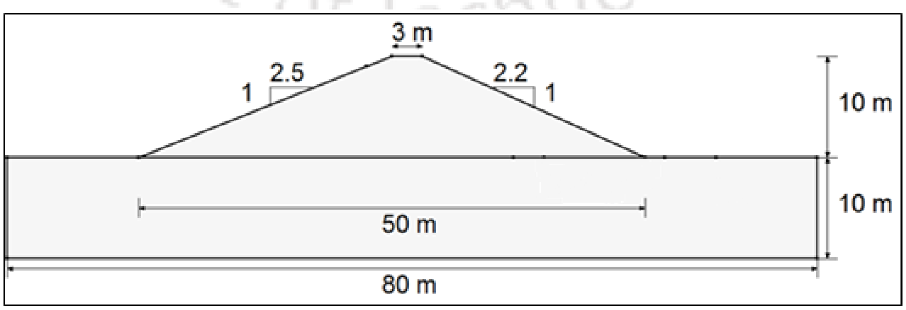

Figure 4.10 Model for the present study with no drainage blanket

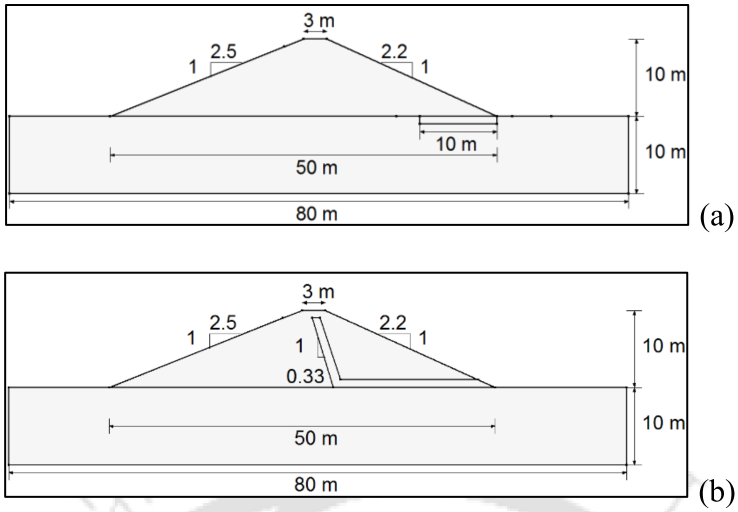

Figure 4.11 (a) Model for the present study with horizontal toe drainage blanket (b) Model for the present study with inclined chimney drainage blanket

The length of the horizontal toe drainage blanket is considered 10 m and its width is 1 m (as per IS 12169: 1987), whereas the inclined chimney drainage blanket has a width of 1 m and an inclination of 0.33H:1V. The development of the model geometry with the help of points, lines and regions were carried out in Geostudio as described in Chapter 3. The effect of clogging in the present study is simulated by reducing the permeability of the drain material in a sequential approach as required to simulate various models of clogging. In order to simulate the different possible scenarios of clogging, the permeability reduction in the drain has been done in different stages, for which the total length or width of the drain has been divided into different sections. A detailed study of various cases is carried out, which includes the reduction of the drain length, the reduction of the drain thickness and a random clogging scenario of the drainage blanket. The clogging of drainage blankets can lead to the reduction of the drain length and width, which can initiate from either ends of the drain (the outlet end or the inlet end, respectively), as shown from Figures 4.12-4.23.

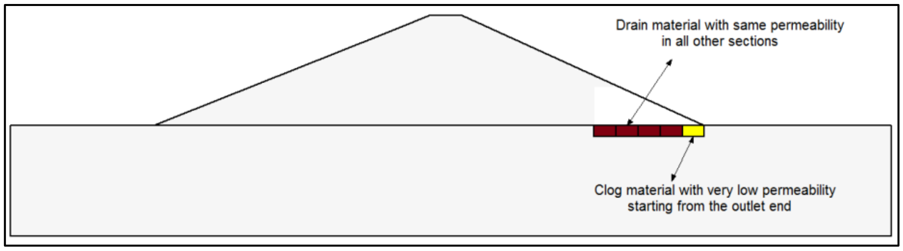

(a)

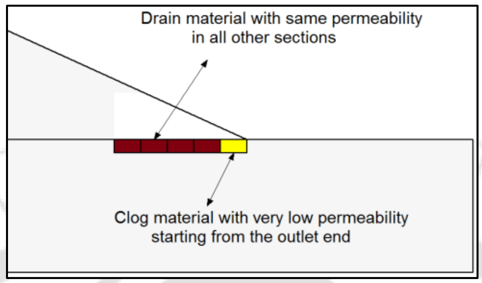

(b)

Figure 4.12 Inward clogging starting from outlet end of horizontal toe drainage blanket (a) Dam section with the clogged drain (b) Enlarged section of the clogged drain

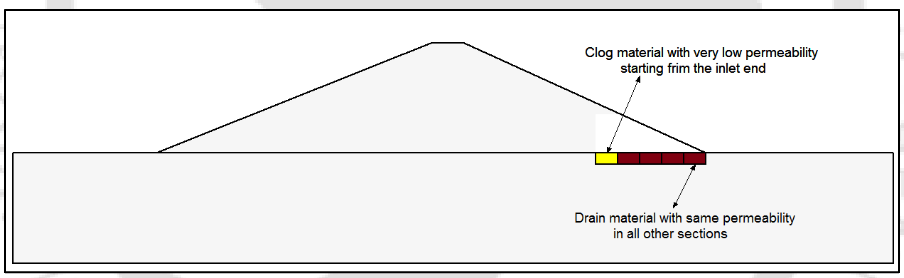

(a)

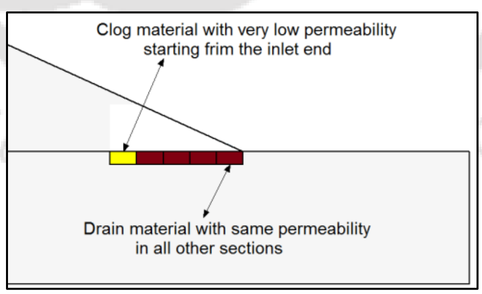

(b)

Figure 4.13 Outward clogging starting from inlet end of horizontal toe drainage blanket (a) Dam section with the clogged drain (b) Enlarged section of the clogged drain.

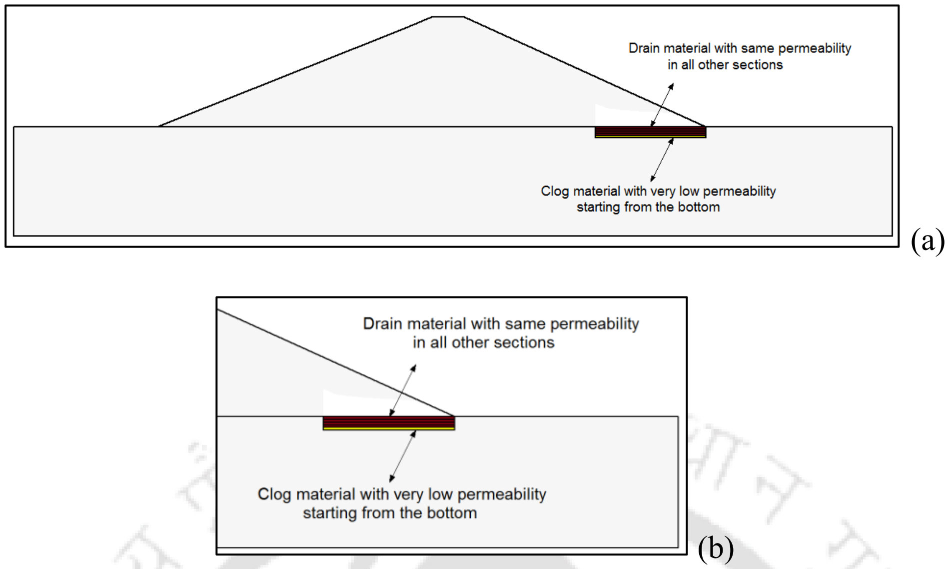

Figure 4.14 Upward clogging starting from the bottom of horizontal toe drainage blanket (a) Dam section with the clogged drain (b) Enlarged section of the clogged drain.

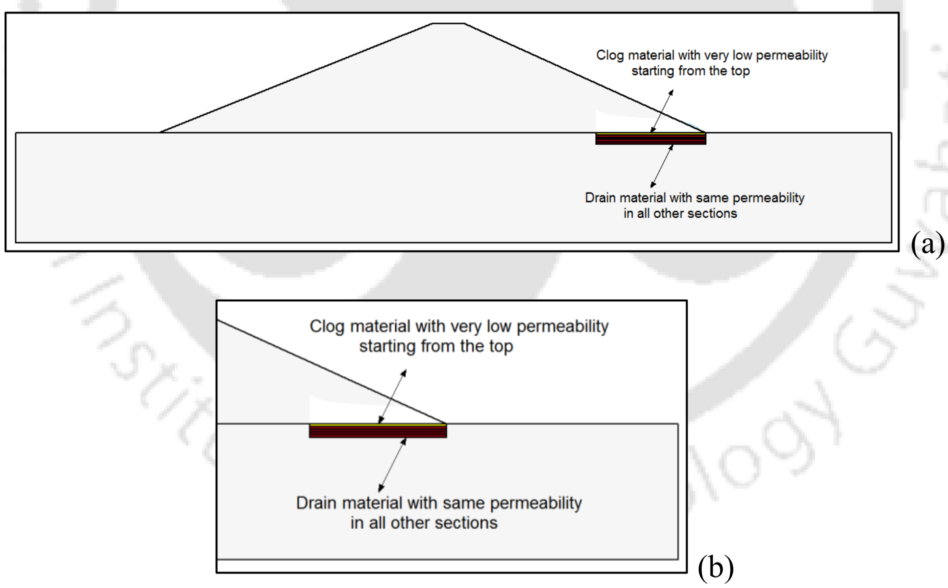

Figure 4.15 Downward clogging starting from the top of horizontal toe drainage blanket (a) Dam section with the clogged drain (b) Enlarged section of the clogged drain

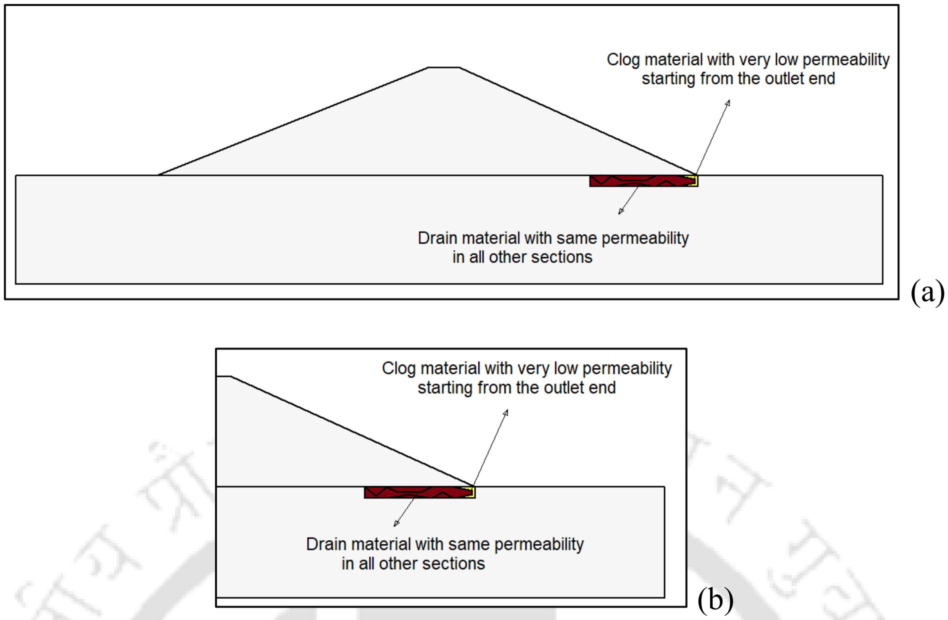

Figure 4.16 Random clogging starting from the outlet end of horizontal toe drainage blanket (a) Dam section with the clogged drain (b) Enlarged section of the clogged drain

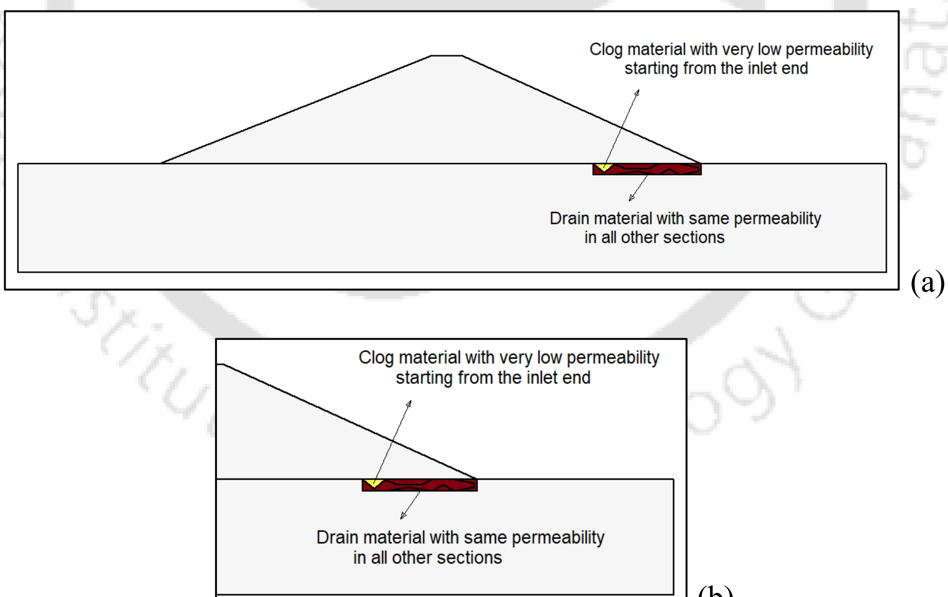

Figure 4.17 Random clogging starting from the inlet end of horizontal toe drainage blanket (a) Dam section with the clogged drain (b) Enlarged section of the clogged drain

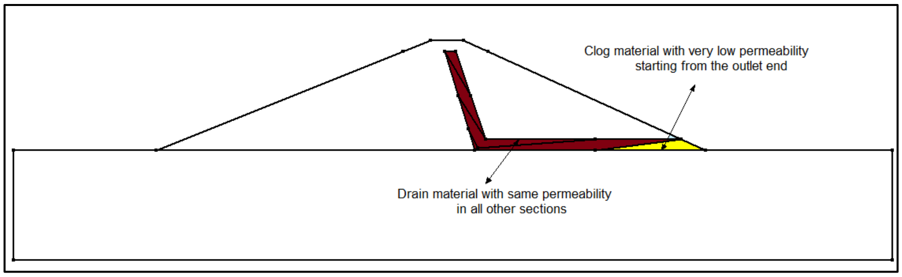

(a)

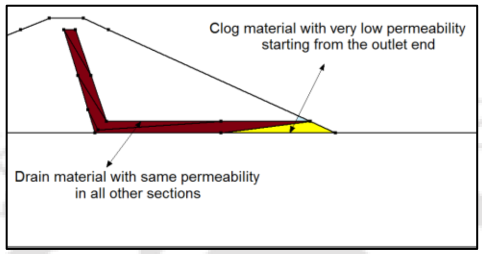

(b)

Figure 4.18 Inward clogging starting from outlet end of inclined chimney drainage blanket (a) Dam section with the clogged drain (b) Enlarged section of the clogged drain

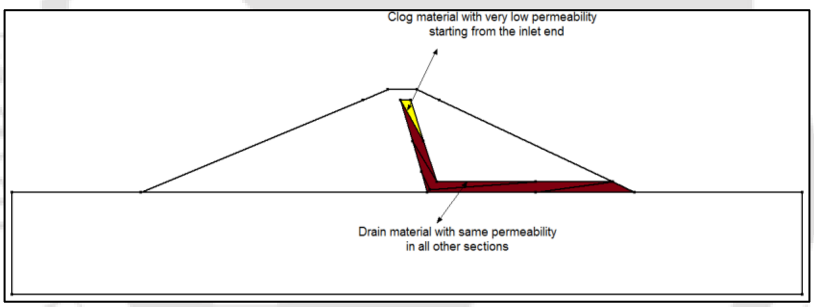

(a)

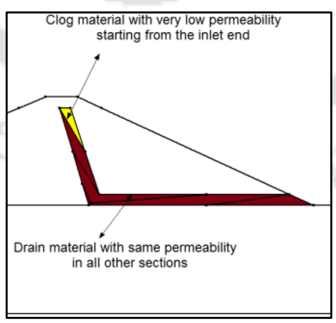

(b)

Figure 4.19 Outward clogging starting from inlet end of inclined chimney drainage blanket (a) Dam section with the clogged drain (b) Enlarged section of the clogged drain

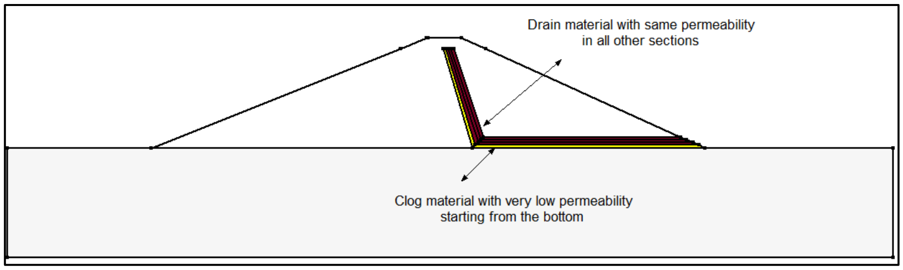

(a)

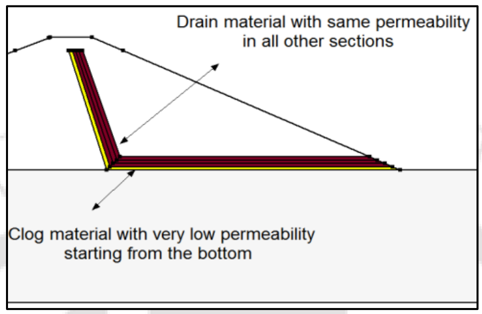

(b)

Figure 4.20 Upward clogging starting from the bottom of inclined chimney drainage blanket (a) Dam section with the clogged drain (b) Enlarged section of the clogged drain

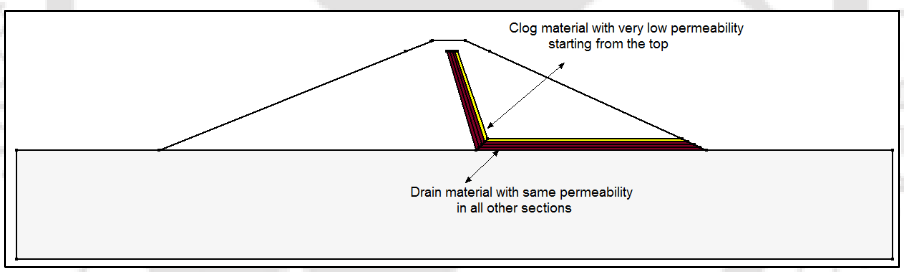

(a)

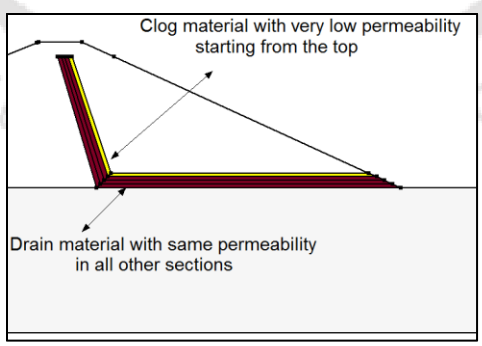

(b)

Figure 4.21 Downward clogging starting from the top of inclined chimney drainage blanket (a) Dam section with the clogged drain (b) Enlarged section of the clogged drain

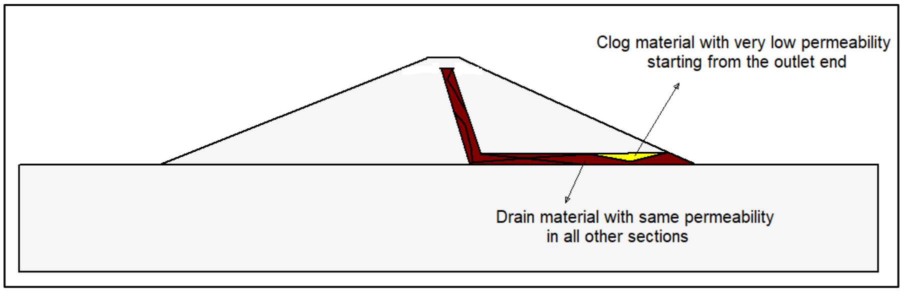

(a)

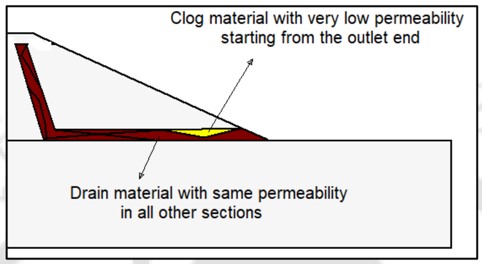

(b)

Figure 4.22 Random clogging starting from the outlet end of inclined chimney drainage blanket (a) Dam section with the clogged drain (b) Enlarged section of the clogged drain

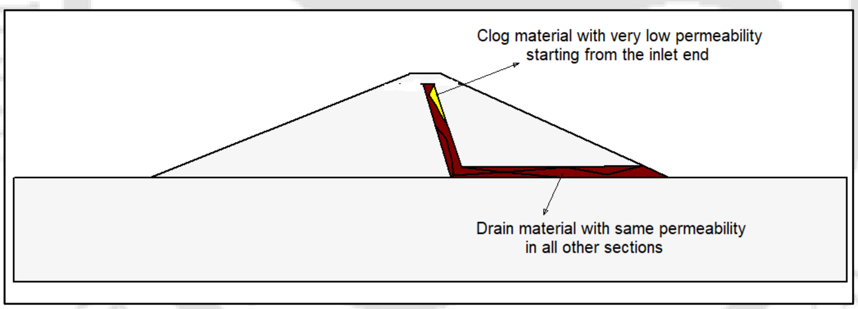

(a)

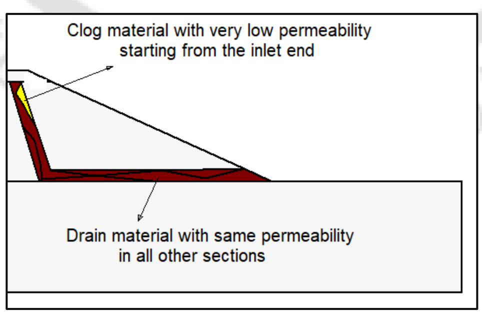

(b)

Figure 4.23 Random clogging starting from the inlet end of inclined chimney drainage blanket (a) Dam section with the clogged drain (b) Enlarged section of the clogged drain

4.3.2 Material Properties

The simulation of different models, comprising different soil characteristics, requires the correct assignment of the material models with proper input parameters. In Seep/W analysis, the earthen dam is modeled using 'saturated/ unsaturated' material model, while the foundation is modeled using 'saturated only' material model. In Sigma/W, the 'elastic-plastic' material model, under 'effective parameters with pore-water pressure change (effective parameters w/PWP change)' category, is used in the deformation analysis. With the aid of Slope/W, to obtain the corresponding stability of the slope face, a stress-based stability analysis is performed using the 'Mohr-Coulomb' material model. The detailed description about the different material models and material categories was provided in Chapter 3. In Sigma/W analyses, the hydraulic conductivity function and the volumetric water content function for the materials representing the earthen dam, foundation, drainage blanket and the clog material are shown in Figure 4.24.

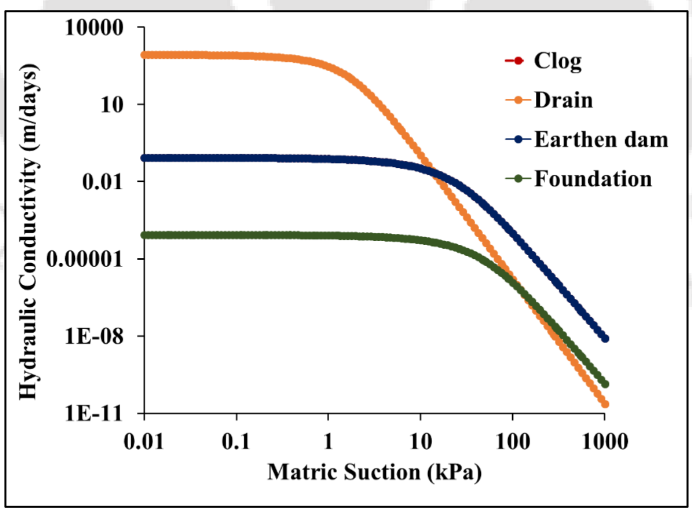

(a)

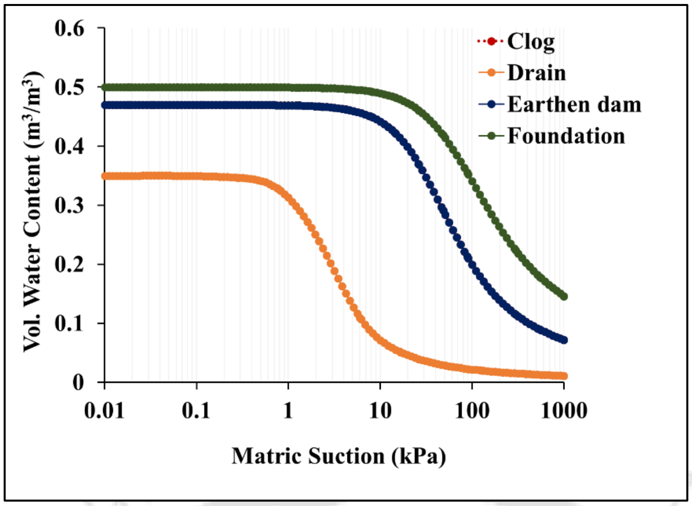

(b)

Figure 4.24 Properties of various material as used for Sigma/W analyses (a) Hydraulic conductivity function (b) Volumetric water content function

The various soil properties used in the modeling are obtained from extensive literature survey (IS 12196; USBR 1987; USBR 2014; Seep/W 2012) and coupled with proper engineering judgment. The strength and stiffness properties of various materials used in the numerical simulation is listed in Table 4.2.

Table 4.2 Material properties of various components used in the simulation of drainage clogging

Material	c (kPa)	$ø$ (degree)	γ (kN/m^3)	$E_{modulus}$ (kPa)	k (m/s)
Earthen dam	10	25	20	15000	10^{-7}
Impervious Foundation	15	20	20	30000	10^{-10}
Drainage blanket	2	30	18	12000	10^{-2}
Clog	10	25	20	15000	10^{-7}

It is observed from Figure 4.24, as well as from Table 4.2, that the properties for the earthen dam material and clog material are the same, as it is considered that finer materials in the earthen dam will migrate and lead to the clogging of the drains. During the clogging process, the materials with which the drain can be clogged cannot have permeability values lower than that of the earthen dam materials. Hence, the plots for clog and earthen dam materials, as shown in Figure 4.24, is considered same, and thus overlapping plots are obtained.

4.3.3 Meshing and Boundary Conditions

The discretization of the models was carried as described in Chapter 3. The models adopted in the present study used a global element size of 1 m, consisting of unstructured pattern of first-order quadrilateral and triangular elements. The number of nodes and elements varied for different simulations within a range of 1100 to 1500. The boundary conditions are, in essence, the driving force that results in the solutions of the numerical problems. In a steady-state analysis, where water pressures and water flow rates do not change with time, all of the boundary conditions comprise either fixed heads (or pressure) or fixed flux values. However, in a transient analysis, where pressure conditions changes with time, the boundary conditions are adopted either to be functions of time or considered as a response to flow volumes exiting or entering the flow regime. In case of steady-state analysis, the present simulation utilizes a fixed total head boundary condition, a potential seepage face boundary condition and a stress/strain boundary condition at the upstream and downstream faces and the base of the earthen dam. However, in the transient analysis, the total head and reservoir elevation is considered a function of time along the upstream face of the dam. The method of application of the boundary conditions and their detailed description are already presented in Chapter 3.

4.3.4 Stages of Analyses

Different stages of analyses were performed for the present study. The simulation of multiple analyses in a single GeoStudio project is already elaborated in Chapter 3. The main objective of this work was to study the flow and deformation response of earthen dams during steady-state and reservoir operation conditions as the drainage blankets are subjected to clogging. To achieve this objective, firstly, using Seep/W, different models were simulated for 'initial steady-state seepage analysis' to establish the in-situ pore-water pressures and total head conditions under steady-state conditions. The initial stress conditions were generated using the 'in-situ analysis' of Sigma/W module. The different clogging scenarios are modeled using the 'Coupled Stress/PWP analysis' in Sigma/W, in which the pore-water pressure generated in the steady-state analysis and stresses generated in the in-situ analysis were used to define the initial conditions for the transient state. A stress-based stability analysis was performed after every stage of construction, with the aid of Slope/W, to obtain the corresponding stability assessment. The entry-exit specification was used to define a wide range of circular slip surfaces in the slope faces of the dam. A detailed analysis and interpretation of the results obtained from the simulations, along with the discussions, is provided in the following section.

4.3.5 Results and Discussions

4.3.5.1 Steady-State Reservoir Operation (Flow/Deformation Analysis)

Under static conditions, i.e. during the normal operation conditions of an earthen dam, the seepage and deformation response of an earthen dam is difficult to predict, as the same is influenced by the complex conditions in the foundation material and also due to the several parameters influencing the evaluation and modeling of the material permeability**.** Seepage is considered as the movement of water from the upstream reservoir towards the downstream water level, through the body of the earthen dam, abutments, and the foundation. Seepage includes porous media (intergranular) flow, flow through fractures, and concentrated flow through 'defects' such as cracks and loose lifts. Steady-state condition of reservoir operation is a time-invariant phenomenon, where the reservoir head is considered constant for sufficient time resulting in a stable flow regime. Usually, this assumption results in a somewhat conservative analysis, as any earthen embankment and dam would experience significant annual fluctuations. Analyses of pore-water pressures in the earthen dam, measured through installed piezometers, have revealed that some of the earthen dams may even take decades to achieve a steady-state phreatic surface. However, given the uncertainties with assigning permeability and modeling the seepage behavior, any conservatism inherent in the assumption of steady-state conditions is usually considered acceptable. Thus, when analyzing flow quantities, gradients, and pore pressures at an earthen dam under its normal operating conditions, a steady-state analysis is usually appropriate. Deformations under static loading, on the other hand, occur because of volumetric changes, lateral spreading, or shear displacements within the earthen dam and foundation materials. Volumetric changes occur either due to an increase in the normal stresses on a soil element causing a decrease in the volume of void or due to the dilation of soil elements undergoing shearing. Lateral spreading and shear displacements are primarily due to squeezing, distortions, and localized shear failures of material, as the materials attempts to adjust to the stress conditions imposed by earthen dam construction and subsequent reservoir operation. These static deformation estimates are used in designing the crest camber, evaluating the possibility of the impervious core cracking, and estimating settlements of structures founded on (surficial or partially embedded) or completely buried within the earthen dam. The magnitude, directions and the rate of occurrence of these deformations largely depends on the rate of dissipation of excess pore-water pressures. It is also largely influenced by the rate at which the steady-state seepage conditions develop within the body of the earthen dam. The development of seepage conditions, in turn, is significantly influenced by several factors such as the material properties of the foundation and earthen dam material, geometry of the abutment and earthen dam, type of construction equipment used, fill placement rates, reservoir loading conditions, and stress distribution within various zones or layers within the earthen dam and its foundation. Thus, the coupled flow/deformation analysis is apt and provides a clear picture of the seepage and deformation behavior of the earthen dams.

Influence of Drainage Scenarios

In this study, pertaining to the horizontal toe drainage blanket and the inclined chimney drainage blanket, three different scenarios are studied. These scenarios are termed as the 'no drainage blanket condition (NDC)', the 'fully functional drainage blanket condition (FDC)' and the 'clogged drainage blanket condition (CDC)'. In case of NDC, there is no drainage blanket provided in the numerical model (as shown in Figure 4.10), whereas for FDC and CDC, the drainage is respectively considered 'fully functional' and 'completely clogged'. To simulate the FDC and CDC, the region demarcating the drainage blanket is considered homogeneous having a singular material with a specific permeability. In case of FDC, the material pertaining to 'drain', as highlighted in Table 4.2, is used. In the case of CDC, the 'earthen dam' material (as highlighted in Table 4.2) is considered to occupy completely the region demarcating drainage blanket. It is worth noting that the permeability of the 'drain' material is significantly higher than the 'earthen dam' material, and the complete replacement of the 'drain' material with the 'earthen dam' material in the region of drainage blanket represents the complete clogging of the same.

The analyses were carried out for 150 days and the results were analyzed at the end of analyzed time. The simulation of different forms of clogging was carried out by dividing the entire region of drainage blanket into different sections, and then sequentially clogging each of the segregated section. In the case of inward, outward, upward and downward cases of clogging, the entire drainage blanket was divided into five (5) smaller subsections, whereas, for the random clogging scenarios, the drain was divided into four (4) smaller subsections (as highlighted in earlier figures in this chapter). Each of these subsections were clogged at an interval of 30 days, i.e. after each sequential clogging of the subsection, the coupled flow-deformation analysis was carried out for 30 days to obtained the initial conditions before the next clogging. The results of various analyses performed during this study are presented in the following sections for both horizontal toe drainage blanket and inclined chimney drainage blanket.

For a steady-state reservoir operating condition, the results of the flow and deformation analyses conducted for an earthen dam without (NDC) and with horizontal toe drainage blanket (FDC and CDC) are presented through Figures 4.25-4.29. Figure 4.25(a) highlights the variation of the pore-water pressure measured along the region encompassing the horizontal toe drainage blanket as shown in Figure 4.25(b).

It is observed that for FDC, the pore-water pressure near the toe drastically reduces and completely dissipates through the functional drainage blanket and finds its path through the drainage blanket towards the downstream. However, in case of NDC and CDC, the seepage water is unable to find any escape path towards the downstream and thereby accumulates at the downstream toe region.

This lead to the abrupt rise in the phreatic surface that intersects with the downstream face, thereby exhibiting unrestricted flow of seepage water through the face itself. Figure 4.26 exhibits the corresponding PWP that provides a visualization of the stated phenomenon. Such a phenomenon can severely jeopardize the stability of the downstream face owing to the saturation of a larger region of the downstream of the earthen dam.

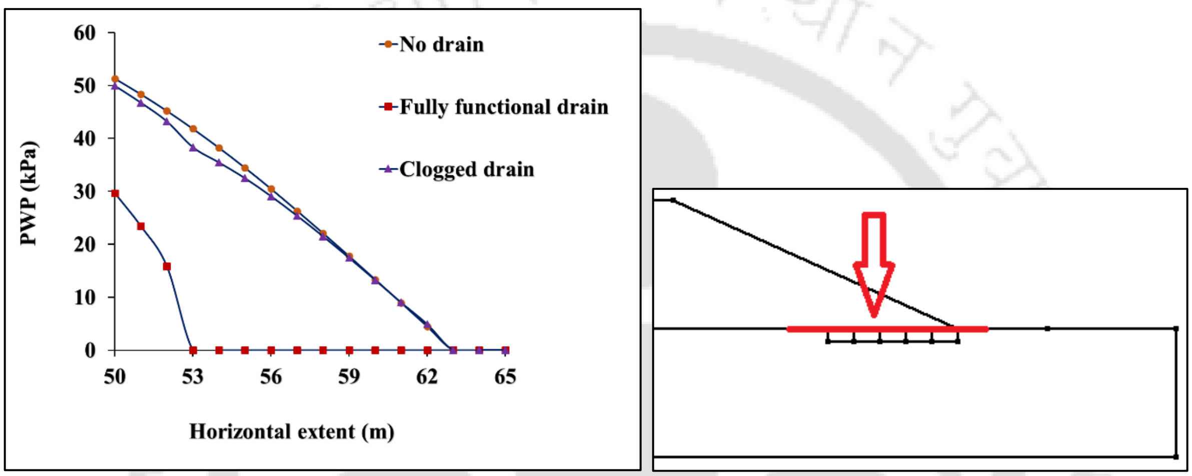

(a) (b)

Figure 4.25 Variation of pore-water pressure in an earthen dam under steady-state reservoir operation (a) Influence of different scenarios of horizontal toe drainage blanket (b) Location where pore-water pressure is measured

For the NDC or CDC conditions, the development of excess pore-water pressure near the toe of the dam and the intersection of phreatic surface with the downstream face results in the reduction of the effective strength of the component materials. This results in increased deformation of the base of the dam as well as the downstream face, as exhibited in Figure 4.27. As compared to the FDC condition, Figure 4.27(a) reveals a higher magnitude of heaving for NDC or CDC conditions, especially towards the downstream side of the dam. On the other hand, the magnitude of settlement of the dam is observed to be in agreement irrespective of the conditions (NDC, CDC or FDC), primarily attributed to the pressure exerted by the reservoir water in steady-state condition.

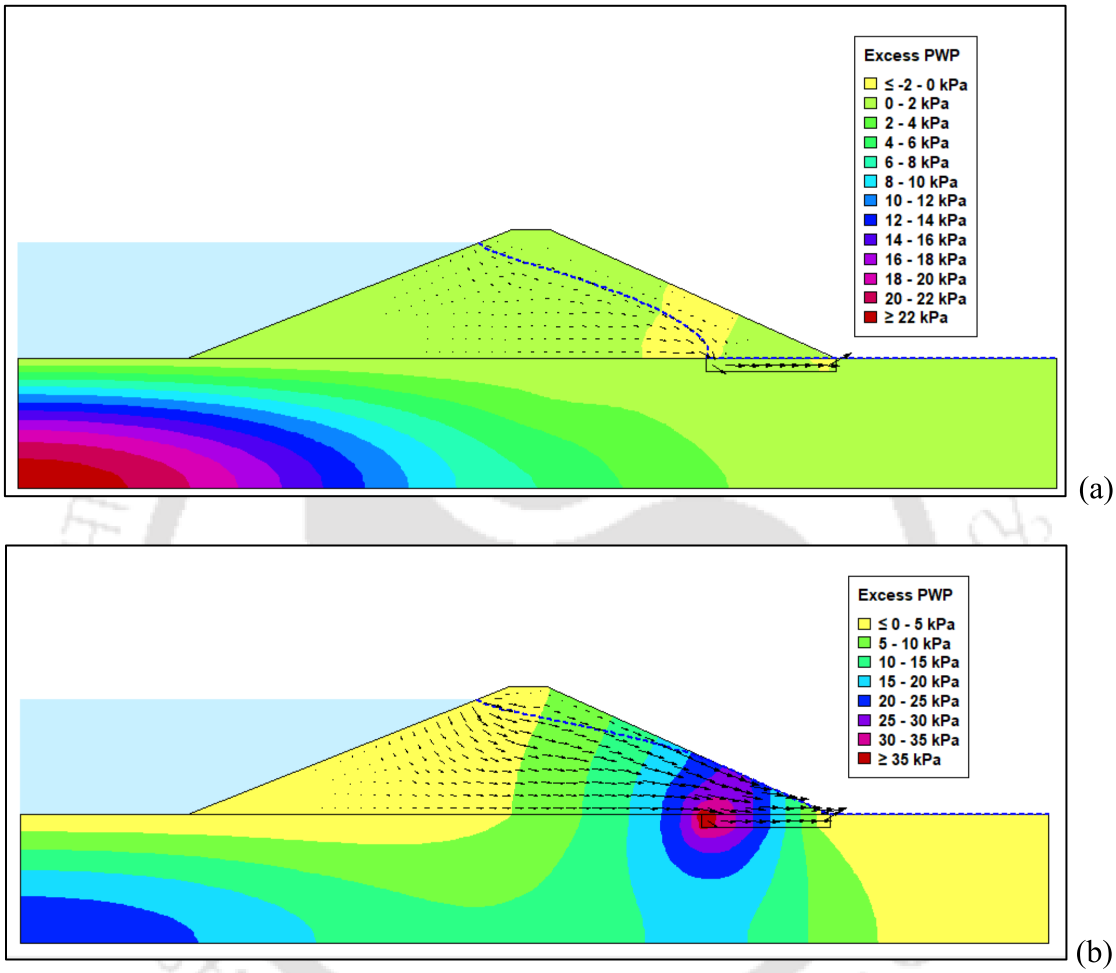

Figure 4.26 Excess PWP contours in an earthen dam under steady-state reservoir operation under various scenarios of horizontal toe drainage blanket (a) FDC (b) CDC or NDC

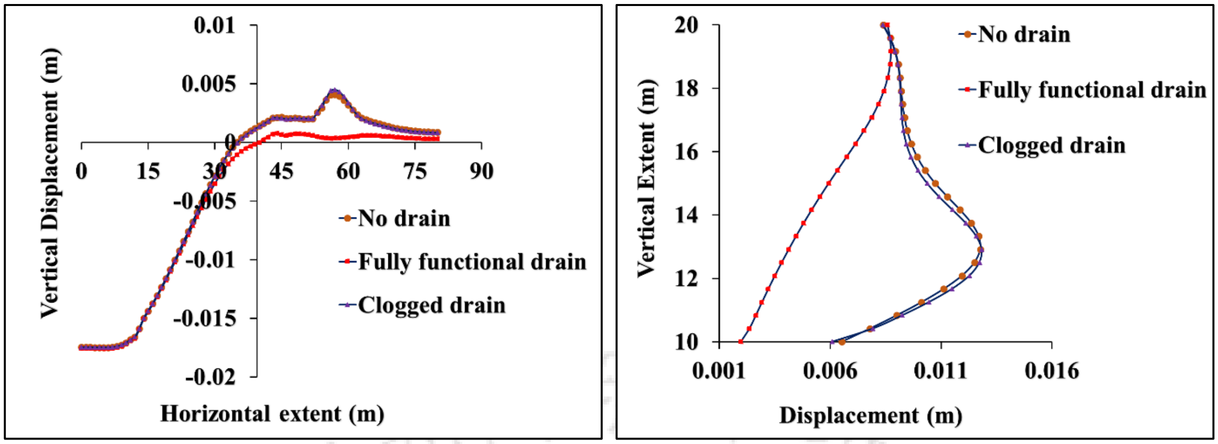

(a) (b)

Figure 4.27 Influence of horizontal toe drainage blanket on the deformation scenario (a) Settlement along the base of earthen dam (b) Deformation along the downstream slope

Figures 4.28 and 4.29 exhibit the hydraulic gradient and velocity contours through the body of the earthen dam for FDC and CDC conditions, respectively. In the scenario of FDC, as exhibited by Figure 4.28(a), the gradient near the toe or the exit region of the dam is equivalent to 0.2, which is noticeably less in comparison to the exit gradient at the same location observed for CDC scenario. For the latter case, the exit gradient is obtained to be approximately 0.5 or greater (Figure 4.29a). However, as shown in Figure 4.28(b) and Figure 4.29(b) respectively, the seepage velocity at the exit point for the FDC scenario is higher than that observed for CDC condition. While the FDC scenario identified the seepage velocity to be 0.12 m/day, the same is obtained as 0.04 m/day for the CDC scenario. This observation is reasonable as higher seepage velocity through a drainage blanket is expected in its fully functional condition, while clogging inhibits the flow path through the blanket resulting in the reduction in seepage velocity and increase in the exit gradient.

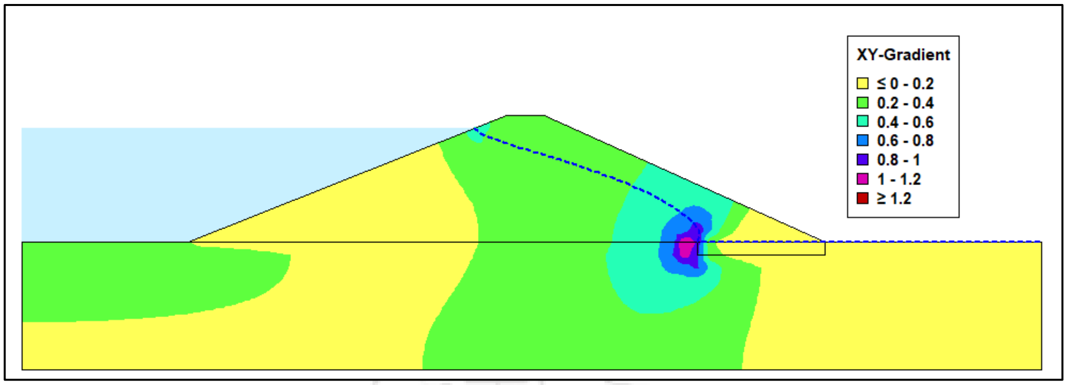

(a)

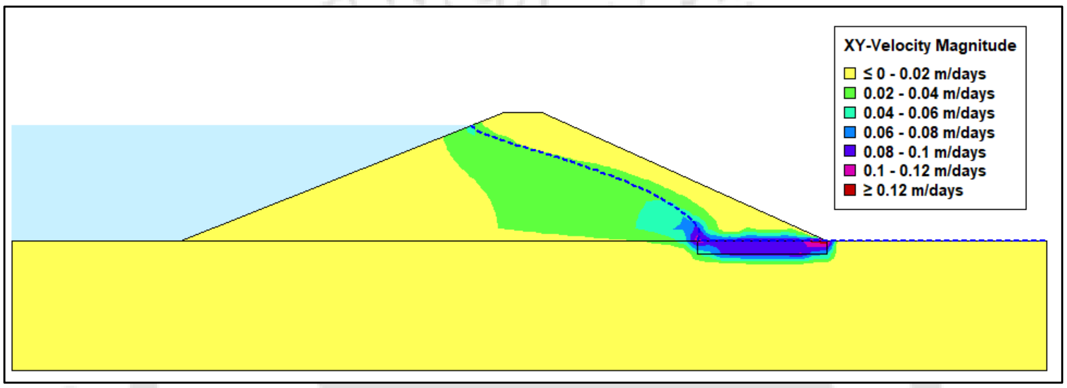

(b)

Figure 4.28 Hydraulic contours within an earthen dam with fully functional horizontal toe drainage blanket (a) Hydraulic gradient (b) Seepage velocity

It is well recognized from earlier researches that an earthen dam are susceptible to piping if both the hydraulic gradient and seepage velocity at the exit region simultaneously achieves high magnitudes. Figures 4.28 and 4.29 exhibit that in neither of the drainage scenarios, the magnitudes of the stated entities are large. In this situation, it is important to recognize that in an impervious foundation made of fine-grained soils with very low permeability, the inter-particle bond make it less likely for these soils to lose strength due to seepage or for individual particles to be easily displaced. Hence, for earthen embankments and dams, the possibility of piping through the body of the dam occurs only when high exit gradients are accompanied by high seepage velocities at the exit region. Otherwise, the evaluation of high exit gradient is an issue more likely to be of concern in pervious foundation.

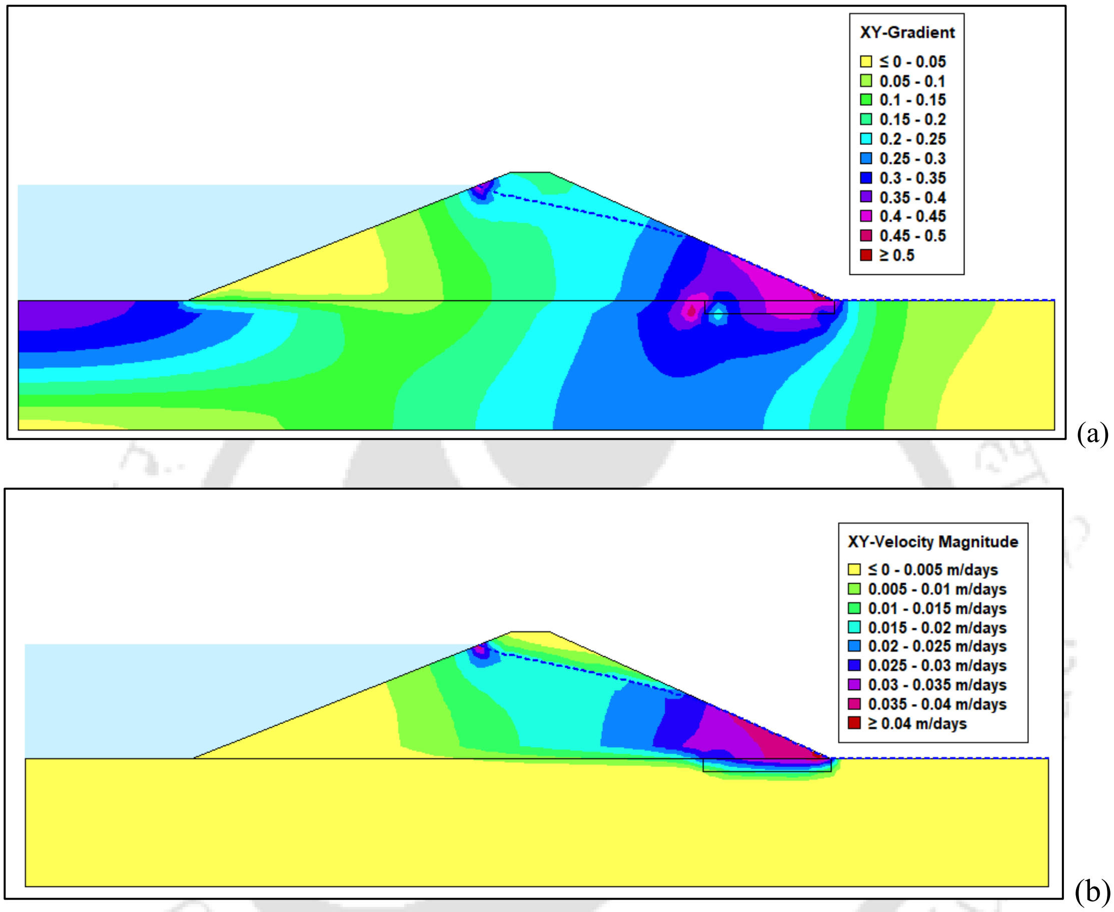

Figure 4.29 Hydraulic contours within an earthen dam with fully clogged horizontal toe drainage blanket (a) Hydraulic gradient (b) Seepage velocity

As conducted for a horizontal toe drainage blanket, the flow and deformation analyses of an earthen dam with/without an inclined chimney drainage blanket, considering various drainage scenarios (namely the NDC, FDC and CDC). Figures 4.30-4.34 illustrate the analyses results.

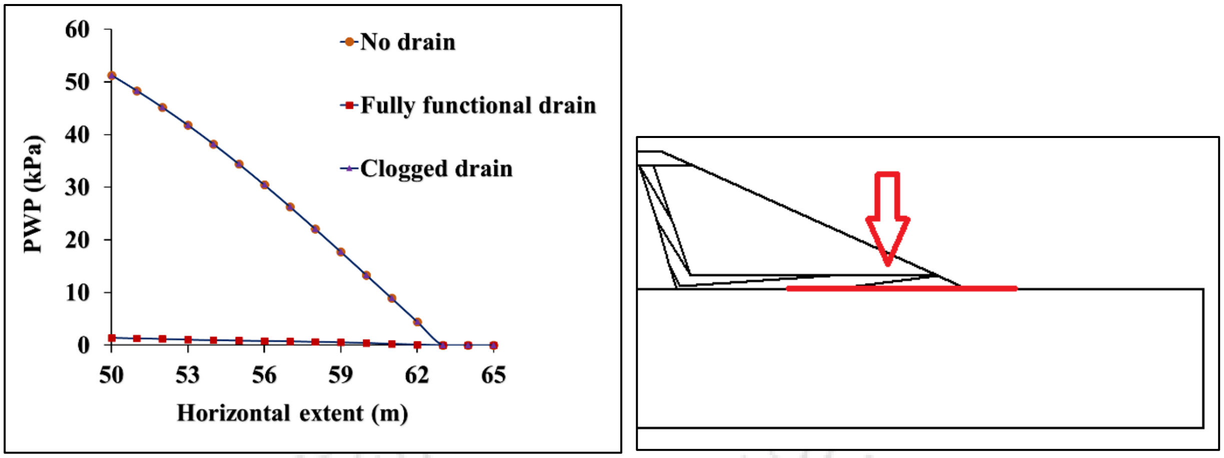

(a) (b)

Figure 4.30 Variation of pore-water pressure in an earthen dam under steady-state reservoir operation (a) Influence of different scenarios of inclined chimney drainage blanket (b) Location where pore-water pressure is measured

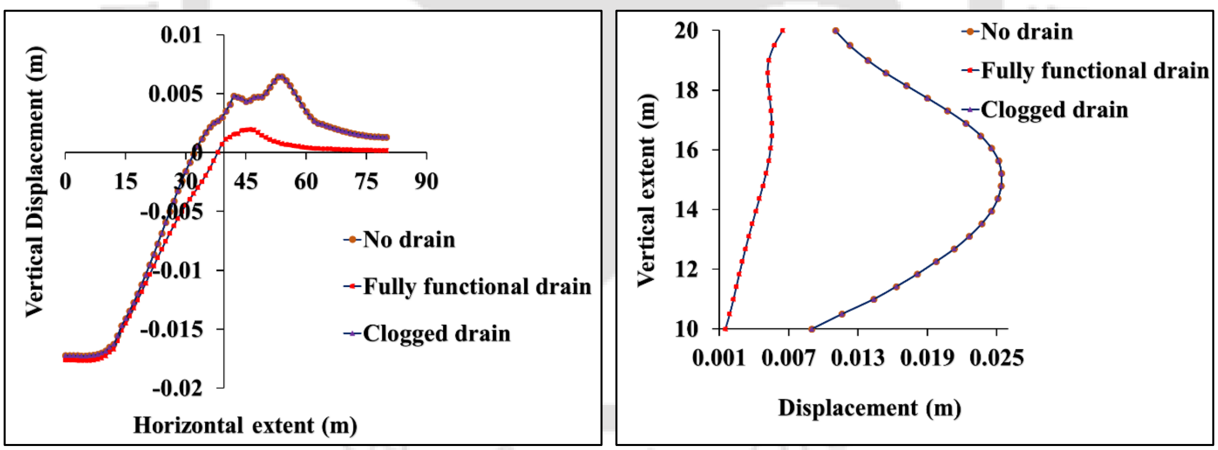

(a) (b)

Figure 4.31 Influence of inclined chimney drainage blanket on the deformation scenario (a) Settlement along the base of earthen dam (b) Deformation along the downstream slope

In general, the flow and deformation characteristics obtained considering inclined chimney drainage blanket showed the same trend and characteristics as obtained for horizontal toe drainage blanket. However, as observed from Figure 4.32(b), the development of excess pore-water pressure owing to the clogged inclined chimney drainage blanket is higher than that obtained for a clogged horizontal toe drainage blanket. Consequently, higher deformations along the downstream slope and the base of the dam are obtained when the clogged inclined chimney drainage blanket is considered.

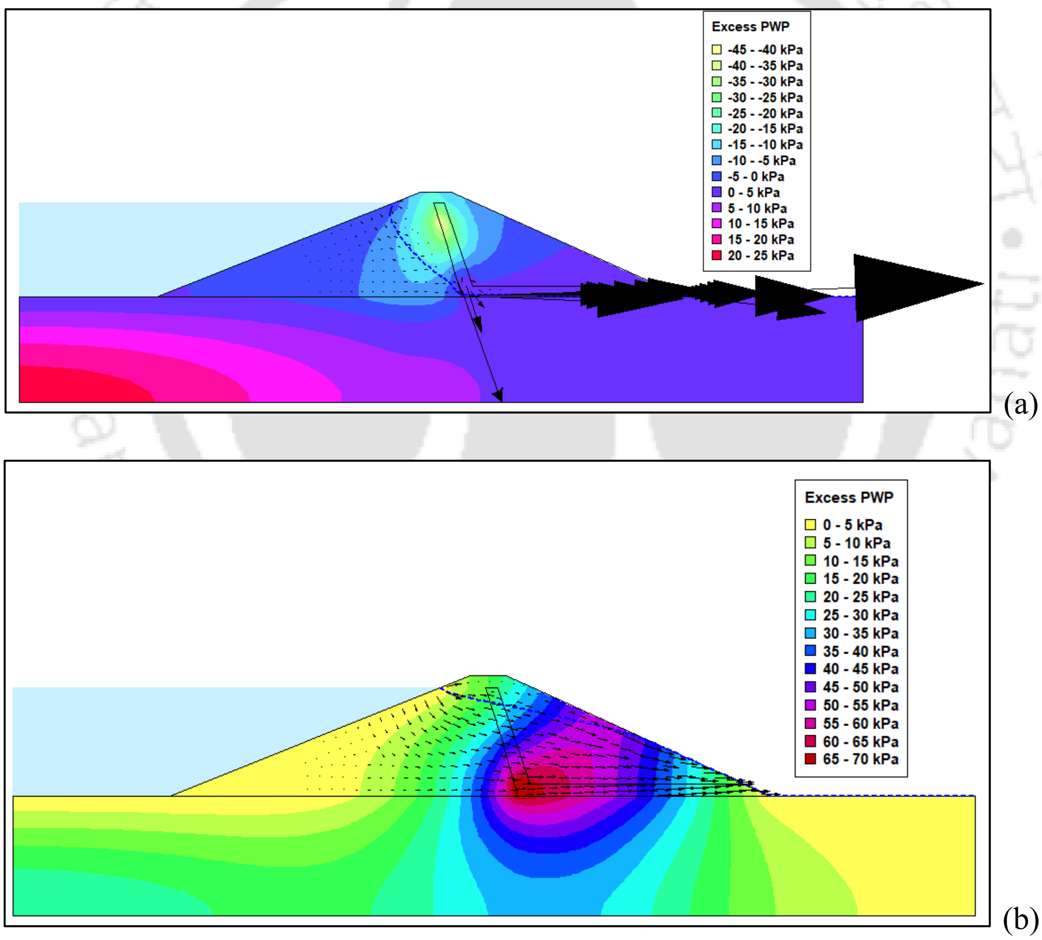

Figure 4.32 Excess PWP contours in an earthen dam under steady-state reservoir operation under various scenarios of inclined chimney drainage blanket (a) FDC (b) CDC or NDC

In case of considering an inclined chimney drainage blanket within the earthen dam, Figure 4.33 indicates that for FDC scenario, the hydraulic gradient near the toe region is 0.2 and the seepage velocity is approximately 18 m/day. Similarly, for the CDC scenario, the hydraulic gradient near the toe region is 0.45 and seepage velocity is approximately 0.35 m/day, as shown in Figure 4.34.

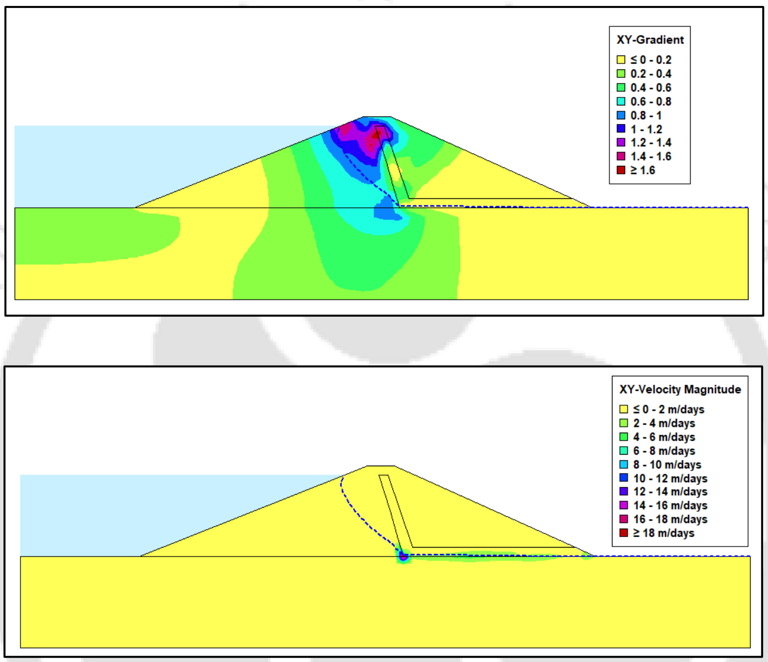

Figure 4.33 Hydraulic contours within an earthen dam with fully functional inclined chimney drainage blanket (a) Hydraulic gradient (b) Seepage velocity

Thus, it is observed that even in the case of application of inclined chimney drainage blanket, the hydraulic gradient and seepage velocity at the exit point in the downstream of the dam are not of high magnitude. The empirically derived critical hydraulic gradients for the initiation of backward erosion and piping for different types of soil, with varying sand content, ranges between 0.048 for fine sand to 0.28 for coarse sand (Perzlmaier et al., 2007). The critical hydraulic gradient, in case of soils containing varying clay content, ranges between 0.9-2.74 (Quanyi et al., 2018). The seepage velocity resulting in initiation of piping ranges between 1.14 x 10^{-6} m/s to 5.39 x 10^{-7} m/s (Okeke and Wang, 2016). Hence, the possibility of piping is not recognizable in the earthen dam considered in the present study.

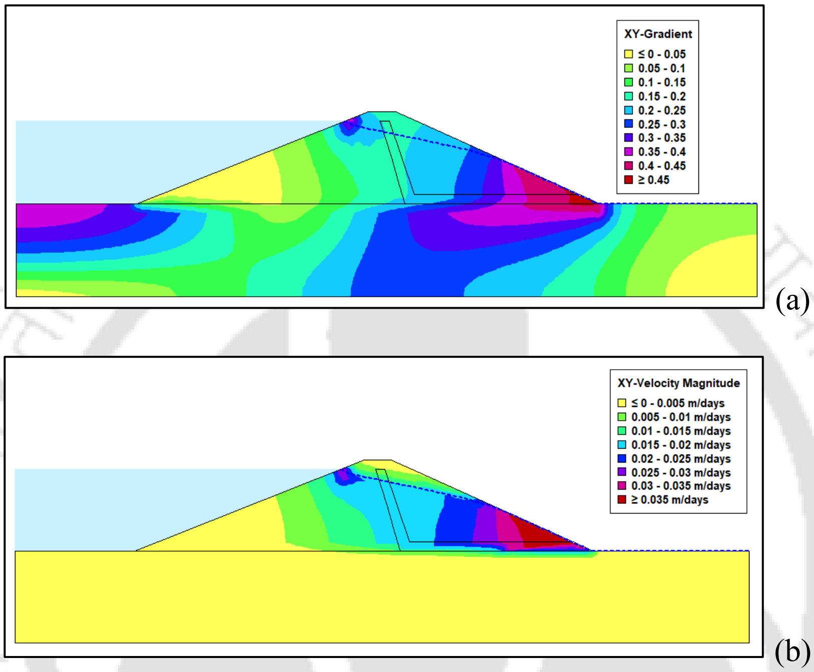

Figure 4.34 Hydraulic contours within an earthen dam with fully clogged inclined chimney drainage blanket (a) Hydraulic gradient (b) Seepage velocity

Influence of Clogging Typology

As mentioned in Section 4.3.1, each type of the drainage blanket, i.e. horizontal toe blanket and inclined chimney blanket, are subjected to four different typologies of sequential clogging and two typologies of random clogging. Figure 4.35 depicts the location near the toe of the dam for which the subsequent figures (Figures 4.36-4.40) highlight the results of the analyses with the stated six different forms of clogging of the horizontal toe and inclined chimney drainage blankets within a homogenous earthen dam resting on an impervious foundation bed. All the plots represent the results obtained at the 90th day i.e. immediately after the 3rd stage of clogging for each case.

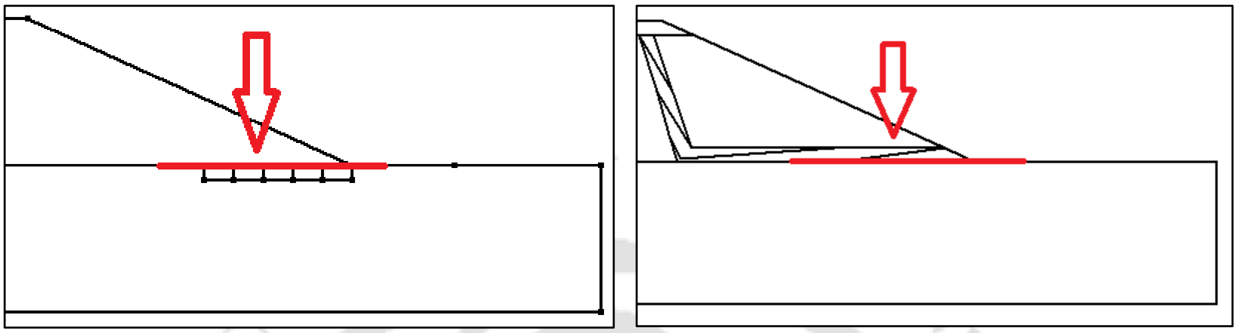

(a) (b)

Figure 4.35 Location of measurement of pore-water pressure to study the influence of clogging typology (a) Horizontal toe drainage blanket (b) Inclined chimney drainage blanket

Figure 4.36 exhibit the variation of the pore-water pressure measured along the toe of the earthen dam, as highlighted in Figure 4.35. It can be observed that for both types of drainage blankets, the inward clogging results in higher PWP, owing to the inhibition of flow of seepage water through the exit region of the downstream face. In general, owing to the greater length of drainage, the inclined chimney drainage blanket is noted to be more effective even during the different forms of clogging; the same is highlighted by lower magnitudes of PWP as compared to that obtained using the horizontal toe drainage blanket. Figure 4.37 shows that for either types of drainage blanket, the settlement along the base of the earthen dam are nearly identical, there highlighting that clogging typology does not noticeably influence the deformation response of the dam.

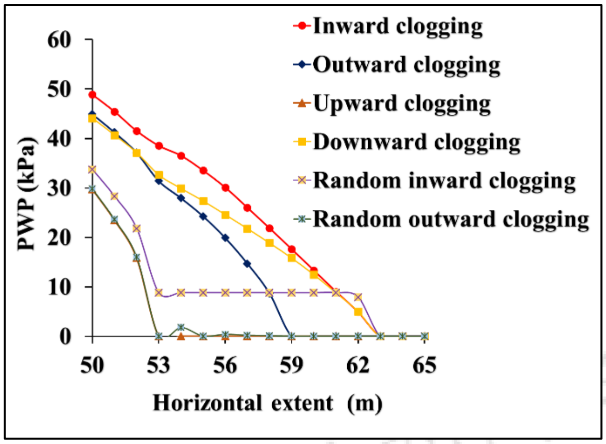

(a)

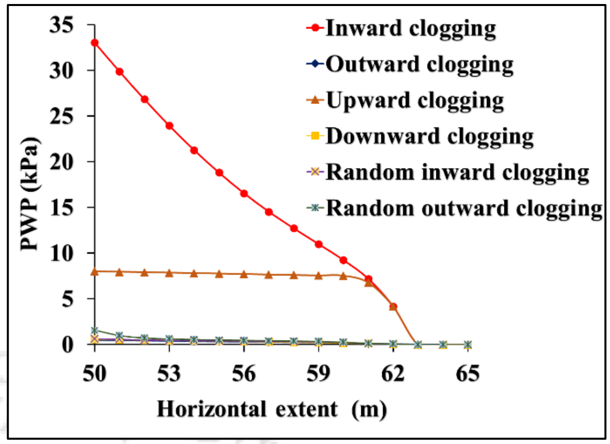

(b)

Figure 4.36 Variation of pore-water pressure as measured along the toe of earthen dam (a) Horizontal toe drainage blanket (b) Inclined chimney drainage blanket

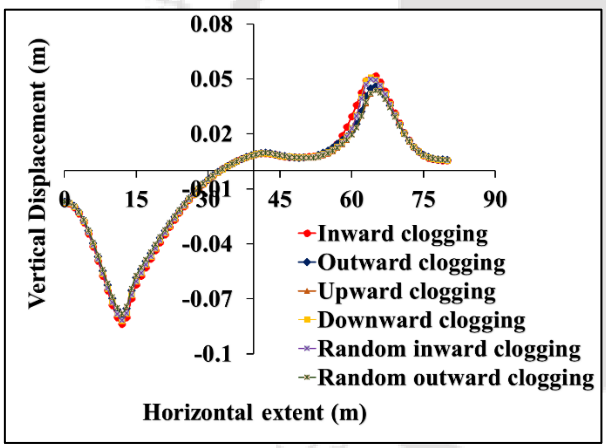

(a)

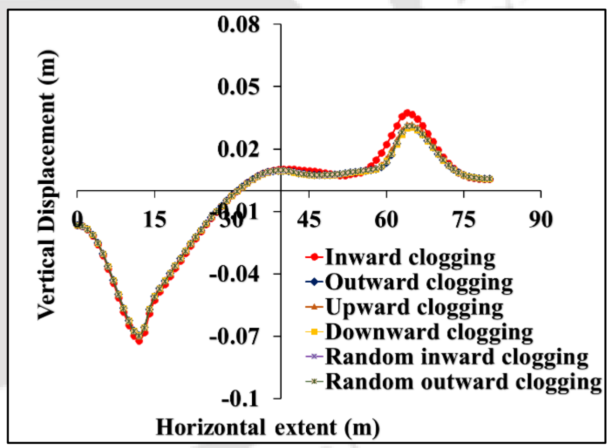

(b)

Figure 4.37 Settlement profile of the base of the earthen dam (a) Horizontal toe drainage blanket (b) Inclined chimney drainage blanket

The deformation along the downstream slope is exhibited in Fig. 4.38. It is observed that the trend of displacement of the downstream slope face is similar for usage of both types of drainage blankets. In both types of drainage blankets, inward clogging results in the highest displacement of the downstream face. However, as compared to that of inclined chimney drainage blanket, the influence of clogging typology is pronouncedly distinct in case of horizontal toe drainage blanket. In case of the inclined drainage blanket, apart from inward clogging scenario, all other forms of clogging results in nearly similar magnitudes of displacement in the downstream face.

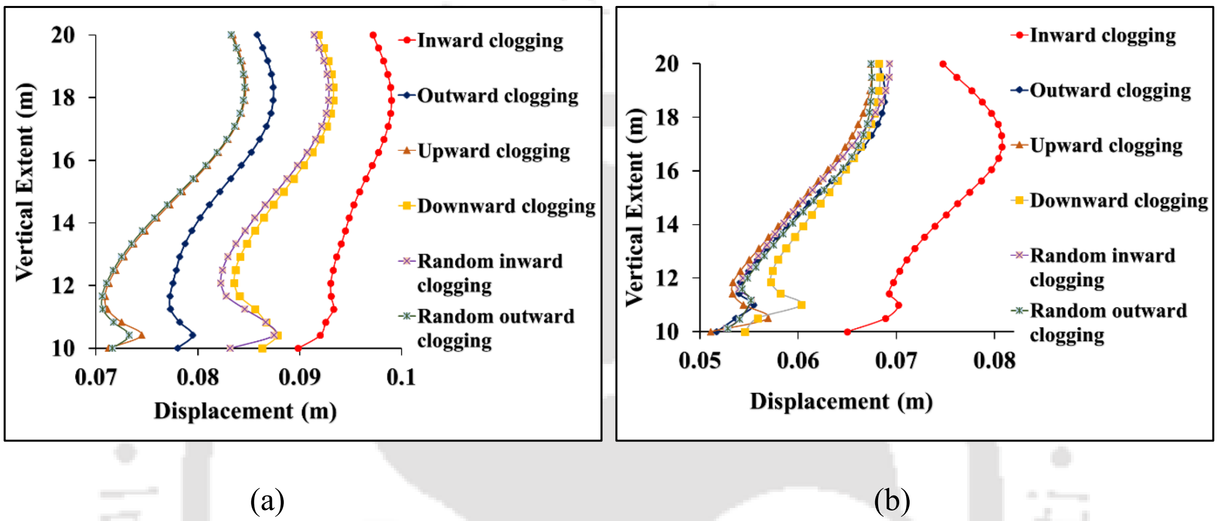

Figure 4.38 Deformation of the downstream face of the earthen dam (a) Horizontal toe drainage blanket (b) Inclined chimney drainage blanket

For an earthen dam with horizontal toe and inclined chimney drainage blanket, the influence of clogging typology on the variation of hydraulic gradient near the exit region towards the downstream of the dam is shown in Figure 4.39(a) and Figure 4.40(a), respectively. For both types of drainage blankets, the maximum exit gradient is obtained for inward clogging; the obtained magnitude being 2.4 and 0.95 for inclined chimney and horizontal toe drainage blanket, respectively. In either of the drainage blankets, for inward clogging, as the outermost section of the drainage blanket near the toe is clogged, the hydraulic gradient develops a potential to reach the critical exit gradient. This phenomenon can possibly lead to either the cracking of impervious foundation or sand boiling in a pervious foundation. Under such cases, the most obvious failure mechanism is associated with the progressive backward erosion, finally leading to dam breaching. In order to check whether such a possibility arise in the present scenario, the seepage velocity near the toe are plotted, as shown in Figure 4.39(b) and Figure 4.40(b), respectively, for horizontal toe and inclined chimney drainage blankets. It is found that although the exit gradients are high and tends to increase near the toe, the presence of low seepage velocities will not possibly initiate ay particle movement in an impervious foundation.

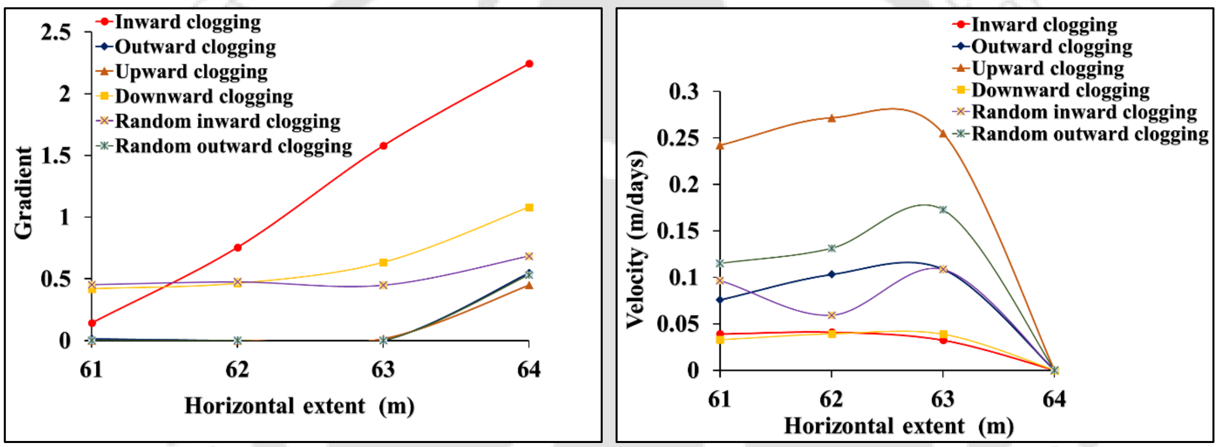

(a) (b)

Figure 4.39 Influence of clogging typology on the hydraulic characteristics at the toe of an earthen dam having horizontal toe drainage blanket (a) Hydraulic gradient (b) Seepage velocity

Based on the earlier results, it is established that the ‘inward clogging’ is the most critical clogging typology affecting the integrity and performance life of an earthen dam. Table 4.3 lists the magnitudes of various measurable entities for earthen dams comprising different types of drainage blanket. It can be well noted that all the measured entities show lower values for the earthen dam comprising inclined chimney drainage blanket. Hence, it can be stated that the presence of an inclined chimney drainage blanket is relatively more effective in enhancing the performance of an earthen dam.

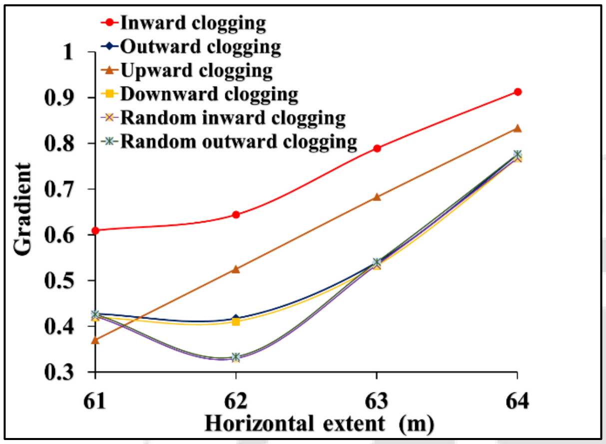

(a)

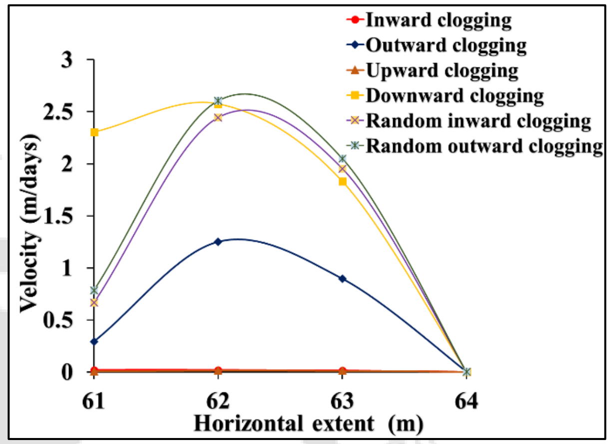

(b)

Figure 4.40 Influence of clogging typology on the hydraulic characteristics at the toe of an earthen dam having inclined chimney drainage blanket (a) Hydraulic gradient (b) Seepage velocity

Table 4.3 Comparative of measured entities in an earthen dam comprising different types of drainage blankets

	Excess PWP (kPa)	Downstream slope deformation (m)	Base settlement (m)	Exit gradient
Horizontal toe drainage blanket	Inward clogging 50	Inward clogging 0.099	Inward clogging 0.09	Inward clogging 2.4
Inclined chimney drainage blanket	Inward clogging 34	Inward clogging 0.08	Inward clogging 0.07	Inward clogging 0.95

4.3.5.2 Transient-State Reservoir Operation (Flow/Deformation Analysis)

Transient flow conditions refer to temporally varying seepage occurring through the body of an earthen dam. During a transient flow, both pore-water pressures and effective stresses vary with time. The transient flow within the earthen dam may be correlated to the influence of fluctuating reservoir levels, which is commonly referred as 'transient-state reservoir operation'. Such operations include the first filling, normal operational cycles, rapid drawdown, seasonal reservoir fluctuations during its operation period of the reservoir, flood loading and their effects on the earthen dams. Under these different loading conditions, the temporal migration of the saturation front through an earthen dam or foundation, as well as the temporal alteration of the phreatic surface, is estimated. The effect of transient state seepage conditions on the development of pore-water pressures, temporal variation of phreatic surface, hydraulic gradients, uplift pressure, effective stresses and deformations within the foundation and body of earthen dam needs to be investigated in detail, as it may lead to serious consequences if left unattended. Seepage can lead to the formation of high pore-water pressures and/or high seepage forces in an earthen dam or its foundation, resulting in excessive deformations that could lead to seepage-related internal erosion in the dam. In this study, the response of a homogeneous earthen dam subjected to clogging of drainage blanket is investigated for the reservoir rise-up and drawdown conditions. The rate of rise-up and drawdown are considered 1.5 m/day as shown in Figure 4.41.

Figure 4.42 exhibits the distribution of pore-water pressure along the base of the earthen dam after 150 days from the completion of drawdown of the reservoir. It is observed that the PWP is higher within the body of the dam for NDC or CDC scenarios, while lower PWP is obtained for a fully functional drainage blanket (FDC scenario). Furthermore, as obvious, the FDC scenario exhibits a zero PWP all along the length of the drainage blanket. As the reservoir water is removed, for all the cases, the PWP at the upstream heel is obtained as zero.

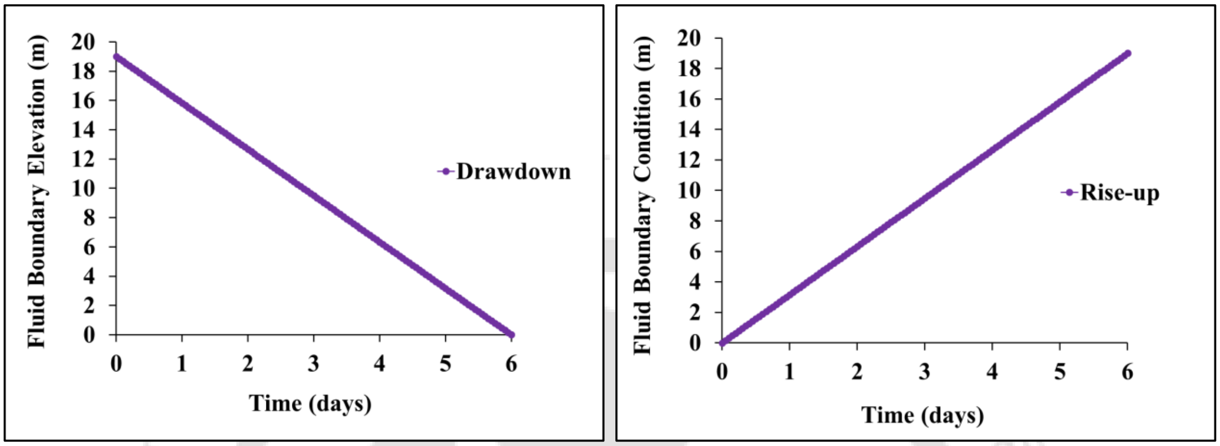

(a) (b)

Figure 4.41 Transient variation in the upstream reservoir level (a) Drawdown (b) Rise-up

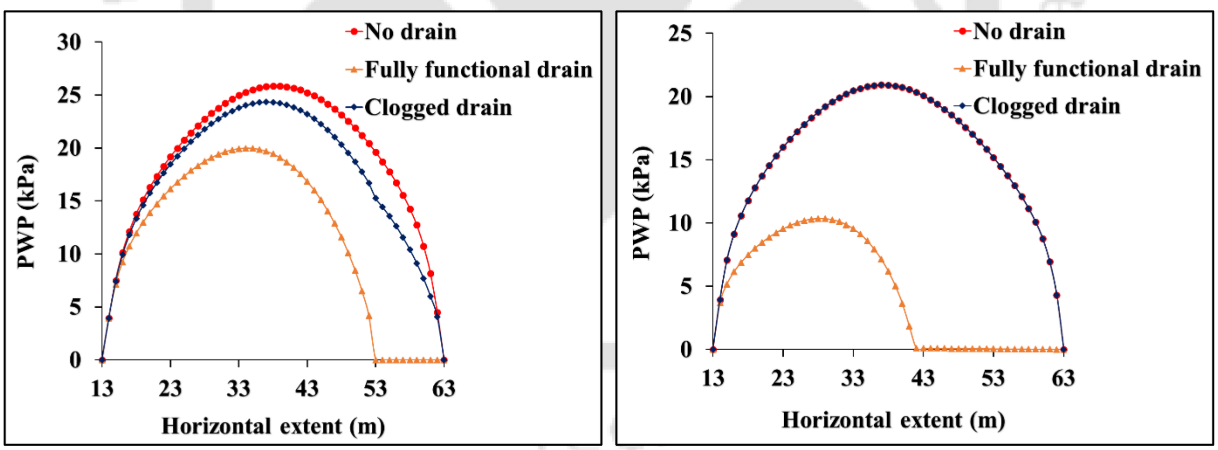

(a) (b)

Figure 4.42 Variation of PWP along the base of earthen dam at 150th day after complete drawdown of upstream reservoir (a) Horizontal toe drainage blanket (b) Inclined chimney drainage blanket

Figure 4.43 displays the PWP contours within the earthen dam and the foundation at the 6th day, i.e. when the reservoir drawdown is just completed. It can be observed that significantly high PWP is obtained along the upstream face when the earthen dam comprises a horizontal toe drainage blanket. As established earlier, compared to a horizontal tow drainage blanket, even though clogging is encountered, an inclined chimney drainage blanket exhibits better performance in the disspation of PWP, and the same is indicated here as well. Furthermore,

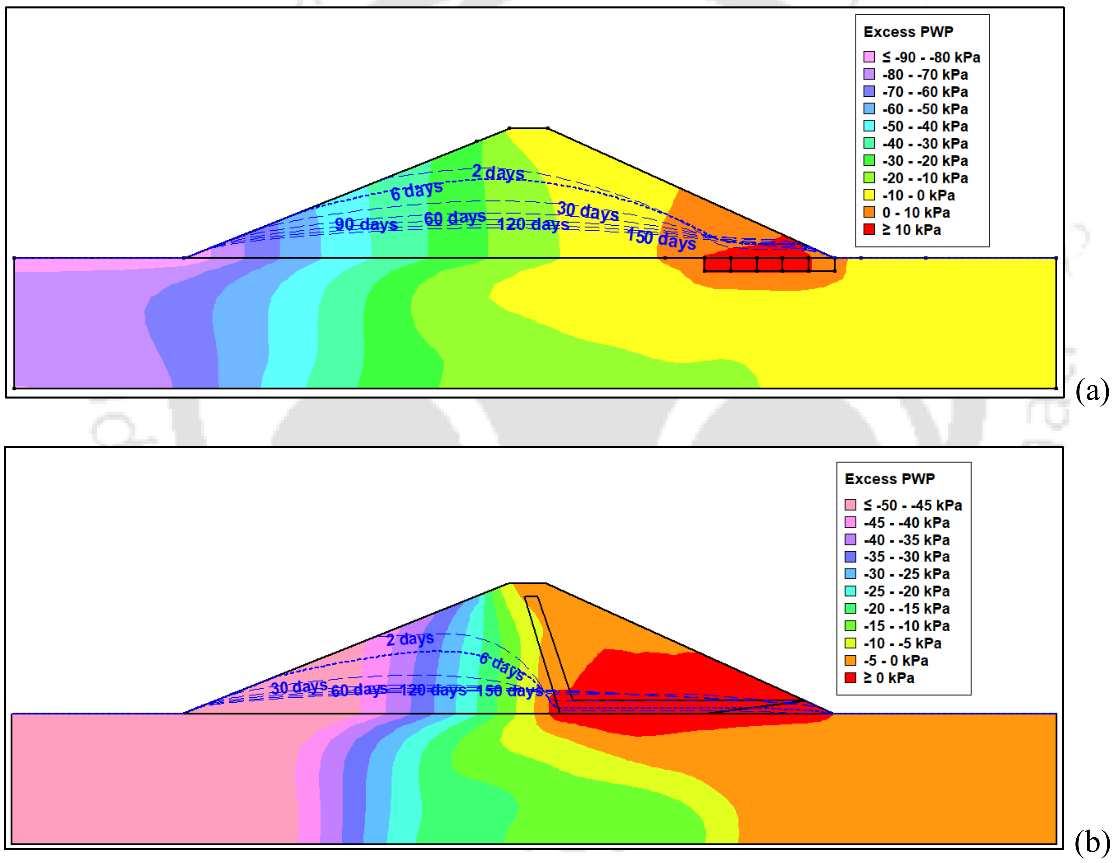

Figure 4.43 PWP contours on the 6th day representing complete drawdown of the reservoir and transient migration of the phreatic surfaces after complete drawdown (a) Horizontal toe drainage blanket (b) Inclined chimney drainage blanket

Figure 4.43 exhibits the temporal migration of the phreatic surface during the transient process. It is observed that even after the drawdown process being complete on the 6th day, for many subsequent days, the gradual dissipation of PWP through the upstream face results in the lowering of the phreatic surfaces towards the upstream. A marginal rise in the phreatic surface towards the downstream region is observed which is attributed to the clogged drainage blanket. The clogged drain would have resulted in a much higher rise in the pore-water pressure and the phreatic surface towards the downstream, but the same is restricted by the simultaneous drawdown of the upstream reservoir. Nevertheless, it is aptly comprehensible that even during and after the upstream reservoir drawdown, clogging has marginal influence on the rise in the phreatic surface towards the downstream of the earthen dam. The effect is more recognizable in earthen dams with horizontal toe drainage blanket, as can be observed from the PWP contours exhibited in Figure 4.43.

Thus, in a nutshell, it can be stated that the clogging of drainage blankets do not substantially influence the hydraulic characteristics during the transient reservoir drawdown conditions. As the sequential and completion of clogging of drainage blanket attempts to raise the PWP in the earthen dam, the simultaneous drawdown of the upstream reservoir leads to the reduction of external water pressure and initiates the dissipation of PWP through the upstream face, thereby nullifying the effect of clogging. As a result, the magnitude and trend of deformation of the upstream and downstream faces of the earthen dam, for any of the NDC, FDC and CDC conditions, are negligibly different, and the same is exhibited in Fig. 4.44. On account of the removal of the water load from the upstream side, a marginal defomration of the earthen dam towards the upstream can be noticed.

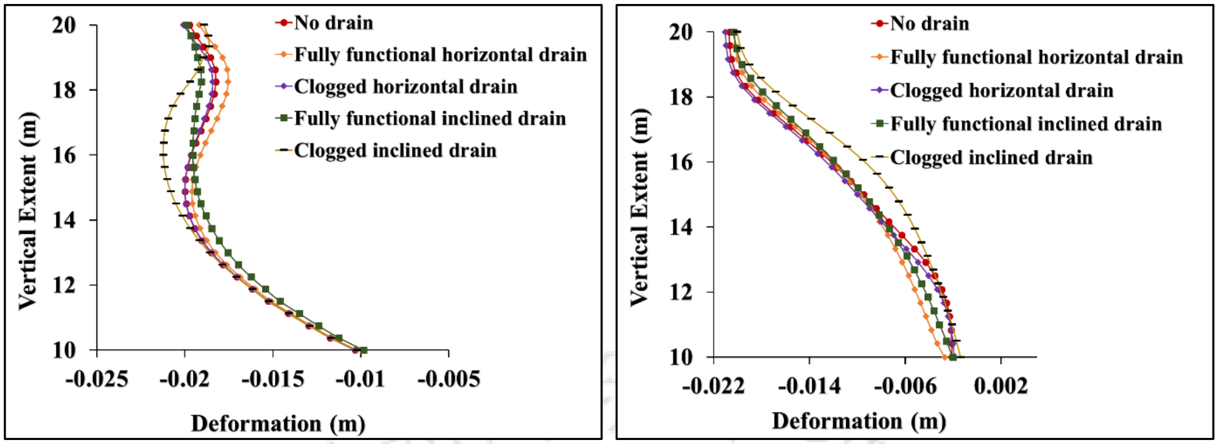

(a) (b)

Figure 4.44 Deformation of the earthen dam at the end of drawdown i.e. at the 6th day (a) Upstream face (b) Downstream face

Alike for drawdown conditions, the influence of clogging of drainage blanket on the response of a homogeneous earthen dam during the reservoir rise-up condition is studied. Similar to the earlier case, a fully functional drainage blanket aids in lowering the PWP with the earthen dam, as exhibited in Figure 4.45 for the 150th day after completion of upstream reservoir rise-up. In contrary to the drawdown condition, Figure 4.46 highlights that for the reservoir rise-up case, the phreatic surface takes time to migrate from the upstream face to reach the downstream face of the earthen dam, and as a result, the pore-water pressure along the drainage blanket near the toe of the dam remains negligible for a significant time. Consequently, during this period at the toe of the earthen dam, the accumulation of pore-water pressure is not yet initiated, and hence the simultaneous clogging of drainage blanket within this period will not pose any impact on the response of earthen dam. For a longer time duration, the clogged drainage blanket would lead to gradual accumulation of the pore-water pressure, thereby leading to a rise in the phreatic surface which proceed to intersect the downstream face of the earthen dam, leading to the reduction of its stability. The migration and rise of phreatic surface with elapsed time is visually represented in Figure 4.46. Upon comparing the rise in the phreatic surface for horizontal toe drainage blanket and inclined chimney drainage blanket, it is evident that the inclined chimney drainage blanket serves better than the former one. Figure 4.46(c) represents a stand alone analysis that is carried out to portray that even with greater drainage length of the horizontal toe drainage blanket (wherein the toe blanket is extended up to the middle of the base of the dam and is comparable to the basal extent of inclined chimney drainage blanket), the performance of inclined chimney drainage blanket is still better. The deformation of the upstream and downstream faces of the earthen dam is observed to be marginally affected by the clogging process during reservoir rise-up condition. Figure 4.47 exhibits similar trend and magnitude of slope face deformations during rise-up condition. It is observed that there is a marginal deformation of the earthen dam towards its downstream, owing to the filling of the upstream reservoir.

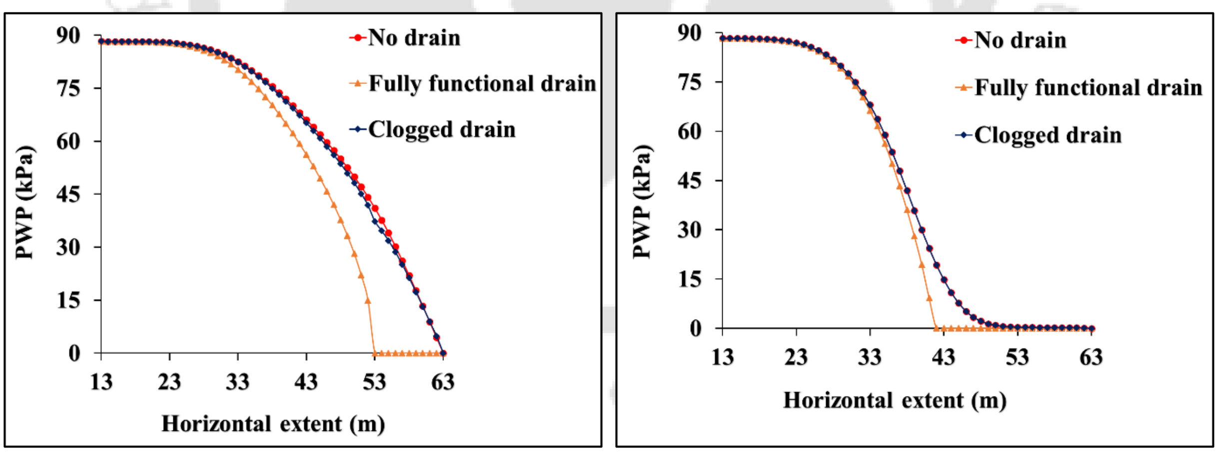

(a) (b)

Figure 4.45 Variation of PWP along the base of earthen dam at 150th day after complete rise-up of upstream reservoir (a) Horizontal toe drainage blanket (b) Inclined chimney drainage blanket

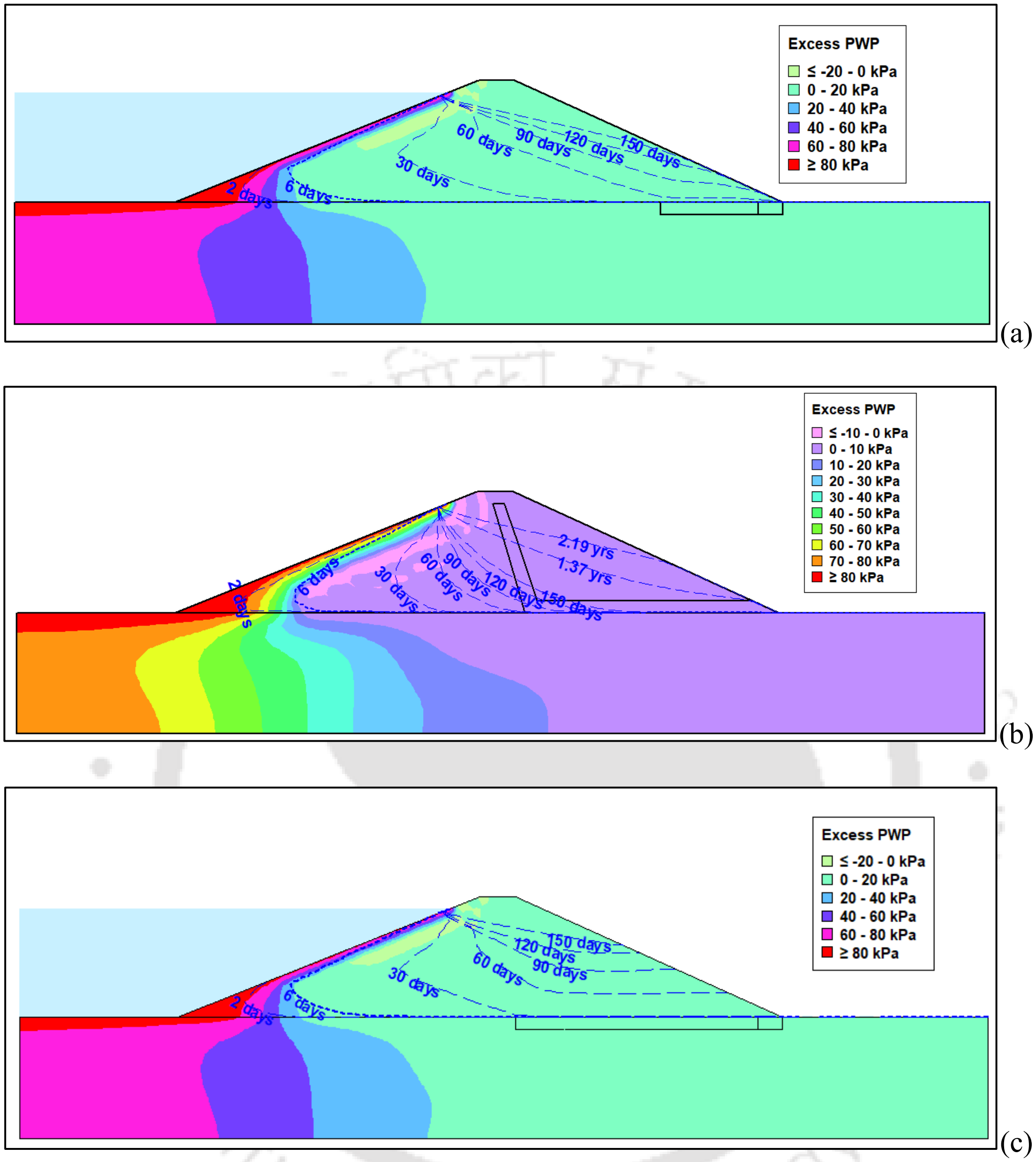

Figure 4.46 PWP contours on the 6^{th} day representing complete rise-up of the reservoir and transient migration of the phreatic surfaces after complete rise-up (a) Horizontal toe drainage blanket (b) Inclined chimney drainage blanket (c) Horizontal toe drainage blanket with length comparable to the basal extent of inclined chimney drainage blanket

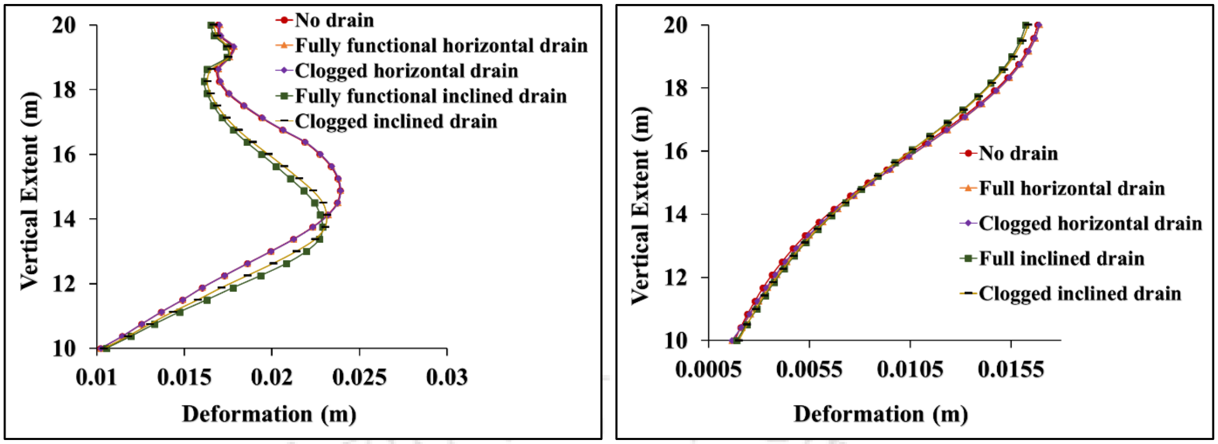

(a) (b)

Figure 4.47 Deformation of the earthen dam at the end of rise-up i.e. at the 6^{th} day (a) Upstream face (b) Downstream face

Figure 4.48 represents the deformation profile along the base of the earthen dam during reservoir rise-up and drawdown conditions. Owing to the removal of the buttressing effect of the reservoir water during drawdown and accompanied by the dissipation of pore-water pressures through the upstream face of the earthen dam, marginal settlement is noted below the crest and base of the earthen dam, as shown in Figure 4.48(a). On the other hand, during reservoir filling, the gradual ingress of the reservoir water in the earthen dam leads to the increase in construction-induced and seepage-induced pore-water pressures, thereby leading to notable heaving in the crest and base of the earthen dam, as shown in Figure 4.48(b). However, despite all these observed features, it is clearly comprehensible that during the transient reservoir operations (i.e., during rise-up and drawdown), simultaneous clogging of drainage blanket does not reveal a significant effect on the settlement profile of the base or sloping face of an earthen dam.

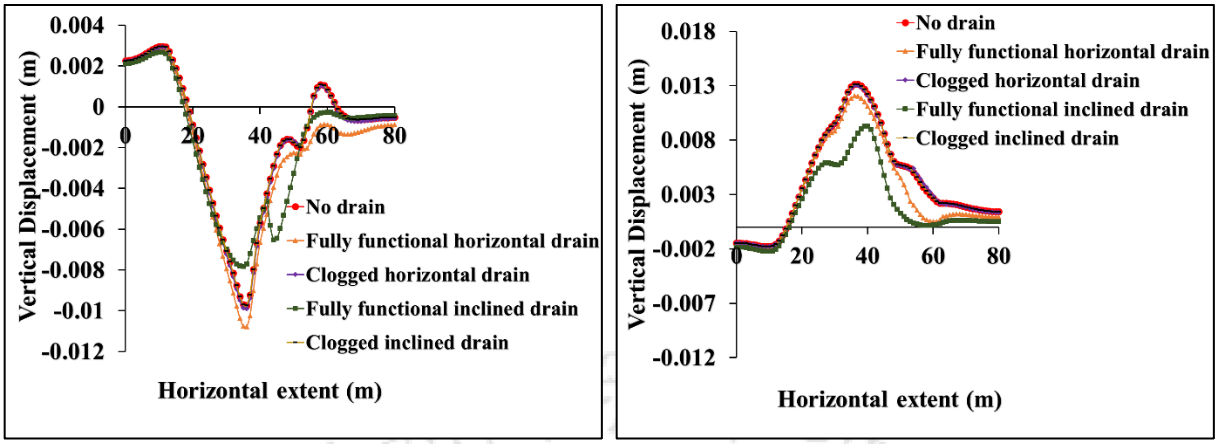

(a) (b)

Figure 4.48 Vertical deformation profile of the base of earthen dam at the end of (a) Reservoir drawdown (b) Reservoir rise-up

4.3.5.3 Influence of Clogging of Drainage Blanket on Stability of Earthen Dam

Based on the pore-water pressures obtained from the Seep/W analysis and the effective stresses obtained from the coupled stress-PWP analysis in Sigma/W, limit-equilibrium based slope stability analysis was performed for various earthen dam model simulations to assess the variation of the stability of the dam face. Figures 4.49 and 4.50 explicitly indicate that the installation of the drainage blankets and their subsequent functional conditions increase the stability of the downstream face. The same is indicated by the increment in Factor of Safety (FoS) in the dam instability. Compared to a homogeneous earthen dam with NDC scenario, horizontal toe drainage blanket in FDC scenario enhances the FoS from 1.26 to 1.358, while an inclined chimney drainage blanket raises the FoS to 1.558. As also observed earlier, the FoS values clearly manifest the efficacy of an inclined chimney drainage over a horizontal toe drainage blanket in enhancing the stability of the downstream face of the dam (the most susceptible region to slope instability). Further, the reduction in the FoS values are noted when the drainage blankets are clogged (CDC scenario), which is attributed to the accumulation of pore-water towards the downstream face, thereby jeopardizing the stability of the slope. It can be noted that the FoS against slope stability obtained for NDC and CDC scenarios are nearly similar. This observation indicates that although the drainage blankets are supposed to ensure the long-term performance and stability of the earthen dam, however their usefulness can be only harnessed if the drainage blankets can be prevented of clogging. A clogged drainage blanket is deleterious to the sustainable life of an earthen dam, which should be prevented to the best possible extent.

Figure 4.51 highlights the variation in FoS of the downstream face of an earthen dam for different clogging typologies and the progression of clogging with time. It is observed that, in general, at the instant of clogging of a particular section of drainage blanket, the FoS of the downstream face sharply decreases due to the abrupt increase in the pore-water pressure. However, as the clogging of the same section of the drainage blanket is maintained over a period of time, the dissipiation of the excess pore-water pressure takes place, thereby leading to a rise in the FoS. This process of temporal alteration of the FoS of the downstream face is represented till the complete clogging of the drainage blanket, as shown in Figure 4.51. It is observed that there is no definite trend of variation of the FoS of downstream face when different clogging scenarios are considered for the analysis. However, in general, the 'inward clogigng' scenario is observed to produce the lowest FoS values, thereby indicaitng that inward clogging of the drainage blanket will be the most jeopardizing to the stability of the downstream face of the dam. Furthermore, in comparison to sequential clogging (inward, outward, upward or downward clogging), randomly clogged drainage blankets exhibited higher stability of the downstream face of the dam. This is attributed to that fact that although clogged, any randoml clog still allows flow channels within the drainage blanket through which the seepage water can be dissipated from the toe of the earthen dam. This phenomenon results in a relatively higher stability to the earthen dam.

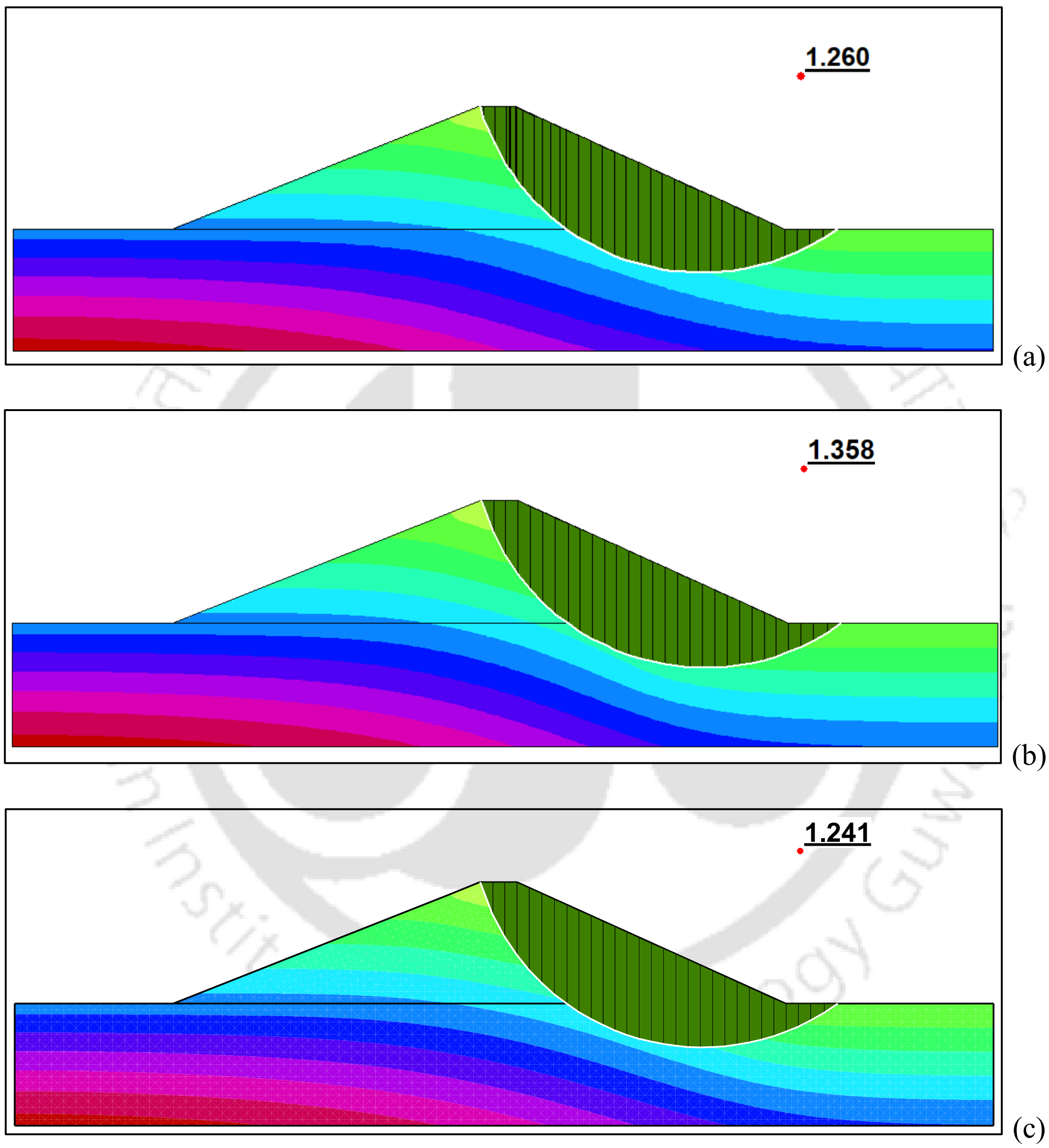

Figure 4.49 Stability of the downstream face of an earthen dam with horizontal toe drainage blanket (a) NDC (b) FDC (c) CDC

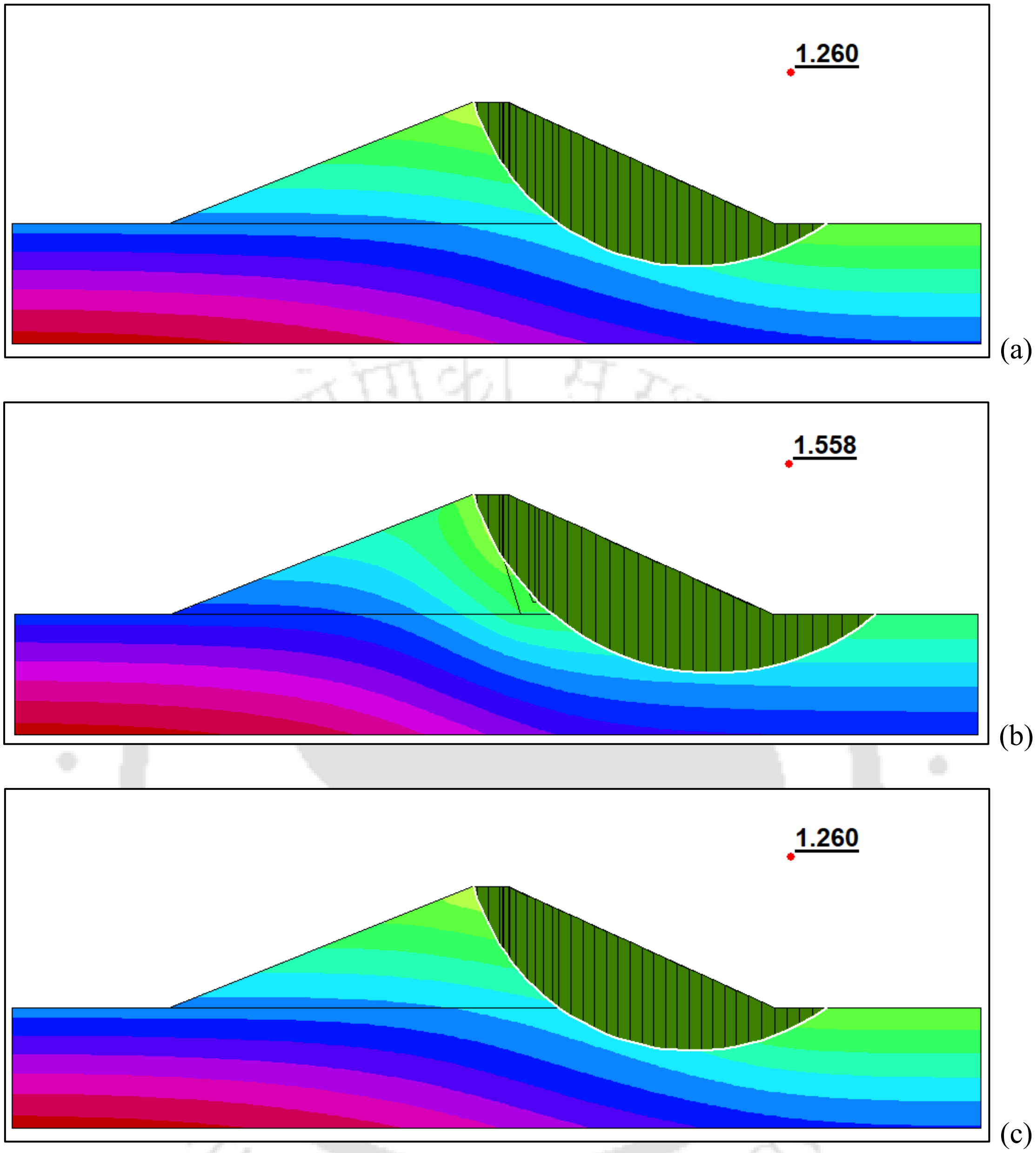

Figure 4.50 Stability of the downstream face of an earthen dam with inclined chimney drainage blanket (a) NDC (b) FDC (c) CDC

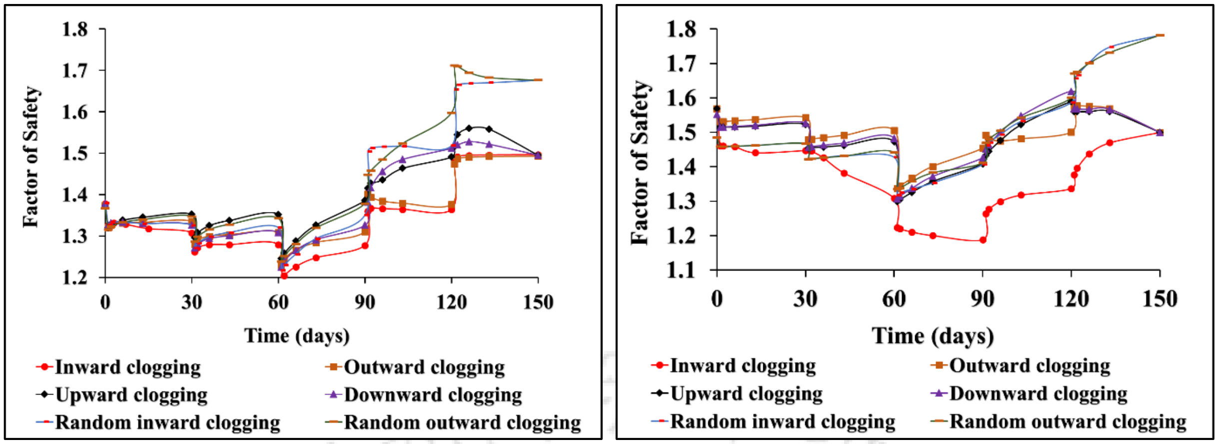

(a) (b)

Figure 4.51 Stability of the downstream face of an earthen dam values subjected to different types of clogging in (a) Horizontal toe drainage blanket (b) Inclined chimney drainage blanket

Figures 4.52 and 4.53 illustrate the temporal variation of the stability of the upstream and downstream faces of the earthen dam when subjected to rise-up and drawdown conditions, respectively. In these figures, the influence of the horizontal toe and inclined chimney drainage blankets in their NDC, FDC and CDC conditions on the stability of upstream and downstream faces of the earthen dam are highlighted. Figure 4.52 shows that during the drawdown condition, owing to the removal of water load from the upstream face, there is an abrupt reduction in the FoS that is irrespective of the type of drainage blanket and their operating conditions (NDC, FDC or CDC). This drastic reduction in the upstream face stability is observed due to hydraulic inequilibrium experienced just after the drawdown, wherein the internal pore-water is trying to drain out through the upstream face due to the removal of the confinement provided by the reservoir water. As the pore-water pressure gradually dissipates after the reservoir drawdown, the stability of the upstream face is marginally regained and a constant FoS is obtained. Figure 4.52(b) exhibits that the stability of the downstream face gradually increases for all conditions, since the drawdown of the upstream reservoir leads to flow of the water towards the upstream, thereby increasing the effective strength in the remaining portion of the earthen dam.

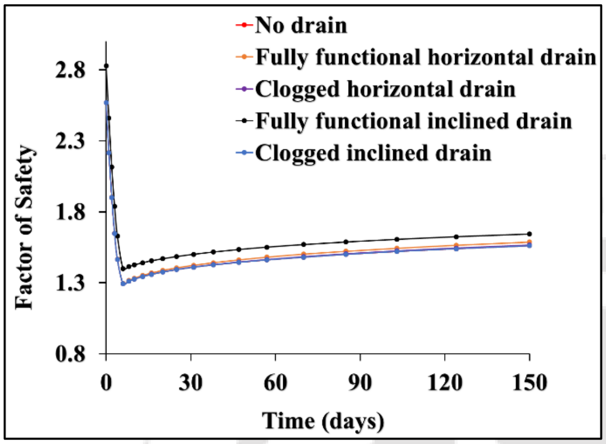

(a)

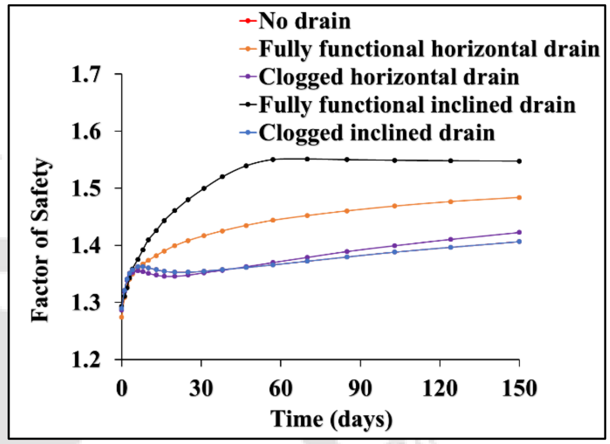

(b)

Figure 4.52 Stability of the earthen dam comprising various types of drainage blanket under varying operating conditions when subjected to reservoir drawdown scenario (a) Upstream face (b) Downstream face

During the reservoir rise-up condition, the sudden buildup of water load on the upstream face results in the momentary increase in the FoS values, as shown in Figure 4.53(a). As the water load on the upstream face stabilizes, gradual dissipation of pore-water pressure takes place through the body of the dam, and the saturation front migrates towards the downstream. This results in a steady decrease of the FoS of the upstream face, until a constant magnitude is achieved. At the same time, Figure 4.53(b) shows that as the waterfront migrates towards the downstream, depending upon the type of drainage blanket and their operating conditions, larger area of the downstream are subjected to saturation owing to the temporal accumulation of pore-water pressure. Thus, the stability of the downstream face of the earthen dam gradually decreases, the decrement being more pronounced for the NDC and CDC conditions. As expected, FDC condition of the drainage blanket sustains the stability of the downstream face, in which the performance of the inclined chimney drainage blanket is observed to be better than the horizontal toe drainage blanket.

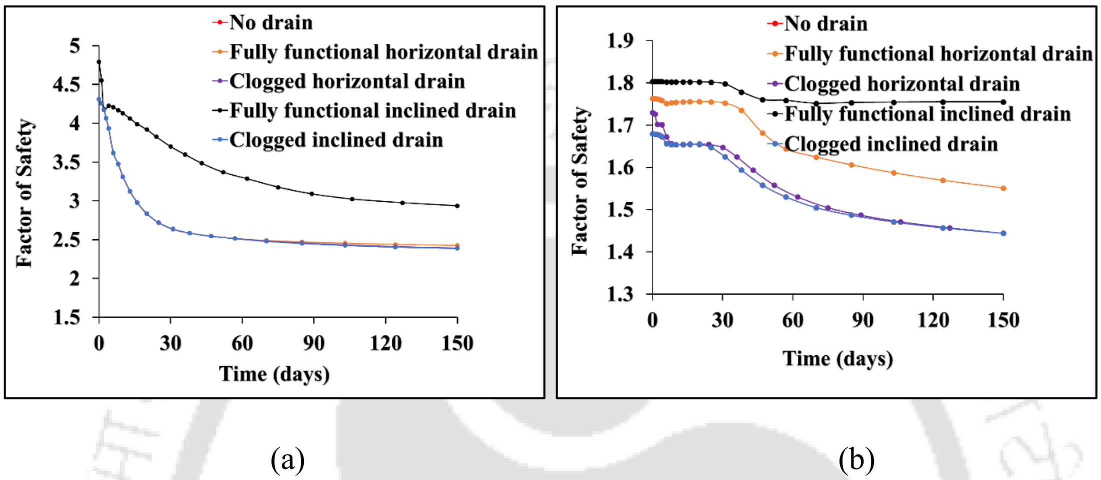

Figure 4.53 Stability of the earthen dam comprising various types of drainage blanket under varying operating conditions when subjected to reservoir rise-up scenario (a) Upstream face (b) Downstream face

4.3.5.4 Influence of Clogging Rate on the Response of Homogeneous Earthen Dam with Drainage Blankets

It is already established in the previous sections that inward clogging of the drainage blankets give rise to the most critical hydraulic and stability response of an earthen dam (as shown in Table 4.3). This section reports about the influence of the rate of inward clogging of the horizontal toe drainage blanket on the response of an earthen dam. The trend of response for the inward clogging of the inclined chimney drainage blanket is expected to be similar, and thus the results are not reported herein. The analyses are carried out for the steady-state and transient reservoir conditions. The clogging rates are calculated by estimating the number of days required to clog the entire drain length. The higher rates considered in the analyses are hypothetical and are introduced in the study for understanding the behavioral differences in the response of the dam if relatively higher rates of clogging take place in the drainage blanket. The length of the horizontal toe drainage blanket is considered 10 m in the study. Accordingly, the entire length of 10 m is considered clogged within 10 days, 100 days and 1000 days, thereby resulting in three different clogging rates as 1 m/day (high rate of clogging), 0.1 m/day (moderate rate of clogging) and 0.01 m/day (high rate of clogging), respectively (Pinyol et al., 2008). The effect of clogging rate on the variation of pore-water pressure is observed for the 3rd stage of clogging i.e., for the 6th day, 60th day (1 month) and 600th day (1.64 years), corresponding to the high, moderate and low rate of clogging respectively.

As highlighted by Figure 4.54, the influence of clogging rate of clogging can be observed for both the steady-state and transient reservoir conditions. Figure 4.54(a) reveals that for the steady-state reservoir condition, the PWP increases with the decrease in clogging rate. A lower clogging rate allows more time for the migration of saturation front through the body of earthen dam towards the downstream, manifested by the rise of phreatic surface, thereby reducing the PWP. Figure 4.55 depicts the influence of the rate of clogging on the location of phreatic surface. However, when the clogging rate is higher, compared to the earlier case, the excess PWP and the saturation front yet did not have enough time to migrate downstream. Hence, when clogging is simulated by their rates, the immediate short term monitoring would bound to show higher magnitudes of pore-water pressure due to lesser dissipation in lesser time, and that is what is manifested in Figure 4.54. However, as mentioned, this response is only for short-term condition to understand the scenario just after the clogging. If the long-term condition were considered, when sufficient time is allowed for the pore-water pressure to dissipate in both the cases, the same rise in the phreatic surface and pore-water pressure distribution would be observed. Figure 4.55 shows that for both the high and low clogging rate, the phreatic surface approximately achieves a similar location with the earthen dam, except being marginally different as it intersects the downstream face, which is attributed to blocking of flow channels by clogging of the drainage blanket itself. Hence, it can be stated that in the steady-state reservoir condition, beyond the time at which the phreatic surface attains its maximum level within the body of earthen dam, the rate of clogging has marginal effect on the subsequent PWP variation.

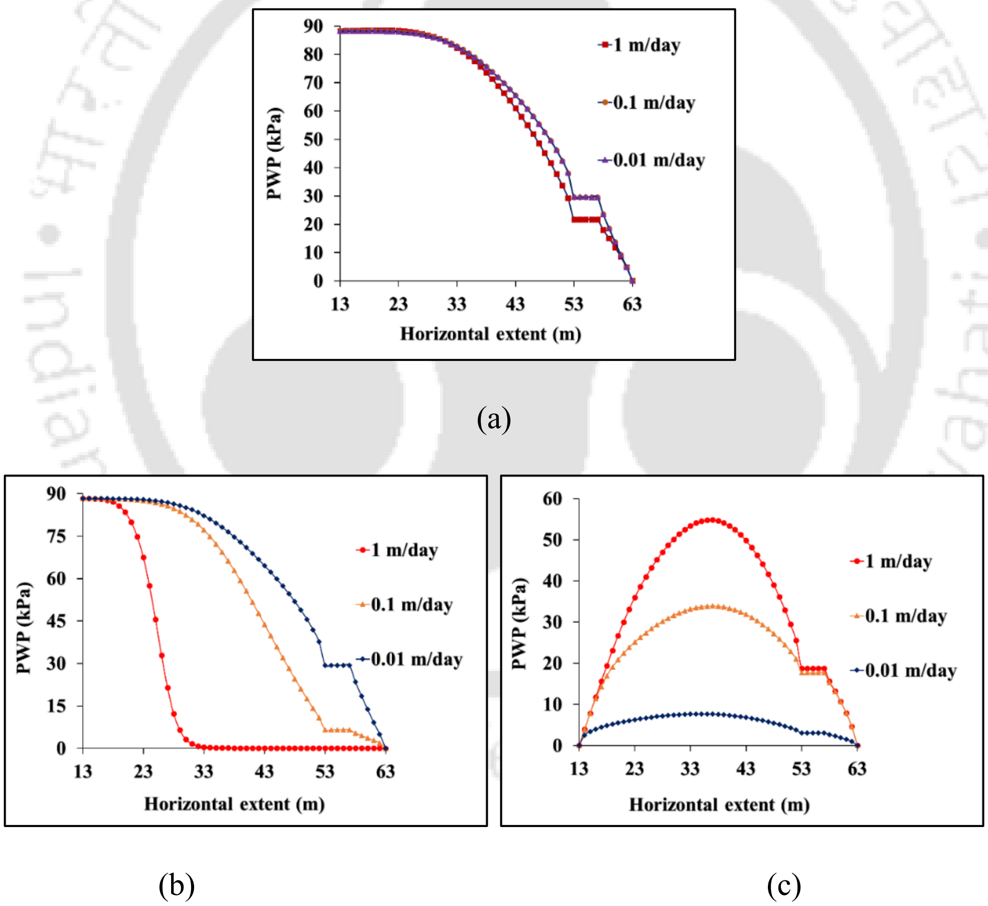

Figure 4.54 Variation of PWP along the base of the dam after the 3rd stage of clogging for different clogging rates (a) Steady-state reservoir condition (b) Reservoir rise-up condition (c) Reservoir drawdown condition

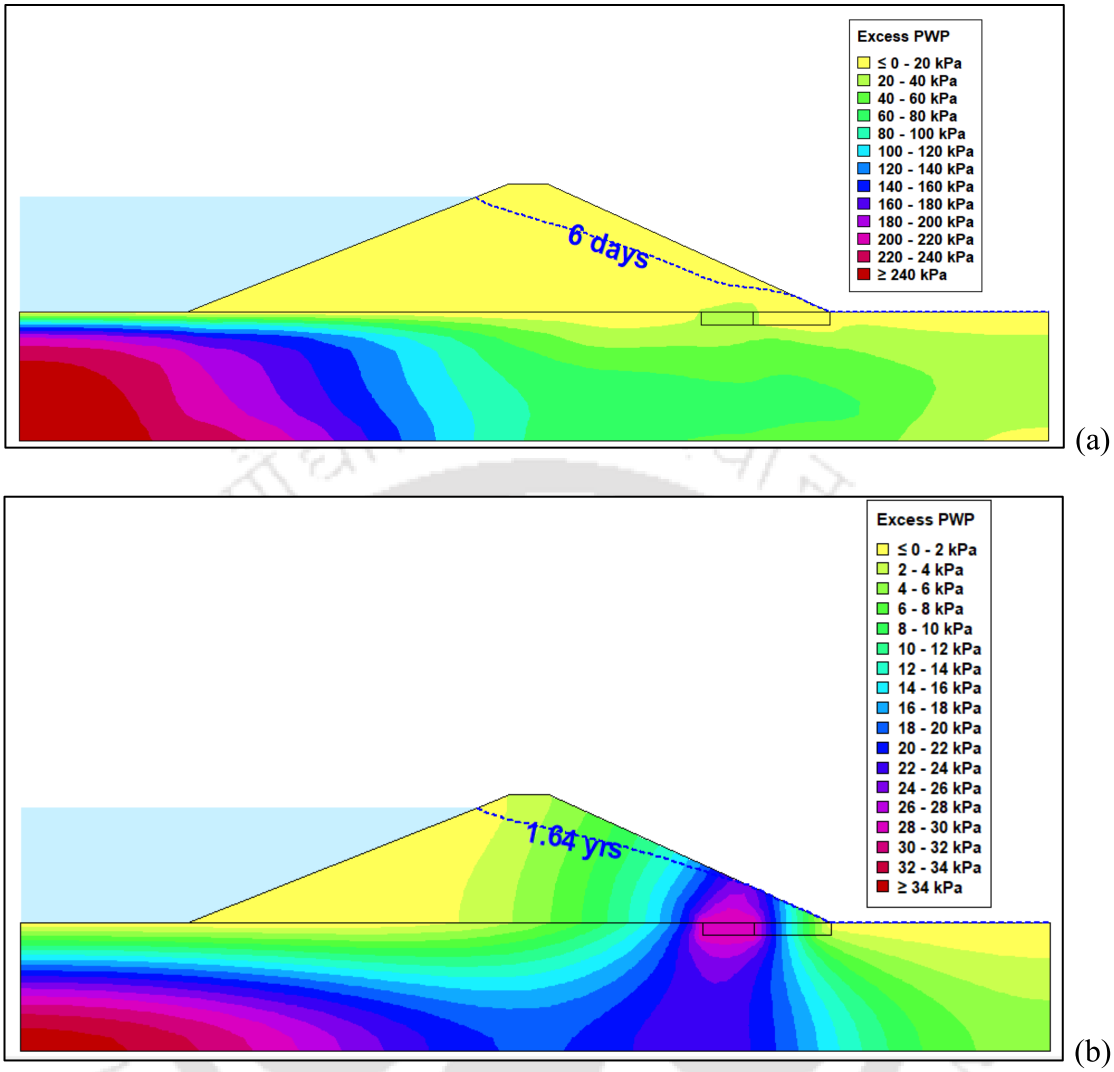

Figure 4.55 Influence of clogging rate on the variation of pore-water pressure within an earthen dam with horizontal toe drainage blanket and a steady-state reservoir condition (a) High rate of clogging, i.e. 1 m/day (b) Low rate of clogging, i.e. 0.01 m/day

For the reservoir rise-up condition, as shown in Figure 4.54(b), it is observed that higher clogging rates result in lower PWP along the base of the earthen dam, and the otherwise is observed for lower rate of clogging. For all the cases of clogging rates considered in the study, the rate of reservoir rise-up is the same, i.e. 1.5 m/day. Thus, for the lower rate of clogging considered (i.e.

0.01 m/day), the reservoir attains its maximum capacity quicker than the progression of clogging in the drainage blanket. Hence, for most of the time required for clogging of the drainage blanket, the reservoir remains full, thereby allowing the excess PWP to migrate towards the downstream. On the other, hand, for higher rates of clogging, the time required for the reservoir to rise to its full capacity is similar to that required for the 3rd stage of clogging. Hence, for higher rates of clogging, the PWP remains concentrated more towards the upstream side of the dam. Figure 4.56 aptly displays the variation of PWP with the body of the earthen dam for various clogging rates.

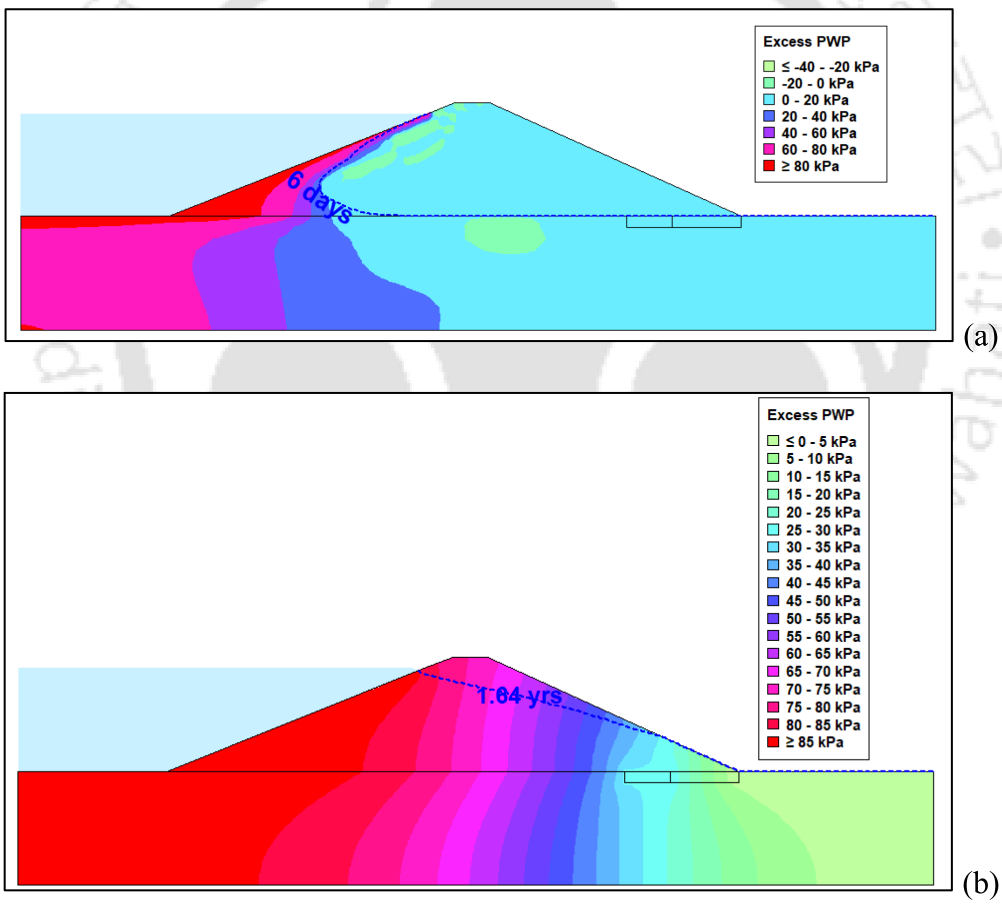

Figure 4.56 Influence of clogging rate on the variation of pore-water pressure within an earthen dam with horizontal toe drainage blanket and a reservoir rise-up condition (a) High rate of clogging, i.e. 1 m/day (b) Low rate of clogging, i.e. 0.01 m/day

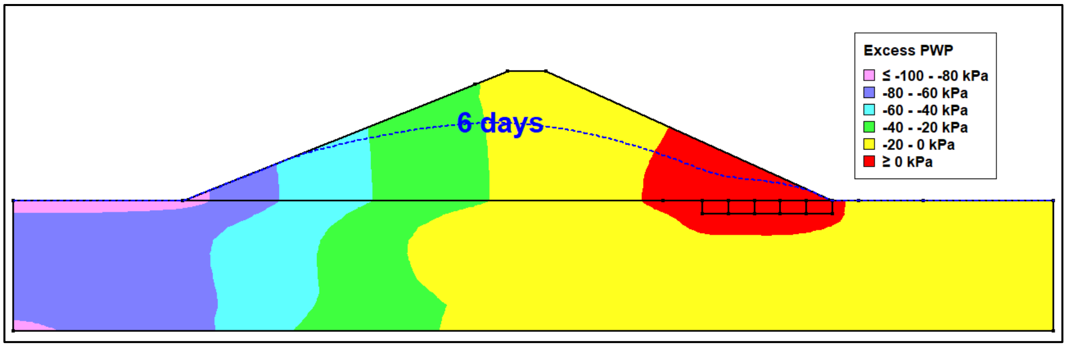

(a)

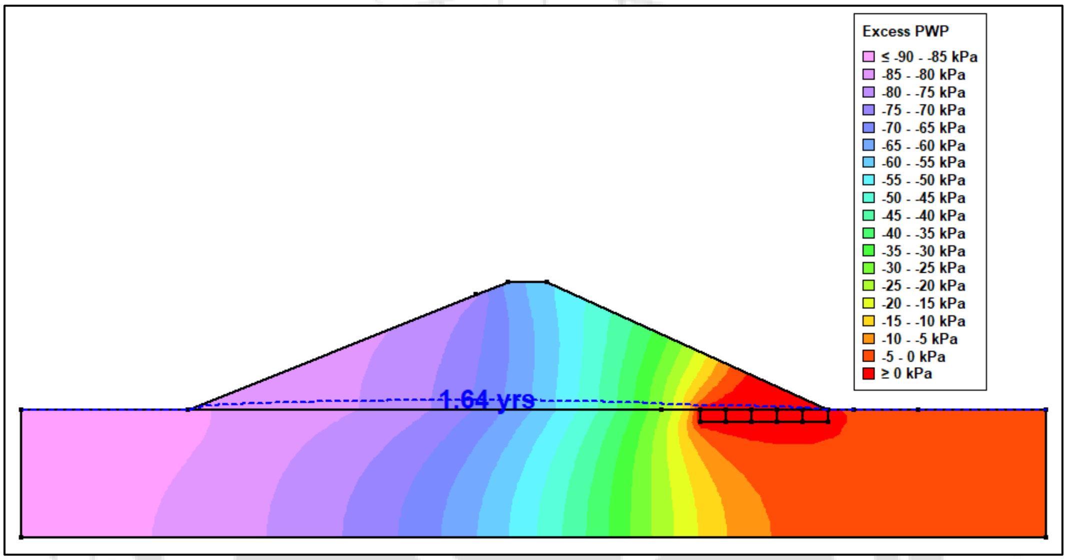

(b)

Figure 4.57 Influence of clogging rate on the variation of pore-water pressure within an earthen dam with horizontal toe drainage blanket and a reservoir drawdown condition (a) High rate of clogging, i.e. 1 m/day (b) Low rate of clogging, i.e. 0.01 m/day

In the case of reservoir drawdown, Figure 4.54(c) shows that higher clogging rates results in more PWP along the base of the earthen dam. Similar to the reservoir rise-up condition, during the drawdown scenario as well, the rate of drawdown is same (i.e. 1.5 m/day), for different clogging rates considered in the study. For higher clogging rate of drainage blanket, the reservoir is drawn down at an approximately similar time required for the 3rd stage of clogging. Hence, the phreatic surface remains at a higher altitude within the body of the dam, and higher magnitude of PWP is yet observed near the drainage blanket. On the other hand, owing to the low clogging rate, the 3rd stage of clogging takes place at sufficiently higher time, within which significant dissipation of PWP takes through the upstream face of the dam. Thus, for lower clogging rates, lesser PWP is observed throughout the base of the dam. The visual representation of the influence of rate of clogging for a reservoir drawdown condition is depicted in Figure 4.57.

Figure 4.55 to Figure 4.57, indicate the generation of excess pwp during the high and low rate of clogging during the steady-state, rise-up and drawdown conditions. It has been clearly observed that the generation excess pwp increases as the rate of clogging decreases for the steady-state and rise-up condition however, the generation of excess pwp decreases with decrease in rate of clogging for the drawdown condition.

4.4 SUMMARY

This chapter presents the response of a homogeneous earthen dam subjected to the clogging of horizontal tow and inclined chimney drainage blankets. Finite element based Seep/W and Sigma/W modules are used to conduct the seepage analysis and stress analysis, respectively, while Slope/W module is used to study the limit-equilibrium based stability analysis. Three different reservoir conditions, namely steady-state condition, reservoir rise-up condition and the reservoir drawdown condition, are used in the present study. A validation study is conducted related to the response of Glen Shira Dam, Scotland, to ascertain the efficacy of the developed models. The influence of different typologies of sequential and random clogging of the drainage blankets are studied for the hydraulic response and stability of the earthen dam. Finally, the influence of rate of clogging and reservoir conditions on the response of homogeneous earthen dam, comprising horizontal toe drainage blanket, are presented. The results presented in this chapter suitably indicates that the clogging typologies and rate of clogging, along with the reservoir fluctuations, have recognizable effects on the response of homogeneous earthen dam.

CHAPTER 5

HYDRAULIC FRACTURING AND CRACKING OF HOMOGENEOUS EARTHEN DAMS

5.1 GENERAL

Development of cracks, fractures and fissures in an earthen dam lead to the generation of weak sections, which may eventually lead to catastrophic failure of dam, thus creating a significant hazard to life and property. Hence, it is immensely important to assess and develop reliable methods of predicting the locations of cracking initiation and to identify the possible extent of cracking. Such understanding can help to adopt suitable mitigation techniques and preventing dam failure, thereby extending the performance life of an earthen dam. The potentiality of finite element method in analyzing tension cracking in earthen dams is a proven issue, and is already used by different researchers in the past (Covarrubias, 1969; Lee and Shen, 1969; Casagrande and Covarrubias, 1970; Covarrubias, 1971). In reality, the formation of cracks during the construction of dams is inevitable. The existence of cracks increases the susceptibility of the soil slopes to erosion, shear strength loss, water seepage, and consequent failures. A hefty percentage of the economic budget is spent every year in the repair and maintenance of such slopes. One such example of it is the expenditure estimated by the geotechnical engineers that was approximately $960,000 for maintaining the slopes and shallow slides in Indiana (Hopkins et al., 1988). The presence and existence of cracks in earthen dams is generally not considered in the conventional design where the fills are hypothesized to be intact and devoid of any cracks and fissures during the construction phase or the reservoir filling phase. Lack of proper information regarding the crack geometry, its initiation and the path of propagation through the earthen dam makes it even difficult to deal with this problem. Thus, it becomes very important to comprehend the mechanisms of cracking, its initiation and the flow of water through the cracks in an earthen dam that would help to adopt suitable mitigation measures and prevent further failures. The following subsections reports the detailed analysis that is attempted to understand the issues related to cracking and hydraulic fracturing in homogeneous earthen dams with the aid of finite element modeling.

5.2 CRACKING IN EARTHEN DAMS

The possibility of hydraulic fracturing in a homogeneous earthen dam follows two different scenarios during the reservoir impounding and drawdown conditions (Ohne and Narita, 1977). The first scenario relates the cause of cracking in the earthen dam to the differential settlement at the base of the earthen dam after its construction. The crack, once initiated, results in erosion during the reservoir operations. When these differential settlements are dominant at the base of the earthen dam, it results in the development of tensile strains on the surface or in the interior of the earthen dam. The tension cracks jack opens as the minor principal stress (σ_3, in terms of total stress) tends to decrease locally with the development of tensile strains. The criterion for the possibility of hydraulic fracturing in this case is given by the following condition

$$\sigma_3 < -p_t \tag{5.1}$$

where, p_t refers to the tensile strength in terms of total stress. The corresponding stress state is shown in Figure 5.1(a). It is observed that the decrease in σ_3 results in the enlargement of initial stress circle (represented by Circle I) towards the left, until it finally touches the failure envelop (represented by Circle II) to open up tension cracks. This type of hydraulic fracturing is mostly associated with the post-construction settlement of the earthen dam before reservoir filling takes place.

The second scenario is the case where pore-water pressure comes into play. As the reservoir filling takes place, the pore-water pressure increases towards the centre of the homogeneous dam which results in the decrease of the minor principal stress ($\sigma_3^{'}$, in terms of effective stress) such that it becomes equal to the effective tensile strength ($p_t^{'}$) to jack open the latent cracks. The stress state for this scenario is shown in Figure 5.1(b). In this case, it is where the initial stress circle (I) touched the failure envelope at the circle (II) by shifting towards the left without any change in the diameter. The criterion for the possibility of hydraulic fracturing in this case is given by the following condition

$$\sigma_3^{'} < -p_t^{'} \tag{5.2}$$

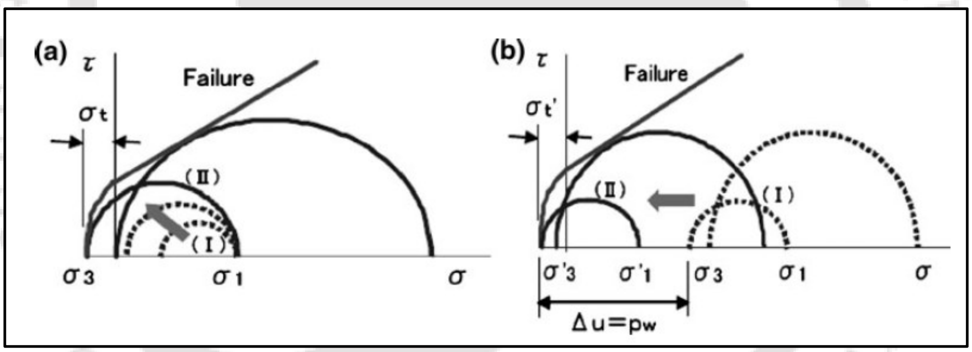

Figure 5.1 Mechanism of hydraulic fracturing in earth dams explained through Mohr's circles based on (a) differential settlement (b) development of seepage-induced pore-water pressure (as per Ohne and Narita, 1977)

5.3 ANALYSIS OF CRACKING AND HYDRAULIC FRACTURING IN HOMOGENEOUS EARTHEN DAM

The detrimental effects of cracks on earthen dams and embankments was first observed by Casagrande (1950). The importance of safety of dams, even with the occurrence of cracks, was hihglighted in the research work. The causes of different types of crack formation in earthen dams was summarized by Sherard (1973). As per the existing literature, the opening of cracks in earthen dams can be broadly classified as longitudinal cracks and transverse cracks (that open parallel and transverse to the dam axis, respectively). They can further be classified as interior or exterior cracks, and on the basis of different circumstances, they may be categorized to devleop in vertical, horizontal or intermediate planes. The occurrence of cracks in erathen dams and embankments have serious consequences and, thus, should be studied in detail in order to develop preventive and healing measures to combat the diastrous effect related to cracking. Many investigators in the USSR and other abroad countries, as well as researchers associated with the International Commission on Large Dams (ICOLD) are involved in solving problems related to cracking. The presence of inhomogeneous soils in earthen dams, as well as the variable water heads, results in a complicated distribution of stresses in earthen dams and embankments. The primary causes of formation of cracks in earthen dams are manifold. They are primarily classified as: (a) differential settlement due to the presence of elements comprising different deformability characteristics, (b) hydro-mechanical forces causing redistribution of stresses in the dam during rapid filling and emptying of the reservoir, thereby promoting the formation of loosened or softened zones in the body of earthen dam, (c) presence of soils placed in the body of the earthen dam and the core of earth-rock dams that has potential to undergo piping, (d) foundation bed comprising compressible, or piping-unstable soils, and (e) marked changes in the topography of the footing and side abutments of the dam. In many cases, cracking is also initiated by seismic forces. Most often, the cracks are formed by a combination of several of the aforementioned causes.

5.3.1 Finite Element Modeling for the Present Study

The finite element analysis for the study is conducted using the commercially available finite element software GeoStudio. The Seep/W and Sigma/W modules of Geostudio are used in this study. Analysis of groundwater seepage and problems related to dissipation of excess pore-water pressure within porous media, such as rock and soil, can be handled by Seep/W; whereas, Sigma/W is a powerful tool for stress-strain and deformation analysis, with special provision to conduct 'Coupled stress-PWP analysis'. Different models are simulated in Seep/W to conduct the initial steady-state seepage analysis, and establish the existing pore-water pressures and total head conditions in the earthen dam. The initial stress conditions are generated using 'In-situ analysis' of Sigma/W. The construction of earthen dam (represented by placing the fill material in single lift or sequential multiple lifts) is simulated using the 'Load/Deformation analysis' in Sigma/W, whereas 'Coupled Stress/PWP analysis' is used to simulate the 'rapid rise-up' and 'rapid drawdown' conditions. In both the analyses types, the pore-water pressure generated in the 'steady-state analysis' of Seep/W and stresses generated in the 'In-situ analysis' of Sigma/W are used to define the initial conditions for the transient reservoir conditions.

5.3.2 Models and Materials used in the Analysis

The flow and deformation responses of homogenous earthen dams are studied to identify the location from where hydraulic fracturing or cracking can possibly initiate. The entire set of analyses is divided under two broad categories, Case I and Case II, for representing and simulating cracking during the construction stage and operational stages of earthen dams. Case I represents those scenarios of cracking initiation that are associated with the construction of earthen dam. In general, the field construction of earthen dam is associated with compaction of sequential multiple layers of earth fill. However, in many instances, the numerical models consider the earthen dams to be constructed of single lift, i.e. the dams are considered 'wish in-place' during the numerical analysis. In such a case, a full-sized numerical model of the dam is analyzed, which does not represent the field construction scenario. Hence, in this study, analysis pertaining to numerical modeling of Case-I considers both single and multiple lifts to represent an earthen dam construction, and assess the influence of commonly adopted single-lift technique on the hydraulic fracturing of earthen dams. For Case II, the transient reservoir operations namely the rapid rise-up and rapid drawdown conditions were simulated to assess their influence on the initiation of hydraulic fracturing of a homogeneous earthen dam. The numerical models used in the present study, along with its relevant dimensions, are shown in Figure 5.2.

The materials of the earthen dam and the foundation are modeled using the 'elastic-plastic' material model in Sigma/W to perform the stress deformation analysis. In Seep/W analysis, the material for earthen dam is modeled using 'saturated/ unsaturated' material model, while the foundation is modeled using 'saturated only' material model. The volumetric water content function and the hydraulic conductivity function that are used as input for the materials chosen for earthen dam and foundation are shown in Figure 5.3. As mentioned earlier, these curves are estimated following the procedures proposed by van Genuchten (1980) and are required to solve the seepage equation in the 'coupled stress-PWP analysis'. The various soil properties used in the modeling was obtained from extensive literature survey (IS 12196; USBR 1987; USBR 2014; Seep/W 2012) coupled with proper engineering judgment. The material properties of the soils used in the models are listed in Table 5.1.

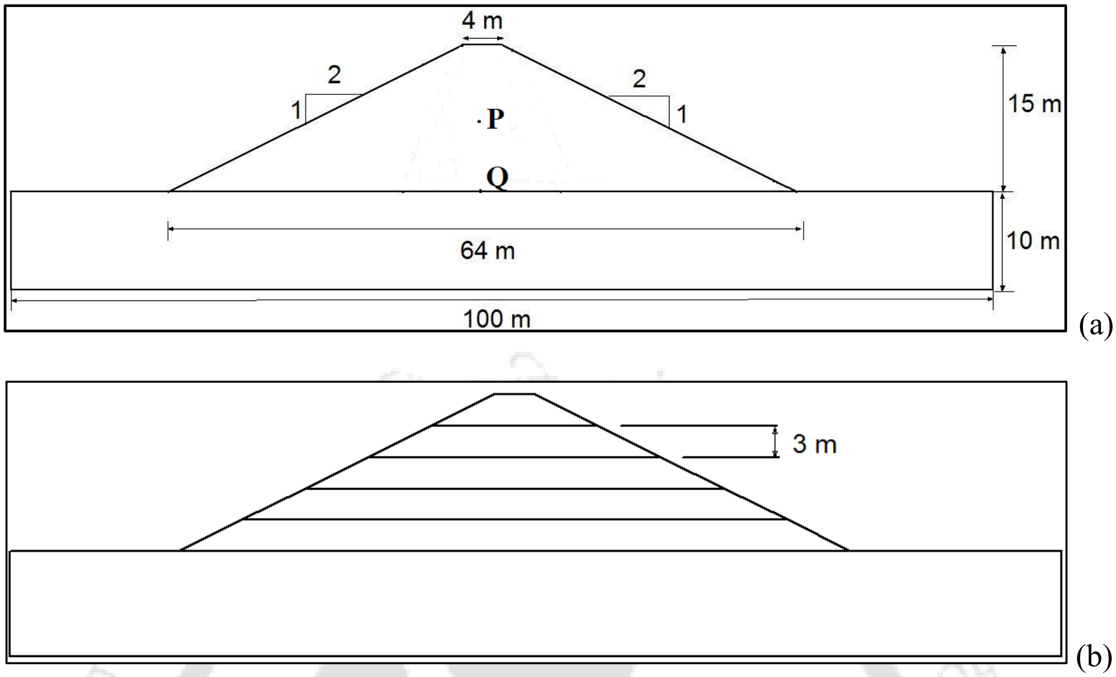

Figure 5.2 Numerical models of earthen dam constructed in (a) simplified single lift (b) real-field multiple lifts

Table 5.1 Material properties used in the simulation of hydraulic fracturing of homogeneous earthen dam

	c (kPa)	$ø$ (degree)	γ (kN/m^3)	$E_{modulus}$ (kPa)	k (m/s)
Embankment	10	25	20	15000	10^{-7}
Foundation	15	20	20	30000	10^{-10}

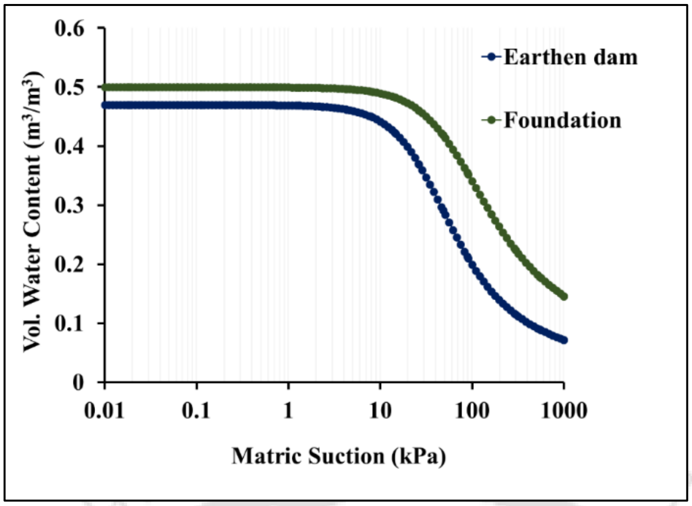

(a)

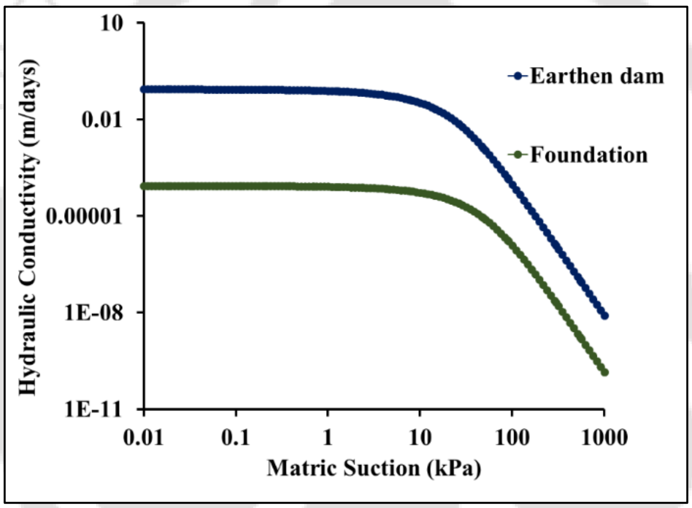

(b)

Figure 5.3 Hydraulic characteristics of materials for earthen dam and foundation (a) Volumetric water content function (b) Hydraulic conductivity function

5.4 INTERPRETATIONS AND DISCUSSIONS

5.4.1 Analysis for Case I: Post-Construction Cracking of Homogeneous Earthen Dam

The simulation of earthen dam construction is carried out using the 'Load/Deformation analysis' in Sigma/W by placing the embankment fill by either single lift or sequential multiple lifts. For the analysis pertaining to multiple lifts, the earthen dam, having height 15 m, was divided into five equal lifts, the height of each lift being 3 m. The foundation is simulated using 'elastic-plastic material model' with the 'effective drained parameters', as it remains submerged by the water table under any stage of analysis. The earthen dam is also simulated with the 'elastic-plastic material model' while considering 'total stress parameters', as this stage of analysis considers only the constructed earthen dam before the commencement of reservoir filling operation. Hence, the water table remains at the base of the earthen dam during the analysis. The outcomes are presented in terms of variation and distribution of minor principal stresses, deformations and strain concentrations at various locations in the faces and body of the earthen dam, as well as within the foundation soil. It is worth mentioning that GeoStudio 2012 describes the minor principal stress as 'minimum total stress (σ_{min})', and the same is expressed as

$$\sigma_{\min} = \frac{\left(\sigma_x + \sigma_y\right)}{2} - \sqrt{\left[\frac{\left(\sigma_x + \sigma_y\right)}{2}\right]^2 + \tau_{xy}^2} \tag{5.3}$$

where, σ_x and σ_y are the horizontal and vertical stresses, while τ_{xy} is the shear stress on any soil element.

Figure 5.4 exhibits the variation of minimum total stress along the upstream and downstream face of the earthen dam simulated by both single and sequential multiple lifts. As mentioned earlier, conventionally, single lift modeling is adopted to conduct analysis of earthen dams through FE modeling. Through this study, an attempt is made to check the verity of the adopted conventional technique, and identify whether there is any marked difference in the response of the dam, in terms of stresses and deformations, if the sequential multiple lift mode of construction is adopted in numerical modeling. Figure 5.4 clearly indicates that the maximum negative stresses occur along the mid-height of the upstream and downstream faces of the earthen dam. Although for multiple lift simulation, the variation of minimum total stresses along the faces of the dam are more jagged, yet the overall variation of stresses along the faces are largely comparable both in magnitude and in their trend. The maximum negative stress in the upstream face of the dam are recorded to be 26.31 kPa and 19.29 kPa, respectively, at heights of 17.02 m and 17.28 m, respectively, for the earthen dam simulated through single and sequential multiple lift modeling. Similarly, along the downstream face, the maximum negative stresses are obtained as 24.61 kPa and 20.5 kPa, respectively, for single and multiple lift modeling, occurring at a height of 17.05 m and 17. 28 m, respectively. Tensile stresses obtained from single lift modeling are noted to be marginally higher than the multiple lift modeling. Hence, it can be stated that the sequential multiple lift modeling of the construction of the earthen dam hardly produces any significant difference in the stress characteristics of the dam, and hence, the single lift modeling is an acceptable model of representing an earthen dam. In both the types of modeling, the appearance of maximum negative stresses at a height of approximately 17-17.3 m, which is approximately 0.5 times the height of the earthen dam, makes it to be the most vulnerable location for post-construction crack initiation along the upstream and downstream faces. It is worth mentioning that in this study, the tensile strength of the constituent material is assumed negligible, and hence, generation of negative minor principal stress would be considered as an indicator for the initiation of the cracking in the earthen dam.

During the construction or just after the construction of the homogeneous earthen dam, the effect of reservoir does not come into play and the soil within the dam body is under compression due to its self-weight, the possibility of crack initiation lies along the side slopes of the dam. The horizontal deformation of the embankment explains the occurrence of the tensile stresses at the mid height of the embankment.

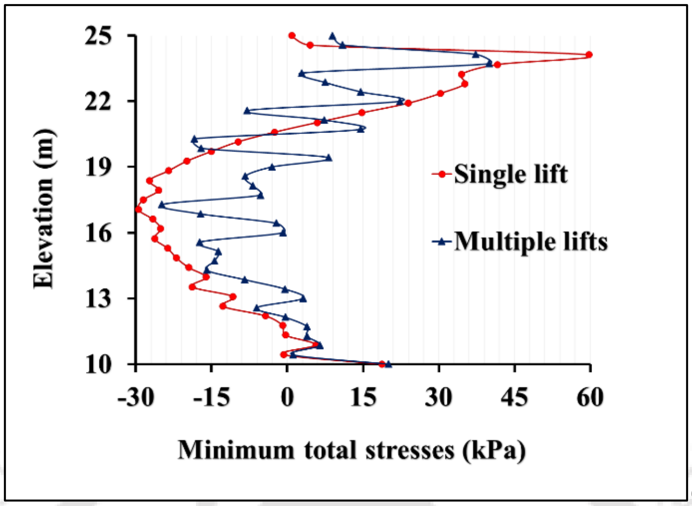

(a)

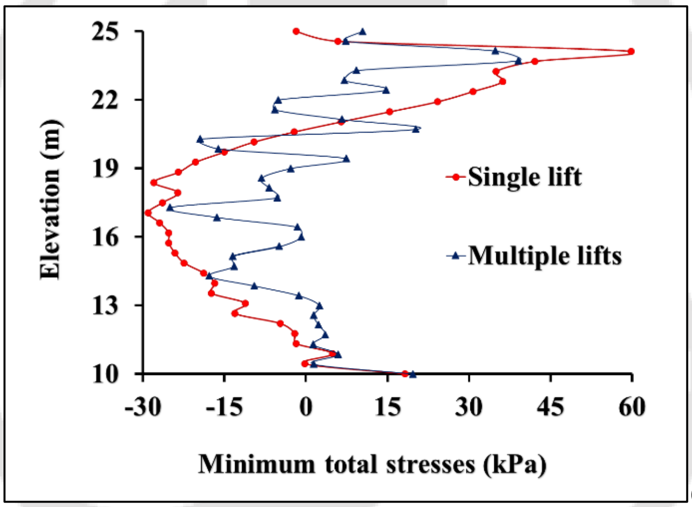

(b)

Figure 5.4 Variation of minimum total stress along the dam faces just after the completion of construction (a) Upstream face (b) Downstream face

Figure 5.5 displays the horizontal deformation contours in the earthen dam modeled using single lift and sequential multiple lifts. As can be observed, prior to reservoir impounding, owing the assumed symmetric compaction control in the field and symmetric distribution of gravity load, symmetric contours of the horizontal displacements were obtained. The contours clearly reflect that the maximum horizontal displacement occurs at 1/2 the height of earthen dam, along both the upstream and downstream faces, irrespective of the way the construction of earthen dam being modeled. For the earthen dam modeled using single lift, maximum horizontal displacement of 50 mm is observed along the upstream and downstream faces, while the same is observed to be approximately 8 mm for the dam modeled using sequential multiple lifts. Hence, based on the results, it can be aptly stated that the single lift mode of modeling the earthen dam is acceptable enough to represent the stress characteristics within the dam, and hence, further analyses reported in this dissertation follows the stated form of modeling of earthen dam. However, the horizontal deformation response of the dam is obtained to be slightly lower for modeling with multiple lifts, which is expected as multiple lifts results in lower sequential stress transfer to the lower fill layers, which are expected to show lower overall deformation. For the same purpose, in practice, the compaction of earthen fills are always carried out in thin layers (mostly 3 m as adopted in the present study), so that the compaction stresses are transferred properly to the lower layers and uniform distribution of compaction stresses are achieved.

Another important factor that plays a very important role in the determination of crack initiation in a homogeneous earthen dam is the post-construction settlement of the earthen dam or its foundation. The differential settlement of the embankment/foundation may cause detrimental cracking in the dam. Figure 5.6 displays the settlement along the base of the earthen dam for the single lift and multiple lift simulations. From the figures, it can be observed that for an earthen dam simulated by single lift technique, the differential settlements at its base are noticeably higher than when it is simulated by sequential multiple lift technique. The maximum settlement for the latter case is 10 mm, whereas for the former case, the settlement is observed as 70 mm.

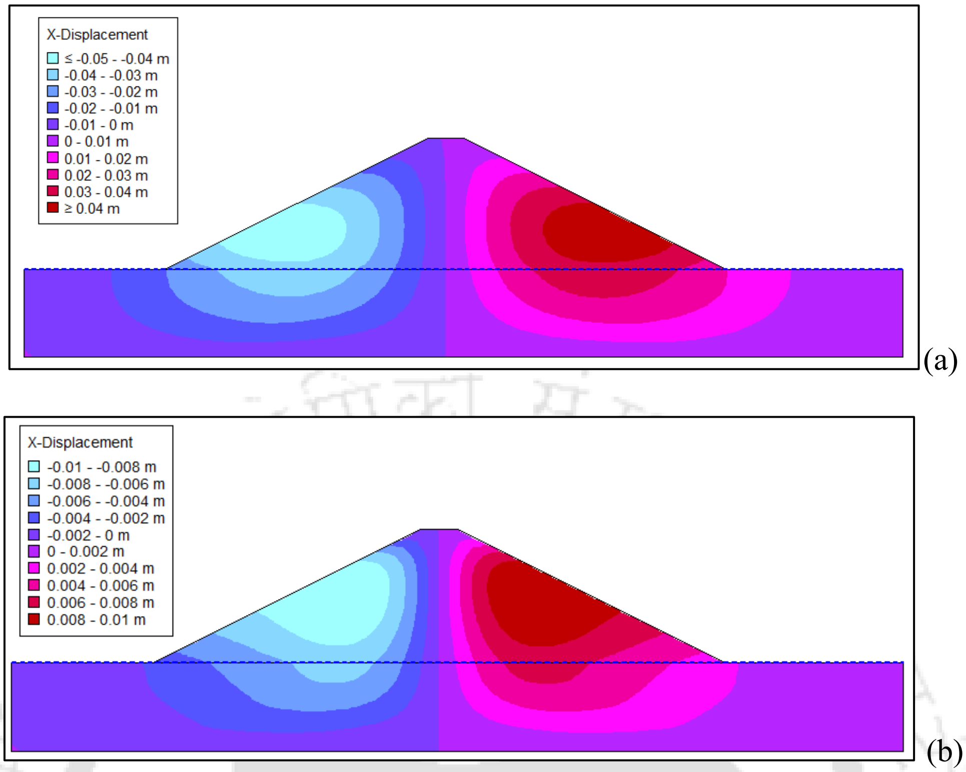

Figure 5.5 Variation of horizontal displacements along the faces of the homogeneous earthen dam (a) Single lift (b) Sequential multiple lift

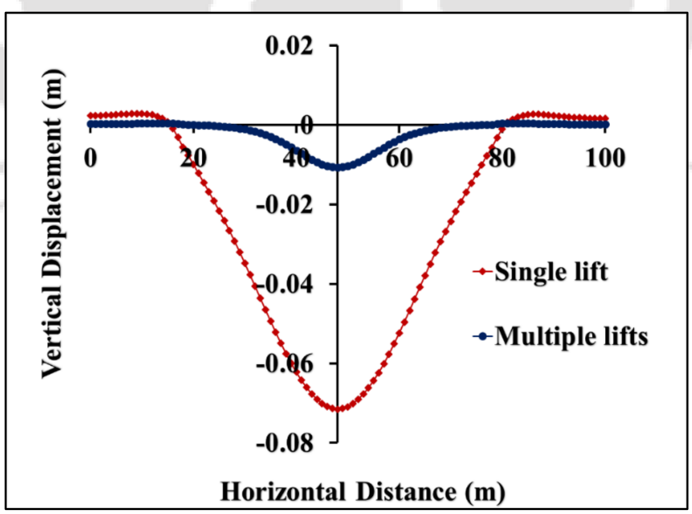

Figure 5.6 Settlement profile along the base of the earthen dam due to adoption of single-lift and multiple-lift techniques for simulating the construction scenario

Figures 5.7 and 5.8 exhibit the variation of strains and their concentration within the earthen dam and its foundation for two different types of adopted modeling scenarios. For the single lift technique, the maximum strain concentration is observed within foundation of the earthen dam, while for the multiple lift scenario, the strain is observed to be concentrated within the body of earthen dam. This is an expected observation as single lift technique considers the dam body to be made of a single entity, and transfers all the bearing stresses generated in the foundation soil. However, for multiple lift technique, each of the sequential lift considers the previous lifts to be the bearing stratum. Hence, for the first lift, the foundation soil acts as the bearing stratum that is subjected to a much lesser load pertaining to a 3 m height of the first fill. However, for the successive lifts, all the previous lifts and foundation are subjected to sequential stress from 3 m lifts. Hence, the stress transfer to foundation soil becomes lesser, and the intermediate layers of fill bear more stresses. Consequently, the strain concentration also remains restricted within the body of the dam. Hence, although the stress characteristics along the face of the dam remains approximately similar for the single-lift and multiple-lift modeling, the horizontal deformation and the strain concentrations are observed to be more realistic pertaining to the multiple-lift modeling. The multiple lift modeling, at the same time, is also more realistic of the field construction technique. Further, the results reveal that the multiple-lift technique will exhibit more deformation and strain concentrations, thereby indicate the dam to be more susceptible to cracking due to post-constructional stresses and deformations.

Hence, it is suggested that the multiple-lift technique would be more appropriate to analyze the post-constructional response of the earthen dam, while the single lift technique is acceptable for further studies subjected to hydraulic fracturing of earthen dam due to reservoir operations, since the initiation of hydraulic fracturing is more dependent on initial stresses than on the strains and deformations. The same will be discussed in the next section.

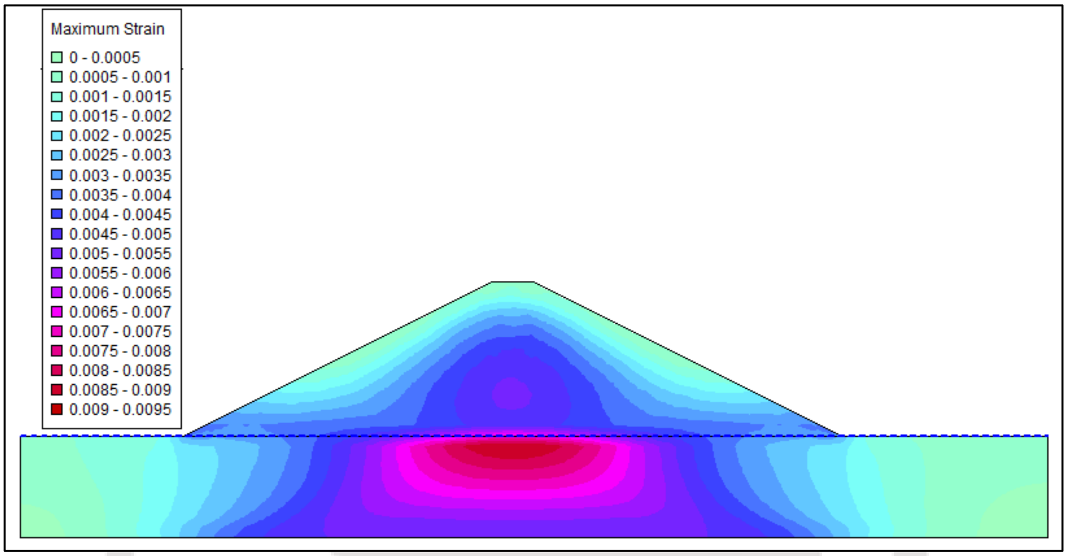

Figure 5.7 Maximum strain contours within the earthen dam and its foundation as obtained from single-lift technique of simulating construction of earthen dam

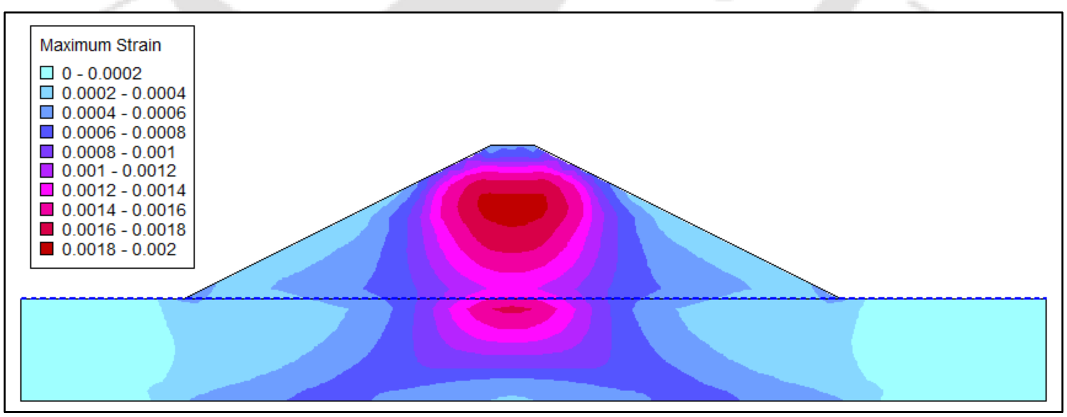

Figure 5.8 Maximum strain contours within the earthen dam and its foundation as obtained from multiple-lift technique of simulating construction of earthen dam

5.4.2 Analysis for Case II: Hydraulic Fracturing of Homogeneous Earthen Dam during Reservoir Rise-up Condition

A reservoir rise-up (RU) condition is simulated using the 'Coupled Stress/PWP analysis' in Sigma/W module of GeoStudio. In this analysis, the simulation of dam construction is first carried out using the 'Load/Deformation analysis', in which the dam construction was simulated in a single lift. At the end of construction, the first impounding of the reservoir is carried out at a rate of 2.8 m/day. Figure 5.9 shows the rate of reservoir rise-up, in which the reservoir of height 24 m was filled in 5 days, leaving a freeboard of 1 m. Stress and deformation analysis is carried out to find out the possibility of crack initiation and its location during the first reservoir filling. The reservoir filling is completed in 5 days, and the analysis is carried out until 1 year after the completion of filling to find out the response of the homogeneous earthen dam during and after the filling process.

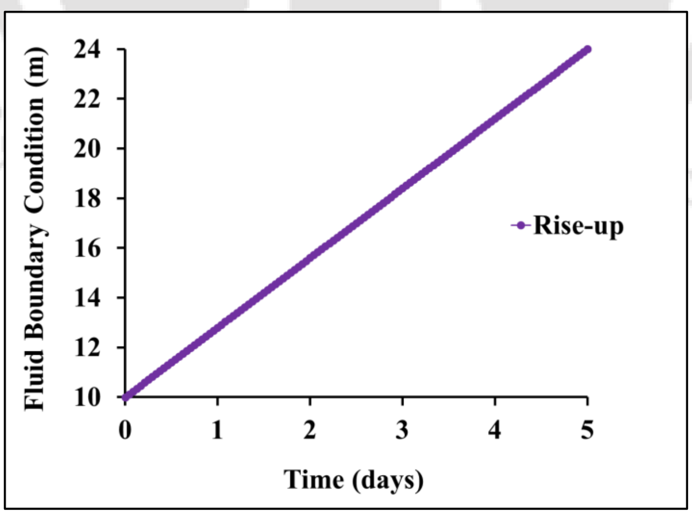

Figure 5.9 Reservoir rise-up (RU) condition and rate adopted in the present analysis

Figure 5.10 highlights the variation of the minimum total stress along the upstream and downstream slopes of the earthen dam for different times during and after the reservoir filling operation. It is observed that along the upstream face, as shown in Figure 5.10(a), the sudden introduction of the water load from the reservoir filling creates a stress in-equilibrium and generates a negative stress at the exposed portion of the upstream face. This is particularly observed in the 2nd day when the reservoir filling has reached a height of 5.6 m from the base of the earthen dam. However, with time, as the reservoir filling progresses towards its completion, on the 5th day, the minimum total stresses on the upstream face increases to the condition that entire upstream face experiences high positive magnitude of minimum total stress. Further, if the reservoir level is maintained in its completely filled condition for a long time, say 146 days, the saturation front gradually moves towards the downstream of the dam. Based on the low hydraulic conductivity of the material of the earthen dam, the dissipation of excess pore-water pressure towards the body of the dam gradually releases the stress, due to which a decrease in the minimum total stress is observed along the upstream face. The process continues until a steady-state of seepage flow is attained, and a marginal change in the PWP profile is observed for further days to come (i.e. 365 days from reservoir filling). In case of the downstream face of the dam, the reservoir filing and steady-state condition has least effect as the minimum total stresses at some portions of the downstream face will increase only when the phreatic surface intersects with the face. Hence, until then, the minimum total stress will change marginally with the reservoir filling operations, as shown in Figure 5.10(b). Figure 5.11 elucidates the variation in the PWP contours, and the progression of the phreatic surface during and after the reservoir filling operation, as is being explained in this section.

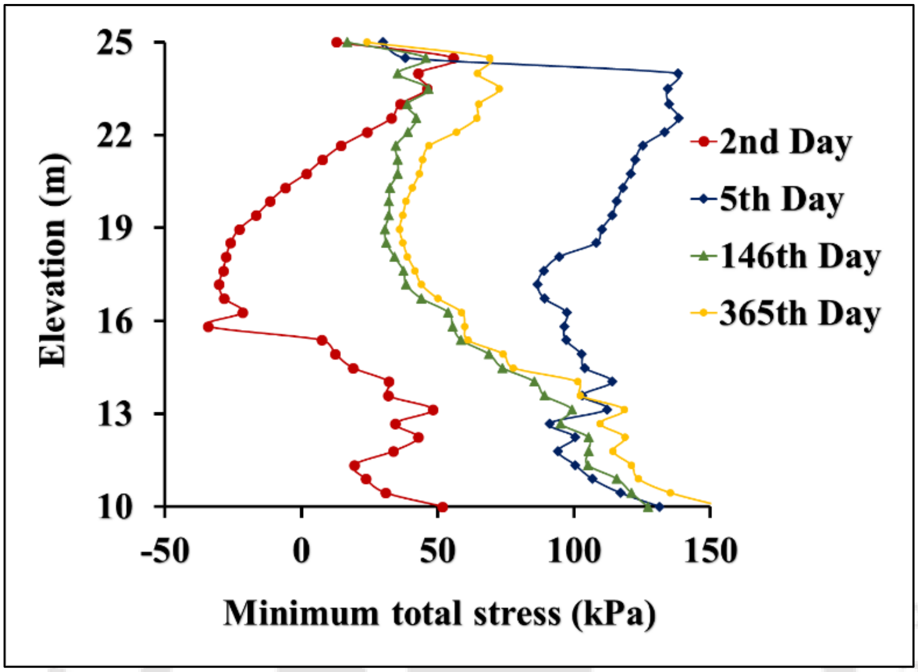

(a)

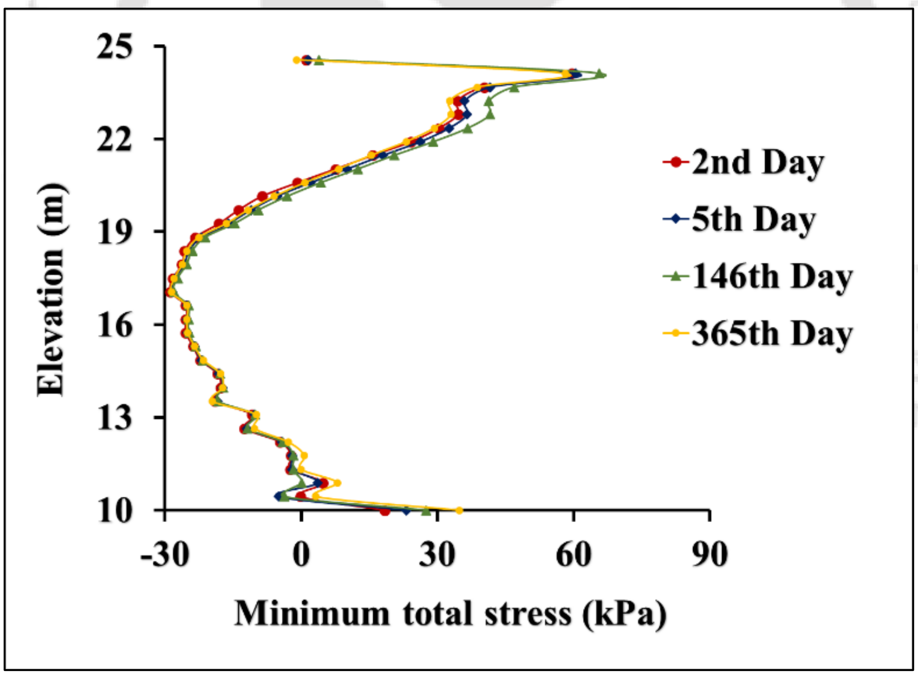

(b)

Figure 5.10 Variation of minimum total stress in the earthen dam during and after the reservoir rise-up (a) upstream face (b) downstream face

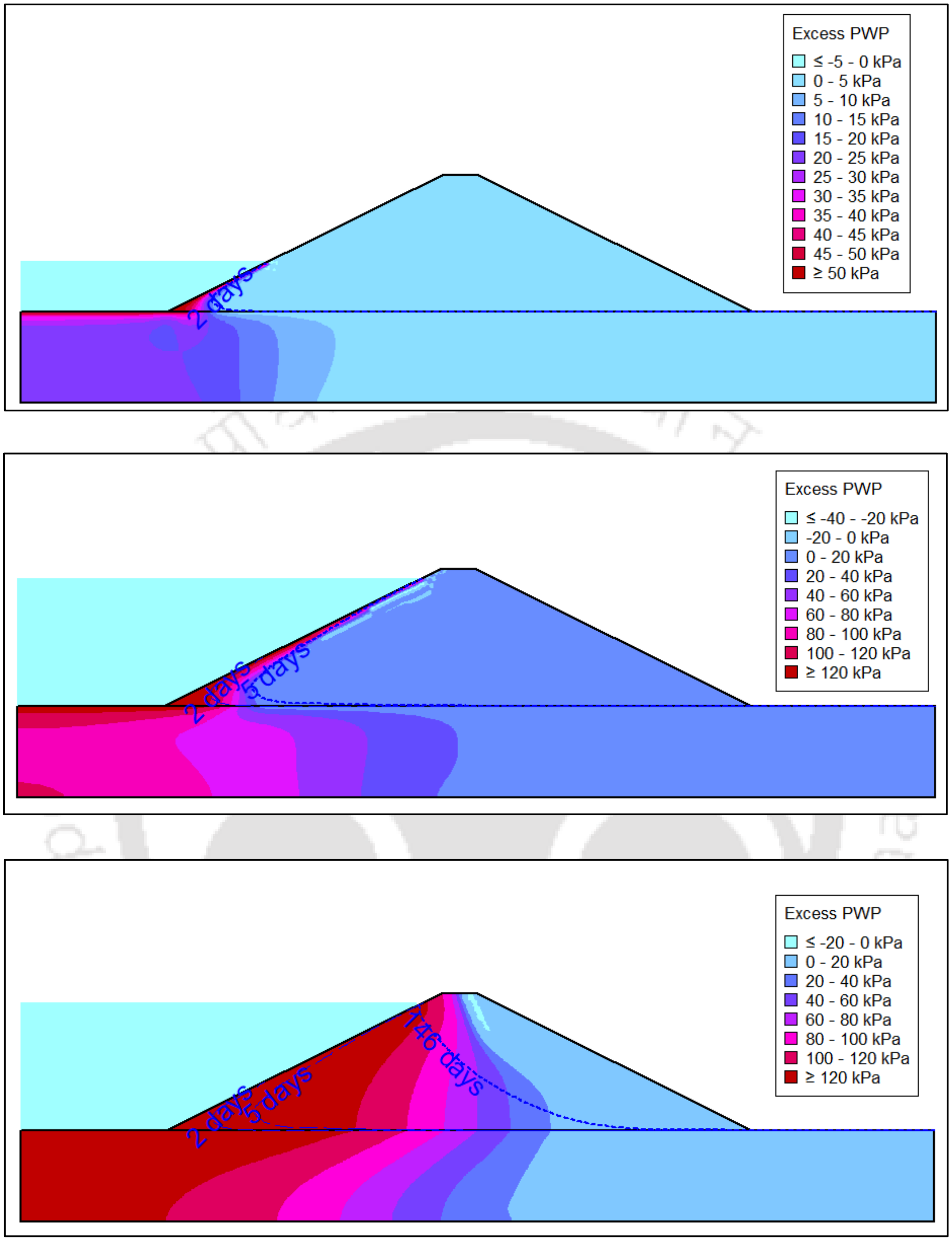
Excess PWP
≤ -5 - 0 kPa
0 - 5 kPa
5 - 10 kPa
10 - 15 kPa
15 - 20 kPa
20 - 25 kPa
25 - 30 kPa
30 - 35 kPa
35 - 40 kPa
40 - 45 kPa
45 - 50 kPa
≥ 50 kPa
2 days
Excess PWP
≤ -40 - -20 kPa
-20 - 0 kPa
0 - 20 kPa
20 - 40 kPa
40 - 60 kPa
60 - 80 kPa
80 - 100 kPa
100 - 120 kPa
≥ 120 kPa
2 days
5 days
Excess PWP
≤ -20 - 0 kPa
0 - 20 kPa
20 - 40 kPa
40 - 60 kPa
60 - 80 kPa
80 - 100 kPa
100 - 120 kPa
≥ 120 kPa
2 days
5 days
146 days

(a)

(b)

(c)

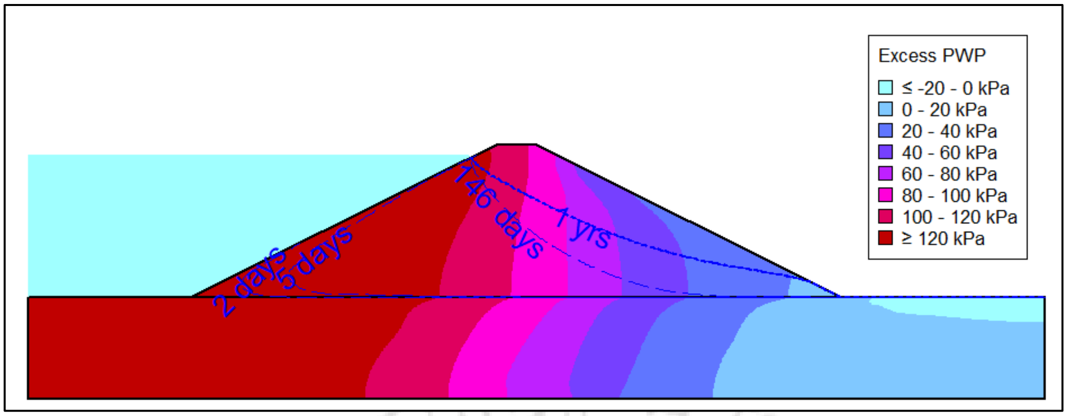

(d)

Figure 5.11 PWP contours and the migration of phreatic surface during and after the reservoir filling operations (a) 2nd day (b) 5th day (c) 146th day (d) 1 year

Thus, from the stress analysis, it can be observed that during the reservoir filling process (i.e. in the initial days of impounding of reservoir until it is filled), there is a high possibility of hydraulic crack initiation in the upstream face as the stress conditions abruptly changes due to the sudden addition of water load. To examine further the possibility of hydraulic fracturing during the rise-up condition, the pore-water pressure is examined along both the slope faces of the earthen dam. As already coined by Ohne and Narita (1977), one criterion for the occurrence or initiation of hydraulic fracture during the reservoir rise-up condition is related to the reduction of effective stress below the effective tensile strength of the earthen dam material, which results in the initiation of cracks. In this study, the identification of the location of hydraulic fracture is carried out by comparing the minimum total stress (i.e. the minor principal stress in terms of total stress) with the pore-water pressure along the dam slopes, as shown in Figure 5.12. In this technique, if the PWP exceeds the minor principal stress, the effective minor principal stress becomes negative, thereby inducing a possibility of development of hydraulic fracturing if its magnitude becomes lesser than the effective tensile strength of the constituent material. It is worth mentioning that in this study, the tensile strength of the constituent material is assumed negligible, and hence, generation of negative effective minor principal stress would be considered as an indicator for the initiation of the hydraulic fracturing. From Figure 5.12(a), it is clearly recognized that in the upstream face of the dam, the pore-water pressure exceeds the minimum total stress values rendering the effective minor principal stress to ne negative, thereby inducing the possibility of hydraulic fracturing along the upstream face. The observation is consistent for both the stages of partial and complete reservoir filling operation. The tentative location of hydraulic fracturing is observed approximately at 0.2-0.25 times the height of the earthen dam, measured from its base. During the reservoir filling operation, it is observed from Figure 5.12(b) that the possibility of hydraulic fracturing does not exist in the downstream face. This is attributed to the fact that the phreatic surface takes long time to reach the downstream face, which occurs only at the steady-state condition. During the reservoir rise-up condition, the pore-water pressure along the downstream face always remain lesser than the minor principal stress, and hence, there is no possibility of negative stresses and consequent initiation of cracking.

Figure 5.13 highlights the horizontal deformation contours as observed with the progress of reservoir rise-up. It is found that the earthen dam experiences horizontal deformation along with the filling of the reservoir due to the introduction of the water load on the upstream face. Such horizontal displacements might lead to the development of cracks on the crest of the dam as well as facilitate favorable conditions for cracks on the upstream face. If the deformations become considerably large, the face can no longer tolerate and result in opening of the latent cracks that might have developed during the construction of the dam. Such a mechanism lead to significant strain accumulation on the upstream face as shown in Figure 5.14. Similar observation is also reported in the past by Khalid et al. (1990). The vertical displacement along the base of the dam is shown in Figure 5.15. Due to the reservoir filling and consequent additional load in the upstream side, additional settlement is observed along the upstream side of the dam leading to heaving towards the downstream side. Based on the combined horizontal and vertical deformations of the dam, it is understood that the reservoir filling renders a marginal anticlockwise rotation of the dam.

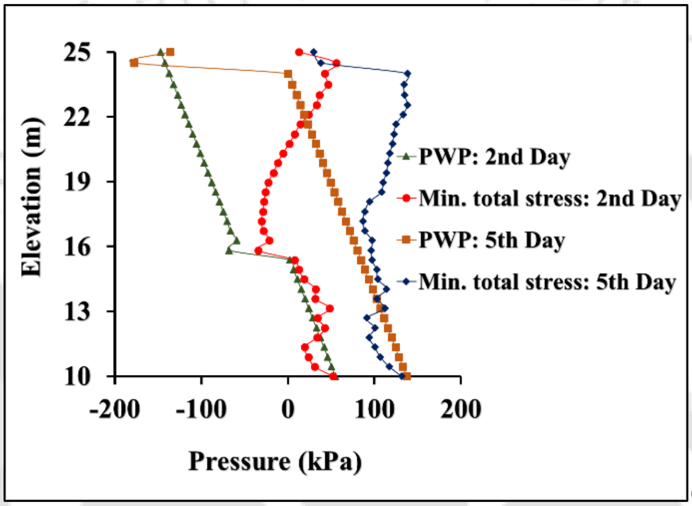

(a)

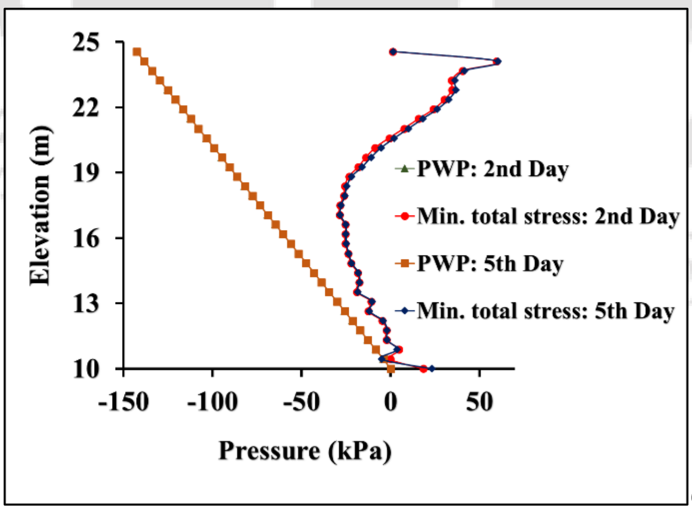

(b)

Figure 5.12 Comparison of total minor principal stress with the developed PWP to identify the possible location of hydraulic fracturing along (a) upstream face (b) downstream face

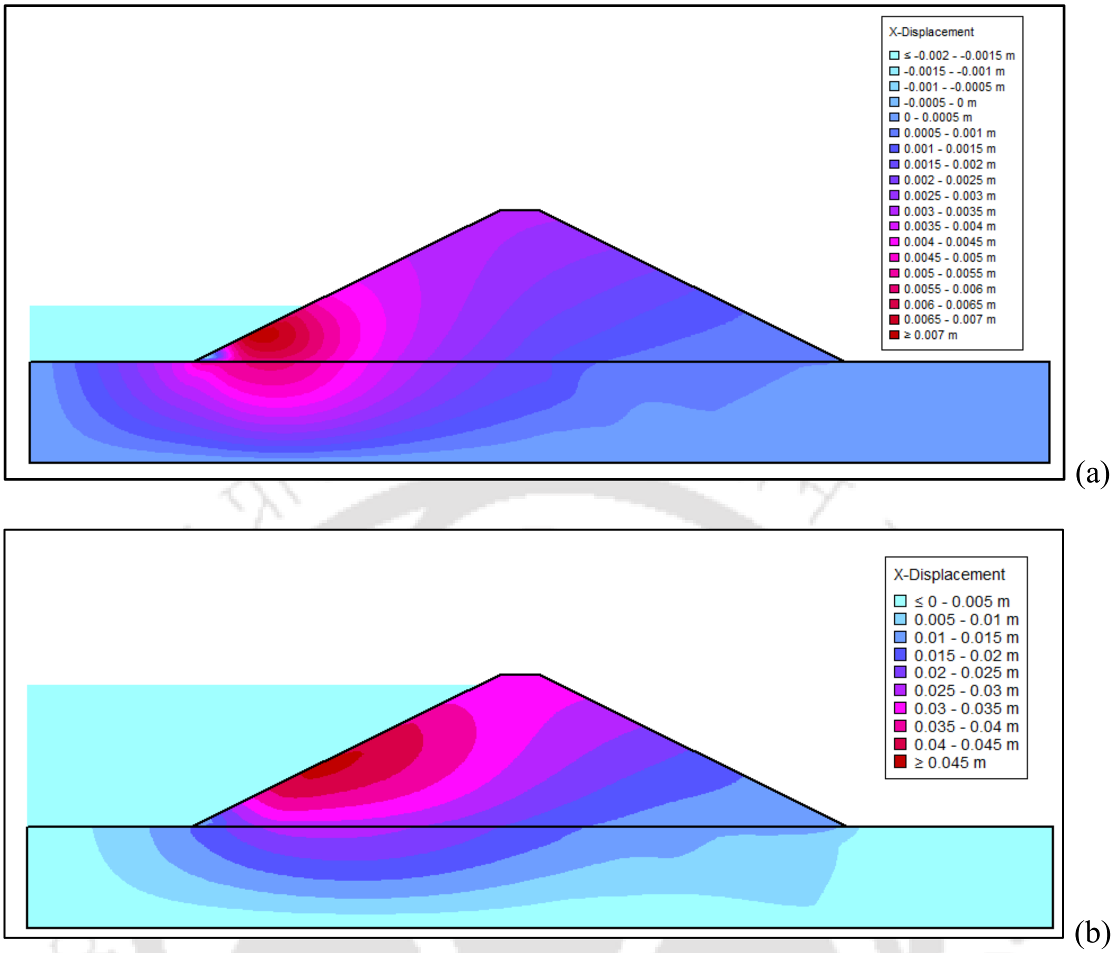

Figure 5.13 Horizontal displacement contours within the earthen dam and foundation during the reservoir rise-up condition at the (a) 2nd day (b) 5th day

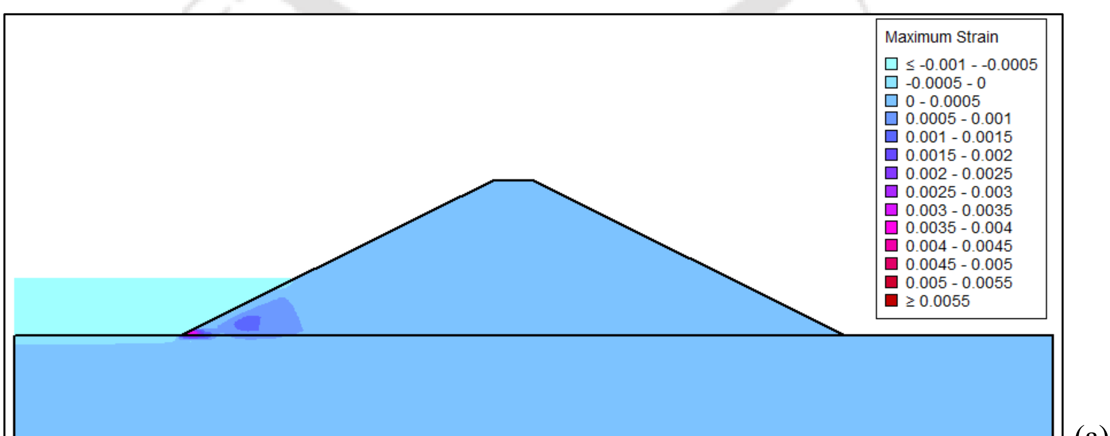

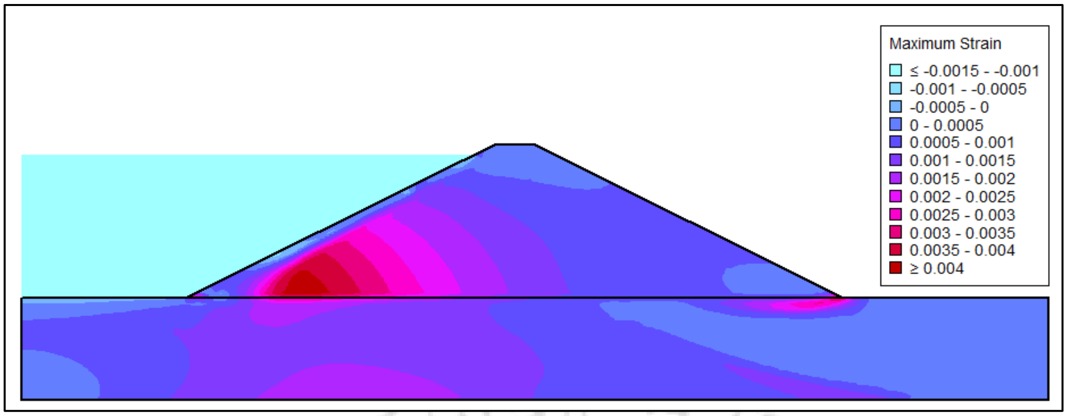

(b)

Figure 5.14 Accumulated maximum strain within the earthen dam and foundation during the reservoir rise-up condition at the (a) 2nd day (b) 5th day

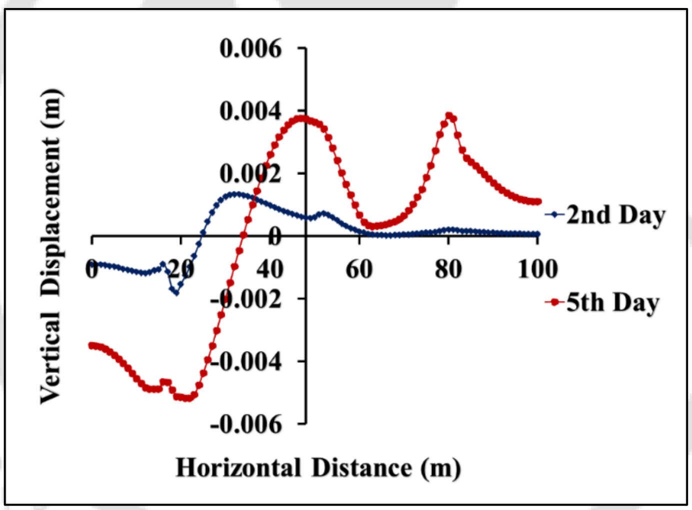

Figure 5.15 Vertical displacement profile along the base of the dam during reservoir filling

5.4.3 Analysis for Case II: Hydraulic Fracturing of Homogeneous Earthen Dam during Reservoir Drawdown Condition

The drawdown condition is a classical scenario in slope stability and it is a very common problem encountered by the riverbanks, dams, embankments and levees, when they are subjected to rapidly declining water levels in their individual upstream side. For earthen dams, the sudden removal of the external hydrostatic pressures may lead to the destabilization of the upstream face and, thus, the drawdown condition is rendered to be critical for the stability of upstream face. There are a number of case histories associated with reservoir drawdown and instability of the upstream face of the earthen dam, as discussed by different researchers (Sherard et al., 1963; von Thun, 1985). However, it is not customary that every drawdown scenario will lead to failure of the upstream face; rather, the failure is strongly governed by the rate of drawdown along with the shear strength and permeability characteristics of the material comprising the earthen dam, especially near the upstream face. The rapid drawdown, if not failure, might induce tension cracking in the upstream of the earthen dam, which may instigate failure of the earthen dam in successive cycles of reservoir filling and drawdown during its performance period. Hence, in this section, only the influence of reservoir drawdown condition on the possibility of crack initiation is assessed and reported. The reservoir drawdown condition is simulated for two scenarios. The first scenario pertains to the condition when drawdown is initiated after the reservoir has been in a steady state for a considerable time so that the phreatic surface within the body of the earthen dam did attain a steady state. The second scenario pertains to the condition when the drawdown is initiated before the phreatic surface has attained a steady state (i.e. the transient migration of the phreatic surface is yet to be complete) under the stead-state reservoir level in the upstream of the dam.

5.4.3.1 Reservoir Drawdown after attaining the Steady-State Phreatic Surface

In order to simulate the drawdown scenario from an initial state wherein the phreatic surface within the body of earthen dam is assumed to have attained a steady state, the reservoir is assumed at its highest level for the in-situ steady-state seepage analysis. Thereafter, the reservoir drawdown (DD) is simulated to the study the flow, stress-strain and deformation characteristics of the earthen dam.

The rate of reservoir drawdown is considered 2.8 m/day, for which the variation of the reservoir water level with time is shown in Figure 5.16.

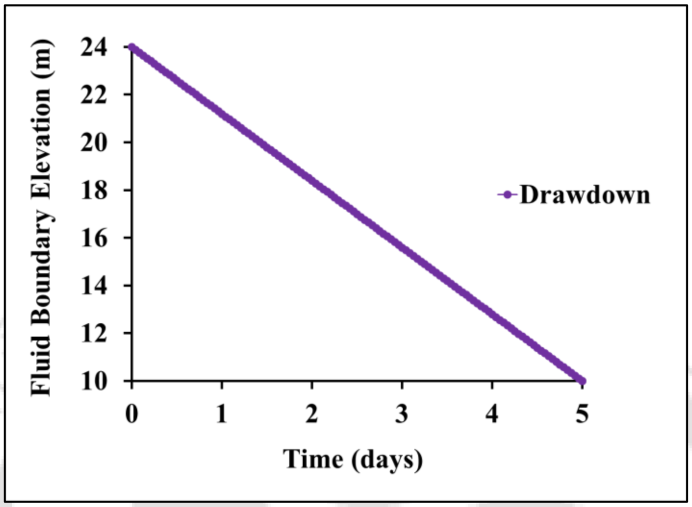

Figure 5.16 Reservoir drawdown (DD) condition and rate adopted in the present analysis where reservoir drawdown is conducted after attaining a steady-state phreatic surface in the earthen dam

Figure 5.17 depicts the variation of minimum total stress along the upstream and downstream face of the dam. It is observed that along the upstream face, tensile stresses are developed very near to the heel region of the earthen dam. The reduction of minimum total stress initiated as soon as the reservoir drawdown commenced, which can be noted by comparing the minimum total stress profile in the 2nd and 5th day from Figure 5.17(a). The reduction of minimum total stresses continued until the completion of drawdown at the 5th day. On the other hand, in the downstream face of the dam, the tensile stresses were observed almost along the entire slope face during and after the completion of drawdown process.

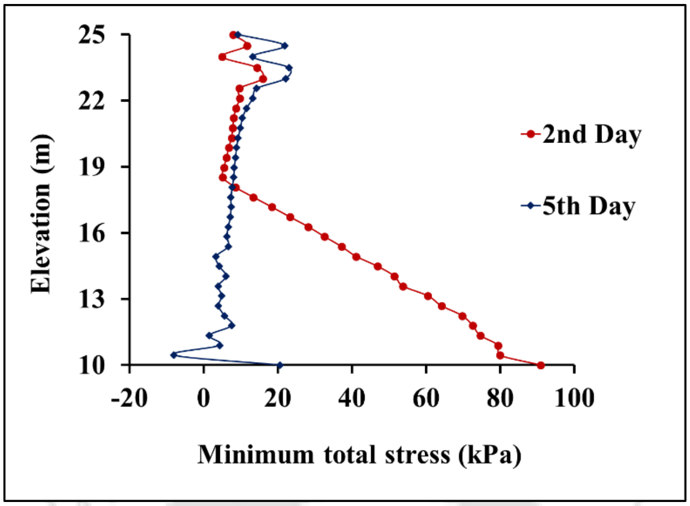

(a)

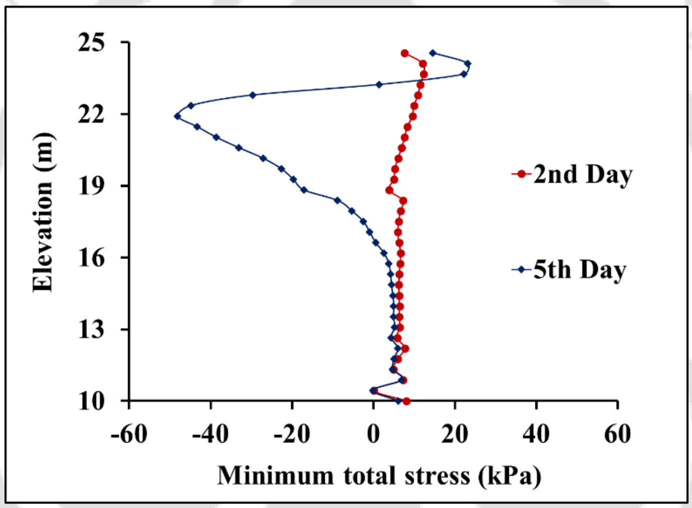

(b)

Figure 5.17 Variation of minimum total stress in the earthen dam pertaining to reservoir drawdown operation initiated after the steady-state phreatic surface is attained (a) upstream face (b) downstream face

Further investigation of identification of possible hydraulic fracturing and its tentative location during the reservoir drawdown was conducted. Figure 5.18 presents the comparison of the PWP and the minimum total stress developed along the upstream and downstream faces during partial and complete drawdown of the reservoir.

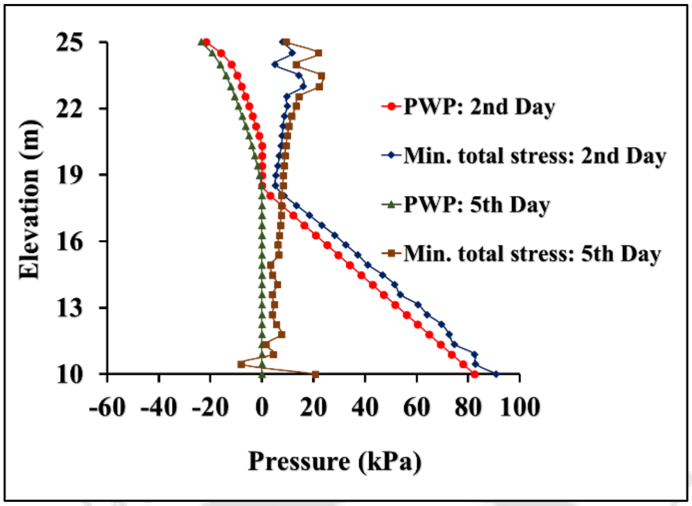

(a)

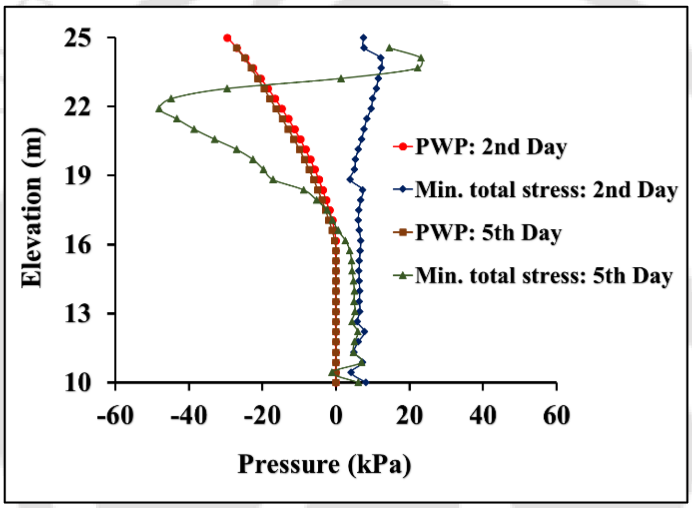

(b)

Figure 5.18 Comparison of total minor principal stress with the developed PWP to identify the possible location of hydraulic fracturing pertaining to reservoir drawdown operation initiated after the steady-state phreatic surface is attained (a) upstream face (b) downstream face

From Figure 5.18(a), it can be clearly stated that the possibility of hydraulic fracturing along the upstream face is extremely marginal as the PWP profile for all conditions is observed to be lesser than the minimum principal stresses. If at all hydraulic fracturing occurs, the tentative location would be near the heel, as the PWP is observed to marginally higher than the minimum total stress at this concentrate region. However, as the drawdown attains completion, along the downstream face of the earthen dam (Figure 5.18b), the pore-water pressure exceeds the minimum total stress, thereby generating a favorable condition for hydraulic fracturing in the downstream face. The tentative location for possible hydraulic fracturing is obtained approximately at 0.5-0.75 times the height earthen dam, measured from its base.

Figure 5.19 displays the horizontal deformation contours at the end of reservoir drawdown. It is clearly highlighted that owing to the removal of the stabilizing hydraulic from the upstream side, the earthen dam depicts a defromation towards the upstream face. The fact is also supported by the significant accumulation of strain along the upstream face, as shown in Figure 5.20. Such significant deformation and strain accumulatio towards the upstream side is the triggering phenomenon for upstream face failure of earthen dams due to raid drawdown of the reservoir, although the actual occurrence of instability depends on several factors as stated earlier. Along with the horizontal movements and deformations, if the earthen dam undergo differential settlement, the outcome might be detrimental for crack initiation on the crest of the dam.

Figure 5.21 presents the vertical displacement profile along the base of the dam was during the reservoir drawdown process. The plot reflects the occurrence of differential settlement the base of the dam, with minor heaving on the upstream end. This behaviour is attributed to the sudden removal of the water load, and generation of stress inequilibrium towards the upstream end. The removal of reservoir load would result in a negative settlement, or heaving, to reach finally a state of stress equilibrium at the end of drawdown. As the drawdown does not have a significant influence on the stress and strain accumulation towards the downstream side (as can be seen from

Figures 5.19 and 5.20), differential settlement due to reservoir drawdown is not observed towards the downstream side of the earthen dam.

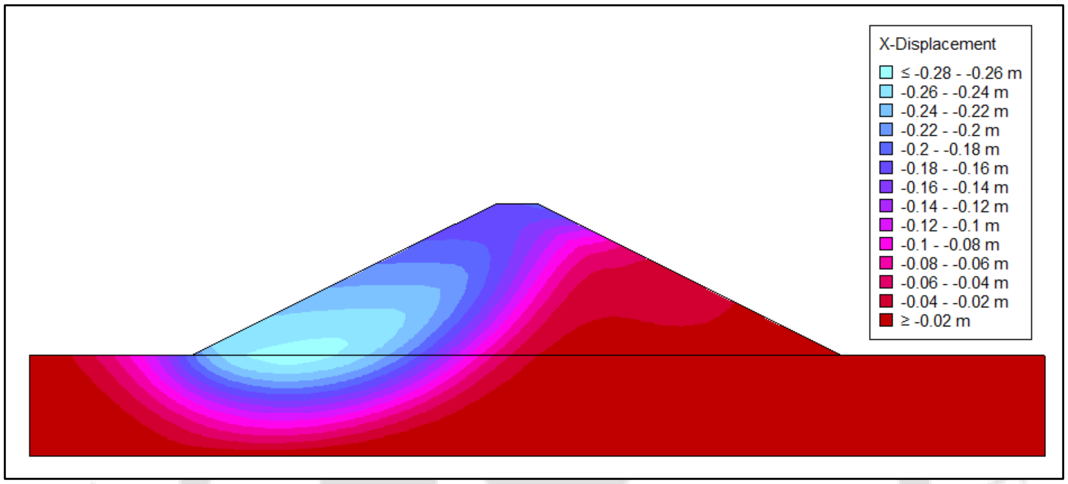

Figure 5.19 Horizontal displacement contours within the earthen dam upon completion of reservoir drawdown on the 5th day

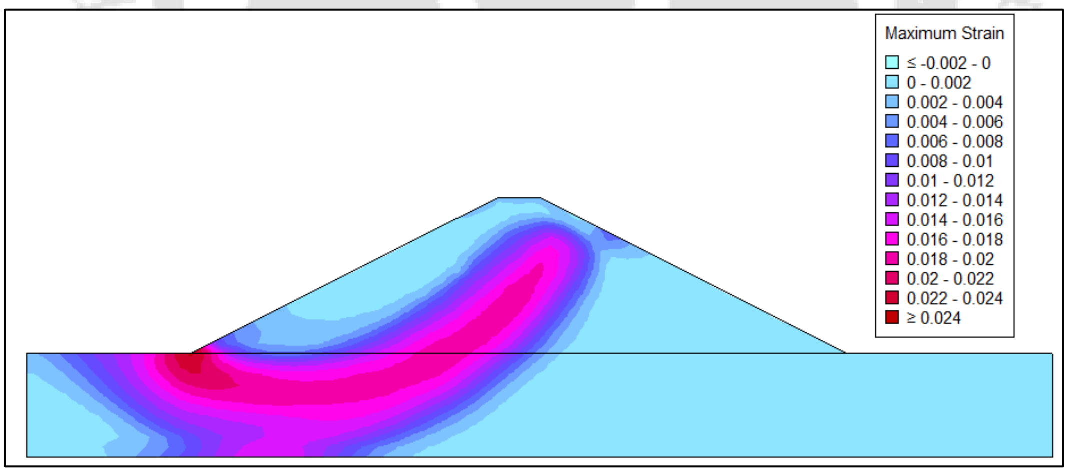

Figure 5.20 Maximum strain contours within the earthen dam upon completion of reservoir drawdown on the 5th day

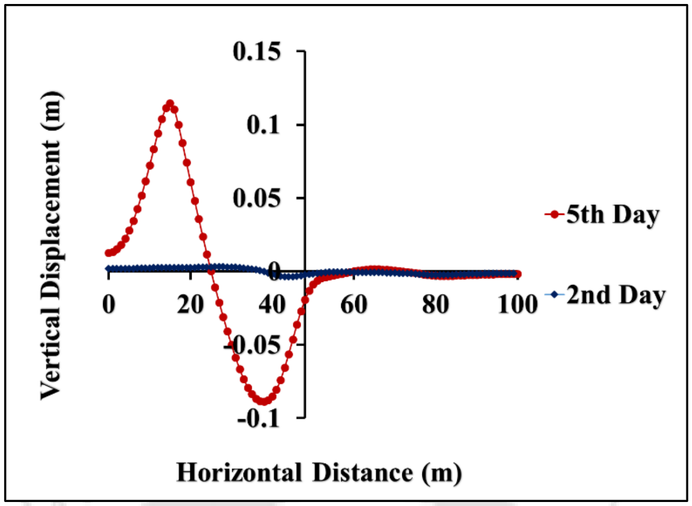

Figure 5.21 Vertical displacement profile along the base of the dam during reservoir drawdown after the steady-state phreatic surface is achieved with the earthen dam

5.4.3.1 Reservoir Drawdown before attaining the Steady-State Phreatic Surface

This case represents a reservoir drawdown scenario much representative of the real-field scenario. In this case, the reservoir is assumed empty in the initial stage, i.e. then earthen dam is in its post-construction condition. Further, the reservoir is filled up in certain number of days, as has been discussed in Section 5.4.2. In this case, as well, the first filling of the reservoir is carried out in 5 days. Thereafter, the reservoir water level is maintained constant for 2 months. During this period, the transient migration of the phreatic surface through the earthen dam is not complete, and it could not intersect with the downstream face. The numbers of days so chosen for the steady-state reservoir condition is from the experience about the time taken to achieve the steady-state phreatic surface, as per the prior analyses in the dissertation work. The adopted steady-state reservoir condition is followed by a drawdown (DD) simulation to the study flow and stress-deformation characteristics of the earthen dam. The rate of reservoir drawdown is considered 2.8 m/day, in which the variation of fluid elevation with time is shown in Figure 5.22.

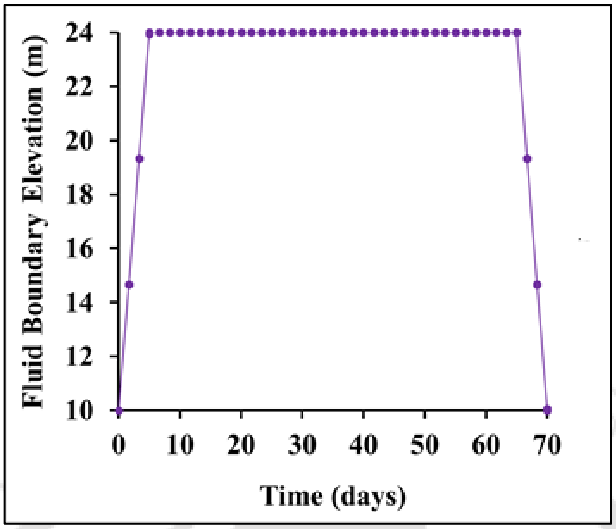

Figure 5.22 Reservoir drawdown (DD) condition and rate adopted in the present analysis where reservoir drawdown is conducted before attaining a steady-state phreatic surface in the earthen dam

Figure 5.23 displays the comparative of the minimum total stress and the PWP profiles along the upstream and downstream faces of the dam, when the drawdown is implemented before the steady-state phreatic surface is attained. It is observed that there is a substantial possibility of hydraulic fracturing along the upstream face, due to a significant release of PWP that accumulated during the reservoir rise-up followed by a constant reservoir level for a certain duration. The tentative location of possible hydraulic fracture along the upstream face is identified approximately within a height of 9 m height from the base of the earthen dam, which approximates to 0.6 times the height of the dam measured from the base (Figure 5.23a). However, along the downstream face of the dam, Figure 5.23(b) reveals that favorable conditions leading to hydraulic fracturing is not generated. This is attributed to the fact that as the migration of phreatic surface within the earthen dam did not attain a steady state, it did not reach the downstream face within the time for which the reservoir was maintained at constant level. Hence, sufficient pore-water pressure was not generated, and it remained sufficiently lower than the minimum total stress, thereby nullifying the possibility of hydraulic fracturing. However, minimum total stress is found to reach negative magnitudes at 0.2-0.6 times the height of the dam measured from its base. This scenario can lead to some tension cracks along the downstream face owing to the reservoir drawdown.

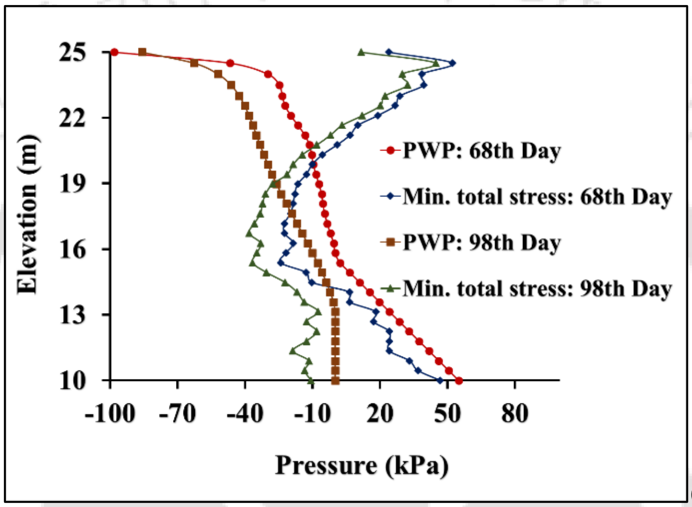

(a)

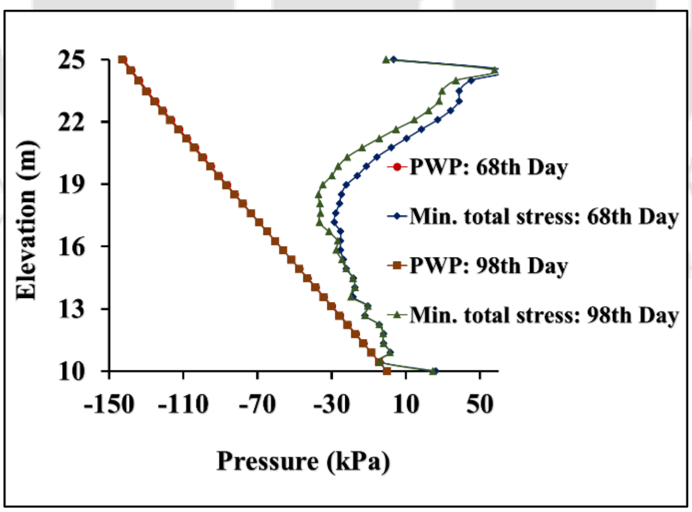

(b)

Figure 5.23 Comparison of total minor principal stress with the developed PWP to identify the possible location of hydraulic fracturing pertaining to reservoir drawdown operation initiated before the steady-state phreatic surface is attained (a) upstream face (b) downstream face

Figure 5.24 presents the horizontal deformation contours within the earthen dam at the 68th day when the dam is subjected to partial reservoir drawdown. It is observed that owing to the removal of hydraulic load from the upstream face due to drawdown, the earthen dam depicts a movement towards the upstream face. The removal of the hydraulic load also resulted in strain accumulation along the upstream face as shown in Figure 5.25. The settlement behaviour of the dam, during drawdown phase, is represented through vertical displacement contours as shown in Figure 5.26. It is clearly observed that differential settlement occurred along the base of the dam, accompanied by marginal heaving on the upstream end. The reason for such a response is already explained in Section 5.4.3.1.

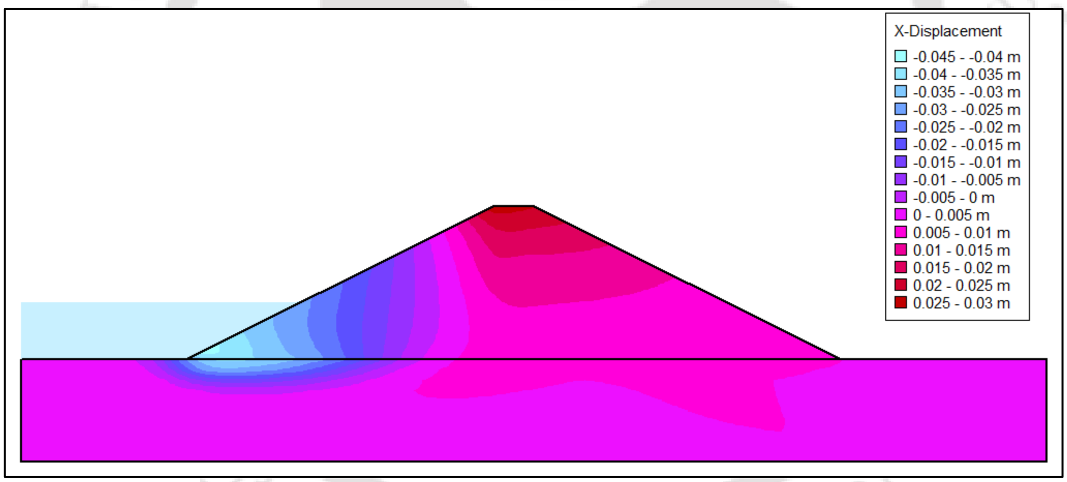

Figure 5.24 Horizontal displacement contours within the earthen dam upon partial drawdown of the reservoir on the 68th day

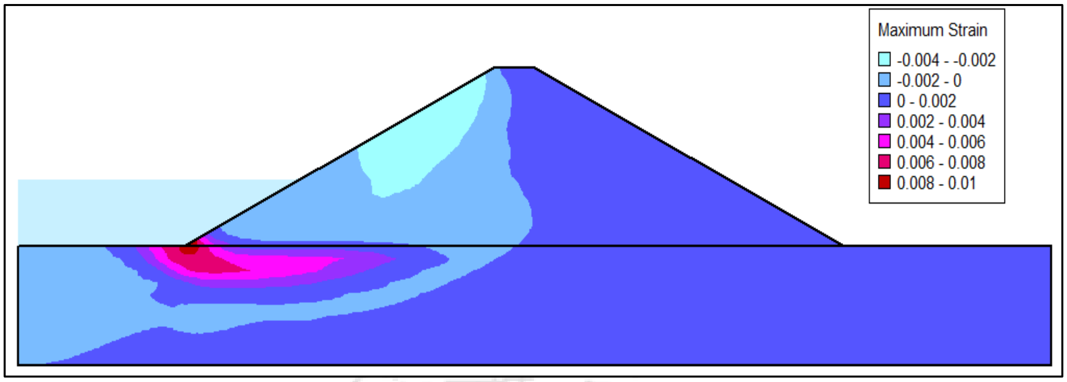

Figure 5.25 Maximum strain contours within the earthen dam upon partial drawdown of the reservoir on the 68th day

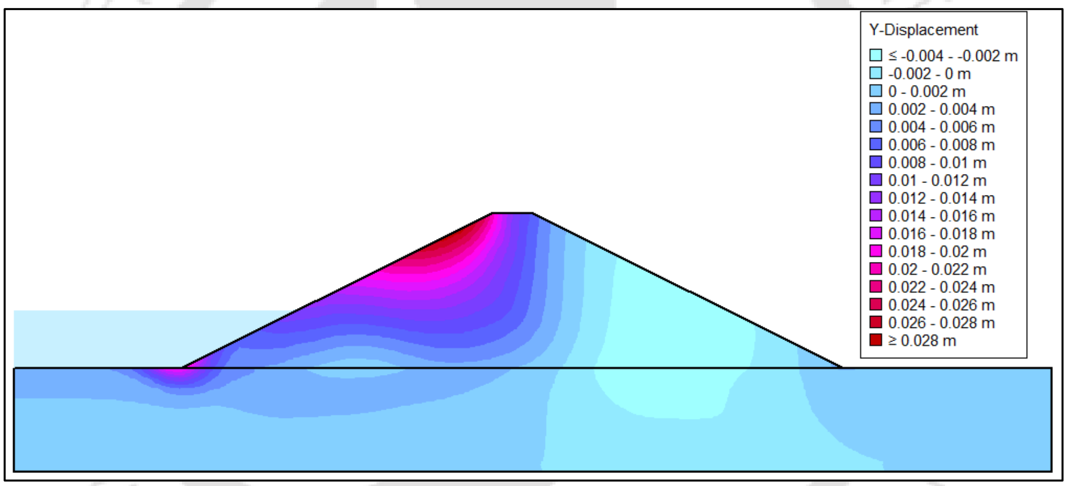

Figure 5.26 Vertical dsiplacement contours within the earthen dam upon partial drawdown of the reservoir on the 68th day

5.7 Summary

The chapter presents the response of homogeneous earthen dam subjected to hydraulic fracturing and cracking. Finite element based Seep/W and Sigma/W modules are used to conduct the seepage analysis and stress analysis, respectively. Based on the existing criteria provided by Ohne and Narita (1977), the tentative locations of possible hydraulic fracturing and cracking of homogeneous earthen dam are identified. The influence of single-lift and multiple-lift modeling technique to assess the response of homogeneous earthen dams on the post-construction cracking are assessed. Based on the negative minor principal stresses generated on the slope faces of the dam, the tentative locations of post-construction cracking are assessed. The behavioral response of the dam are further represented in terms of horizontal deformations of the faces, strain accumulation in the dam, and the differential settlement at the base of the dam. The influence of transient reservoir operations, i.e. reservoir rise-up and reservoir drawdown, on the tentative generation of hydraulic fracturing and their possible locations on the dam faces are investigated. Two different drawdown scenarios are investigated, i.e. when the drawdown is initiated either before or after the steady-state phreatic surface is achieved within the body of earthen dam. The influence of partial and complete rise-up and drawdown conditions on the stress, strain accumulation, deformation and differential settlement characteristics of the earthen dam are also highlighted. The results presented in this chapter suitably indicates that either the upstream face or the downstream face, or both, may undergo cracking (under total stress condition) or hydraulic fracturing (under the influence of pore-water pressure generation). It is important to have a thorough understanding of the tentative location of the developed fracture so that proper mitigation measure can be adopted as per requirement.

CHAPTER 6

HYDRAULIC FRACTURING AND CRACK PROPAGATION IN ZONED EARTHEN DAMS WITH A CENTRAL IMPERVIOUS CORE

6.1 GENERAL

Hydraulic fracturing of the central core is one of the most important factors affecting the safety of earthen and rockfill dams. It is a serious concern that mostly occurs in the upstream face of the dam core, which is initiated by significant reduction in the vertical effective stress in the core to the extent that it results in the occurrence of tension fracture. Such a situation may arise when the total stress in the core is reduced by an arching effect where the core settles relatively more to the rockfill or the earthen shell of the dam. In most of the cases, the central core of the zoned earthen dams are made of fine-grained materials with severely low permeability, that render the core to be nearly impermeable and thereby inhibiting the free flow of seepage through the body of the dam. The effective stress in the central core can also undergo reduction as the pore-water pressure on the core increases during the reservoir filling process, which may lead to hydraulic fracturing of the upstream face of central core. There are many examples in the literature where the cause of dam failures is attributed to hydraulic fracturing. One such example is the failure of Stockton and Wister dams in USA (Sherard, 1973). The leakage from the Viddalsvatn dam in Norway was investigated to identify that hydraulic fracturing is the possible cause of failure (Vestad, 1976). The failure of Teton dam in USA during the first reservoir filling is also attributed to hydraulic fracturing as a possible cause (Chadwick et al., 1976). In order to understand the mechanism of hydraulic fracturing in the upstream face of the dam core, the effects of time of construction and rate of impounding of the dams that experienced hydraulic fracturing were studied. Lo and Kaniaru

(1990) studied and compared the embankment construction and impoundment rates of five dams; Balderhead, Hyttejuvet, Viddalstavn, Teton and Yard's Creek dams that experienced hydraulic fracturing. It was reported that neither the time of embankment construction nor the rate of impoundment had any effect on hydraulic fracturing on the clay core of the rockfill dam. There are a number of well-studied cases in which dams have failed or been damaged by concentrated leaks for which the cause remained unidentified. In some of these experiences, investigators concluded that differential settlement were the probable causes of cracking, even though no cracks were seen on the surface of the dam at its crest. In several unsolved problems on the safety of the earth-rock fill dam, the problem of hydraulic fracturing in the central core of the dam attracts wide attention by designers and researchers. Hydraulic fracturing is generally considered as a main reason to induce the leakage of the dam during first filling. The likelihood of the occurrence of hydraulic fracturing increases with increasing water level or the crack depth. The lower part of the dam core is the zone in which the phenomenon of hydraulic fracturing may be induced easily. In this scenario, it becomes pertinent to have a thorough study to analyze and identify the mechanism of hydraulic fracturing in the surface as well as the central core of the zoned earthen dams, as these type of dams comprises the biggest share of earthen dams worldwide.

6.2 ANALYSIS OF ZONED EARTHEN DAMS WITH CENTRAL IMPERVIOUS CORE

Assessment of hydraulic fracturing in dams has an inherent inevitable difficulty. The verification of hydraulic fractures by direct visual observation is not possible, as hydraulic fractures occur only when the water pressure comes into play and they are confined within the dam. As for the unsatisfactory dam performance or dam failures due to hydraulic fracture, it is observed that the development of high pore-water pressure at the downstream of the core or erosive leakage appeared abruptly without any warning sign. The Teton Dam failure, which is attributed to hydraulic fracturing, failed just within few hours after the first leakage was spotted (Seed and Duncan, 1981). There is always a difference of opinions and arguments among the investigators regarding the origin of the initial leak resulting in the dam breaching. Determination of the cause of initial leak is virtually impossible, as erosion inadvertently destroys any existing proof. It was often concluded by the majority of researchers that the sole reason for the initial leak is differential settlement cracking. However, there has been a sufficient debate regarding this issue, and any strong conclusion is yet to be reached. In a zoned earthen dam, the presence of different layers of different stiffness can lead to the interior failure of the dams. One of such imminent danger is due to hydraulic fracturing that can lead to interior failure over a prolonged period. Due to differences in stiffness of the core and its abutment zone of an earthen dam, differential settlements occur to induce arching within the body of the dam, especially at the interface of the core and the shell. These differential settlements between the core and shell results in the development of cracks within the core. These cracks may develop during the first impounding, thereby causing internal erosion of the dam core (Sherard, 1991; Ng and Small, 1999; Narita, 2000). At times, development of tension cracks are also observed in the cohesionless shells that further worsens as the water starts penetrating through it and finally lead to its widening. The differential PWP arising at various sections within the dam, owing to the materials of different permeability, are primary causative agent for differential settlements. Hence, it is important that the integration of the components of the earthen dam be maintained during its performance period. The stability of an earthen dam should be assured by restricting the developed stresses at acceptable levels at any anticipated events. Different factors, namely the size and shape of core, constituent materials for the dam and their placement etc., play a role to determine the potential of arching induced horizontal cracking.

Until 1972, the very few existing stated that hydraulic fracturing led to concentrated leaks resulting in further failure or erosion damage of dams (Kjaernsli and Torbla, 1968). Lofquist (1951) was the first to report about the existence and implication of arching in rockfill dams. Based on the real-time pressure measurements, the implication of the stress decrement on the settlement of the core of the dam was highlighted. In later years, a few considerations about load transfer mechanism at the interface of the shell and core of the dam were undertaken (Nonvieller and Anognosti, 1961). Since 1975, with renewed interest by various researchers, different literatures were published on various aspects of development of concentrated leaks by hydraulic fracturing phenomenon (Dascal et al., 1984; Jworski et al., 1981; Seed et al., 1981). Kulhawy and Gurtowski (1976) stated that the load transfer phenomenon within zoned dams would occur due to the differences in stiffness of various materials used in the construction of the dam.

A series of studies have been carried out by various researchers to simulate hydraulic fracturing through a homogeneous or heterogeneous body. A method for predicting hydraulic fracturing was presented using special joint elements for modelling the fluid flow and fracture (Ng and Small, 1999). The simulation of crack propagation in a concrete dam was attempted by using a cohesive fracture model that requires mesh updating at the crack tip during the successive cracking (Secchi and Schrefler, 2012). A three-dimensional (3D) cohesive crack propagation method was presented by Barani and Khoei (2014) for saturated porous media. Wang et al. (2016) thought that the mechanism of hydraulic fracturing can be explained by fracture mechanics, and the crack propagation may follow any of Mode I, Mode II, and Mixed mode III. Mode I is primarily tensile opening mode where the crack faces separate in a direction normal to the plane of the crack. Mode II is an in-plane sliding mode and the crack faces are mutually sheared in a direction normal to the cracking front. Mode III is tearing or anti-plane shear mode and the crack faces are sheared parallel to the crack front. Liu et al. (2017) presented a stabilized extended finite element formulation to simulate the hydraulic fracturing process in an elastoplastic medium. Li et al. (2007) used the smeared cracking theory to simulate the process of hydraulic fracturing in certain earth and rockfill dams. Tang et al. (2008) gave fracture spacing in layered materials for which numerical simulations were carried out to show that the critical value of the fracture spacing to layer thickness ratio is strongly dependent on the mechanical disorder in the fractured layer. The spacing-to-thickness ratio decreases with increasing heterogeneity of the mechanical properties. Thus, different mechanical parameters to different material units were introduced by using a certain statistical distribution. Different researchers have presented the extended finite element method (XFEM) for simulating crack propagation in homogenous material such as rock and concrete materials (Belytschko and Black, 1999; Moes et al., 1999, Gordeliy and Peirce, 2015). By using XFEM, the crack is allowed to pass through the element; thus, cracks with complex shapes can be simulated in regular mesh without any need of re-meshing. Today, it is a well-known fact that unusually large settlements are not always the 'villain' to initiate cracking of dams; rather, in many studies it is evident that cracks have developed near the impervious section of the dams due to hydraulic pressure. Hence, there is a need to conduct thorough research in regard to identify the root cause of hydraulic fracturing in zoned earthen dams, their tentative locations and their path of propagation through the central core, and the same is reported in this chapter.

6.2.1 Finite Element Analysis

The study reported in this chapter is conducted using the finite element software GeoStudio. The Seep/W module is used for seepage/flow analysis of the problem, whereas the deformation analysis is carried out by Sigma/W module. For the numerical analysis, the entire domain of the model is discretized into an unstructured mesh, comprising first order quadrilateral and triangular elements. The entire domain consists of 1636 nodes and 1531 elements. The global element size used for the basic model in this problem is 1 m, while refined elements are adopted at those regions that are supposed to portray stress or strain concentrations. The initial steady-state seepage analysis of the models is simulated in Seep/W to establish the existing pore-water pressures and total head conditions, followed by the in-situ analysis in Sigma/W to generate the initial stress conditions. The Load/Deformation analysis in Sigma/W is used to simulate the construction of the dam by placing the embankment fill in single layer, whereas the response to the reservoir rise-up and drawdown conditions are simulated using the Coupled Stress/PWP analysis in Sigma/W. The pore-water pressures generated in the steady-state analysis and the stresses generated in the in-situ analysis are used to define the initial conditions for the subsequent transient state.

6.2.2 Model and Materials used in the Analysis

A zoned earthen dam section is considered in which the nearly impervious central core is flanked by the shell comprising relatively pervious material. The shell is used to enclose, support, and protect the central core. The flow and deformation response of the dam is studied to investigate core cracking during reservoir rise-up and drawdown conditions. For the rise-up condition, the earthen dam is simulated using the single-fill technique as discussed in Chapter 5, which is further subjected to reservoir impounding. For the drawdown condition, the reservoir is initially considered at its maximum capacity with a freeboard of 1 m, which is subsequently subjected to drawdown. The model used in the present study, along with its relevant dimensions, is shown in Figure 6.1. As shown in the figure, the height of the earthen dam is 15 m and its width is 64 m. The upstream and downstream slope has an inclination of 2H:1V. The earthen dam has a crest width of 4 m and a freeboard of 1 m. The height and width of the foundation are 10 m and 100 m, respectively. The central core has an inclination of 0.4H:1V in both of its slopes.

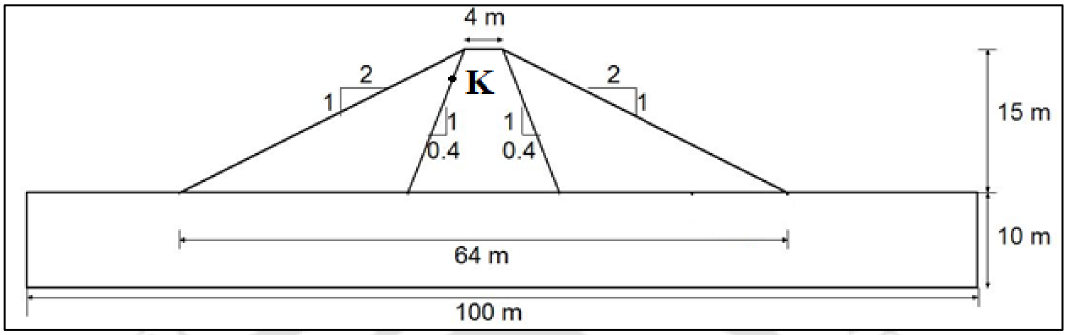

Figure 6.1 Model of the zoned earthen dam used for the present study

For performing the stress-deformation analysis, the 'elastic-plastic' material model in Sigma/W is assigned to the earthen dam and foundation soil. The shell and the core regions are modeled using 'saturated/ unsaturated' material model, while the foundation is modeled using the 'saturated only' material model in the Seep/W analysis. To solve the seepage equation in the coupled analysis, it is required to specify the volumetric water content function and the hydraulic conductivity function for the shell and core material. In this study, they are estimated following the procedures proposed by van Genuchten (1980). Figure 6.2 shows the estimated volumetric water content function and hydraulic conductivity functions for the shell and core material that are used in the present study.

The properties of various materials used in the modeling is obtained from extensive literature survey and is adopted from specific literature (IS 12196; USBR 1987; USBR 2014; Seep/W 2012; Sigma/W 2012), coupled with proper engineering judgment. The adopted material properties are listed in Table 5.1.

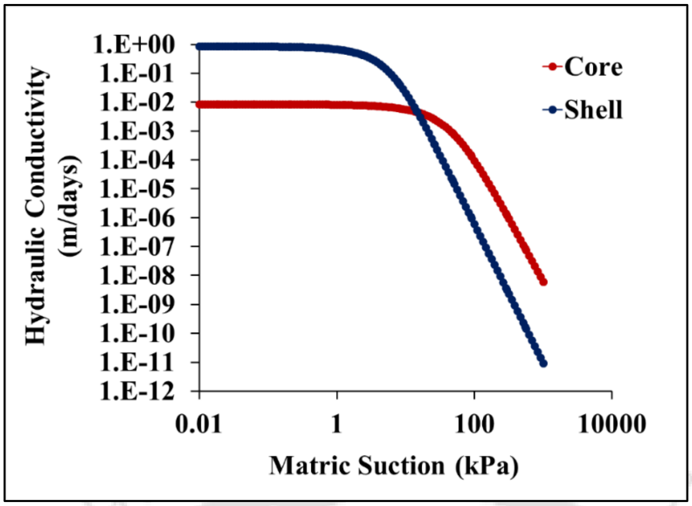

(a)

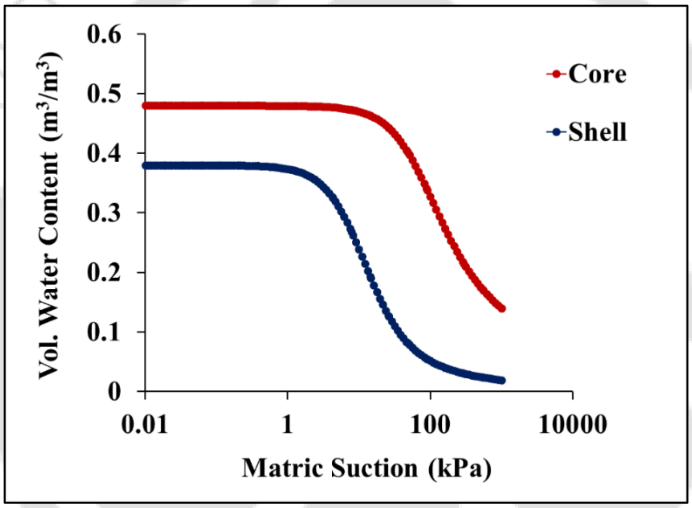

(b)

Figure 6.2 Hydraulic characteristics of materials for the core and shell of the earthen dam (a) Volumetric water content function (b) Hydraulic conductivity function

Table 6.1 Material properties for the simulation of hydraulic fracturing of zoned earthen dam

	c (kPa)	$ø$ (degree)	γ (kN/m^3)	$E_{modulus}$ (kPa)	k (m/s)
Shell	5	28	18	15000	10^{-6}
Core	10	32	20	9000	10^{-8}
Foundation	15	20	20	30000	10^{-10}

6.3 HYDRAULIC FRACTURING OF ZONED EARTHEN DAMS DUE TO RESERVOIR RISE-UP AND DRAWDOWN OPERATIONS

6.3.1 Flow/Deformation Response of Zoned Earthen Dam due to Reservoir Rise-up

Coupled Stress/PWP analysis is used to simulate the reservoir Rise-up (RU) condition for the present study. The earthen dam is simulated using the single-lift technique and the response of the construction of the dam is obtained through Load/Deformation analysis in Sigma/W module. Further, the earthen dam is subjected to reservoir impounding. The rate of reservoir rise-up is considered 0.5 m/day. The variation of the height of reservoir with time is shown in Figure 6.3.

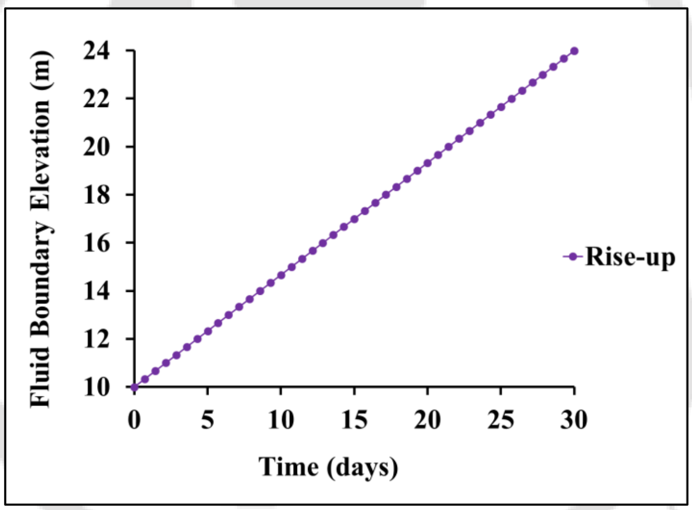

Figure 6.3 Reservoir rise-up (RU) and its rate adopted in the present analysis

The possibility of crack initiation on the upstream face of the core by hydraulic fracturing is investigated through the stress-deformation analysis based on the reservoir filling as the applied load. The reservoir filling is completed in 30 days, leaving a free board of 1 m. In order to understand the behaviour of the zoned earthen dam during and after the filling process, the analysis is extended until 1 year after the completion of reservoir filling. The two main criteria that govern hydraulic fracturing, i.e. the water pressure exceeding the total stress and the existence of differential settlement, are taken into consideration. The minimum total stress and the pore-water pressure along the upstream face of the central core is evaluated for different time intervals, and the comparison is shown in Figure 6.4.

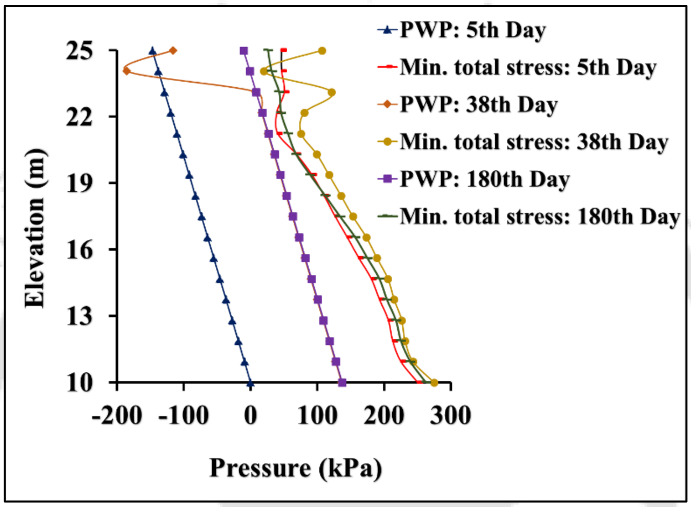

Figure 6.4 Variation of minimum total stress and PWP along the upstream face of the central core of the earthen dam during and after the reservoir rise-up condition

It can be observed that along the upstream face of the central core, the possibility of hydraulic fracturing just at the initial stages of the reservoir filling is substantially less. This is attributed to the fact that the build-up of pore-water pressure would not reach the magnitudes of minor principal stress along the upstream face of the dam, as seen in the case of corresponding plots for 5th day. However, just after the completion of the reservoir rise-up, the possibility of hydraulic fracturing increases as the pore-water pressure along the upstream face of the core increases, and the same approaches the magnitude of the minor principal stress along the corresponding locations, as can be observed from the comparative plots of 38th day. The slow dissipation of excess pore-water pressure due to very low conductivity of the material of central core did not inflict substantial change in the pore-water pressure and total stress profiles after long time from the completion of reservoir rise-up, as can be observed from the comparative plots of 180th day.

Figure 6.4 indicates that for all the depicted cases during and after the reservoir rise-up, the PWP profile remains lower than the minimum total stress profile. In accordance to the criterion for hydraulic fracturing proposed by Ohne and Narita (1977), none of the profile indicate a conclusive occurrence of hydraulic fracturing along the upstream face of the central core. However, considering on the uncertainty on the constituent properties, compaction control in the field, and uncertainty associated with the construction processes of the dam, it is decided to define a modified limiting condition that can be considered for the conceptual detection of hydraulic fracturing. In this regard, the temporal variation of the stress ratio (ratio between the minimum total stress and PWP) is investigated. As per the criterion of Ohne and Narita (1977), under the ideal conditions, hydraulic fracturing will initiate when the stress ratio would be equal to or greater than 1 (one). Figure 6.5 depicts the variation of stress ratio with time for the present study. It can be observed that approximately until the 25th day, the stress ratio is transient, which is indicative of the transient development of the PWP during the reservoir rise-up. However, from the 35th day, i.e. after the reservoir rise-up is complete, the stress ratio increases and arrives at a stable magnitude thereby indicative of the stabilization of the pore-water pressure fluctuations on the upstream face of the central core. Figure 6.5(b) depicts the plot of maximum stress ratio obtained from each of the time plot from Figure 6.5(a). It can be observed that the stress ratio increases with time and attains a stable magnitude of 0.8. Hence, based on the finding, it can be stated that considering different uncertainties associated with dam construction, the hydraulic fracturing can be reasonable said to initiate when the stress ratio at the upstream face of the central core reaches a magnitude 0.8.

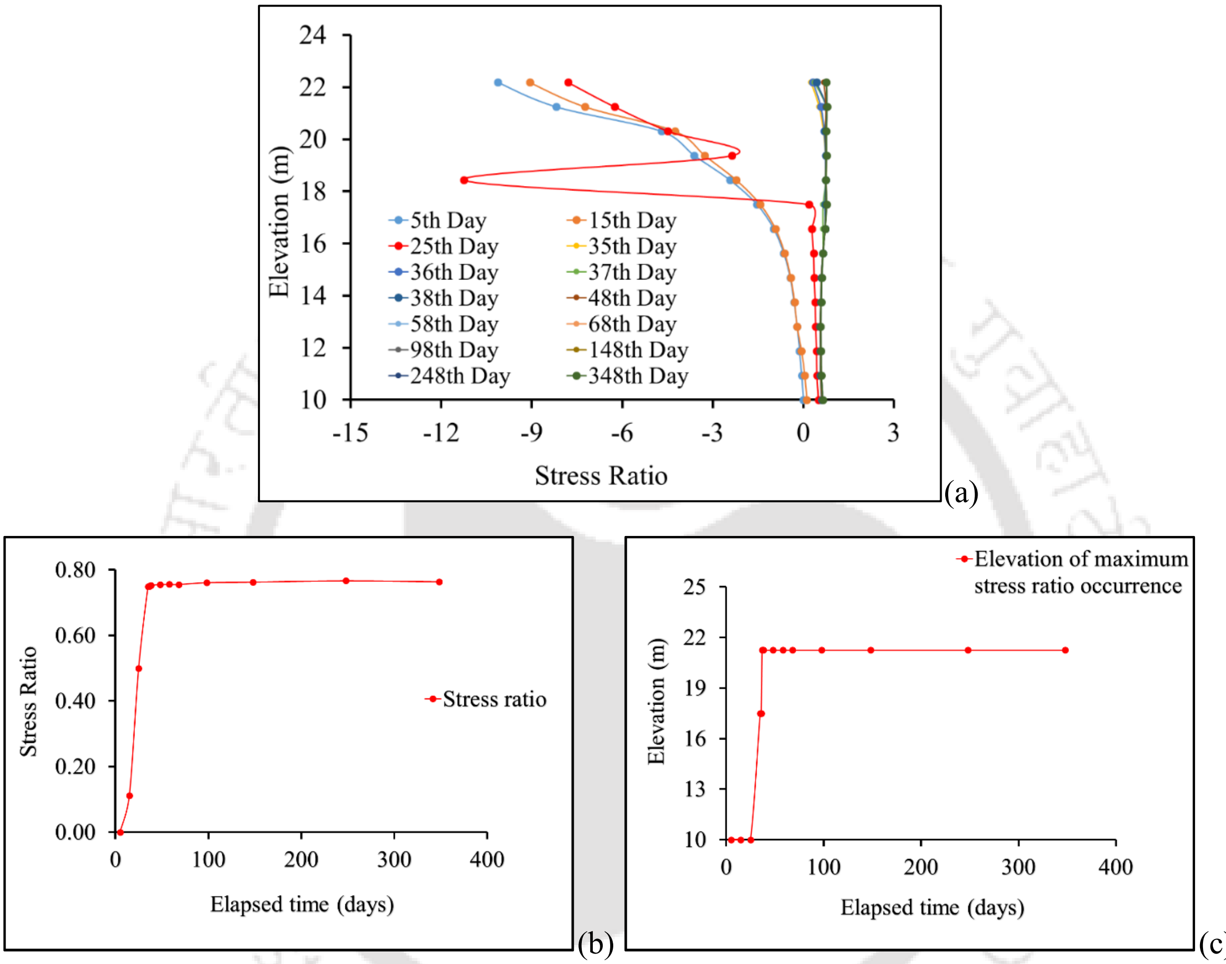

Figure 6.5 (a) Variation of stress ratio along the upstream face of the central core during and after the reservoir rise-up scenario (b) Variation of the maximum stress ratio with elapsed time (c) Variation of the elevation of occurrence of maximum stress ratio with elapsed time

Further, it is also required to identify the tentative location through which the hydraulic fracturing would initiate. In this regard, Figure 6.5(c) depicts the elevation at which the maximum stress ratio occurs at different time instances, and the same can be obtained as a derivative of Figure 6.5(a). It can be observed that upon the completion of the reservoir rise-up, and even during the post rise-up condition, the maximum stress ratio occurred at an elevation of 11.25 m from the base of the dam which conforms the occurrence of hydraulic fracturing is approximately at 3/4th the height of the dam, measured from the base. Based on the findings, it is observed that the hydraulic fracturing at the upstream face of the central core takes place after few days (at the 38th day) from the completion of the reservoir rise-up (30th day). This delay is possibly the time taken by the phreatic surface and the saturation front to migrate from the upstream face of the dam to the upstream face of the core. The critical location of the initiation of hydraulic fracturing is observed approximately at 2 m below the full-capacity reservoir level, which is reasonable as the phreatic moves downward after entering the body of the dam and meets the shell-core interface.

Figure 6.6 depicts the temporal variation of the vertical displacement at the base of the zoned earthen dam. It is observed that during the initial stages of the reservoir rise-up, as expected, the vertical displacement is negligible. However, after the reservoir filling is completed, the vertical displacement along the base of the dam showed evidences of both settlement and heaving. The introduction of the water load and a complex interaction of materials of different conductivities along their interface leading to complicated build-up and dissipation of the excess pore-water pressure resulted in such differential vertical displacement along the base of the dam. This kind of differential displacement would be favourable to jack open the cracks existing in the soil fabric during the construction and compaction of the dam.

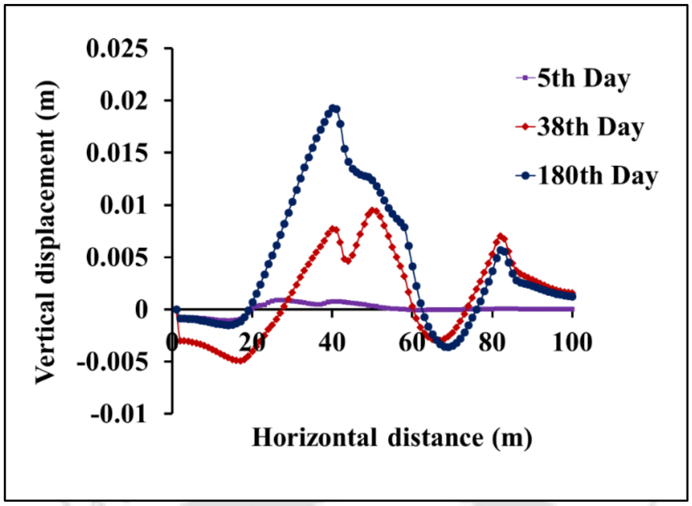

Figure 6.6 Vertical displacement profile along the base of the dam during reservoir filling

Such differential displacements along the base of the dam can be responsible to develop arching at the shell-core interfaces as they have different compressibility and result in strain accumulations a certain portions of the zoned earthen dam. The resulting strain concentrations further influence the redistribution of internal stresses that results in the alteration of the internal pressure at different places within the dam body, which in turn might govern the initiation of cracks. Figure 6.7 depicts the maximum strain contours evaluated just after the completion of reservoir rise-up, i.e. on the 38th day, to investigate and identify the most probable location for crack initiation. It is observed that the maximum strain concentration occurs on the upstream face of the core at about 3/4th of the height of the dam, measured from the base. Thus, it can be concluded that the maximum possibility of occurrence of the initial leak during the gradual reservoir filling condition would be after the completion of the rise-up condition.

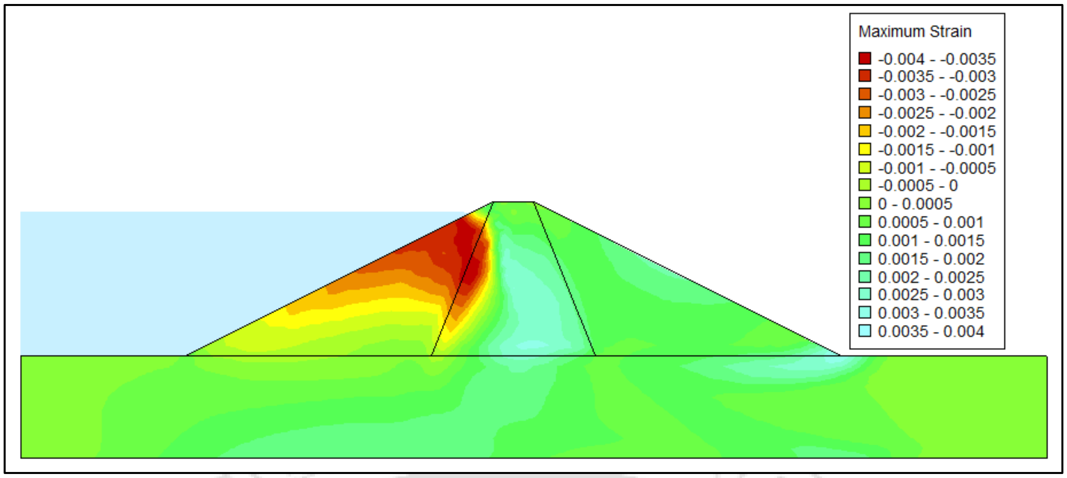

Figure 6.7 Maximum strain contours in the zoned earthen dam at the 38th day after the initiation of reservoir rise-up

Figure 6.8 depicts the temporal variation of seepage velocity at a Point K (as shown in Figure 6.1) on the upstream face of the central core which is identified as the most probable location for the initiation of hydraulic fracturing (based on the findings of Figure 6.6). The figure clearly indicates that as the reservoir rise-up is completed, pore-water pressure within the body of the dam rises and within an interval of 2-3 days, the saturation front migrates from the upstream face of the dam to the upstream face of the core. This is clearly indicated by a marked rise in the seepage velocity at Point K, the abrupt rise being attributed to the hydraulic inequilibrium generated due to the transition from unsaturated to saturated characteristics of the constituent material. With further passage of time, it may be noted that the seepage velocity reduces and attains a constant magnitude as the seepage water follows a saturated flow path through the body of the dam.

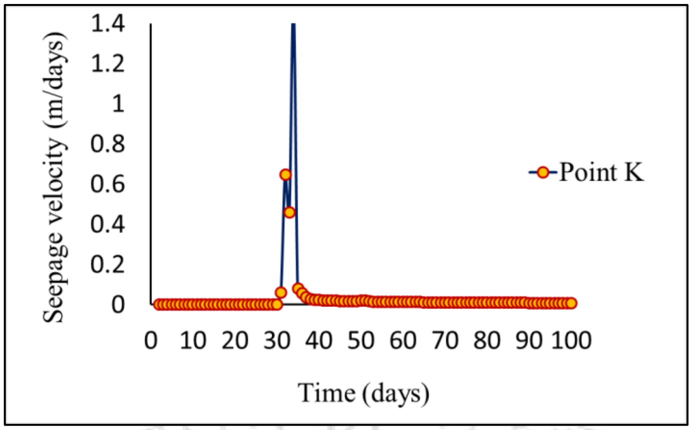

Figure 6.8 Temporal variation of seepage velocity at Point K along the upstream face of the core

Figure 6.9 highlights the hydraulic gradients within the zoned earthen dam at the 38th day that exhibited a very high seepage velocity. The examination of hydraulic gradient along with the seepage velocity is necessary investigate the development of conducive conditions of internal erosion and possibility of piping through earthen dams. The figure reveals that the hydraulic gradients are very high at point K as well as its adjacent regions that are identified as most critical for hydraulic fracturing. High gradients along with high seepage velocity gives sufficiently favourable conditions for internal erosion and piping through the dam core.

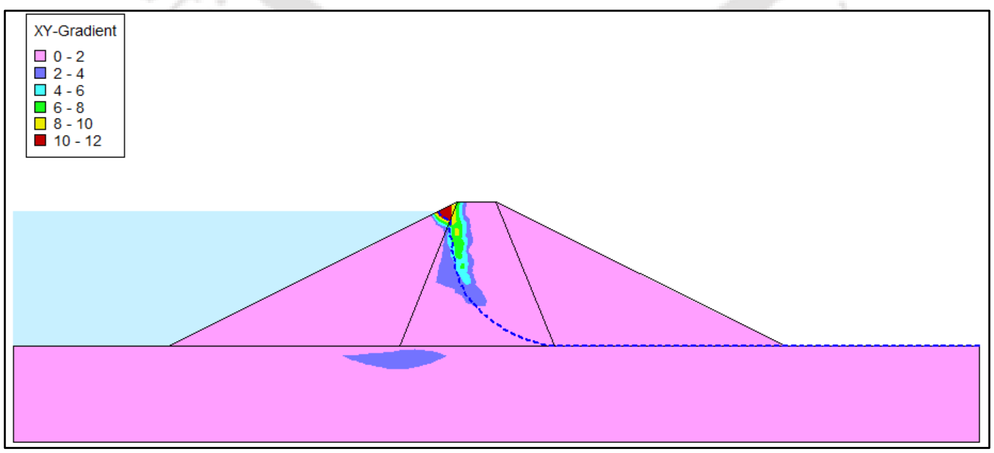

Figure 6.9 Hydraulic gradient contours within the earthen dam at the 38th day

6.3.2 Flow/Deformation Response of Zoned Earthen Dam due to Reservoir Drawdown

6.3.2.1 Reservoir Drawdown after attaining the Steady-State Phreatic Surface

The investigation for hydraulic fracturing of the central core of the zoned earthen dam was carried out during and after the drawdown of the upstream reservoir. The minimum total stress and the pore-water pressure were compared for different time intervals to identify the possibility of hydraulic fracturing. The drawdown condition (DD condition) is simulated using Coupled Stress-PWP analysis in Sigma/W to study for the flow and stress-deformation response of the earthen dam. The rate of reservoir drawdown is considered 0.5 m/day, for which the variation in the elevation of upstream reservoir is shown in Figure 6.10.

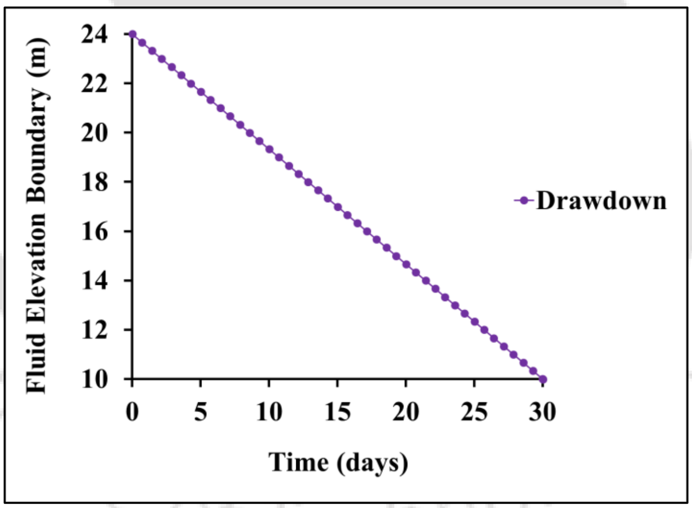

Figure 6.10 Reservoir drawdown (DD) and its rate adopted for the case when the drawdown is initiated after the steady-state phreatic surface is attained in the post rise-up scenario

Figure 6.11 provides the comparison of the pore-water pressures with minimum total stresses along the upstream face of the dam core. It can be clearly observed that as the drawdown takes place, the difference between the PWP and minimum total stresses gradually increases with the passage of time. This is attributed to the dissipation of the PWP towards the upstream of the earthen dam due to the removal of the reservoir load. Hence, it can be stated that for the reservoir drawdown initiated after the phreatic surface attained a steady-state, the hydraulic fracturing at the upstream face of the central core of the dam is possible only at the early stages of drawdown. In the figure, it can be noticed that at the 5th day of drawdown, the PWP and minimum total stress is closest and nearly reaching the magnitude of 1 (one) that corresponds to the criterion of initiation of hydraulic fracturing. Figure 6.11 also shows that at the early stages of drawdown, the tentative location of hydraulic fracturing at the upstream face of the core can be identified at 3/4th height of the earthen dam, measured from its base. As more time passes after the drawdown, the pore-water pressure decreases to reduce the stress ratio and avert any possibility of hydraulic fracturing.

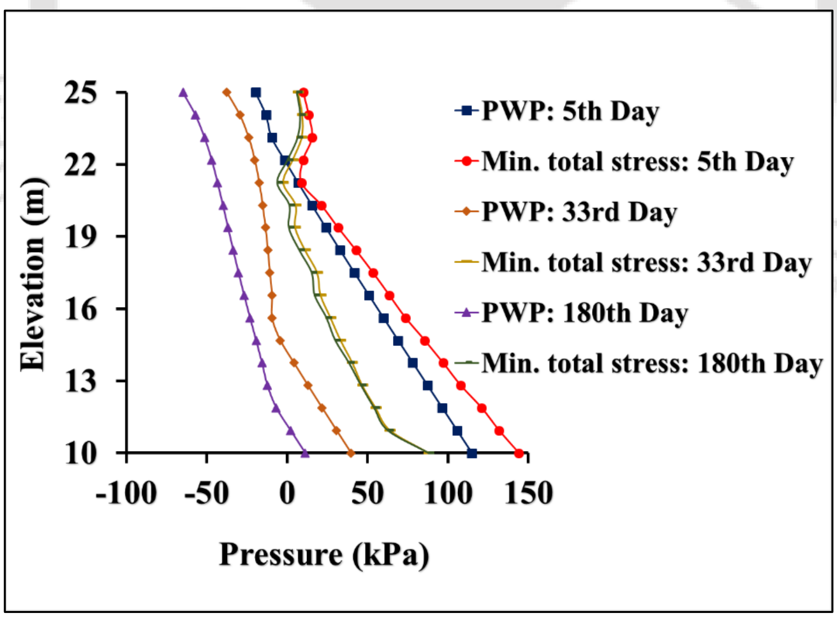

Figure 6.11 Variation of minimum total stress and PWP along the upstream face of the central core of the earthen dam during subjected to reservoir drawdown condition initiated after a steady-state phreatic surface is attained

Figure 6.12 highlights the vertical displacement contours in the zoned earthen dam for the 5th day that is identified as the possible time of hydraulic fracturing for the present study. It can be noticed that the settlement of the core is comparatively more than the settlement of adjacent shells, which causes an arching action in the core-shell interface. The settlement contours are found to extend up to the mid-height of the earthen dam, and are concentrated along the dam core. Such differential displacements between the core and the shell results in strain accumulation throughout the earthen dam, as shown in Figure 6.13. The maximum strain concentration is observed to be along the upstream face of the core. Such strain accumulations along the core face indicates the possibility of hydraulic fracturing during the drawdown condition.

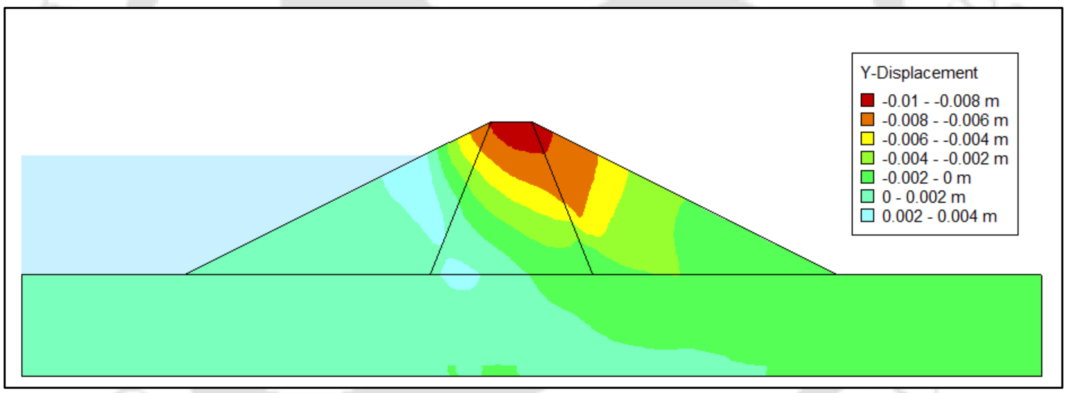

Figure 6.12 Vertical displacement contours in the zoned earthen dam at the 5th day during reservoir drawdown that is initiated after a steady-state phreatic surface is attained in the earthen dam

Figures 6.14 and 6.15 highlight the distribution of hydraulic gradient and seepage velocity, respectively, within the zoned earthen dam. It is seen that for the drawdown condition, high gradients are more concentrated along the downstream face of the core. However, the seepage velocity contours indicated very low seepage velocities. Hence, even though high gradients exist, the presence of low seepage velocity indicated a very low possibility of internal erosion and piping through the zoned earthen dam. Hence, based on all these findings, it can be concluded that although there exists a possibility of crack initiation through hydraulic fracturing during reservoir drawdown, still the conditions are not favorable for internal erosion of the dam.

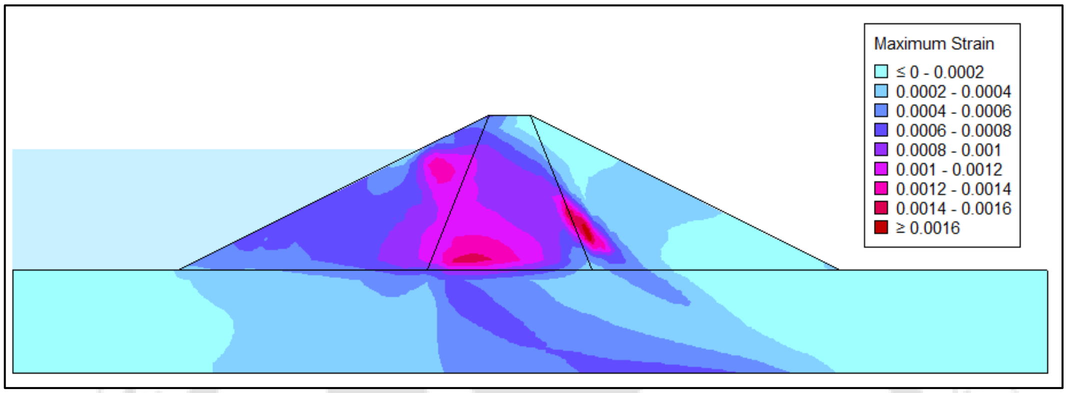

Figure 6.13 Maximum strain contours in the zoned earthen dam at the 5th day during reservoir drawdown that is initiated after a steady-state phreatic surface is attained in the earthen dam

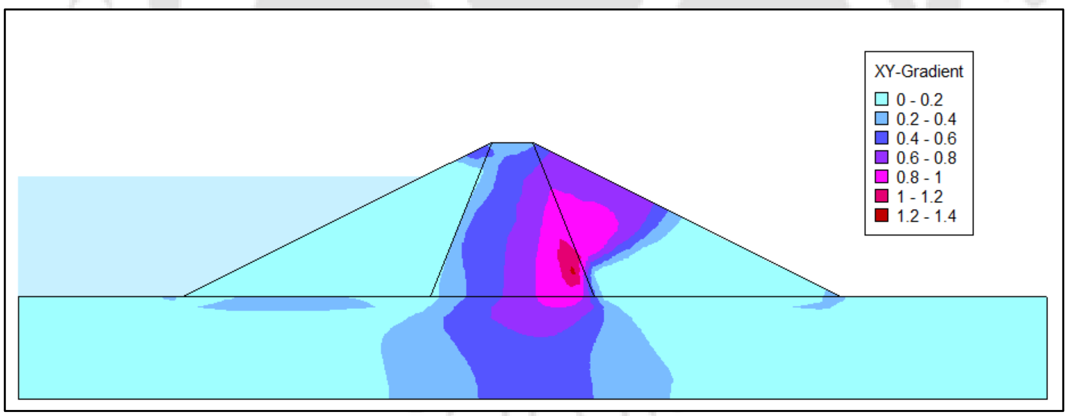

Figure 6.14 Contours of hydraulic gradient in the zoned earthen dam at the 5th day during reservoir drawdown that is initiated after a steady-state phreatic surface is attained in the earthen dam

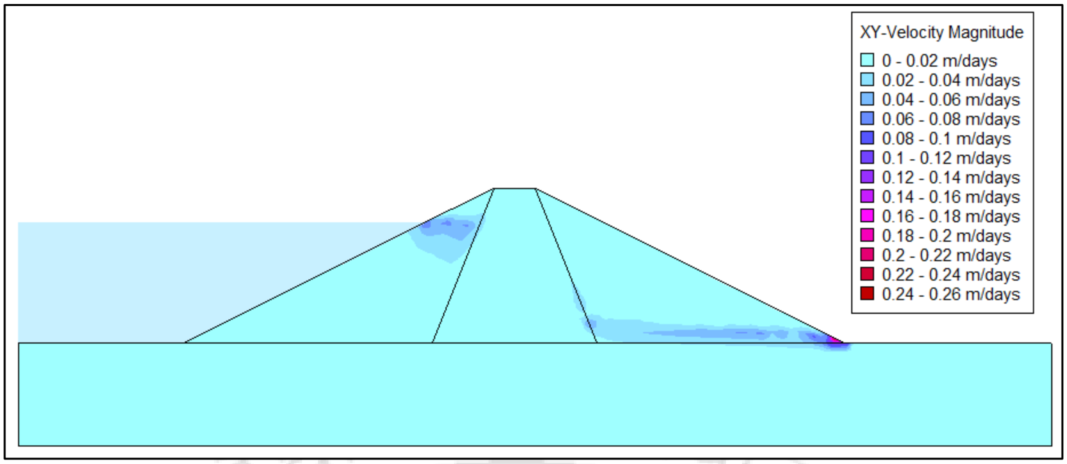

Figure 6.15 Seepage velocity contours in the zoned earthen dam at the 5th day during reservoir drawdown that is initiated after a steady-state phreatic surface is attained in the earthen dam

6.3.2.2 Reservoir Drawdown before attaining the Steady-State Phreatic Surface

In this section, the influence of drawdown phase on the hydraulic fracturing of zoned earthen dam is investigated for the condition wherein the drawdown is carried out before the steady-state phreatic level is achieved after reservoir rise-up. In this section, firstly, the zoned dam is subjected to a reservoir filling in 30 days (which is identical to the rise-up scenario described in Section 6.2.3.1). Thereafter, water level in the reservoir is maintained constant for 2 months, followed by a drawdown carried out before the steady-state phreatic surface developed within the zoned earth dam. The rate of reservoir drawdown is considered 0.5 m/day. The complete sequence of rise-up and drawdown condition of the reservoir is represented in Figure 6.16.

Figure 6.17 highlights the variation of the PWP and minimum total stress along the upstream face of the central core of the zoned earthen dam. It is clearly observed that irrespective at the beginning or completion of drawdown, the PWP always remains significantly lesser than the minimum total stress. Hence, under the stated drawdown scenario, the possibility of hydraulic fracturing is almost negligible. The only possible case of hydraulic fracturing can occur at or before the 91st day that indicate the stress ratio reaching close to 0.8 at some portions of the upstream face of the core. This situation is similar to as described for the zoned dam subjected to reservoir rise-up condition (Section 6.2.3.1). Based on this criterion, the tentative location pertaining to the maximum possibility of hydraulic fracturing remains near the crest. As the drawdown progresses, the pore-water pressure decreases, thereby generating an unfavourable condition for hydraulic fracturing.

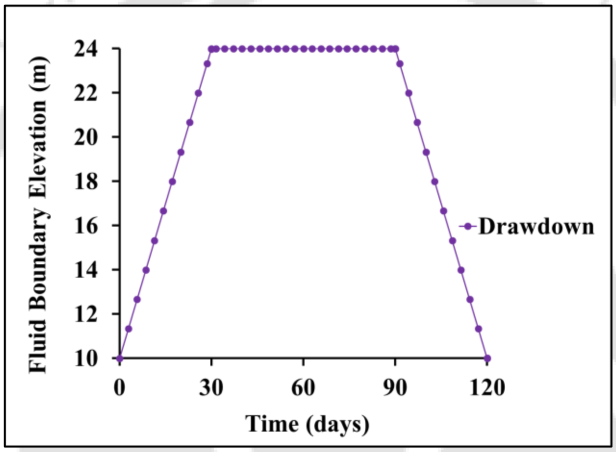

Figure 6.16 Reservoir drawdown (DD) and its rate adopted for the case when the drawdown is initiated before the steady-state phreatic surface is attained in the post rise-up scenario

Figure 6.18 depicts the vertical displacement contours for the 91st day. The figure does not reveal any distinctive differential settlement between the core and shells, which reduces the possibility of hydraulic fracturing. Figure 6.19 portrays the maximum strain accumulation in the body of the zoned earthen dam at the 91st day. It is observed that the recognizable concentration is at a location on the upstream face of the central core and near the crest. This observation reinforces the understanding that maximum possibility of hydraulic fracturing is at the 91st day when the stress ratio is maximum near the crest of the dam.

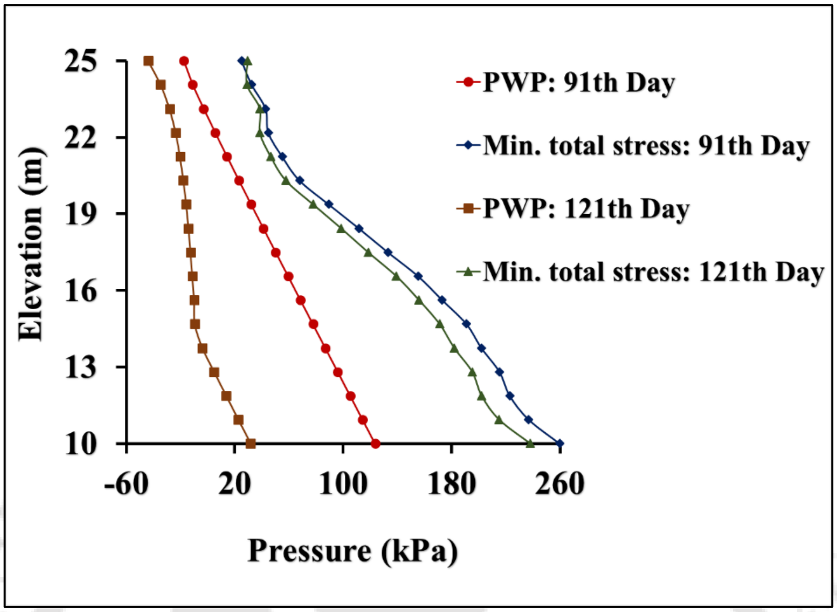

Figure 6.17 Variation of minimum total stress and PWP along the upstream face of the central core of the earthen dam during subjected to reservoir drawdown condition initiated before a steady-state phreatic surface is attained

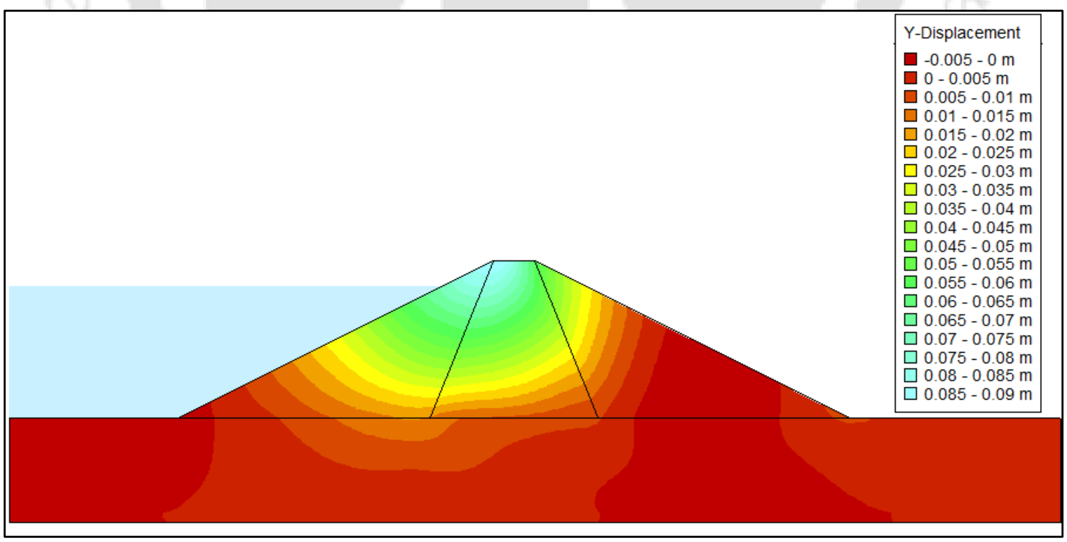

Figure 6.18 Vertical displacement contours in zoned earthen dam at the 91st day during reservoir drawdown that is initiated before a steady-state phreatic surface is attained in the earthen dam

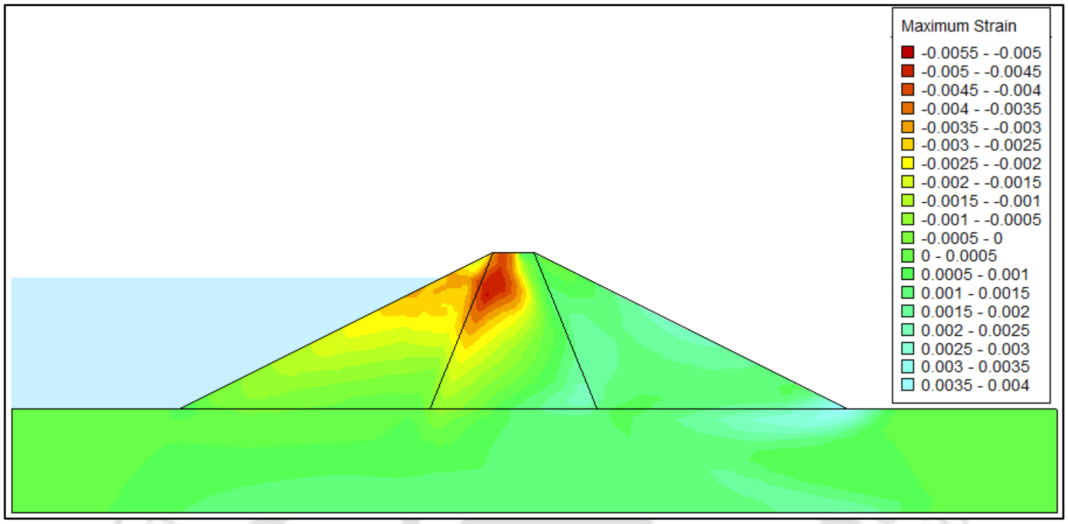

Figure 6.19 Maximum strain contours in zoned earthen dam at the 91st day during reservoir drawdown that is initiated before a steady-state phreatic surface is attained in the earthen dam

Figures 6.20 and 6.21 illustrates the hydraulic gradient contours and seepage velocity contours, respectively, within the body of the zoned earthen dam at the initial stages of the drawdown process (at the 91st day). It is observed that high gradients are mostly concentrated along the downstream face of the core, while the higher seepage velocities are found to be concentrated towards the upstream face of the core. Hence, as the maximum gradients and maximum seepage velocity at a particular location are not simultaneously high, the possibility of internal erosion and piping through the zoned earthen dam is extremely low.

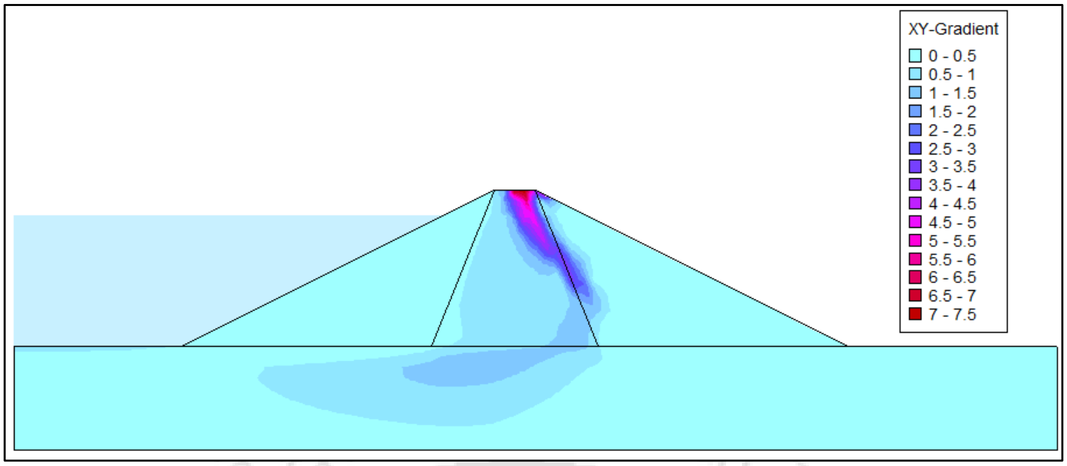

Figure 6.20 Hydraulic gradient contours in zoned earthen dam at the 91st day during reservoir drawdown that is initiated before a steady-state phreatic surface is attained in the earthen dam

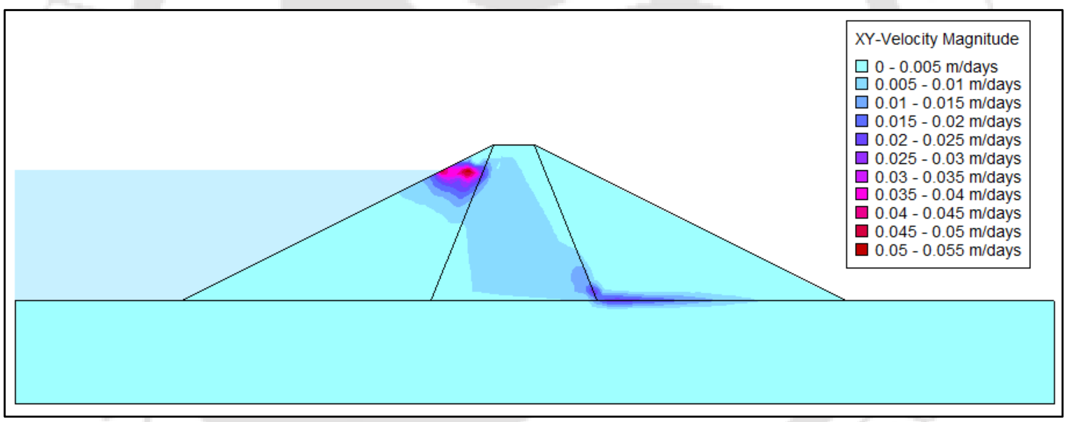

Figure 6.21 Seepage velocity contours in zoned earthen dam at the 91st day during reservoir drawdown that is initiated before a steady-state phreatic surface is attained in the earthen dam

6.4 EFFECTIVENESS OF DRAINAGE BLANKETS IN A ZONED EARTHEN DAM WITH A CRACKED CORE

Section 6.3 has elaborately described the response of zoned earthen dams and identification of the tentative locations of hydraulic fracturing subjected to different types of reservoir operations. The zoned earthen dams comprise a central impervious (or, nearly impervious) core that is flanked, enclosed, supported and protected by the shells of relatively pervious materials. The upstream pervious zone provides the stability against rapid drawdown, while the downstream pervious zone aids in controlling the seepage flow and lowering of the phreatic surface. It is interesting to note that for zoned earthen dams, in case there a breach of the central impervious core through sustained hydraulic fracturing and internal erosion, the downstream shell (comprising relatively pervious material) would be immediately jeopardized, and so do the stability of the downstream of the earthen dam. In many cases, to amend the unfortunate situation, a drainage blanket may be necessary at the interface of the central core and downstream shell, as well as beneath the downstream shell near the toe of the dam. These drainage blankets must definitely meet filter criteria so that the migration of particles can be prohibited while the seeping water can freely flow through them. These drainage blankets can be single- or multi-layered for enhancing their performance. The type and shape of the drainage blankets (horizontal toe drainage blanket or inclined chimney drainage blanket) governs the protective buffer that can be provided in case of larger volume of water flow through the breached central core. The drainage blankets can keep a control over the phreatic surface developed due to the core cracking, and attempt to maintain the performance of the earthen dam by lowering down the phreatic line in its downstream. Chapter 4 has illustrated the utilization of drainage blankets towards the stability and flow-deformation response of homogeneous earthen dams, and successfully highlighted the change in the response of the same under different scenarios of clogging of drainage blankets. In this section, the utilization of the horizontal toe and inclined chimney drainage blankets are explored for their effectiveness in preventing the failure of a zoned earthen dam with a cracked core.

6.4.1 Model and Materials used for the Present Study

The present study explores the implication of having a fully functional horizontal toe or inclined chimney drainage blanket on the flow and deformation responses of the zoned earthen dam subjected to hydraulic cracking and internal erosion. The numerical models used in the present study, along with its relevant dimensions, are shown Figure 6.22.

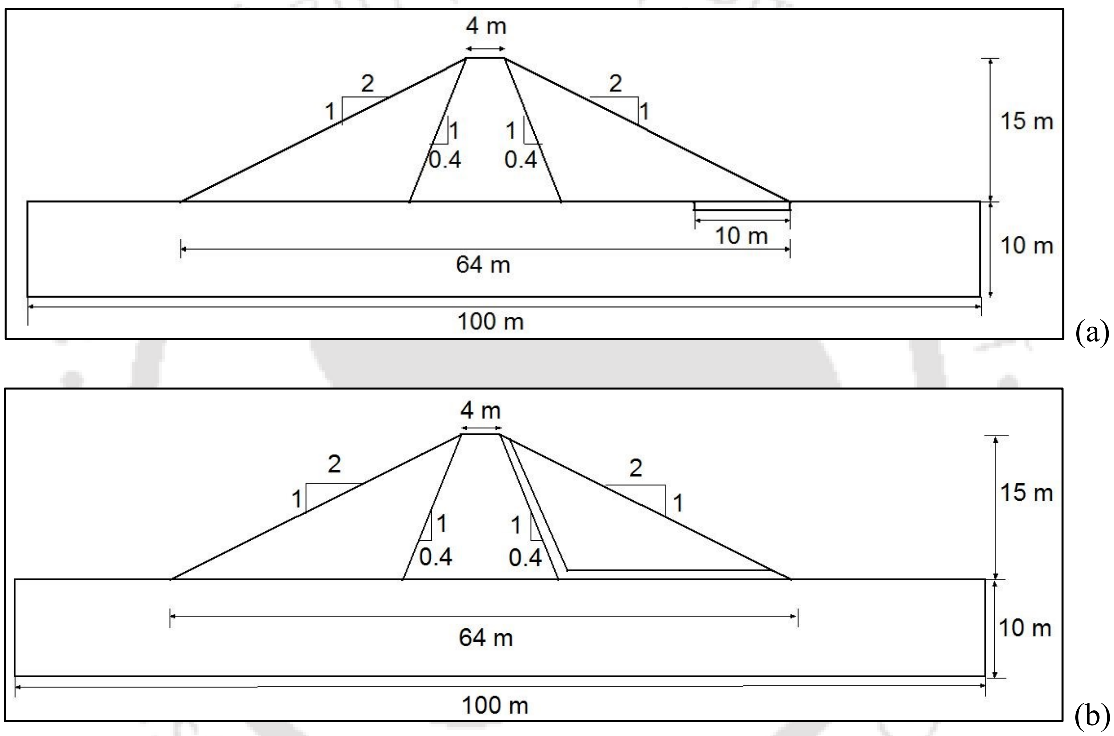

Figure 6.22 Model of a zoned earthen dam with (a) horizontal toe drainage blanket (b) inclined chimney drainage blanket

Further details about the dimensions and constituent material used for the zoned dam remain same as described in Section 6.2.2. The material characteristics of the drainage blankets remain same as described in Section 4.3.2. The details of the FE models, about the boundary conditions, meshing and stages of analyses, remain same as described in Sections 4.3.3 and 4.3.4. Since this study is only to highlight the efficacy of the utilization of drainage blankets in the zoned earthen dams, all the analyses reported for the present study involves a steady-state reservoir level, leaving a freeboard of 1 m from the crest of the dam. Additional studies with operational reservoir conditions are not reported herein.

6.4.2 Interpretations and Inferences

The functionality of the drainage blanket in a zoned earthen dam is to collect the seepage water and maintain the phreatic surface away from the downstream face, so that the downstream slope can be prevented from failure. Figure 6.23 exhibits the comparison of the steady-state phreatic surface within a zoned earthen dam without a drainage blanket as well as comprising a fully functional horizontal toe or inclined chimney drainage blanket. It can be observed that the presence of the impervious core, if not suffered hydraulic fracturing, is effective enough in lowering the phreatic surface even in the absence of drainage blankets (as seen in Figure 6.23a). The presence of a fully functional drainage blanket is observed to offer only additional support in altering the exit point at which the phreatic surface dips and intersects with the base of the dam.

For zoned earthen dam without drainage blanket and comprising horizontal toe or inclined chimney drainage blanket, Figure 6.24 and 6.25 highlights the hydraulic gradient and seepage velocity contours, respectively. As mentioned earlier, a thorough scrutiny of simultaneously high magnitudes of hydraulic gradients and seepage velocity within the dam is necessary to identify possible scenarios of internal erosion or its initiation.

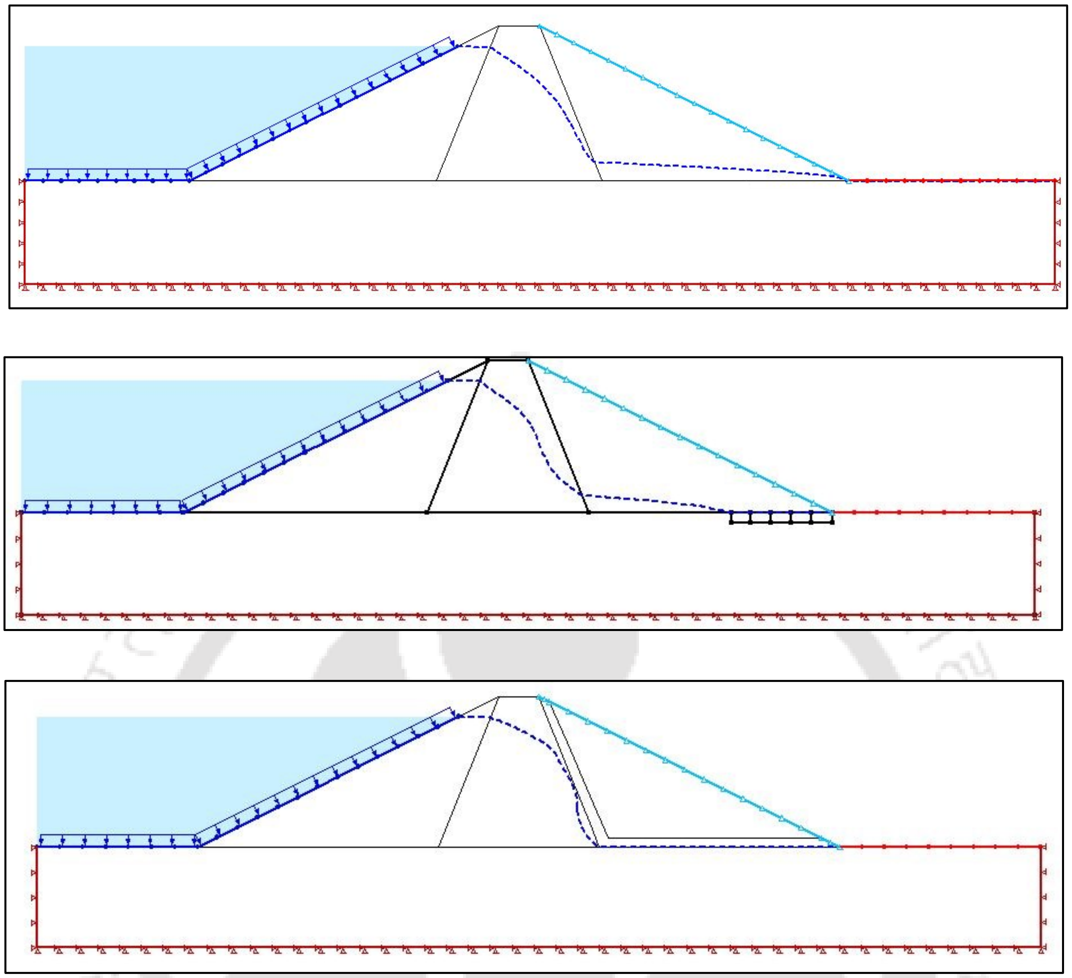

(a)

(b)

(c)

Figure 6.23 Comparative of steady-state phreatic surface within the zoned dam having a central impervious core and comprising (a) no drainage blanket (b) horizontal toe drainage blanket (c) inclined chimney drainage blanket

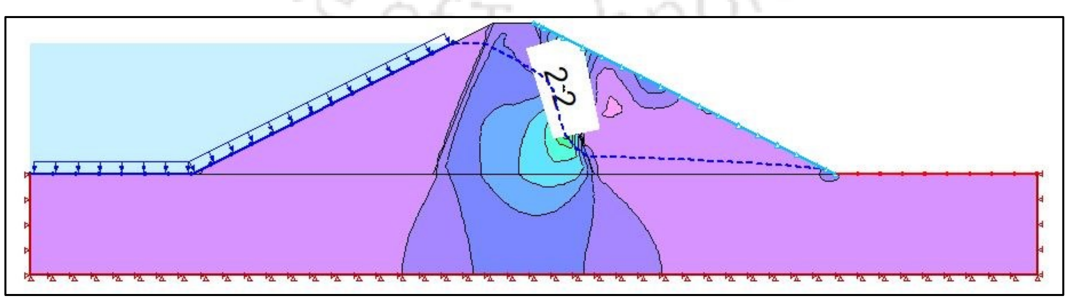

(a)

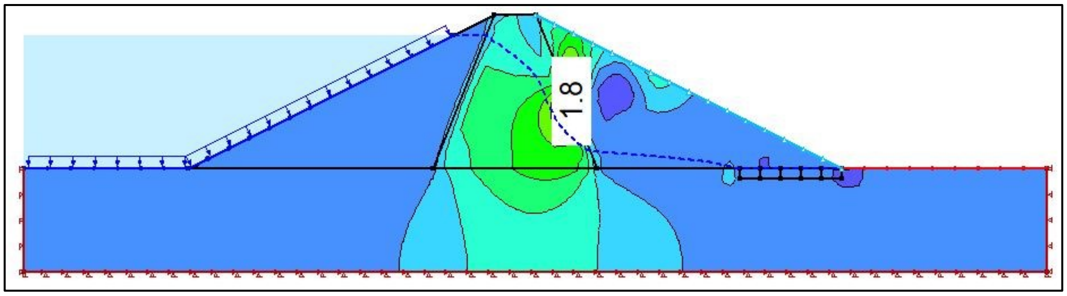

(b)

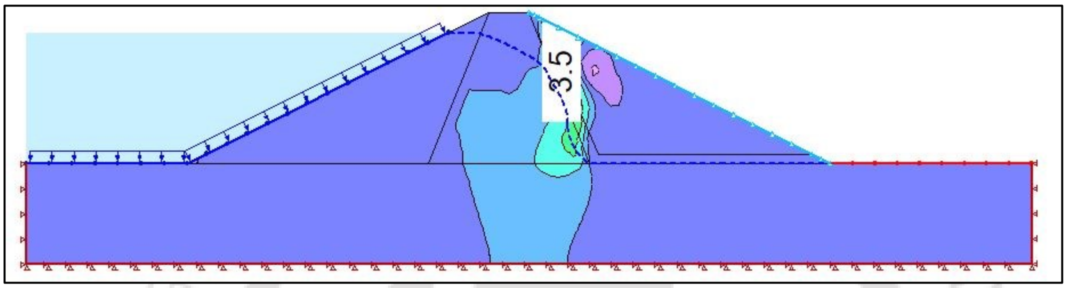

(c)

Figure 6.24 Comparative of hydraulic gradients within the zoned dam having a central impervious core and comprising (a) no drainage blanket (b) horizontal toe drainage blanket (c) inclined chimney drainage blanket

The internal hydraulic gradients that are capable of initiating internal erosion are likely to be quite different at various places along the seepage pathway. As the seepage path is undoubtedly tortuous and considerably meandering, and seepage flows experiencing different amounts of head loss at different locations along the way, it becomes exceedingly difficult to assess accurately the hydraulic gradients along the seepage path. It is worth reinforcing the concept that the internal gradient that might lead to the initiation of internal erosion may be as low as 0.02-0.08 for particularly susceptible soils (Schmertmann, 2000). These internal gradients are substantially lower than the critical gradient of 1.0 that is often assumed for exit gradients at the toe region of the dam.

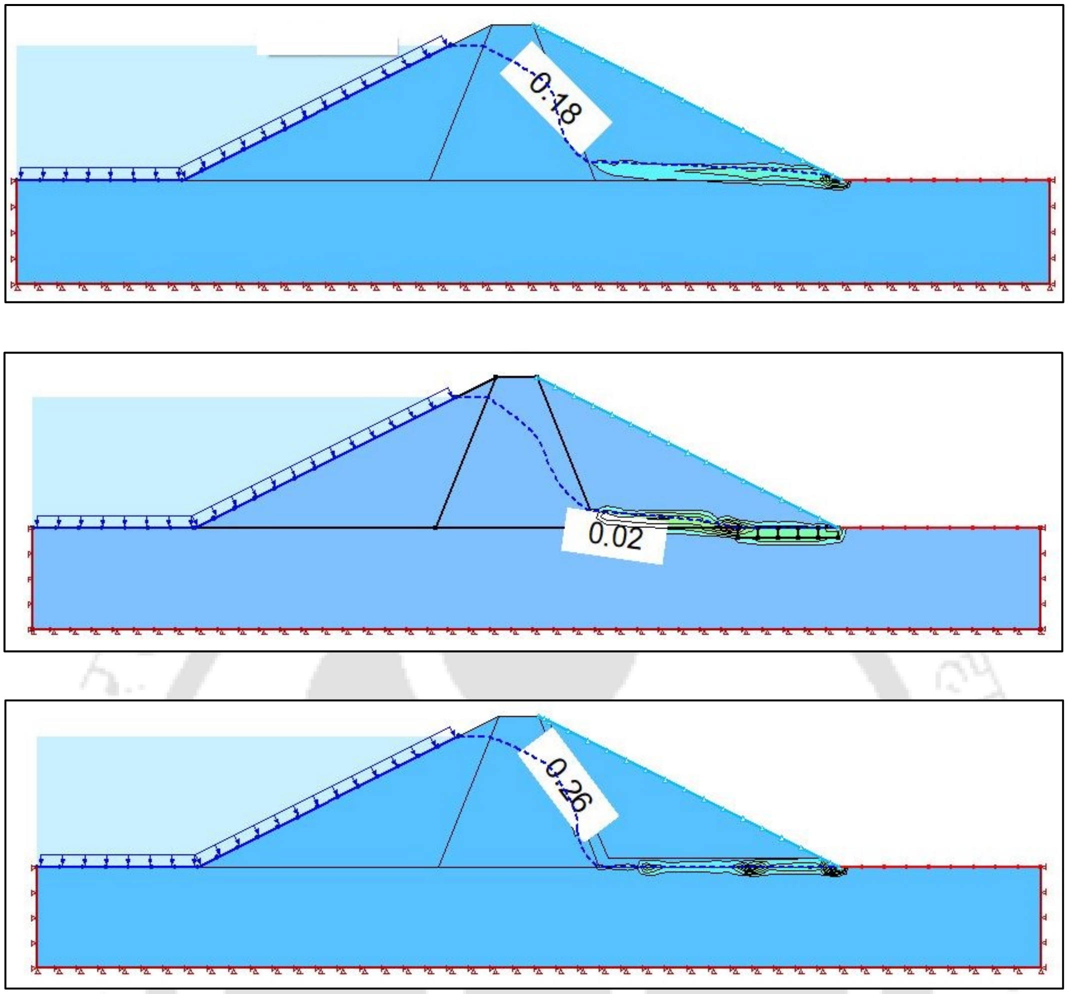

(a) (b) (c)

Figure 6.25 Comparative of seepage velocities (m/day) within the zoned dam having a central impervious core and comprising (a) no drainage blanket (b) horizontal toe drainage blanket (c) inclined chimney drainage blanket

Figure 6.24 shows that the location for high internal gradients are approximately same for all the cases. High gradients are observed along the downstream part of the core in contact with the shell. Upon comparing the three cases depicted in Figure 6.24, it can be seen that dam with inclined chimney drainage blanket has the maximum gradient and velocity. However, for all the cases, the gradients are high enough to initiate the internal erosion within the dam. However, from Figure

6.25, it can be seen that the seepage velocities are obtained as 0.18 m/day, 0.02 m/day and 0.26 m/day for the three cases, respectively. It can be noticed that the seepage velocity at the interface of the downstream face of the core and downstream shell is lowest for the zoned earthen dam comprising horizontal toe drainage blanket. Hence, for the earthen dam without the drainage blanket or with inclined chimney drainage blanket, the susceptibility to internal erosion is apparently higher. Now, whether such combination of gradients and velocities, for each of the case, are potentially harmful or not is a matter of further debate, research, and engineering judgment with due consideration to a number of additional factors such as soil gradation and mean size of the constituent materials apart from compaction state and its uniformity across the dam. Thus, a detailed study to evaluate the potential for internal erosion to initiate, by considering particle gradation and particle migration, is a subject of thorough analysis and research, which is out of scope of the present research.

From the above analyses, it is observed that for a zoned dam with a central impervious core and resting on an impervious foundation, the presence of the drainage blanket does not play significant role in preventing the potential risk for internal erosion or hydraulic fracturing within the core. Further investigation is conducted to ascertain whether the drainage blankets have a positive role to play in withholding the performance of a zoned earthen dam in case it experiences a complete core breaching through hydraulic fracturing. In order to conduct this study, the earlier numerical model of the dam is considered with a predefined crack through the impervious central core, schematically represented in Figure 6.26. In this numerical model, a very thin section, representing the crack, is introduced wherein the impervious material of the core is replaced by the pervious materials of the upstream shell. In this way, the phreatic surface is forced to move through the crack path and meet the downstream face of the core at a specified location.

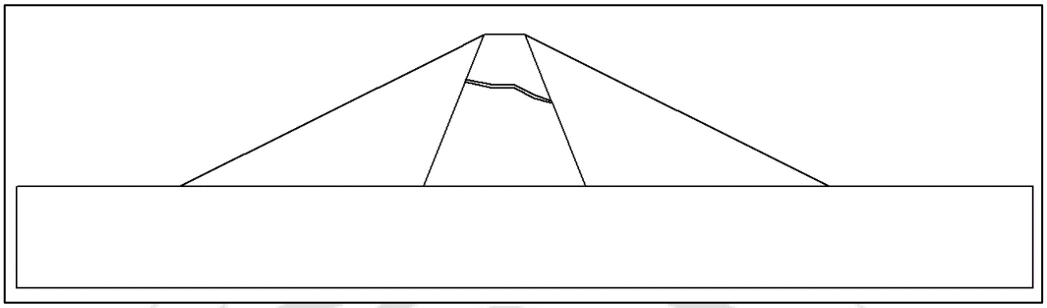

Figure 6.26 Schematic diagram of a zoned earthen dam with a predefined crack in the central impervious core used for the present study

Figure 6.27 highlights the implication of using drainage blankets as a protective measure and enhancement of the performance life of zoned earthen dam with a breached core. In all the figures, it can be observed that the phreatic surface is successfully developed along the predefined crack. Further, for the zoned dam without any drainage blanket, it enters the downstream shell of the accompanied by high seepage velocities as indicated by the larger size of the flow magnitudes (Figure 6.27a). In this process, for the steady-state scenario, the phreatic surface saturates most of the downstream portion of the dam, and moves ahead to intersect with the downstream face of the dam. This combination of flow path and high seepage velocities can be detrimental for the long-term performance of the dam. Figure 6.27b and 6.27c indicates that the presence of a drainage blanket, whether horizontal toe or inclined chimney drainage blanket, successfully directs the flow towards and through the drainage blanket, thereby preventing the phreatic line to migrate towards the downstream face, and protecting the safety and stability of the downstream face of the dam. As can be easily understood, the inclined chimney drain provided at the downstream face of the core and downstream shell of the dam is instrumental in channelizing the phreatic surface right from the core-shell interface and prevents larger portion of the downstream shell from being saturated.

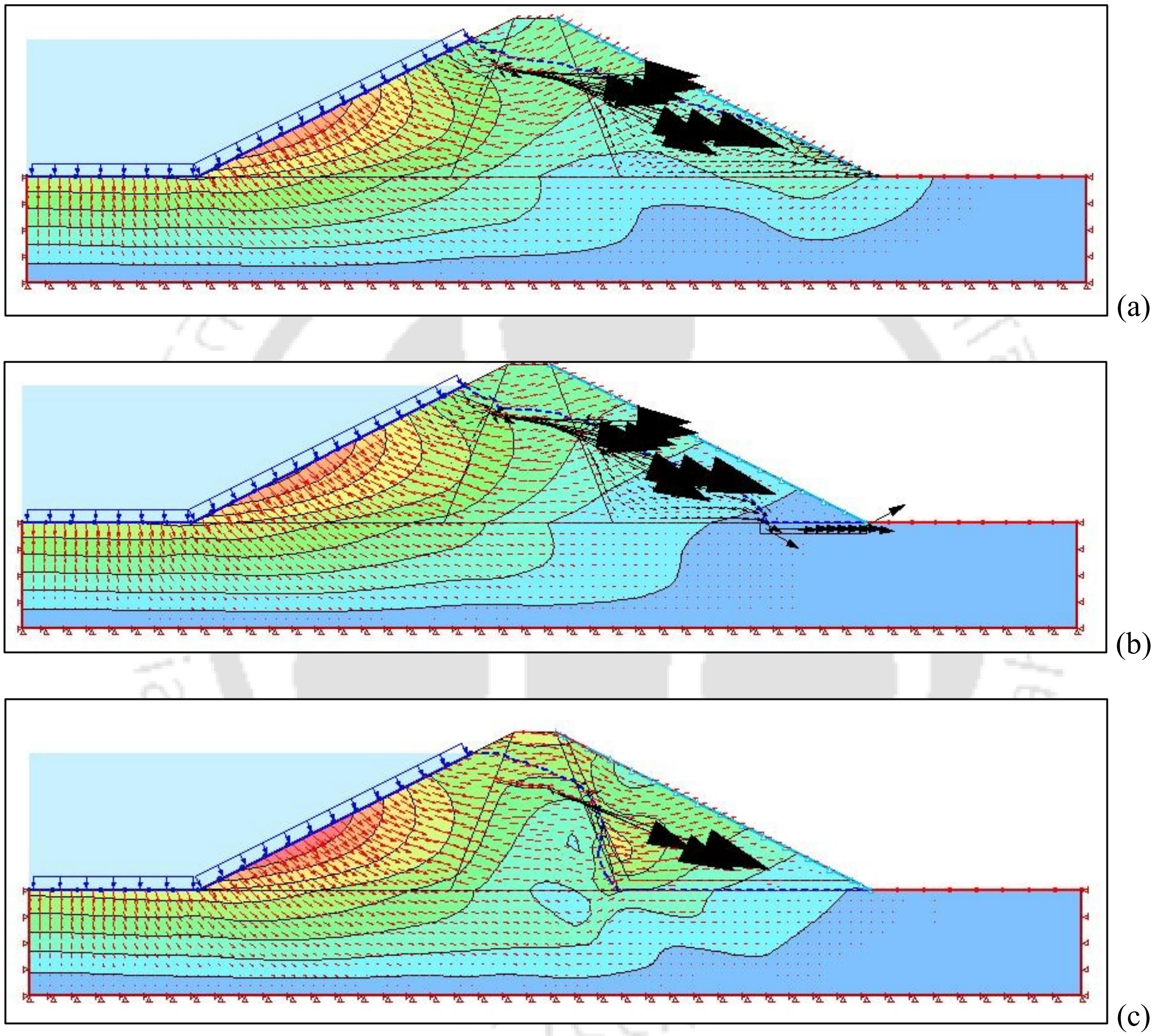

Figure 6.27 Comparative of seepage velocities (m/day) within the zoned dam having a central impervious core and comprising (a) no drainage blanket (b) horizontal toe drainage blanket (c) inclined chimney drainage blanket

Hence, concisely, it can be stated that the presence of drainage blanket does not necessarily reduce the possibility of core cracking through hydraulic fracturing. However, their presence is immensely necessary for maintaining the performance of a zoned earthen dam that suffered a core breaching. The presence of the drainage channels directs and diverts the phreatic line through them, thus controlling the saturation front from migrating towards the downstream.

6.5 IDENTIFICATION OF THE PATH OF CRACK PROPAGATION THROUGH A BREACHED CENTRAL CORE IN ZONED EARTHEN DAM

Section 6.4 was mainly intended to highlight the importance of having drainage blankets in the zoned earthen dams that is manifested through a predefined crack region through the central core. However, it is understandable that in reality, the crack would evolve through the central core, rather than following a predefined path as assumed in the previous section. Hence, this section explores for a methodology that can be used to identify the evolution of crack propagation through the central core of zoned earthen dam, for the case of initial location of hydraulic fracturing being known. It is already revealed in Section 6.3 that the initiation of hydraulic fracturing in the upstream face of the core of a zoned earthen dam is mostly conducive just after a reservoir rise-up condition. It was also revealed that the tentative location for crack initiation along the upstream face of the core is approximately at 3/4th height of the dam, measured from its base, which occurred at 38th day as highlighted in Figure 6.5. The location of the crack at the upstream face of the core was observed to be approximately at 2 m below the steady-state reservoir level. Based on this information, the initial state of zoned dam and the initial location of hydraulic fracturing on the upstream face of the core is simulated, and further attempt is made to simulate and identify the path of crack propagation path through the core central of the dam.

The primary objective of this analysis is to identify the path of crack propagation through the central core after its initiation. Numerical modelling as adopted for the rest of the dissertation is followed in this study as well. Additionally, the outcome of each step of the analysis at each of the node points and Gauss points are minutely scrutinized. Figure 6.7 had already depicted the development of the regions of strain concentration on an event of initiation of hydraulic fracturing of a zoned earthen dam after the completion of reservoir rise-up. Utilizing the plots of maximum strain contours, the propagation path is traced by identifying all those the nodal points, around the location of crack initiation, where the stress ratio was approximately equal to or higher than 1 (one), as shown in Figure 6.28(a). Apart from the nodal stress ratio, the identification process is reinforced with engineering judgment based on the outcomes of the analysis conducted for the 38th day using the distributions of strain, hydraulic gradient and seepage velocity (Figure 6.7-6.9). Based on all the above, the region of hydraulic fracture between the upstream face of the dam and core is identified. Further, the identified region is replaced by a high permeable material in the numerical simulation, as shown in Figure 6.28(b). This approach virtually generates a region of higher permeability that implies nearly free percolation of water, thereby indicating the demarcated region as the most feasible path of water percolation towards the upstream face of the core.

Considering the demarcated crack region, for further analysis, the various stages of analyses, as discussed earlier, are repeated for the 39th day. Similar to that obtained for 38th day, the corresponding contour plots for maximum strain, hydraulic gradient and seepage velocity are estimated, as shown in Figure 6.29. These findings help to develop the idea of successive demarcation of the nodal points with maximum stress ratio (approximately equal to or greater 1) for the next day, i.e. the 39th day. Further, on identification of the possible region of crack enhancement from the results of 39th day, as earlier, a high permeable material is assigned and the analyses is carried forward for the successive days. Based on the outcomes from the analysis for the 39th day, Figure 6.30 demarcates the results obtained from the analysis of 40th day. Hence, an iterative and repetitive process is devised, and the same steps are applied for the analysis of consecutive days.

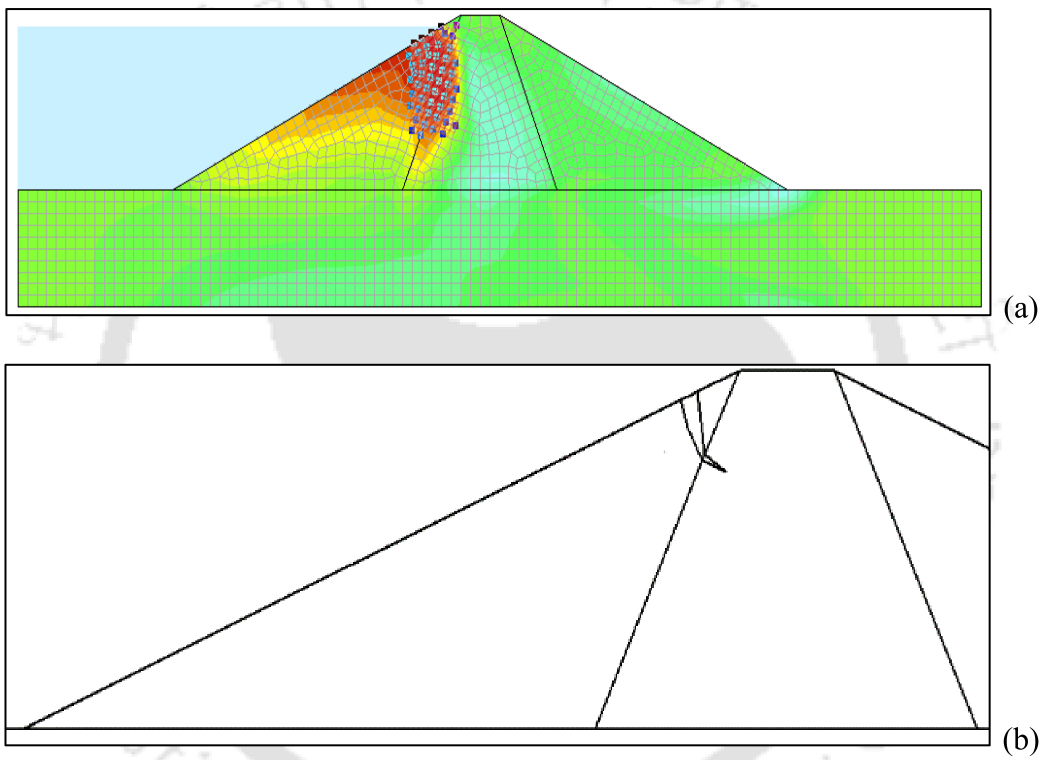

Figure 6.28 Simulation of crack propagation in a zoned earthen dam (a) Nodal points demarcating the maximum stress ratio in the region of maximum strain on the 38th day (b) Demarcated region assigned with high permeable material to simulate virtual flow path of water due to cracking

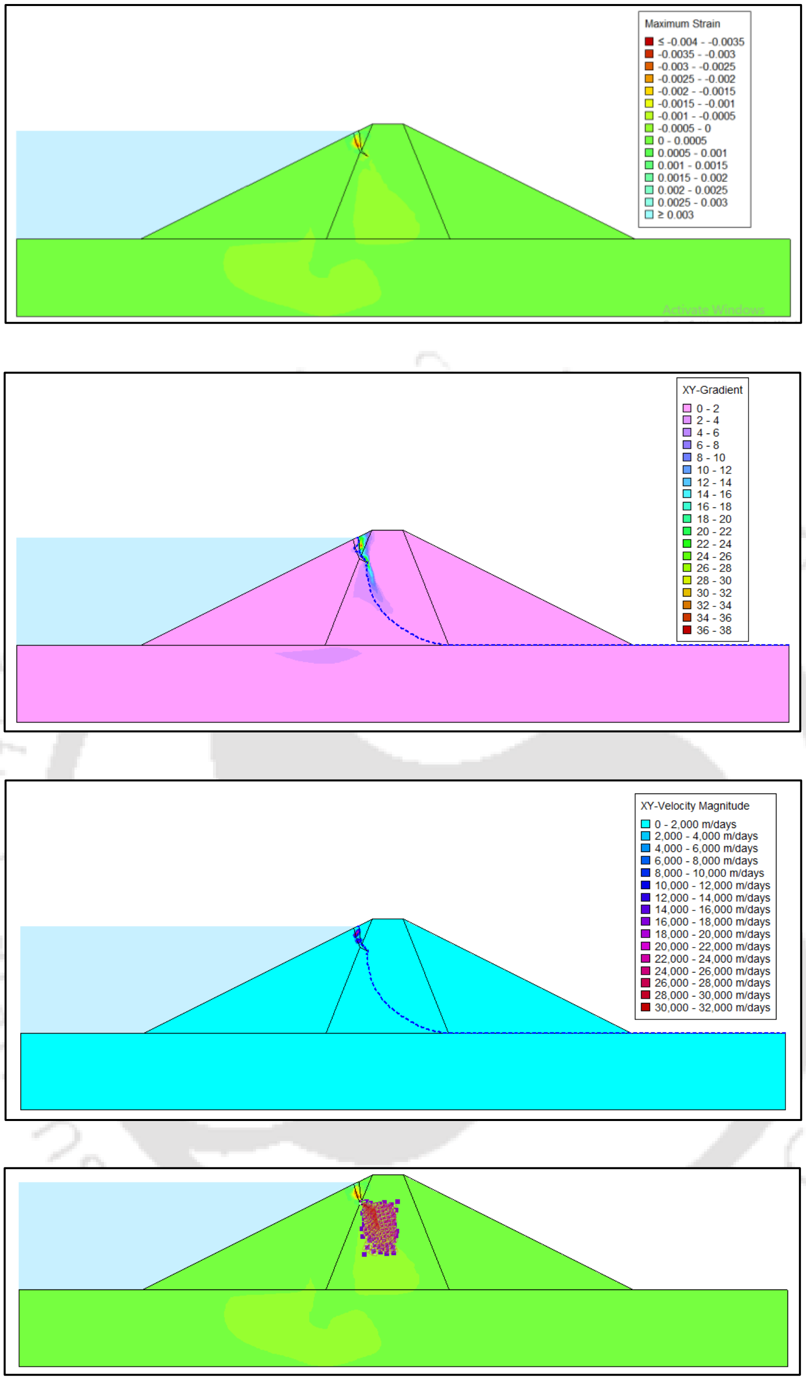

(a) (b) (c) (d)

Figure 6.29 Elements of identification of crack propagation on 39th day based on the analysis of demarcated crack region on 38th day **(**a) Maximum strain contours (b) Hydraulic gradient contours (c) Seepage velocity contours (d) Nodal points demarcating maximum stress ratio in the region of maximum strain on the 39th day

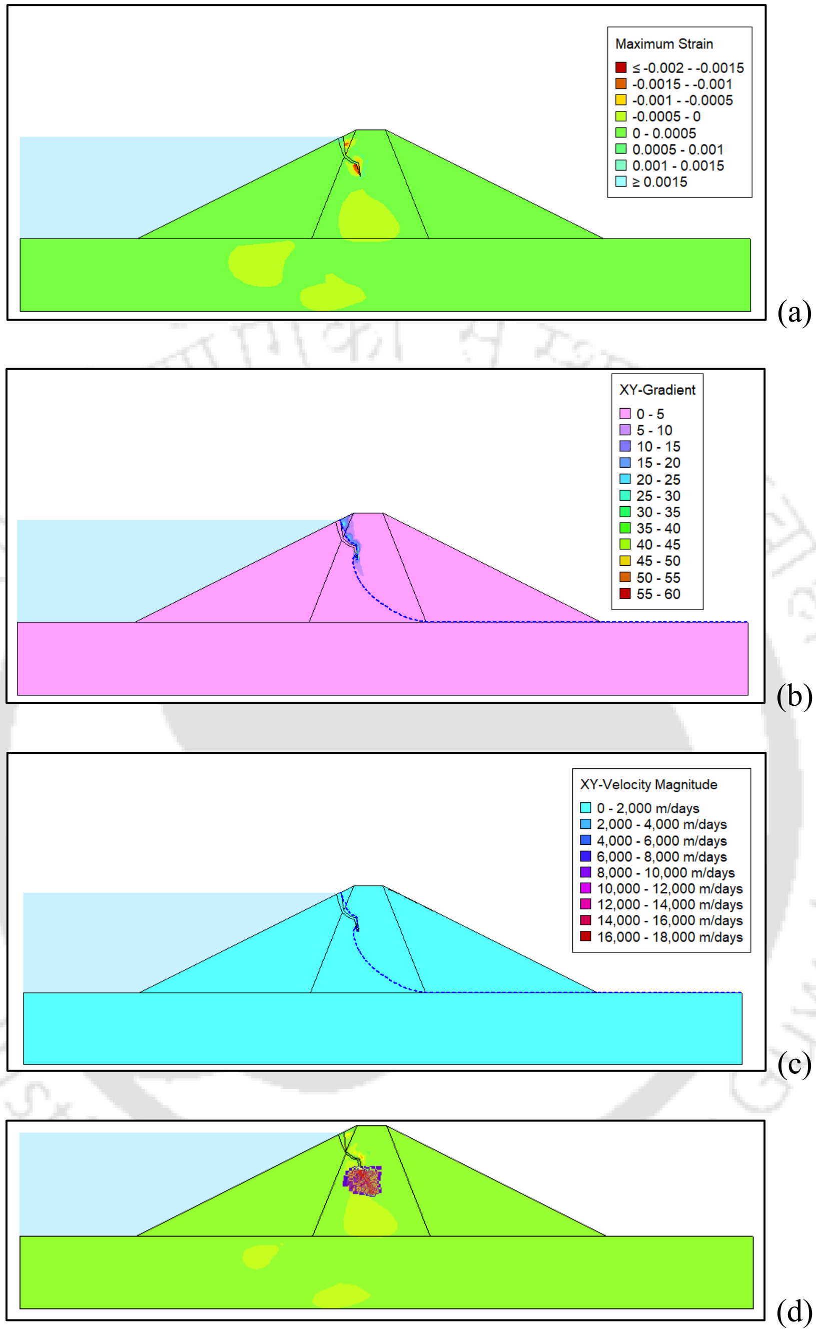

Figure 6.30 Elements of identification of crack propagation on 40th day based on the analysis of demarcated crack region on 39th day (a) Maximum strain contours (b) Hydraulic gradient contours (c) Seepage velocity contours (d) Nodal points demarcating maximum stress ratio in the region of maximum strain on the 40th day

The repetitive analysis, as described through the Figures 6.28-6.30, is conducted progressively for successive days. The recursive process is stopped once the crack propagates and the tip of the identified crack merges with the downstream face of the central core. Hence, with the aid of this recursive process, as described, the path of crack propagation through the central core of the dam is identified, as indicated in terms of the velocity contours in Figure 6.31. This analysis can be easily repeated for crack propagation in the presence of a drainage blanket in the earthen dam. It can be observed from Figure 6.31, a concentration is hydraulic velocity develops at the interface of the downstream face of the core and downstream shell. In the presence of a drainage blanket, this gradient concentration will be dissipated through the drainage blankets, as the seeping water will find a channelized path to flow out of the dam. Apart from that, all the basic inferences remain same as already described in Section 6.4, and hence the detailed study of the same is not included in the dissertation report.

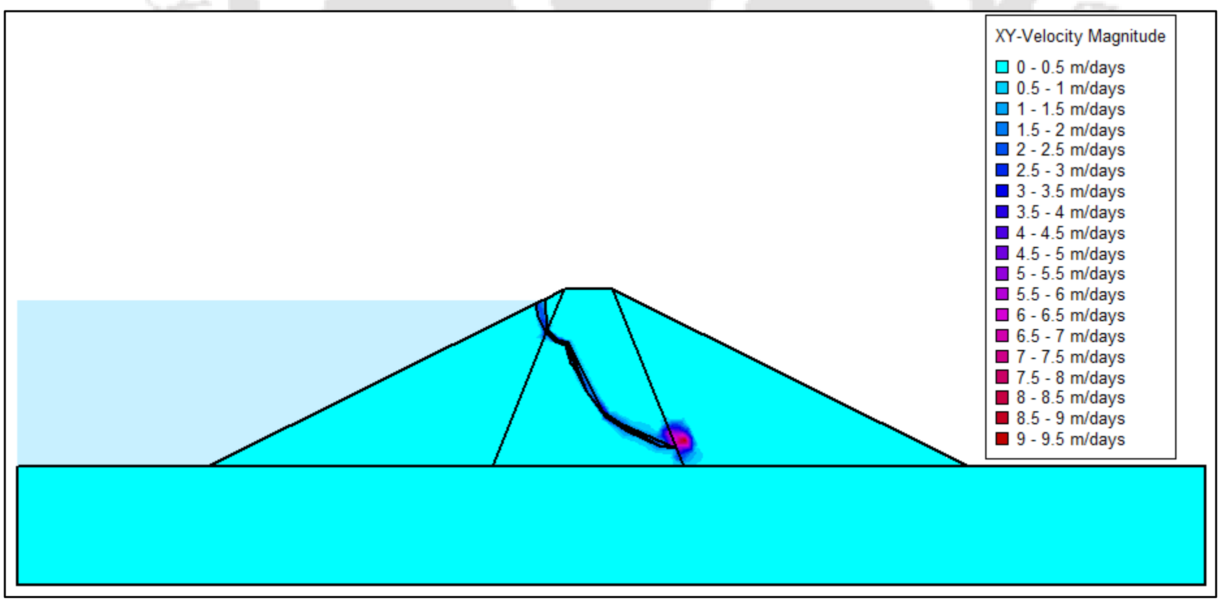

Figure 6.31 Path of crack propagation through the central core of the dam represented in terms of velocity contours

6.6 SUMMARY

This chapter highlighted the response of zoned earthen dams comprising a central core when subjected to hydraulic fracturing. Detailed FE analyses have been conducted to identify the influence of reservoir rise-up and drawdown scenarios on the hydraulic fracturing of central core. Based on the analysis, the possible instances and locations of hydraulic fracturing are reported. Further, the influence of drainage blanket in a zoned earthen dam on the possibility of prevention of hydraulic fracturing are investigated. It was observed that the drainage blankets do not necessarily put a check on the hydraulic fracturing. However, they are immensely useful in case the central core of the zoned dam is breached by hydraulic fracturing. The presence of drainage blanket lowers the phreatic level and prevents the saturation front to migrate to the downstream face of the dam, thereby enhancing the performance life of an earthen dam with a breached impervious core. Finally, the chapter reports a recursive technique that is devised with simple iterative numerical simulations to identify and track the path of crack propagation through the impervious central core.

CHAPTER 7

FINAL REMARKS AND CONCLUSIONS

7.1 SUMMARY OF THE DISSERTATION

This dissertation reports about the hydraulic response and stability analysis of earthen dams subjected to drainage blanket clogging and hydraulic fracturing of the central core. Finite element analyses is resorted to for conducting the numerical investigations. The assessment of drainage clogging subjected to different drainage configurations are deciphered and the phenomenon of hydraulic fracturing for different reservoir loading conditions is understood. The study is further extended to identify the tentative locations of cracking in an earthen dam, subjected to various loading scenarios, and crack propagation path through zoned dams.

The detrimental effect of the clogging of drainage blanket, which has resulted in the failure of dams, was already emphasized by different researchers. Thus, flow analysis, stress-deformation analysis, and the stability analysis of homogeneous earthen dams, without or with fully functional or clogged drainage blankets, were investigated and reported in the dissertation. In this direction, various types of clogging scenarios are incorporated in the drainage blankets to study their influence on the response of homogeneous earthen dams. The study helped in identifying the comparatively efficient drainage configurations that can serve its purpose even when they are partially clogged. From the different clogging typologies analysed in the study, the most detrimental clogging scenario is identified. The influence of the clogging rate of the drainage blankets on the response of the earthen dam was also ascertained.

Hydraulic fracturing in impervious clay core is a common phenomenon in earthen dams and the experience from different dam failure incidents suggested that concentrated leaks induced by hydraulic fracturing often goes unrecognized. Understanding the initiation of core cracking is an ever-challenging problem for the engineers. Therefore, in this work, an attempt is made to investigate numerically the possible locations of core cracking along the upstream and downstream face of homogeneous earthen dam during the transient reservoir operations. The study is extended to identify the tentative location of crack initiation on the faces of the central impervious core in a zoned earthen dam. Further, the path of crack propagation through the core is also identified through recursive numerical investigation and imposition of standard criterion involving effective minor principal stress and generated pore-water pressure.

7.2 CONCLUSIONS

Based on the investigations and numerical simulations conducted for the present study, the following conclusions are drawn:

- Validation of the developed FE numerical model against the well-documented case history of Glen Shira dam failure established the suitability of using the Geostudio 2012 software package in investigating the stability and hydraulic response of earthen dams.
- Installation of drainage blanket results in significant reduction of pore pressure within the earthen dam, especially at the downstream end. However, the drainage blankets are effective only up to the extent that they are not substantially clogged. In the latter cases, the response of the earthen dam with clogged drainage blankets become equivalent to an earthen dam devoid of any drainage blanket.

- Inward clogging of drainage blanket proved to be the most critical clogging scenario resulting in high and drastic generation of pore-water pressure in the downstream, thereby jeopardizing the stability of the downstream face of earthen dam. In this clogging scenario, the clogging of the toe at the outset of sequential clogging leads to substantial rise of the phreatic surface within the body of earthen dam. Hence, provision of efficient filter materials to prevent drainage blanket clogging is recommended for higher life performance of earthen dams.
- Clogging of horizontal toe drainage blanket is observed to be more detrimental as compared to clogging of inclined chimney drainage blankets, owing to the more drainage area provided by the latter. Therefore, it is preferable to use inclined chimney drains in case of homogeneous or zoned earthen dams.
- Clogging of drainage blankets have marginal influence on the response of earthen dams during the transient reservoir operations. The detrimental influence of clogging should be critically assessed for the long-term steady-state performance of earthen dams.
- The influence of the clogging rate is pronounced only when the reservoir level or the phreatic level within the body of the earthen dam had attained steady-state conditions. During the transient reservoir operation conditions (rise-up or drawdown), the influence of clogging rate is minimal.
- The drainage blankets do not have influence in reducing the potential risk of hydraulic fracturing of the central impervious core of a zoned earthen dam. However, the drainage blankets (especially the chimney drainage blanket) are instrumental in reducing additional distress by dissipating the pore water pressure once the central core suffers hydraulic fracturing and cracking.

- Numerical modeling of homogeneous earthen dams can be carried out by following the conventional single-lift technique or more detailed realistic multiple-lift technique. It is concluded that both types of modeling technique results in similar stress distribution along the face of the dam. However, during the sequential multiple-lift technique of modeling, simulating lifts of lesser thickness reduces the unrealistic generation of stress-based cracking along the dam slopes. In such cases, if cracking occurs, the most probable location is at the mid-height of the earthen dam and on the slope face.
- During the transient reservoir rise-up condition, the tentative location of hydraulic fracturing along the upstream face of a homogeneous earthen dam is approximately at 0.2-0.25 times the height of the earthen dam, measured from its base. During the reservoir filling operation, the possibility of hydraulic fracturing does not exist in the downstream face.
- The possibility of hydraulic fracturing along the upstream face of a homogeneous earthen dam is extremely marginal during drawdown condition (after a steady-state phreatic surface is attained). However, possibility of hydraulic fracturing exists along the downstream face, and the tentative location for possible hydraulic fracturing is approximately at 0.5-0.75 times the height earthen dam, measured from its base.
- During the reservoir drawdown condition (before a steady-state phreatic surface is attained), the tentative location of possible hydraulic fracturing along the upstream face of a homogeneous earthen dam is approximately within 0.6 times the height of the dam, measured from its base. Along the downstream face of the dam, no favorable conditions leading to hydraulic fracturing is generated; however, the minimum total stress attained negative magnitudes at 0.2-0.6 times the height of the dam, measured from its base. The

negative magnitudes indicate the possibility of tension crack formation along the downstream face owing to the reservoir drawdown.

- For a zoned earthen dam subjected to reservoir rise-up condition, the tentative location of hydraulic fracturing along the upstream face of the central core is approximately at 3/4th the height of the dam, measured from its base.
- For a zoned dam subjected to reservoir drawdown condition (after a steady-state phreatic surface is attained), the tentative location of hydraulic fracturing along the upstream face of the core is at 3/4th height of the earthen dam, measured from its base.
- For a zoned earthen dam subjected to drawdown condition (before a steady-state phreatic surface is attained), the tentative location pertaining to the maximum possibility of hydraulic fracturing at the upstream face of the dam remains near its crest.
- The hydraulic fracturing of the central core (i.e. core cracking) of a zoned earthen dam, if any, occurs in a very short time-span of 1-2 weeks after the complete reservoir rise-up, and is prominently located approximately at 2 m below the attained reservoir level.
- Cracking of central impervious core of a zoned earthen dam is not pronounced during the drawdown conditions, and simultaneous internal erosion of the core is also negligible during such transient reservoir operation.
- From the numerical finite element modeling, and applying the standard inequality criterion relating the effective minor principal stress and pore-water pressure, the path of crack propagation is effectively traced from the upstream to the downstream face of the central impervious core of a zoned earthen dam. The path or the direction of crack propagation path is identified based on the progressive development of stress-ratio, velocity gradient,

and maximum seepage velocity in the regions of evolving maximum strain concentration within the core of the dam.

7.3 MAJOR CONTRIBUTIONS FORM THE PRESENT STUDY

The following are the major contributions from the present study:

- Providing a simplistic modeling technique for simulating various possible mechanisms of drainage blanket clogging and their influence on the stress-flow-deformation response of earthen dams.
- Showcasing the importance and efficacy of drainage blankets, especially the inclined chimney drainage blankets, in establishing the continuous functioning and long-term safety of earthen dams, even after the same gets partially clogged.
- Highlighting the importance of the inclined chimney drains in ascertaining the performance of a zoned earthen dam with the presence of a cracked central impervious core.
- Based on numerical modeling and standard stress-PWP criterion, assessing the tentative locations of initiation of cracking and hydraulic fracturing of the shell and core of homogeneous and zoned earthen dams, respectively.
- Tracing and identifying the path of crack propagation through the central impervious core through recursive finite element analysis.

7.4 LIMITATIONS AND SCOPE OF FUTURE RESEARCH

Any research work performed has its own limitations and thus paves the way and scope for further research. Some of them, as applicable for the present study, are listed as follows:

- The phenomenon of hydraulic fracturing in dams during the dynamic conditions should be rigorously evaluated. Seismic activity is a major source of sudden and substantial rise in pore-water pressure that may result in local liquefaction, lateral spreading and hydraulic fracturing in the interior of an earthen dam, which needs ample attention.
- Simulation of particle migration through discrete element or discontinuum modeling, thereby simulating the piping and internal erosion within the earthen dam, should be conducted for both steady and transient reservoir operation.
- Detailed study about the processes of filtration, interface behavior, and time-dependent changes within the filter medium or drainage blanket in a dam should be investigated, as the combination of drainage blankets and filters play an important role in preventing particle migration.
- Earthen dams and embankments are mostly constructed with the locally available soils. Hence, the applicability of various local available sustainable resources (LASR) should be investigated for their suitability in such dams.
- The influence of different constitutive model, representing the behavior of material in the earthen dam, is to be studied on the stability and hydraulic response of the earthen dam through coupled stress-deformation-PWP analysis. Amalgamation of flow through porous media and suitable constitutive behavior of piping should be ventured or developed to estimate the nature of piping through a dam, which yet remains a relatively grey area. Such a model should incorporate particle migration through very narrow and tortuous channels guided by gravity and/or pressure gradients.
- Experimental investigations of piping through earthen dams with respect to its initiation and evolutions should be carried out along with the supportive numerical studies.

- Response of earthen and earthen/rockfill dams located on semi-impervious foundation beds with anisotropic permeability should be studied.
- Overtopping of earthen dams forms one major type of hydraulic failure due to uncontrollable rise in reservoir water due to flood or extreme rainfall, leading to formation of notch and subsequent breaching of the dam and wreaking havoc. Significant amount of studies should be carried out to understand breaching and overtopping of earthen dams.
- All the analysis conducted in the present research conform to plane-strain conditions, which is suitable for internal sections of the regular shaped earthen embankments and dams. For irregular shaped dams, complete three-dimensional static and seismic analyses would be the requirement to be fulfilled.

REFERENCES

1. Aberg, B. (1993). Washout of grains from filtered sand and gravel materials. ***Journal of Geotechnical Engineering, ASCE***, *119(1),* 36-53.

2. Aitchison, G. D. (1960). Discussion on Cole and Lewis (1960). ***Proceedings of Third Australia-New Zealand Conference on Soil Mechanics and Foundation Engineering***, Sydney, Australia, 260.

3. Aitchison, G. D., Ingles, O. G., and Wood, C. C. (1963). Post-construction deflocculation as a contributory factor in the failure of earth dams. ***Proceedings of Fourth Australia-New Zealand Conference on Soil Mechanics and Foundation Engineering***, Adelaide, Australia, 275-279.

4. Alamdari, N. Z., Banihashemi, M., and Mirghasemi, A. (2012). A numerical modeling of piping phenomenon in earth dams. ***International Journal of Civil, Environmental, Structural, Construction and Architectural Engineering****, 6(10),* 772-774.

5. Alonso, E. E., and Pinyol, N. M. (2016). Numerical analysis of rapid drawdown: Applications in real cases. ***Water Science and Engineering****, 9(3),* 175-183.

6. Annandale, G. W., Murthy, R., and Beckwith, G. (2004). Simulation of dam breach initiated by cracks and earth fissures in semi-arid and arid environments. ***Proceedings of the ASDSO Dam Safety Conference***, Phoenix, Arizona, USA.

7. Arulanandan, K., and Perry, E. B. (1983). Erosion in relation to filter design criteria in earth dams. *Journal of Geotechnical Engineering, ASCE***,** *109(5),* 682-698.

8. Arulanandan, K., Loganathan, P., and Krone, R. B. (1975). Pore and eroding fluid influences on surface erosion of soil. ***Journal of Geotechnical Engineering Division, ASCE****, 101(1),* 51-66.

9. Aubeny, C. P., and Lytton, R. L. (2004). Shallow slides in compacted high plasticity clay slopes. ***Journal of Geotechnical and Geoenvironmental Engineering, ASCE***, *130(7),* 717-727.

10. Barani, O. R., and Khoei, A. R. (2014). 3D modeling of cohesive crack growth in partially saturated porous media: a parametric study. ***Engineering Fracture Mechanics***, *124-125,* 272-286.

11. Bass, J. M. (1986). Avoiding failure of leachate collection systems at hazardous waste landfills. ***Proceedings of the Seventh Annual Madison Waste Conference Municipal and Industrial Waste***, Madison, USA.

12. Belytschko. T., and Black, T. (1999). Elastic crack growth in finite elements with minimal remeshing. ***International Journal for Numerical Methods in Engineering***, *45(5),* 601-620.

13. Berilgen, M. M. (2007). Investigation of stability of slopes under drawdown conditions. ***Computers and Geotechnics**, 34(2),* 81-91.

14. Bertram, G. B. (1940). An experimental investigation of protective filters. ***Publications of the Graduate School of Engineering**,* Soil Mechanics Series, Harvard University, 267, 1-21.

15. Bjerrum, L., Nash, J. K., Kennard, R. M., and Gibson, R. E. (1972). Hydraulic fracturing in field permeability testing. ***Geotechnique**, 22(2),* 319-332.

16. Bligh, W. G. (1910). Dams, barrages and weirs on porous foundation. ***Engineering News***, *64(26),* 708-710.

17. Bligh, W. G. (1911a). Reply to sheet piles as a means of decreasing permeability of porous foundations. ***Engineering News***, *65(4),* 109-110.

18. Bligh, W. G. (1911b). Weirs on porous foundations and with pervious floor. ***Engineering News***, *65(15),* 444-445.

19. Bligh, W. G. (1913). Lessons from the failure of a weir and sluices on porous foundations. ***Engineering News**, 69(6),* 266-270.

20. Bonala, M. V. S., and Reddi, L. N. (1998). Physicochemical and biological mechanisms of soil clogging: An overview. ***ASCE Geotechnical Special Publication**, 78,* 43-68.

21. Bonelli, S., and Benahmed, N. (2010). Piping flow erosion in water retaining structures: Inferring erosion rates from hole erosion tests and quantifying the failure time. ***Proceedings of the 8th ICOLD European Club Symposium on Dam Safety-Sustainability in a Changing Environment**,* ATCOLD Austrian National Committee on Large Dams, Innsbruck, Austria, *6*, 467-472.

22. Brinkgreve, R. B. J., Kumarswamy, S., and Swolfs, W.M. (2015). **Plaxis 2015 Reference Manual**. Plaxis BV, Delft, Netherlands.

23. Casagrande, A. (1950). **Notes on the Design of Earth Dams**. Harvard University, London.

24. Casagrande, A., and Covarrubias, S. W. (1970). Cracking of earth· and rockfill dams: Tension Zones in Embankment caused by conduits and cut-off walls. ***Contract Report No. S-70-7***, U. S. Army Engineers Waterways Experiment Station, Vicksburg, Mississippi.

25. Cedergren, H. R. (1994). America's pavements: World's longest bathtubs. ***Civil Engineering, ASCE**, 64(9)*, 56-58.

26. Chadwick, W. L., Cassagrande, A., Coombs, H. A., Dowd, M. W., Fucik, E. M., Higginson, R. K., Leps, T. M., Peck, R. B., Seed, H. B., and Jansen, R. B. (1976). Failure of Teton Dam. ***Report to U.S. Department of the Interior and the State of Idaho on Failure of Teton dam*** by the Independent panel to review cause of Teton dam failure, U.S. Bureau of Reclamation, Denver, Colorado, USA.

27. Chang, D. S., and Zhang, L. M. (2012). Critical hydraulic gradients of internal erosion under complex stress states. ***Journal of Geotechnical and Geoenvironmental Engineering, ASCE**, 139(9),* 1454-1467.

28. Chang, D.S., and Zhang, L.M. (2010). Simulation of the erosion process of landslide dams due to overtopping considering variations in soil erodibility along depth. ***Natural Hazards Earth System Science*, *10,*** 933-946.

29. Chen, W.F., and Zhang, H. (1991). **Structural Plasticity: Theory, Problems, and CAE Software**. Springer-Verlag, New York, USA.

30. Cheng, K., Liu, H., and Zhou, Y. (2006). Studies on the design of sand/gravel anti-filter layer. ***Journal of Shihezi University (Natural Science)**, 24(2),* 241-244.

31. Childs, E. C., and Collis-George, N. (1950). The permeability of porous materials. ***Proceedings of the Royal Society of London A**, 201*, 392-405.

32. Cho, S. E., and Lee, S. R. (2001). Instability of unsaturated soil slopes due to infiltration. ***Computers and Geotechnics***, *28(3),* 185-208.

33. Cividini, A. and Gioda, G. (2004). Finite-element approach to the erosion and transport of fine particles in granular soils. ***International Journal of Geomechanics, ASCE**, 191(4),* 1532-3641.

34. Clibborn, J., and Bresford, J. S. (1902). **Experiments on the Passage of Water through Sand**. Government of India, Central Printing Office, New Delhi.

35. Cooling, L., and Marsland, A. (2011). Soil mechanics studies of failures in the sea defence banks of Essex and Kent. ***Proceedings of the Conference on the North Sea Floods of 31 January/1 February 1953***, London, UK, 58-73.

36. Covarrubias, S. W. (1969). Cracking of earth and rockfill dams: A theoretical investigation by means of the finite element method. ***Contract Report S-69-5***, U. S, Army Engineers Waterways Experiment Station, Vicksburg, Mississippi.

37. Covarrubias, S. W. (1971). Cracking of earth and rockfill dams. Comparison of observed and theoretical tensile strains in the crests of two earth and rockfill dams. ***Contract Report S-71-11***, U. S, Army Engineers Waterways Experiment Station, Vicksburg, Mississippi.

38. Dakshanamurthy, V., Fredlund, D. G, and Rahardjo, H. (1984). Coupled three-dimensional consolidation theory of unsaturated porous media. ***Proceedings of the Fifth International Conference on Expansive Soils**,* Adelaide, Australia*,* 99 -103.

39. Das Neves, E. M. (1989). Analysis of crack erosion in dam cores. The crack erosion test. ***De Mello Volume: A Tribute to Prof. Victor de Mello***, Ed. Edgard Blucher Ltda, Sao Paulo, Brazil, 284-298.

40. Das, K., Saikia, M. D., and Kalita, U. C. (2017). Modelling of embankment breaching with special reference to Barak Valley, Assam. ***Indian Geotechnical Conference, GeoNEst 2017****,* Guwahati, India*,* 1-4.

41. Dascal, O. (1984). Peculiar behavior of the Manicouagan 3 Dam's core. ***Proceedings of the First International Conference on Case Histories in Geotechnical Engineering****,* Missouri-Rolla, USA, 561-569.

42. Decker, R. S., and Dunnigan, L. P. (1977). Development and use of the soil conservation service dispersion test. ***ASTM Special Technical Publication***, *623,* 94-109.

43. Fell, R., Wan, C. F., Cyganiewicz, J., and Foster, M. (2003). Time for development of internal erosion and piping in embankment dams. ***Journal of Geotechnical and Geoenvironmental Engineering, ASCE***, *129(4),* 307-314.

44. Fenton, G.A., and Griffiths, D.V. (1997). Extreme hydraulic gradient statistics in a stochastic earth dam. ***Journal of Geotechnical and Geoenvironmental Engineering, ASCE****, 123(11),* 995-1000.

45. Forsythe, P. (1977). Experiences in identification and treatment of dispersive clays in Mississippi dams. ***ASTM Special Technical Publication****, 623*, 135-155.

46. Foster, M., Fell, R., and Spannagle, M. (2000a). The statistics of embankment dam failures and accidents: Part 1. ***Canadian Geotechnical Journal****, 37(5),* 1000-1024.

47. Foster, M., Fell, R., and Spannagle, M. (2000b). The statistics of embankment dam failures and accidents: Part 2. ***Canadian Geotechnical Journal****, 37(5),* 1025-1061.

48. Franca, M. J., Gezero, L., Ferreira, R. M. L., Amaral, S. and Montenegro, H. D. B. (2008). The failure of the Fonte Santa mine tailing dam (Northeast Portugal). ***Proceedings and Monographs in Engineering Water and Earth Sciences***, 1153-1160.

49. Franco, G. E., and Bagtzoglou, A. C. (2002). An elastic contact mechanics fracture flow model. ***Proceedings of 15th ASCE Engineering Mechanics Conference, ASCE***, New York, USA, 1-7.

50. Fread, D. L. (1980). Prediction of flood inundation from breached dams due to earthquakes. ***Tsunamis and Flood Wave Hazard Definition and Design Consideration***, Subcommittee 8 – Tsunamis and Floodwave Interagency Committee on Sismic Safety in Construction, *5*, 1-39.

51. Fredlund, D. G. and Xing, A. (1994). Equations for the soil-water characteristic curve. ***Canadian Geotechnical Journal****, 31,* 521-532.

52. Fredlund, D. G., and Morgenstern, N. R. (1976). Constitutive relations for volume change in unsaturated soils. ***Canadian Geotechnical Journal****, 13,* 261-276.

53. Fredlund, D. G., and Morgenstern, N. R. (1977). Stress state variables for unsaturated soils. ***Journal of the Geotechnical Engineering Division, ASCE**, 103(5),* 447-464.

54. Fredlund, D. G., and Rahardjo, H. (1993). **Soil Mechanics for Unsaturated Soils**. Wiley and Sons Inc, New York, USA.

55. Gao, Y., Zhu, D., Zhang, F., Lei, G. H., and Qin, H. (2014). Stability analysis of three-dimensional slopes under water drawdown conditions. ***Canadian Geotechnical Journal,** 51(11),* 1355-1364.

56. Geostudio Seep/W (2012). **Engineering Book for Seepage Modeling with Seep/W**, Geo-Slope International Ltd., Calgary, Alberta, Canada.

57. Geostudio Sigma/W (2012). **Engineering Book for Stress-Deformation Modeling with Sigma/W**, Geo-Slope International Ltd., Calgary, Alberta, Canada.

58. Geostudio Slope/W (2012). **Engineering Book for Stability Modeling with Slope/W**, Geo-Slope International Ltd., Calgary, Alberta, Canada.

59. Gordeliy, E., and Peirce, A. (2015). Enrichment strategies and convergence properties of the XFEM for hydraulic fracture Problems. ***Computer Methods in Applied Mechanics and Engineering***, *283,* 474-502.

60. Grass, A. J. (1970). Initial instability of fine bed sand. ***Journal of Hydraulics Division, ASCE***, *96(3),* 619–632.

61. Grass, L. B., Willardson, L. S., and Lemert, R. A. (1979). Soil sediment deposits in subsurface drains. ***Transactions of ASAE,** 22(5),* 1054-1057.

62. Green, R. E., and Corey, J. C. (1971). Calculation of hydraulic conductivity: A further evaluation of some predictive methods. ***Soil Science Society of America Proceedings**, 35,* 3-8.

63. Griffith W. M. (1913). The stability of weir foundations on sand and soil subject to hydrostatic pressure. ***Minutes of the Proceedings of the Institute of Civil Engineers,** 197(3),* 221-232.

64. Haimson, B. (1968). Hydraulic fracturing in porous and non-porous rock and its potential for determining in-situ stresses at great depths. ***Doctoral Thesis***, University of Minnesota, USA.

65. Hill, R. (1950). **The Mathematical Theory of Plasticity**. Oxford University Press, Oxford, UK.

66. Hoffmans, G., and Van Rijn, L. (2018). Hydraulic approach for predicting piping in dikes. ***Journal of Hydraulic Research**, 56(2),* 268-281.

67. Hopkins, T. C., Allen D. L., Deen R. C., and Grayson, C.G. (1988). Slope Maintenance and slide restoration. ***Report No. FHWA-RT- 88-040***, FHWA Office of Implementation, Virginia, USA.

68. International Commission on Large Dams (2012). **Internal Erosion of Existing Dams, Levees, and Dikes, and their Foundations.** ICOLD, Paris, France, Bulletin Preprint-164

69. Indraratna, B. and Raut, A. K. (2006). Enhanced Criterion for Base Soil Retention in Embankment Dam Filters. ***Journal of Geotechnical and Geoenvironmental Engineering, ASCE**, 132(12),* 1621-1627.

70. Indraratna, B., and Radampola, S. (2002). Analysis of critical hydraulic gradient for particle movement in filtration. ***Journal of Geotechnical and Geoenvironmental Engineering, ASCE**, 128(4),* 347-350.

71. Indraratna, B., and Vafai, F. (1997). Analytical model for particle migration within base soil-filter system. ***Journal of Geotechnical and Geoenvironmental Engineering*, *ASCE**, 123(2),* 100-109.

72. Indraratna, B., Raut, A. K., and Khabbaz, H. (2007). Constriction-based retention criterion for granular filter design. ***Journal of Geotechnical and Geoenvironmental Engineering, ASCE**, 133(3),* 266–276.

73. Indraratna, B., Vafai, F., and Dilema, E. L. G. (1996). An experimental study of filtration of a lateritic clay slurry by sand filters. ***Proceedings Institute of Civil Engineers, Geotechnical Engineering**,* London, England*, 119(2),* 75-83.

74. IS 12169 (1987 Reaffirmed 2020). **Criteria for Design of Small Embankment Dams**, Bureau of Indian Standards, New Delhi, India.

75. Jantzer, I., and Knutsson, S. (2007). Seepage and critical hydraulic gradients in tailings dams and natural formations. ***Proceedings of 2nd International Conference on Porous Media and its Applications in Science and Engineering***, Hawaii, USA, 1-11.

76. Jaworski, G. W, Duncan, J. M., and Seed, H. B. (1981). Laboratory study of hydraulic fracturing. ***Journal of Geotechnical Engineering Division, ASCE**, 107(6),* 713-732.

77. Jimenez-Rodriguez, R., Sitar, N. and Chacon, J. (2006). System reliability approach to rock slope stability. ***International Journal of Rock Mechanics and Mining Sciences***, *43(6),* 847-859.

78. Jones, J. A. A. (1981). **The Nature of Soil Piping: A Review of Research**, British Geomorphological Research Group (BGRG) Research Monograph No. 3. Geo Books, Norwich.

79. Kakuturu, S. P. (2003). Modeling and experimental investigations of self-healing or progressive erosion of earth dams. ***Ph.D. Thesis***, Kansas State University, USA.

80. Kakuturu, S. P., and Reddi, L. N. (2006). Evaluation of the Parameters influencing Self-Healing in Earth Dams. ***Journal of Geotechnical and Geoenvironmental Engineering, ASCE**, 132(7),* 879-889.

81. Kakuturu, S. P., and Reddi, L. N. (2006). Mechanistic model for self-healing of core cracks in earth dams. ***Journal of Geotechnical and Geoenvironmental Engineering, ASCE**, 132(7),* 890-901.

82. Kapadia, V. P. (2013). Addressing failure of canal embankments in swelling soils: A case study of Sardar Sarovar project. ***Proceedings of the Indian Geotechnical Conference GANGA 2013***, Roorkee, 1-18.

83. Kennard, R. M. (1970). The measurement of soil permeability in-situ by constant head test. ***Doctoral Thesis***, University of London, UK.

84. Kenney, T. C., Chahal, R., Chiu, E., Ofoegbu, G. I., Omange, G. N., and Ume, C. A. (1985). Controlling constriction sizes of granular filters. ***Canadian Geotechnical Journal**, 22,* 32-43.

85. Khalid, S., Singh, B., Nayak, G. C., and Jain, O. P. (1990). Nonlinear analysis of concrete face rockfill dam. ***Journal of Geotechnical and Geoenvironmental Engineering, ASCE**, 116(5),* 822-837.

86. Kim, H., Daliri, F., Simms, P. H., and Sivathayalan, S. (2011). The influence of desiccation and over-consolidation on monotonic and cyclic shear response of thickened gold tailings. ***Proceedings of the 64th Pan-American Canadian Geotechnical Conference**,* Toronto, Canada, 1-8.

87. Kjaernsli, B., and Torblaa, I. (1968). Leakage through horizontal cracks in the core of Hyttejuvet Dam. ***Norwegian Geotechnical Institute Publication,** 80,* 39-47.

88. Koerner, R. M., and Koerner, G. R. (1991). Landfill leachate clogging of geotextile (and soil) filters. ***EPA Project Summary EPA/600/S2–91/025***, US Environmental Protection Agency, Risk Reduction Engineering Laboratory, Cincinnati, Ohio.

89. Kuhn, J. A., and Zornberg, J. G. (2006). Field suction and effect of cracking in highly plastic clay. ***Report No. FHWA/TX-07/0-5202-2***, Texas Department of Transportation, Austin, USA.

90. Kulhawy, F. H., and Gurtowsky, T. M. (1976). Load transfer and hydraulic fracturing in zoned dams. ***Journal of the Geotechnical Division, ASCE**, 102(9),* 963-974.

91. Lane, E. W. (1934). Security from under-seepage masonry dams on earth foundations. ***Transactions of the ASCE***, *60(7),* 929-966.

92. Lebreton, A. (1964). Les ruptures et accidents graves de barrages. ***La Houille Blanche,*** 529-544.

93. Lee, K. L., and Shen, C. K. (1969). Horizontal movements related to subsidence. ***Journal of the Soil Mechanics and Foundations Division, ASCE****, 95(1),* 139-151.

94. Leonards, G. A., and Davidson, L. W. (1984). Reconsideration of failure initiating mechanism for Teton Dam**.** ***Proceedings of the First International Conference on Case Histories in Geotechnical Engineering****,* Missouri-Rolla, USA, 1103-1113.

95. Leonards, G. A., Haung, A. B., and Ramos, J. (1991). Piping and erosion test at Conner Run Dam. ***Journal of Geotechnical Engineering, ASCE****, 117(1),* 108-117.

96. Li, A., Merifield, R., and Lyamin, A. (2008). Stability charts for rock slopes based on the Hoek-Brown failure criterion. ***International Journal of Rock Mechanics and Mining Sciences***, *45(5),* 689-700.

97. Li, D. Y., Yin, K. L., and Leo, C. (2010). Analysis of Baishuihe landslide influenced by the effects of reservoir water and rainfall. ***Environmental Earth Sciences****, 60(4),* 667-687.

98. Li, Q., Zhang, B. Y., Yu, Y. Z., and Wang, J. (2007). Numerical simulation of the process of hydraulic fracturing in earth and rockfill dams. ***Chinese Journal of Geotechnical Engineering***, *29(2),* 212-217.

99. Liu, F., Gordon, P., Meier, H., and Valiveti, D. (2017). A stabilized extended finite element framework for hydraulic fracturing simulations. ***International Journal for Numerical and Analytical Methods in Geomechanics***, *41(5),* 654-681.

100. Lo, K. Y., and Kaniaru, K. (1990). Hydraulic Fracture in earth and rockfill dams. ***Canadian Geotechnical Journal****, 27(4),* 496-506.

101. Locke, M., Indraratna, B., and Adikari, G. (2001). Time-dependent particle transport through granular filters. ***Journal of Geotechnical and Geoenvironmental Engineering, ASCE***, *127(6),* 521-529.

102. Lofquist, B. (1951). Earth pressure in a thin impervious core. ***Transactions of the 4th International Congress on Large Dams****,* New Delhi, India*, 1,* 99-109.

103. Lofquist, B. (1957). Discussion on cracking in earth dams. ***Proceedings of the 4th International Conference of Soil Mechanics and Foundation Engineering***, London UK, 261-262.

104. Lorenz, F. M. (2003). The protection of water facilities under international law. ***Report No. SC-2003/WS/40***, IHP-6, Technical Documents in Hydrology, Research Project sponsored by the International Water Academy, Oslo, Norway.

105. Louis, C. (1969). A study of groundwater flow in jointed rock and its influence on the stability of rock masses. ***Rock Mechanics Research Report No. 10***, Imperial College of Science and Technology, London, England.

106. Low, B. (2007). Reliability analysis of rock slopes involving correlated non-normals. ***International Journal of Rock Mechanics and Mining Sciences***, *44(6),* 922-935.

107. Luo, Y. L. (2012). A continuum fluid-particle coupled piping model based on solute transport. ***International Journal of Civil Engineering, Transaction B: Geotechnical Engineering***, *11(1),* 38-44.

108. Lytton, R. L., Picornell, M., Garcia, C., and Huang C. C. (1987). Detection and sizing of surface cracks in expansive soil deposits. ***Report No. FHWA/TX-87/187-13***, Texas Transportation Institute, College Station, USA.

109. Macchione, F., and Sirangelo, B. (1988). Study of earth dam erosion due to overtopping. ***Hydrology of Disasters***, ***Proceedings of the Technical Conference***, Geneva, 1-8.

110. Marshall, A. F., and Workman, J. P. (1977). Identification of dispersive clays in the Texas Gulf Coast area. ***ASTM Special Technical Publication***, *623,* 274-286.

111. Massarsch, K. R., and Broms, B. B. (1977). Fracturing of Soil Caused by Pile Driving in Clay. ***Proceedings of the 9th International Conference on Soil Mechanics and Foundation Engineering***, Tokyo, Japan, *1(40),* 197-200.

112. McCook, D. K. (2004). A comprehensive discussion of piping and internal erosion failure mechanisms. ***Proceedings the 2004 Annual Dam Safety Officials, ASDSO***, Phoenix, Arizona, 1-6.

113. Mesri, G., and Ali, S. (1988). Discussion on Hydraulic fracturing in embankment dams. *Journal of Geotechnical Engineering, ASCE, 114(6),* 742-746.

114. Metcalf and Eddy, Inc. (191). **Wastewater Engineering: Treatment, Disposal, Reuse**. 3rd Edition, McGraw-Hill, New York.

115. Mhach, H.K. (1991). An experimental study of hydraulic fracture and erosion. ***Doctoral Thesis***, City University London.

116. Moes, N., Dolbow, J., and Belytschko, T. (1999). A finite element method for crack growth without remeshing. ***International Journal for Numerical Methods in Engineering***, *46(1),* 131-150.

117. Moffat, R. A., and Fannin, R. J. (2006). A large permeameter for study of internal stability in cohesionless soils. *Geotechnical Testing Journal, ASTM*, *29(4),* 273-279.

118. Morgenstern, N. R., and Vaughan, P. R. (1963). Some observations on allowable grouting pressures. ***Grouts and Drilling Muds in Engineering Practice***, Butterworths, London, 36-43.

119. Morgenstern, N.R., and Price, V.E. (1965). The analysis of the stability of general slip surfaces. *Geotechnique, 15(1),* 79-93.

120. Mufute, N. L., Senzanje, A., and Kaseke, E. (2008). The development of a risk of failure evaluation tool for small dams in Mzingwane catchment, Zimbabwe. ***Physics and Chemistry of the Earth A/B/C**, 33(8-13)*, 926-933.

121. Narita, K. (2000). **Design and Construction of Embankment Dams**. Department of Civil Engineering, Aichi Institute of Technology, Japan.

122. Nawari, O., Hartmann, R., and Lackner, R. (1997). Stability analysis of rock slopes with the direct sliding blocks method. ***International Journal of Rock Mechanics and Mining Sciences***, *34(3-4),* 220e1-220e8.

123. Ng, A. K. L., and Small, J. C. (1999). A case study of hydraulic fracturing using finite element methods. *Canadian Geotechnical Journal, 36(5),* 861-875.

124. Nobari, E. S., Lee, K. L., and Duncan, J. M. (1973). Hydraulic fracturing in zoned earth and rock fill dams. ***Contract Report No. S-73-2***, US Army Engineers Waterways Experiment Station, Vicksburg, Mississippi, USA.

125. Ohne, Y., and Narita, K. (1977). Discussion on cracking and hydraulic fracturing in fill-type dams. ***Proceedings of the 9th International Conference on Soil Mechanics and Foundation Engineering**,* Special Session 8 - Deformation of Earth-rockfill Dams, Tokyo, 60–63.

126. Okeke, A. C. U., and Wang, F. (2016). Critical hydraulic gradients for seepage induced failure of landslide dams. ***Geoenvironmental Disasters**, 3(9),* 1-22.

127. Paton, J. (1956). The Glen Shira Hydroelectric Project. ***Proceedings of the Institution of Civil Engineers,*** Sheffield, United Kingdom, 593-618.

128. Paton, J., and Semple, N. G. (1961). Investigation of the stability of an earth dam subjected to rapid drawdown including details of pore pressure recorded during a controlled drawdown test. ***Pore Pressure and Suction in Soils***. Butterworths, London, 85-90.

129. Peck, R. (1990). Interface between the core and downstream filter. ***Proceedings of the H. Bolton Seed Memorial Symposium**,* Vancouver, Canada, 237–251.

130. Perzlmaier, S., Muckenthaler, P., and Koelewijn, A. R. (2007). Hydraulic criteria for internal erosion in cohesionless soil. Assessment of risk of internal erosion of water retaining structures: dams, dykes and levees. ***Intermediate Report of the European Working Group of ICOLD***, Technical University, Munich, 30–44.

131. Pinyol, N. M., Alonso, E. E., and Olivella, S. (2008). Rapid drawdown in slopes and earthen dams. ***Water Resources Research**, 44(5)*, W00D03, 1-22.

132. Quanyi, X., Liu, J., Han, B., Li, H., Li, Y., and Li, X. (2018). Critical hydraulic gradient of internal erosion at the soil–structure interface. ***Processes***, *6(92)*, 1-15.

133. Reboul, N., Vincens, E., and Cambou, B. (2010). A computational procedure to access the distribution of constriction sizes for an assembly of spheres. ***Computers and Geotechnics**, 37(1),* 195-206.

134. Reddi, L. N., Xiao, M., Hajra, M. G., and Lee, I. M. (2000). Permeability reduction of soil filters due to physical clogging. ***Journal of Geotechnical and Geoenvironmental Engineering, ASCE**, 126(3),* 236-246.

135. Richards, K. S., and Reddy, K. R. (2007). Critical appraisal of piping phenomena in earth dams. ***Bulletin of Engineering Geology and Environment***, *66*, 381-402.

136. Richards, L.A. (1931). Capillary conduction of liquids through porous mediums. ***Journal of Applied Physics**, 1(5),* 318-333.

137. Ritchie, J. A. (1963). Earthwork tunneling and the application of soil testing procedure. ***Journal of the Soil Conservation Service of New South Wales***, *21,* 81-89.

138. Ruggeri, G. (2004). Uplift Pressures under Concrete dams: Chapter 5 - Drain Maintenance and Cleaning. ***Final Report of the Working Group***, ICOLD European Club.

139. Rutenback, T., and Day, G. (1999). An evaluation of water jetting for Bureau of Reclamation use in cleaning concrete dam foundation drains. ***Report No. DSO-98-16***. Materials Engineering and Research Laboratory. United States Department of Interior Bureau of Reclamation Dam Safety Office.

140. Sail, Y., Marot, D., Sibille, L., and Alexis, A. (2011). Suffusion tests on cohesionless granular matter. *European Journal of Environmental and Civil Engineering, 15(5),* 799-817.

141. Savvidou, C. (1981). Fracture and Permeability Changes in Soils. ***M Phil. Dissertation***, Cambridge University, UK

142. Schmertmann, J. H. (2000). The no-filter factor of safety against piping through sands. ***ASCE Geotechnical Special Publication, Judgment and Innovation,*** *111,* 65-132.

143. Schuler, U. (1996). Scattering of the composition of soils: An aspect for the stability of granular filters. ***Proceedings of GeoFilters '96***, Montreal, Canada, 21-34.

144. Secchi, S., and Schrefler, B. A. (2012). A method for 3-D hydraulic fracturing simulation. ***International Journal of Fracture***, *178(1-2),* 245-258.

145. Seed, H. B., and Duncan, J. M. (1981). The Teton Dam failure-A retrospective review. ***Proceedings of the 10th International Conference on Soil Mechanics and Foundation Engineering***, Stockholm, Sweden*, 4,* 214-238.

146. Segerlind, L. J. (1984). **Applied Finite Element Analysis**. Wiley and Sons, New York, USA.

147. Sellmeijer, J.B. (1988). On the mechanism of piping under impervious structures. ***Doctoral Dissertation.*** TU Delft, Netherlands.

148. Sellmeijer, J. B., and Koenders, M. A. (1991). A Mathematical model for piping. ***Applied Mathematical Modelling***, *15(6),* 646-651.

149. Sellmeijer, J.B. (2006). Numerical computation of seepage erosion below dams (piping). ***Proceedings Third International Conference on Scour and Erosion,*** Gouda, Netherlands, 596-601.

150. Sharif, Y. A., Elkholy, M., Chaudhry, M. H., and Imran, J. (2015). Experimental Study on the Piping Erosion Process in Earthen Embankments, ***Journal of Hydraulic Engineering, ASCE***, *141(7),* 04015012-1-9.

151. Sherard, J. L. (1973). Embankment dam cracking. ***Embankment Dam Engineering. Casagrande Volume***, Eds. R. C. Hirschfeld and S. J. Poulos, John Wiley, New York, 324-328.

152. Sherard, J. L. (1979). Sinkholes in dams of coarse, broadly graded soils. ***Proceedings of 13th ICOLD Congress,*** International Commission on Large Dams, India, *2,* 25-35.

153. Sherard, J. L., Woodward, R. J., Gizienski, S. F., and Clevenger, W. A. (1963). **Earth and Earth-Rock Dams, Engineering Problems of Design and Construction**. Wiley, New York.

154. Sherard, J., Dunnigan, L., and Talbot, J. (1984). Basic properties of sand and gravel filters. ***Journal of Geotechnical Engineering*, ASCE**, *110(6),* 684-700.

155. Sherard, J. L. (1991). Cracking and hydraulic fracturing in embankment dams. ***US Army Corps of Engineers***, 301-327.

156. Shire T., and O'Sullivan, C. (2017). A network model to assess base-filter combinations. ***Computers and Geotechnics***, *84,* 117-128.

157. Shuckrow, A. J., Pajak A. P., and Osheka J. W. (1981). Concentration technologies for hazardous aqueous waste treatment. ***Contract Report 68-03-2766***, United States Environmental Protection Agency, Cincinnati, Ohio.

158. Shukla, S. K., Khandelwal, S., Verma, V., and Sivakugan, N. (2009). Effect of surcharge on the stability of anchored rock slope with water filled tension crack under seismic loading condition. ***Geotechnical and Geological Engineering***, *27(4),* 529-538.

159. Silva, D. J. F. (2015). Clogging of drains and its influence on the stability of concrete dams. ***Proceedings of the 49th US Rock Mechanics/Geomechanics Symposium***, American Rock Mechanics Association, San Francisco, California, 15-140.

160. Silveira, A. (1965). An analysis of the problem of washing through in protective filters. ***Proceedings of the 6th International Conference of Soil Mechanics and Foundation Engineering****,* Montreal, Canada*, 2,* 551-555.

161. Sjah, J., and Vincens, E. (2013). Determination of the constriction size distribution of granular filters by filtration tests. ***International Journal for Numerical and Analytical Methods in Geomechanics****, 37(10),* 1231-1246.

162. Skempton, A. W., and Brogan, J. M. (1994). Experiments on piping in sandy gravels. ***Geotechnique****, 44(3),* 449-460.

163. Smith, I.M., and Griffiths, D.V. (2014). **Programming the Finite Element Method**. 5th edition, John Wiley and Sons, Sussex, UK.

164. Song, K., Yan, E., Zhang, G., Lu, S., and Yi, Q. (2015). Effect of hydraulic properties of soil and fluctuation velocity of reservoir water on landslide stability. ***Environmental Earth Sciences****, 74(6),* 5319-5329.

165. Talbot, J. R., and Deal, E. (1993). Rehabilitation of cracked embankment dams. ***Geotechnical Practice in Dam Rehabilitation, Geotechnical Special Publication****, 35,* 267-283.

166. Tang, C. A., Liang, Z. Z., Zhang, Y. B., Chang, X., Tao, X., Wang, D. G., Zhang, J. X., Liu, J. S., Zhu, W. C., and Elsworth, D. (2008). Fracture spacing in layered materials: a new explanation based on two-dimensional failure process modeling. ***American Journal of Science***, *308(1),* 49-72.

167. Taylor, H. F., O'Sullivan, C., and Sim, W. W. (2015). A new method to identify void constrictions in micro-CT images of sand. ***Computers and Geotechnics****, 69,* 279–290.

168. Terzaghi, K. (1925). **Erdbaumechanik auf Bodenphysikalischer Grundlage**. Deuticke, Leipzig, Germany.

169. Terzaghi, K. (1929). Effect of minor geologic details on the safety of dams. ***Technical Publication 215,*** Geology and Engineering for Dams and Reservoirs. American Institute of Mining and Metallurgical Engineering, New York, 31-46.

170. Terzaghi, K. (1939). Soil mechanics: A new chapter in engineering science. The 45th James Forrest Lecture. ***Journal of the Institution of Civil Engineers****, 12(7),* 106–142.

171. Terzaghi, K. (1943). **Theoretical Soil Mechanics**. John Wiley and Sons, New York, USA.

172. Terzaghi, K., Peck, R. B., and Mesri, G. (1996). **Soil Mechanics in Engineering Practice**. 3rd Edition. John Wiley and Sons, Canada.

173. Thandaveswara, P. B. (2012). History of dam failures. ***NPTEL Lecture Material***, IIT Madras, Chennai, India.

174. Tomlinson, S., and Vaid, Y. (2000). Seepage forces and confining pressure effects on piping erosion. ***Canadian Geotechnical Journal**, 37(1),* 1-13.

175. United States Army Corps of Engineers. (2011). Summary of Actual 2010 Regulaton: Missouri River Basin. ***Missouri River Basin Water Management Division***. U.S. Army Corps of Engineers, Northwestern Division, Omaha, Nebraska.

176. United States Bureau of Reclamation (1987). **Design of Small Dams**, A Water Resources Technical Publication, USA.

177. United States Bureau of Reclamation (2014). Design Standards No. 13 Embankment Dams - Chapter 8: Seepage, ***Report No. DS-13(8)-4.1: Phase 4 (Final)***, USBR, USA.

178. Van Beek, V. M., Bezuijen, A., and Zwancnburg, C. (2010). Piping: Centrifuge effects on scaling effects and levee stability. ***Proceedings of the 7th International Conference on Physical Modelling in Geotechnics,*** Zurich, Switzerland, 183-189.

179. Van Beek, V. M. (2015). Backward erosion piping, initiation and progression. ***Doctoral Thesis***. Delft University of Technology, Delft, Netherlands.

180. van Genuchten, M. Th. (1980). A closed-form equation for predicting the hydraulic conductivity of unsaturated soils. ***Soil Science Society of America Journal**, 44,* 892-898.

181. Vaughan, P. R. (1976). Cracking of embankment dam cores and the design of filters for their protection. ***Boletin de la Sociedad Espanola de Mecanica del Suelo Y Cimentaciones***, Madrid Leecture, Spain, 23-34.

182. Vaughan, P. R. (1978). Design of filters for the protection of cracked dam cores against internal erosion. ***Proceedings of the ASCE Convention and Exposition**,* Chicago, USA, 1-22.

183. Vaughan, P. R., and Soares, H. F. (1982). Design of filters for clay cores of dams. ***Journal of Geotechnical Engineering, ASCE**, 108(1*), 17-31.

184. Vestad, H. (1976). Viddalsvatn dam: A history of leakages and investigations. ***Proceedings of the 12th International Congress on Large Dams**, ICOLD.* Mexico*, 2,* 369-390.

185. Vick, S. (1996). Failure of the Omai Tailings dam. ***Geotechnical News***, *14(3)*, 34-40.

186. Viratjandr, C., and Michalowski, R.L. (2006). Limit analysis of submerged slopes subjected to water drawdown. ***Canadian Geotechnical Journal**, 43(8),* 804-812.

187. von Thun, J. L. (1985). San Luis dam upstream slide. ***Proceedings of the 11th International Conference on Soil Mechanics and Foundation Engineering**,* San Francisco, USA, 2593-2598.

188. Wang, J. J., Zhang, H. P., Zhang, L., and Liang, Y. (2012). Experimental study on heterogeneous slope responses to drawdown. ***Engineering Geology**, 147-148,* 52-56.

189. Wang, J. J., Zhu, J. G., Mroueh, H., and Chiu, C. F. (2016). Hydraulic fracturing of rock-fill dam. ***International Journal of Multiphysics***, *1(2),* 199-219.

190. Wang, Z., Zhao. B., and Royal A. C. D. (2017). Investigation of erosion of cement-bentonite via piping. ***Advances in Materials Science and Engineering**, 17(1),* 1-8.

191. Wersocki, W. S. (2014). Problem of clogging in drainage systems in the examples of the Zur and Podgaje dams. ***Archives of Hydro-Engineering and Environmental Mechanics***, *61(3–4)*, 183–192.

192. Wilson, G. V., and Fox, G. A. (2013). Pore-water pressures associated with clogging of soil pipes: Numerical analysis of laboratory experiments. ***Soil Science Society of America Journal**, 77(4),* 1168–1181.

193. Witt, K. (1993). Reliability study of granular filters. ***Filters in Geotechnical and Hydraulic Engineering. Proceedings of the 1st International Conference on Geo-Filters***, Karlsruhe, Germany, 35-42.

194. Worman, A., and Olafsdottir, R. (1992). Erosion in a granular medium interface. ***Journal of Hydraulic Research**, 30(55),* 639-655.

195. Xu, T., and Zhang, L. (2013). Simulation of piping in earth dams due to concentrated leak erosion. ***Proceedings of the Geo-Congress 2013, ASCE**,* 1091-1099.

196. Yan, Z. L., Wang, J. J., and Chai, H. J. (2010). Influence of water level fluctuation on phreatic line in silty soil model slope. ***Engineering Geology**, 113(1-4),* 90-98.

197. Yang, X. L., and Zou, J. F. (2006). Stability factors for rock slopes subjected to pore water pressure based on the Hoek-Brown failure criterion. ***International Journal of Rock Mechanics and Mining Sciences***, *43(7),* 1146-1152.

198. Yang, X. L., Li, L., and Yin, J. H. (2004). Stability analysis of rock slopes with a modified Hoek-Brown failure criterion. ***International Journal for Numerical and Analytical Methods in Geomechanics***, *28(2),* 181-190.

199. Young, C.W., Nummo, T. J., Jasniksi, M. P., Cogley, D. R., and Capone, S. V. (1982). Clogging of leachate collection systems used in hazardous waste disposal facilities. ***Draft White Paper for U.S. EPA***, Research Triangle Park, North Carolina, USA.

200. Zhang, T., Yan, E., Cheng, J., and Zheng, Y. (2010). Mechanism of reservoir water in the deformation of Hefeng landslide. ***Journal of Earth Science**, 21(6),* 870-875.

201. http://duluthreader.com/articles/2018/04/26/13157_a_sampling_of_16_earthen_dam_failures (last visited 20/05/2019)

202. http://planetsave.com/2012/01/06/13000-homeless-9-dead-from-dam-break-in-brazil (last visited 20/05/2019)

203. http://www.assamtribune.com/scripts/detailsnew.asp?id=apr2216/state051 (last visited 20/05/2019)

204. http://www.cwc.gov.in/national-register-large-dams (last visited 20/052019)

205. http://www.icold-cigb.org/GB/Dams/role_of_dams.asp (last visited 20/052019)

206. http://www.npdp.stanford.edu/index.html (last visited 20/052019)

207. http://www.tailings.info/casestudies/merriespruit.htm (last visited 20/052019)

208. http://www.un.org/waterforlifedecade/water_and_sustainable_development (last visited 20/052019)

209. http://www.wise-uranium.org/mdaf.html (last visited 20/052019)

210. https://divyamarathi.bhaskar.com/news/MAH-PUN-panshet-dam-burst-compeled-54-years-massive-flooding-in-pune-5051412-PHO.html (last visited 20/052019)

211. https://en.wikipedia.org/wiki/List_of_tailings_dam_failures (last visited 20/052019)

212. https://history.info/on-this-day/1976-collapse-of-the-teton-dam-in-idaho/ (last visited 20/052019)

213. https://www.aljazeera.com/news/americas/2012/01/20121634911486308.html/(last visited 20/052019)

214. https://www.apnnews.com/flood-situation-remains-grim-in-assam/(lastvisited 20/05/2019

215. https://www.bbc.co.uk/news/resources/idt-sh/brazil_dam_disaster(last visited 20/05/2019

216. https://www.indiawaterportal.org/articles/machhu-dam-disaster-1979-gujarat-discussion-book-tom-wooten-and-utpal-sandesara (last visited 20/05/2019)

217. https://www.internationalrivers.org/resources/the-forgotten-legacy-of-the-banqiao-damcollapse (last visited 20/05/2019)

218. https://www.internationalrivers.org/resources/the-forgotten-legacy-of-the-banqiao-damcollapse (last visited 20/05/2019)

219. https://www.pratidintime.com/assam-reeling-under-soil-erosion-flood-threats/(last visited 20/05/2019)

220. https://www.time8.in/breaking-majulis-main-embankment-gives-way/(last visited 20/05/2019)

221. www.cwc.gov.in (last visited 20/05/2019)

LIST OF PUBLICATIONS

Book Chapters (Published/Accepted)

1. **Talukdar, P.** and Dey, A. (2018) "Effect of varying geometrical configuration of sheet piles on exit gradient and uplift pressure in Geotechnical Applications", ***Lecture Notes in Civil Engineering Vol. 13***, Ed. I. V. Anirudhan, S. Banerjee, Springer, Singapore, pp. 135-142: ISBN No. 978-981-13-0367-8.
2. **Talukdar, P.** and Dey, A. (2018) "Numerical modeling of earthen dam: Validation with field data" (Accepted for Book Chapter in Springer Publications).
3. **Talukdar, P.** and Dey, A. (2018) "Influence of the rate of construction on the response of earthen dam on PVD improved soft ground" (Accepted for Book Chapter in Springer Publications).
4. **Talukdar, P.** and Dey, A. (2018) "Sequential drawdown and rainwater infiltration based stability assessment of earthen dams" (Accepted for Book Chapter in Springer Publications).
5. **Talukdar, P.** and Dey, A. (2017) "Response of Earth Dams to Toe Drain Clogging" (Accepted for Book Chapter in Springer Publications).

Journal Publications (Published/Communicated/To be communicated)

1. **Talukdar, P.,** Bora, R. and Dey, A. (2018) "Numerical investigation of hill slope instability due to seepage and anthropogenic activities" ***Indian Geotechnical Journal (Springer)***, Vol. 48, Iss. 3, pp. 585-594. (DOI: 10.1007/s40098-017-0272-4)
2. **Talukdar, P.** and Dey, A. (2019) "Hydraulic failures of earthen dams and embankments" ***Innovative Infrastructure Solutions (Springer)***, Vol. 4, Paper No. 42, pp. 1-20 (DOI: 10.1007/s41062-019-0229-9)
3. **Talukdar, P.** and Dey, A. (2019) "Hydraulic fracturing and crack propagation through the impervious central core of zone earthen dams" ***International Journal of Geomechanics*** (ASCE) (Manuscript communicated).
4. **Talukdar, P.** and Dey, A. (2019) "Hydraulic Fracturing and Crack Initiation in Homogeneous Earthen Dams" ***International Journal of Geoengineering*** (Manuscript communicated).
5. **Talukdar, P.** and Dey, A. (2019) "Response of Homogeneous Earthen Dams to Clogging of Drainage Blanket" ***International Journal of Geotechnical Engineering*** (Manuscript communicated).
6. **Talukdar, P.** and Dey, A. (2019) "Efficacy of Drainage Blankets towards the Performance of Zoned Earthen Dam Comprising a Cracked Core" ***International Journal of Civil Engineering*** (Manuscript communicated).

7. **Talukdar, P.** and Dey, A. (2019) "Influence of Drainage Blanket Clogging on Response of Homogeneous Earthen Dams" ***Acta Geotechnica Slovenica*** (Manuscript communicated).

Conference: National/International (Published)

1. **Talukdar, P.** and Dey, A. (2018) "Sequential drawdown and rainwater infiltration based stability assessment of earthen dams" ***International IACMAG Symposium***, Gandhinagar, India, Paper No. 236, pp. 1-11.
2. **Talukdar, P.** and Dey, A. (2018) "Numerical modeling of earthen dam: Validation with field data" ***International Conference on Infrastructure Development (ICID)***, Jorhat, India.
3. **Talukdar, P.** and Dey, A. (2018) "Influence of the rate of construction on the response of earthen dam on PVD improved soft ground" ***Indian Geotechnical Conference (IGC-2018)***, Bangalore, India, pp. 1-7
4. **Talukdar, P.** and Dey, A. (2017) "Response of Earth Dams to Toe Drain Clogging", ***Indian Geotechnical Conference, IGC***, Department of Civil Engineering, IIT Guwahati, India, pp. 1-4.
5. **Talukdar, P.,** Bora, R. and Dey, A. (2017) "Finite Element Based Identification of the Triggering Mechanism of a Failed Hill Slope" ***15th International Conference of International Association for Computer Methods and Advances in Geomechanics (IACMAG),*** Wuhan, China, pp. 1-11.
6. **Talukdar, P.,** Bora, R. and Dey, A. (2016) "Stability analysis of ash pond dyke under static, pseudo-static and seismic conditions" ***1st International Conference on Civil Engineering for Sustainable Development – Opportunities and Challenges (CESDOC)***, Guwahati, India, pp. 1-6.
7. **Talukdar, P.,** Bora, R. and Dey, A. (2016) "Forensic investigation of the failure of a marginally stable hill slope" ***5th International Conference on Forensic Geotechnical Engineering***, Bangalore, India, pp. 389-400.
8. **Talukdar, P.** and Dey, A. (2016) "Effect of varying geometrical configuration of sheet piles on exit gradient and uplift pressure" ***Geotechnology towards Global Standards, Indian Geotechnical Conference, IGC 2016***, IIT Madras, India, pp. 1-4.